CARDIAC EFFECTS OF OVARIAN HORMONES AND GENDER IN A MOUSE MODEL OF OBESITY

Inauguraldissertation

zur

Erlangung der Würde eines Doktors der Philosophie

vorgelegt der

Philosophisch-Naturwissenschaftlichen Fakultät

der Universität Basel

von

Sonia Lebboukh

aus Frankreich

Basel, 2018

Genehmigt von der Philosophisch-Naturwissenschaftlichen Fakultät auf Antrag von:

Prof. Dr. Markus A. Rüegg
Prof. Dr. Marijke Brink
Prof. Dr. Thierry Pedrazzini

Basel, 17th October 2017

Prof. Dr. Martin Spiess

Dekan der Philosophisch-Naturwissenschaftlichen Fakultät

I dedicate my thesis to my parents and especially to my mother who is always here for me. I hope to be able to return you the favour and more soon.

TABLE OF CONTENTS

LIST OF FIGURES AND TABLES

LIST OF SUPPLEMENTAL FIGURES AND TABLES

LIST OF ABBREVIATIONS

4EBP1: eukaryotic translation initiation factor 4E-binding protein 1

ACC: acetyl-CoA carboxylase

ACO: acyl CoA oxidase

AGEs: advanced glycation end-products

AMPK: AMP activated protein kinase

ANP: atrial natriuretic peptide

AS160: Akt substrate 160

Atg: autophagy related genes

ATP: adenosine triphosphate

βARKO: beta cell selective androgen receptors deficiency

BNP: brain natriuretic peptide

β-MHC: beta myosin heavy chain

BP: blood pressure

BW: body weight

CPT-I/II: carnitine palmitoyl transferase I/II

CRP: C-reactive protein

CTD: control diet

DAG: diacylglycerol

DBP: diastolic blood pressure

Ca^{2+}: calcium

CD36: cluster of differentiation 36

CO: cardiac output

CoA: Coenzyme A

CT: carnitine/acylcarnitine transferase

CHD: coronary heart disease

CVD: cardiovascular disease

CVS: cardiovascular system

DHEA: dehydroepiandrosterone

E1: estrone

E2: estrogen

E3: estriol

EDPVR: end-diastolic pressure volume relationship

EF: ejection fraction

EGF: epidermal growth factor

ER: estrogen receptor

ERE: estrogen receptor element

ERα: estrogen receptor alpha

ERβ: estrogen receptor beta

ER stress: endoplasmic reticulum stress

ERE: estrogen response element

ERK: extracellular signal-regulated kinase

ERR: estrogen related receptor

ESPVR: end-systolic pressure volume relationship

FA: fatty acid

FABPpm: plasma membrane isoform of fatty acid binding protein

FACS: fatty acyl CoA synthetase

$FADH_2$: flavin adenine dinucleotide

FAO: fatty acid oxidation

FAT: fatty acid transporter

FATP 1/6: fatty acid transport protein

FFA: free fatty acid

FOXO: forkhead box O

FS: fractional shortening

FSH: follicle-stimulating hormone

GAPDH: glyceraldehyde-3-phosphate-dehydrogenase

GH: growth hormone

GLUT: glucose transporter

GnRH: gonadotropin-releasing hormone

GO: glucose oxidation

GPER: G-protein-coupled receptor estrogen receptor

GSIS: glucose-stimulated insulin secretion

GSK3: glycogen synthase kinase 3

GTT: glucose test tolerance

GW: gastrocnemius weight

HF: heart failure

HFD: high fat diet

HFpEF: heart failure with preserved ejection fraction

HFrEF: heart failure with reduced ejection fraction

HRT: hormonal replacement therapy

Hsp: heat shock protein

IκBα: I kappa B alpha

IKK: IκBα kinase complex

IL: interleukin

i.p.: intraperitoneal

IR: ischemia-reperfusion

IRS: insulin receptor substrate

IVCT: isovolumic contraction time

IVRT: isovolumic relaxation time

JNK: c-Jun N-terminal kinase

KO: knock-out

LA: left atria

LC3B: microtubule-associated protein 1 light chain 3 beta

LH: luteinizing hormone

LW: liver weight

LV: left ventricle

MCD: malonyl CoA decarboxylase

MCP-1: monocyte chemotactic protein-1

MEF2C: myocyte enhancing factor-2C

MMP: matrix metalloproteinase

mTOR: mammalian or mechanistic target of rapamycin

$NADH_2$: nicotinamide adenine dinucleotide

NF-κB: nuclear factor kappa-light-chain-enhancer of activated B cells

p70-S6K1: p70 ribosome S6 kinase 1

OVX: ovariectomy/ovariectomized

PDC: pyruvate dehydrogenase complex

PDH: pyruvate dehydrogenase

PDK: pyruvate dehydrogenase kinase

Ped: end-diastolic pressure

PGC1α: peroxisome-proliferator activated receptor gamma coactivator 1 alpha

PHLPP1/2: PH-domain leucine rich repeat containing protein phosphatase 1/2

PI3K: phosphoinositol 3 kinase

PIP_3: phosphatidylinositol (3,4,5) triphosphates

PKB: protein kinase B (Akt)

PKC: protein kinase C

PLN: phospholamban

PP1: protein phosphatase-1

PPAR: peroxisome-proliferator activated receptor

PP2A: protein phosphatases 2A

PSR: Picrosirius Red

PTEN: phosphatase and tensin homolog

PV: pressure-volume
PVL: pressure-volume loop
RT: room temperature
RV: right ventricle
SBP: systolic blood pressure
SERCA: sarcoplasmic reticulum calcium-ATPase 2
SIRT: silent information regulation
SP1: specificity protein 1
SR: sarcoplasmic reticulum
StAR: stereoidenogenic acute regulatory protein
STZ: streptozotocine
SV: stroke volume
T2DM: type II diabetes mellitus
TAG: triacylglycerol
TCA: tricarboxylic acid cycle
TEM: transmission electron microscopy
TFAM: mitochondrial transcription factor A
TFBM2: mitochondrial transcription factor B2
TIMP: tissue inhibitor of metalloproteinase
TL: tibia length
TNFα: tumor necrosis factor alpha
TSC1/2: tuberous sclerosis complex 1/2
VFW: visceral fat weight
VW: ventricular weight
WGA: wheat germ agglutinin
WHO: world health organization

Summary

Men are at higher risk to develop obesity, cardiovascular disease and hypertension than women. However, this tendency is inversed in the postmenopausal population when women lose their advantage while ovarian hormone levels decrease. This raises the question as to why and how this occurs. Many studies suggested that estrogen is cardioprotective, however the underlying mechanisms are still unknown. Additionally, hormone replacement therapies failed to prove the beneficial effect of estrogen on the cardiovascular system. Hence the need to characterize and better understand the mechanisms underlying the effects of estrogen in the cardiovascular system. Thus, the aim of this thesis project was to describe gender- and ovarian hormone-specific effects of obesity in the heart. To this end we analyzed the effect of HFD, gender and ovariectomy on cardiac function and structure and investigated the mechanisms involved in a mouse model.

Male and female mice were fed for 22 weeks with a regular chow diet and a high-fat diet (HFD) containing 45% calories derived from saturated fat and 17% from sucrose aiming to mimic the diet used in western countries, which contains a lot of saturated fat and carbohydrates. The following gender-specific changes were demonstrated after HFD feeding. At the systemic level, male showed a stronger increase of plasma insulin than female mice, suggestive of higher insulin sensitivity in the female mice. Cardiac function analysis revealed that the peak filling and emptying rates were decreased by the HFD in male mice only, suggesting that their ventricular relaxation is impaired. As for the female mice, they exhibited decreased E/A ratios as well as a moderate wall thickness increase, suggestive of mild diastolic dysfunction and cardiac remodeling, respectively. Ejection fractions were preserved in these female mice.

To evaluate the role of female hormones in changing cardiac structure and function, we ablated the ovaries (OVX) 4 weeks before starting the diet. At the systemic level, we demonstrated that ovarian hormones are involved in increasing plasma insulin and maintaining glucose tolerance in response to HFD, since the OVX-female mice were not able to increase plasma insulin levels and had greater glucose intolerance than the sham-female mice after HFD. When investigating cardiac function, we revealed that the sham-female but not the OVX-female mice were able to reduce the end-diastolic pressure in response to HFD. This difference unveiled that OVX-female had higher end-diastolic pressures than sham-female mice after HFD following cardiac stress induced by the beta-adrenergic agonist dobutamine. This suggests that estrogen is implicated in the adaptation to the increased cardiac work induced by dobutamine. Finally, we demonstrated that OVX-female had higher cardiac PDK4 mRNA than sham-female mice when fed with regular chow, suggesting that ovarian hormones are important for preserving normal glucose oxidation. In conclusion, these data suggest that estrogen plays a role in insulin and glucose homeostasis as well as in the adaptation of the heart to HFD-induced obesity.

1. Introduction

The prevalence of obesity and insulin resistance increased in the developed and emerging countries, obesity has more than doubled since 1980 (WHO, 2016). Although genetic factors have been implicated in the onset of insulin resistance, this pathology is principally due to feeding behavior and the increase of sedentary lifestyle. Metabolic syndrome is characterized by the association of obesity, diabetes, and cardiovascular disease and is described as an abdominal obesity with increased triglyceride, decreased high-density lipoprotein cholesterol, glucose intolerance and hypertension.[1] The associated increased prevalence for cardiovascular disease (CVD) is linked to a higher risk to develop atherosclerosis and myocardial ischemia, hypertension and diabetic cardiomyopathy, hypercoagulability, sleep-disordered breathing and atrial fibrillation.

Different observations from clinical studies introduced that premenopausal women present a lesser risk to develop cardiovascular diseases than age-matched men.[2-4] Hence, the statement that female hormones are cardioprotective, which has been proved at preclinical levels. Nevertheless, different hormonal replacement therapies (HRT) studies failed to prove any benefits on CVD.[5,6] The disparity between these clinical trials and experimental models is not yet clearly understood. However, it is noteworthy that a “timing hypothesis” has been proposed since HRT in younger patients, who are still in the perimenopausal period, showed improved cardiovascular benefits. In 2014, new clinical trials have been designed to explore this finding, and similarly the early HRT improved cardiovascular risks.[7] Recently, trials performed by Manson et al. within the scope of the women health initiative, have driven to the statement that HRT “has a harmful effect on coronary heart disease among older women, whereas the results in younger women remain inconclusive”.[8] More in detail they affirmed that conjugated equine estrogen treatment was protective for myocardial infarction, coronary artery bypass grafting/percutaneous coronary intervention and all cardiovascular events, and had a harmful effect on deep veins thrombosis in early menopausal women only, strengthening the age-dependent effects.

Estrogen deficiency is associated with insulin resistance, impaired glucose tolerance and increased abdominal fat. Obesity is a high-risk factor for the development of type II diabetes mellitus (T2DM). Diabetic patients have a higher risk to develop CVD, and interestingly the female advantage regarding the cardiovascular risk incidence is not anymore found in the context of T2DM.[9,10] Indeed, the Framingham Heart Study revealed a 5-fold increase in risk of heart failure (HF) in diabetic women compared to a 2-fold increase in males.[2] This difference might be linked to increased susceptibility to develop coronary disease, impaired insulin sensitivity, and hyperglycemia. Diabetic females are also more prone to develop acute myocardial infarction than diabetic males.[11,12] As previously noted,

menopause in women increases the CVD risk and is associated with an enhanced incidence of insulin-resistance and diabetes, but whether estrogen deficiency exacerbates the CVD risk in diabetic compared to non-diabetic women is still unknown. It has been observed that T2DM females are more susceptible to develop other cardiovascular risk factors (dyslipidemia, obesity, hypertension) and that these risks have a greater probability to lead to CVD.[13]

Hereafter, I will introduce the cardiovascular system (CVS) as well as two well-known methods to investigate cardiac function, echocardiography and pressure volume loop (PVL), relevant for the understanding of my thesis project. This general introduction will be followed by key information about cardiac metabolism and CVD, and a summary of the existing literature on the role of estrogen in this context. My introduction concludes with the overall aims of my studies.

1.1 Cardiovascular system

1.1.1 General

The cardiovascular system (CVS) is composed of the heart and the blood vessels. The heart is divided in four chambers: left/right atria, and left/right ventricles (LV and RV respectively). The left ventricle receives the blood from the pulmonary system via the pulmonary veins and redistributes it to all the organs as a pump, whereas the right ventricle gathers blood coming from the organs via the inferior and superior vena cava, before to send it to the pulmonary system for replenishment. Figure 1 shows the anatomy of the heart with its four chambers and the major veins and arteries.

Blood vessels transport the blood from the heart to the organs and back from the organs to the heart. Different types of blood vessels exist with different characteristics. The arterial vessels are composed of endothelial and smooth muscle cells as well as connective tissue with high elastic properties. Importantly, they possess a thick wall to cope with the high-pressure blood coming from the left ventricle, and are branching into arterioles. Arterioles are highly resistant and contain a high density of smooth muscle cells innervated by sympathetic adrenergic nerve fibers, which give them the susceptibility to trigger vasoconstriction or vasodilatation stimulation of α1 and β2 adrenergic receptors, respectively. Finally, arterioles distribute the blood into capillaries, which constitute the site of nutrient and gas exchange between blood and tissues. The blood that results from this exchange will return to the right atria via venules and veins. The veins are not as rich in

elastic tissue as the arteries hence their particularity to have a large capacitance, meaning that they can hold a large volume of blood.[14]

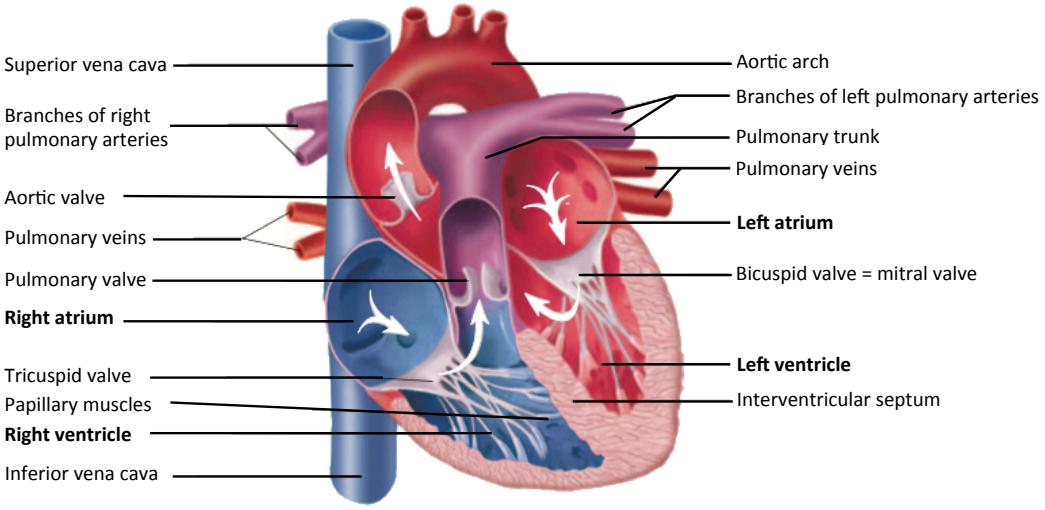

Figure 1: Schematic representation of the anatomy of the heart.
The heart is composed of four chambers: the right and left atria and the right and left ventricles. Blood coming from the lungs enters the left atrium via the pulmonary veins. When the left ventricle pressure is higher than the atrium pressure, the mitral valve opens and blood flows into the left ventricle during the relaxation phase. While the left ventricle contracts the pressure increases until it gets higher than the aortic pressure. At this moment, the aortic valve opens and the blood is ejected into the aorta to perfuse organs with oxygenated blood. After passage through the organs, the deoxygenated blood comes back to the right atrium via the inferior and superior vena cava. Similar as for the left ventricle, the blood is filling the right ventricle before to be ejected to the lungs through the left pulmonary arteries to be reoxygenated. Copied from "Essentials of Anatomy and Physiology", 6th Edition- Seeley, Stefens, Tate.

1.1.2 Blood circuit

The heart propels the blood rich in oxygen from the left ventricle into the arterial blood vessels through the aorta, to reach the peripheral capillaries. It is in the capillaries where nutrients, gases, water and solutes are exchanged between the blood and the tissues. The blood continues its way to the venules and veins before to reach the right atrium via the vena cava. The blood flows then into the right ventricle and is propelled into the pulmonary artery to the lungs where exchanges will also happen between the blood and the alveolar gas. This blood rich in oxygen will return to the left atria (LA) by the pulmonary veins and a new cycle will start.

The cardiac output is the rate at which blood is ejected by the heart (L/min). Each organ receives a different percentage of this cardiac output. The renal system, gastrointestinal

tract, and skeletal muscles receive the highest percentage of cardiac output, with 25% each, the brain receives 15% and the skin and the coronaries 5% of the cardiac output. All these attributed percentages of cardiac output are susceptible to change according to the immediate needs of each organ and to their individual vital character.

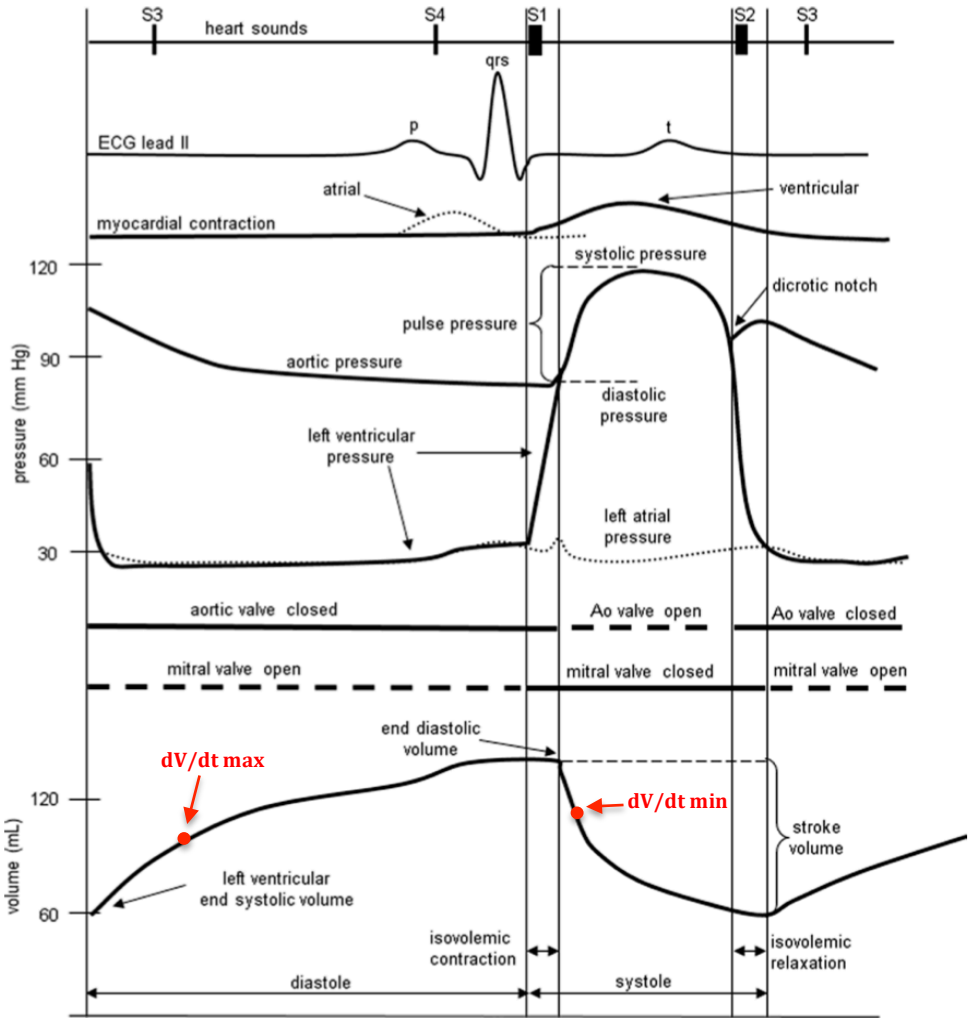

Figure 2: Electrical and mechanical events of a cardiac cycle within the left ventricle.
The LV volume at peak dV/dt max was added as well as the peak dV/dt min, which occurs during LV ejection. Copied from "Handbook of cardiac anatomy, physiology, and devices", Springer, Paul A. Iaizzo.

1.1.3 Cardiac cycle

The normal heart rate is 60-80 beats per minute at a resting state. The cardiac cycle is divided into 4 phases, which take place within less than a second. The different electrical and mechanical events of a cardiac cycle in a normal left heart are shown in Figure 2.[15] The blood coming from the veins enter the atria and when the pressure is sufficiently high the cuspide valve (atrioventricular: mitral for the LV and tricuspide for the RV) opens to let the

blood flow passively into the relaxed ventricle, this is the diastole. Active atrial contraction pushes further blood volume into the LV, the LV pressure becomes higher than the atrium, and the atrio-ventricular valve closes marking the end of the diastole. The electrical stimulus of the sinus node that induced atrial contraction (atrial systole) is propagated to the ventricles through His bundle and left and right bundle branches. This depolarization of ventricular cells will trigger the contraction and increase progressively intraventricular pressures until they are above those in the atria, which results in the closure of the atrioventricular valves. The ventricular pressure continues to rise, this is the isovolumic contraction, until it is above the pressure in the semilunar valves (pulmonary and aortic valve). Blood is rapidly ejected from the ventricle to the aorta and pulmonary artery where the pressures rise while the ventricles continue to contract, this phase is called rapid ejection phase. In the right ventricle, similar steps are present, but the pressure developed and required to open the pulmonary valve are lower because the resistance is lower in the pulmonary vascular system. The ventricles decrease their contraction and the intraventricular pressures decrease below those in the aorta and pulmonary arteries provoking a rapid closure of the semilunar valves. Rapidly, the intraventricular pressures fall and the ventricles relax. All the cardiac valves are closed, this is the isovolumetric relaxation phase.

1.1.4 Echocardiography

Echocardiography is a non-invasive method used to evaluate cardiac morphology and function in patients and has also been adapted for the analysis of murine models.[16,17] Different parameters assessed by echocardiography are important to evaluate systolic and diastolic dysfunction. The 2D imaging “B-mode” is used to obtain a parasternal short and long axis view (Figure 3) and visualize the LV anterior and posterior walls as well as the intraventricular septal and lateral wall. The LV internal dimension corresponds to the LV lumen. The 1D imaging “M-mode” is used to obtain fine measurements of cardiac dimensions (Figure 4). These parameters are used to assess systolic function.

Ejection fraction (EF) and fractional shortening (FS) are commonly used to study systolic function in a clinical setting and also in animal experimentation. The EF corresponds to the ratio between the stroke volume (SV) and the end-diastolic volume. The SV is the amount of blood expelled during one cardiac cycle. Thus, the ejection fraction is the actual percentage of blood ejected during one cycle. In non-pathologic cases, the fractional shortening reflects the EF and is similarly used to estimate myocardial contractility. In ischemia or myocardial infarction models, EF calculation may not be accurate because of the changes in cardiac geometry, and FS is preferentially used to describe systolic function.

The EF and FS parameters are afterload-dependent, which is their main limitation. Indeed, an increase in systemic blood pressure and myocardial stiffness will reduce these parameters. The LV posterior thickening is also used as a parameter of systolic function. These parameters are calculated according to the following formulas:[17-20]

- **Stroke volume = end-diastolic volume – end-systolic volume**
- **EF = stroke volume / end-diastolic volume (x 100, %)**
- **FS = (LV end-diastolic diameter – LV end-systolic diameter) / LV end-diastolic diameter (x 100, %)**
- **LV posterior wall thickening = (Posterior wall thickness at systole – Posterior wall thickness at diastole) / Posterior wall thickness at diastole (x100, %)**

Another parameter recorded by echocardiography is the cardiac output (CO). It is the volume of blood pumped out of the left or right ventricle per unit of time (L/min). This is the product of heart rate (beats/min) and stroke volume (L/beat). The LV mass as well as wall thickness are also calculated from echocardiography. The LV mass is measured using M-mode from targeted short axis view or a parasternal long axis view at the end of the diastole in which the ventricular dimension or volume is the largest. Geometric formulas are used to calculate the volume of the LV myocardium, which is then converted to mass by multiplying this volume of the myocardium by the myocardial density (1.04 g/mL), the formula used is as follow:[21]

$$\textbf{LV mass} = 0.8 \times 1.04 \times [(IVS+LVID+PWT)^3 - LVID^3)] + 0.6g$$

(IVS: interventricular septum; LVID: LV internal diameter; PWT: posterior wall thickness)

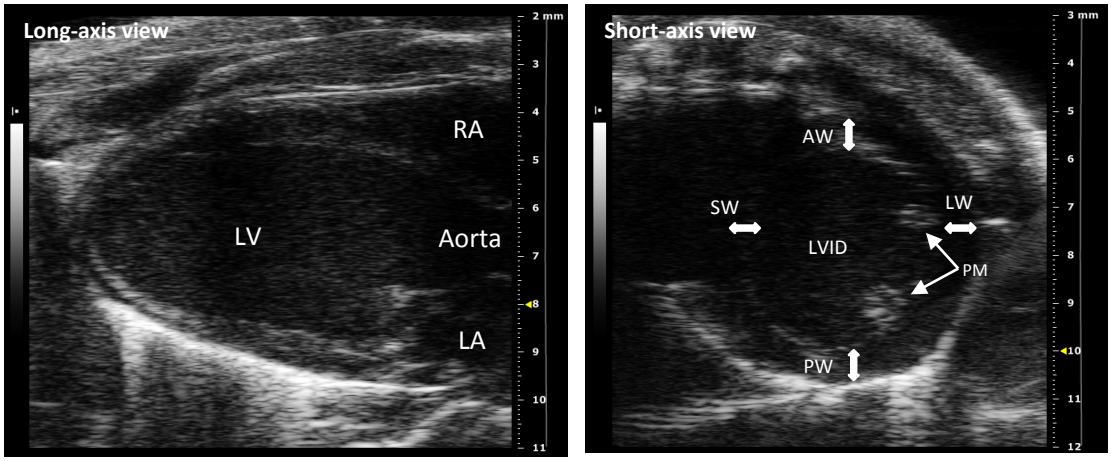

Figure 3: Representative 2D echocardiographic image of mouse cardiac tissue using the B-mode.

A: long-axis view; B: short-axis view; LV, left ventricle; RA, right atrium; LA, left atrium; SW, intraventricular septal wall; AW, anterior wall; LW, lateral wall; PW, posterior wall; LVID, LV internal dimension; PM, papillary muscle.

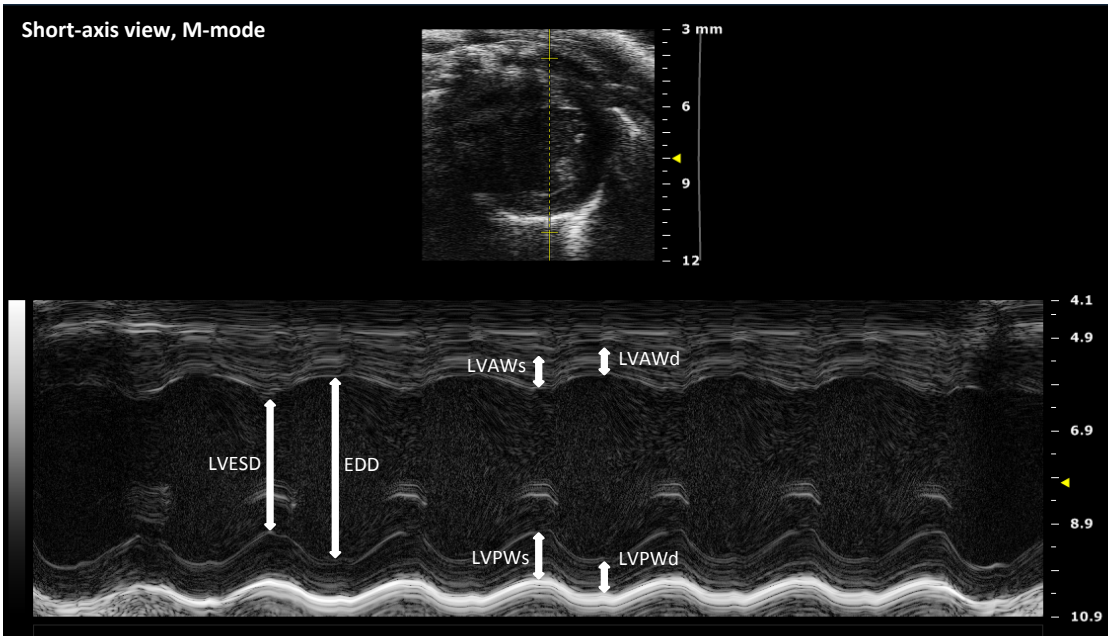

Figure 4: Representative 1D echocardiography images of mouse cardiac tissue using the M-mode.
The M-mode cursor was positioned perpendicular to the interventricular septum wall (SW) and posterior wall (PW) of the LV at the level of the papillary muscles. LV end-systolic and -diastolic dimensions, as well as diastolic and systolic LV wall thickness were measured. ESD, end-systolic diameter; EDD, end-diastolic diameter; LVAWs, LV anterior wall at systole; LVAWd, LV anterior wall at diastole.

Cardiac remodeling is defined as alterations in size, geometry, shape, composition and function of the heart induced by cardiac load or injury.[22] Cardiac remodeling, or more precisely LV remodeling, is observed in pathologic conditions such as hypertension. This adaptive response is the consequence of increase LV workload to overcome the elevated aortic pressure and is leading to LV wall hypertrophy. This compensatory hypertrophy in response to systemic hypertension is explained by the Laplace law,[23] which states that pressure correlates directly with tension and wall thickness and inversely correlates with the radius as described with the following formula:

$$T = P \times r / 2h$$

(T: tension or stress in the LV wall; P: LV pressure; r: radius; h: LV wall thickness)

In other words, the Laplace law says that the greater the thickness of the LV wall, the greater the pressure can be developed, and this is also why the LV is thicker than the RV as it has to develop more pressure to expel the blood. A sustained elevated blood pressure will increase the LV wall stress and results in LV wall thickening and LV mass elevation. This adaptive response leads to the normalization of the wall stress and the onset of concentric hypertrophy as a result of a pressure overload. In case of increased blood volume, the chamber radius would increase resulting in eccentric hypertrophy (volume overload). The LV geometry can be described according to the LV mass and the relative wall thickness

(RWT). The relative wall thickness derives from the Laplace law and is defined as the ratio of twice the LV posterior wall thickness to the LV internal diameter measured at the end-diastole. Together with the LV mass, the RWT can describe four LV geometric patterns:[21,24]

1. normal LV geometry: normal LV mass and lower value of RWT
2. eccentric LV hypertrophy: increased LV mass and lower value of RWT (≤0.42)
3. concentric LV hypertrophy: increased LV mass and RWT (>0.42)
4. concentric LV remodeling: normal LV mass and increased RWT

Hypertrophy is the main mechanism used by the heart to reduce LV wall stress to palliate pressure overload. It involves different cellular events such as increased protein synthesis and stability. In concentric hypertrophy the width of the cardiomyocytes is increased through the parallel addition of sarcomeres (the force-generating units). As for eccentric hypertrophy, it is characterized by increased cardiomyocyte length caused by the addition of new sarcomeres in series.[23,25]

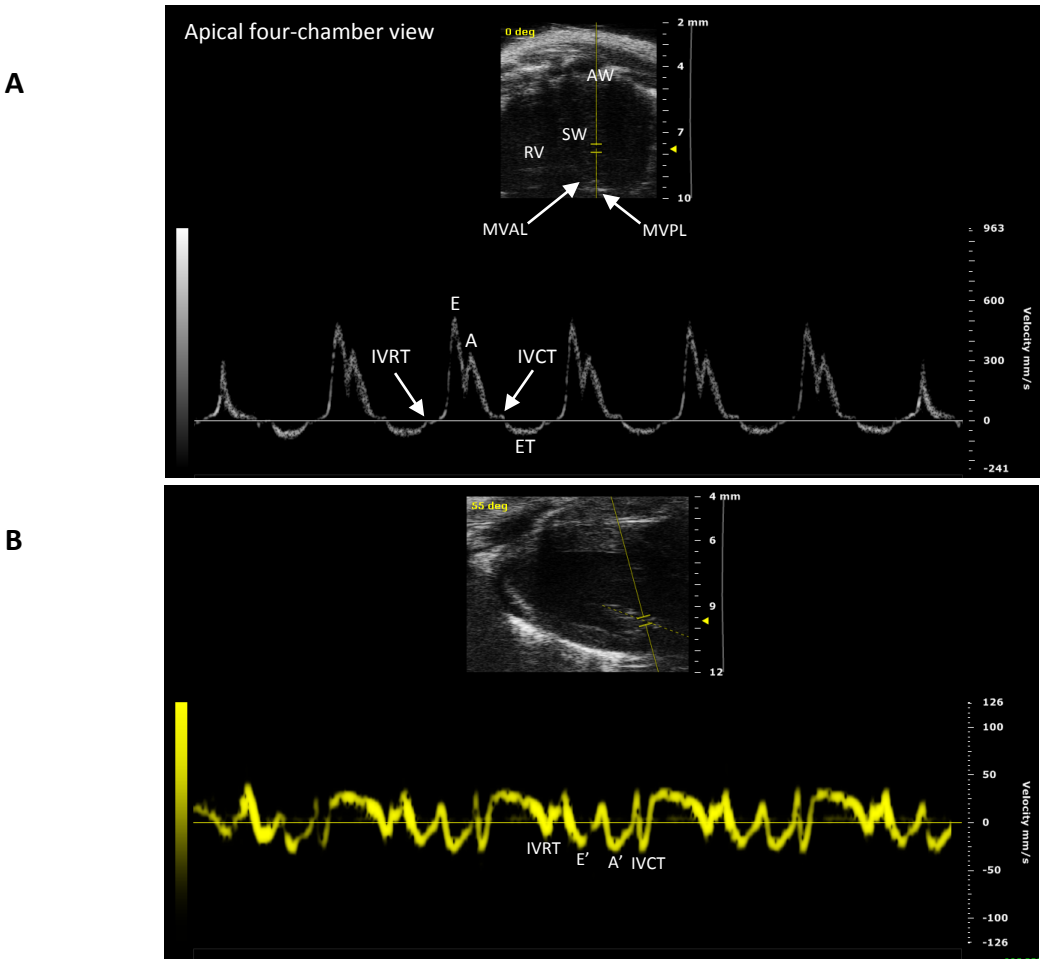

Figure 5: Representative echocardiography images of mouse cardiac tissue.
A: pulse-waved Doppler is used to determine the intramitral flow velocity at early (E) passive filling of the ventricle and late active atrial (A) systole. The isovolumic relaxation and contraction time and the ejection time are also measured via this method. B: tissue Doppler imaging to measure velocity and wall motion. AW, anterior wall; ET, ejection time; IVCT, isovolumic contraction time; IVRT, isovolumic relaxation time; LV, left ventricle; MVAL, mitral valve anterior leaflet; MVPL, mitral valve posterior leaflet; PW, posterior wall; RV, right ventricle; SW, interventricular septum wall.

Left diastolic function can be evaluated by echocardiography using the following three parameters:

1) The mitral inflow pattern, including the measure of the E/A ratio, the deceleration time and the isovolumic relaxation time.
2) The mitral annulus velocity recorded with tissue Doppler: E/E' ratio, which is an indicator of LV relaxation.
3) The pulmonary venous inflow pattern

The pulse-waved Doppler tool appreciates the blood flow velocity, to study diastolic function imaging the evaluation of the transmitral flow patterns is essential. This is because the velocity curve reflects the instantaneous pressure gradient between the LA and the LV. As the pressure difference is high, the velocity will be higher at this time point. When the pressure in the atrium equals the pressure of the ventricle, no pressure gradient exists anymore and the flow ceases. Pulse-waved Doppler records mitral inflow velocity at the mitral valve leaflet tips level. Two waves are then visualized, one representing the early passive filling of the LV (E-wave) and one representing the late active filling in response to atrial systole (A-wave) (Figure 5). The atrial contraction contributes to 20% of the LV filling in young, healthy subjects, and this proportion increases with aging without exceeding 50% generally. Loading conditions and filling pressure determine the mitral flow pattern, an increased LA pressure will lead to an increased peak E-wave velocity. On the contrary, a decreased LA pressure can lead to a decrease in peak E-wave velocity as well as an increase in deceleration time independently from the intrinsic relaxation properties of the LV which rely on the distensibility, elasticity, wall-thickness, cavity dimensions and pericardial constraint.

These parameters are used to describe the progression of diastolic dysfunction into several grades: [26-28]

- Normal diastolic function: E>A, normal LV filling
- Grade 1: E<A, impaired relaxation
- Grade 2: E>A, pseudonormal mitral valve inflow
- Grade 3: E>>A, restrictive filling

Diastole consists of 4 phases:[29]

1- isovolumetric relaxation, which starts from the end-systole until the LV pressure falls below atrial pressure causing the mitral valve opening. This ATP-dependent process is initiated by the release of the actin-myosin cross-bridges.
2- the rapid early ventricular filling ensues where blood flows from the LA to the LV by active and passive process, this phase corresponds to the E-wave.

3- diastasis corresponds to the completion of the active ventricular relaxation, the pressure between the LA and LV are nearly equal causing a slower blood flow of atrial filling from the pulmonary venous flow.
4- atrial systole takes place, the atria contracts then, increasing the transmitral pressure gradient and leading to the acceleration of blood flow from the atria to the ventricle, this phase corresponds to the A-wave.

Diastolic filling depends on creating and maintaining a pressure gradient between the LA and the LV, which determines the blood flow rate. Blood is first pulled out from the atria to the ventricle because the LV pressure is rapidly decreased during relaxation leading to a suction phenomenon. This happens during the early diastole. In late diastole, the atria contracts, the pressure is increased above ventricle pressure and the blood is pushed out through the valve to the LV.[28]

The deceleration time, the isovolumic relaxation time of mitral inflow (IVRT) and the isovolumic contraction time (IVCT) are also used as indicators of diastolic function. The deceleration time of the early filling velocity is the time interval from early peak inflow velocity (E-wave) to the end of the rapid early filling phase. This data is obtained by tracing the deceleration curve from the maximal point of the E-wave velocity to the baseline. In other words, the deceleration time represents the time needed for the pressure to be equal between the LA and the LV.

The IVRT is the interval of time between the closing of the aortic valve to mitral valve opening and the start of the transmitral flow. This parameter depends on the rate of LV relaxation and LA pressure. A prolongation of the IVRT is associated with impaired relaxation while a shorter IVRT is associated with an elevation of atrial pressure.

Additionally, tissue Doppler imaging is used to measure velocity of myocardial motion. It measures peak myocardial velocities at the mitral annulus or the LV posterior wall. The waveform will show four peaks: (1) IVRT, (2) the E’ wave which represents the motion of the mitral annulus during early LV diastolic filling, (3) the A’ wave corresponding to the atrial systole during late filling and (4) the IVCT. These parameters are important to determine diastolic function. A decreased of the E’/A’ ratio is indicative of diastolic dysfunction.[30]

1.1.5 Ventricular pressure-volume loop

The pressure-volume loop (PVL) method is the "gold-standard" method to study cardiac function. It was initially used in large animals and human and was progressively adapted to be used in small animals such as mice. Unlike the echocardiography and cardiac MRI, this method assesses systolic and diastolic dysfunction in a load-dependent or -independent manner. PVL is commonly used to assess real-time cardiac function and is sometimes combined with a cardiac stress inducer such as the β-adrenergic agonist dobutamine. The technique uses a pressure-conductance catheter, which is inserted into the left or right ventricle to record the changes in pressure and volume during cardiac cycles.

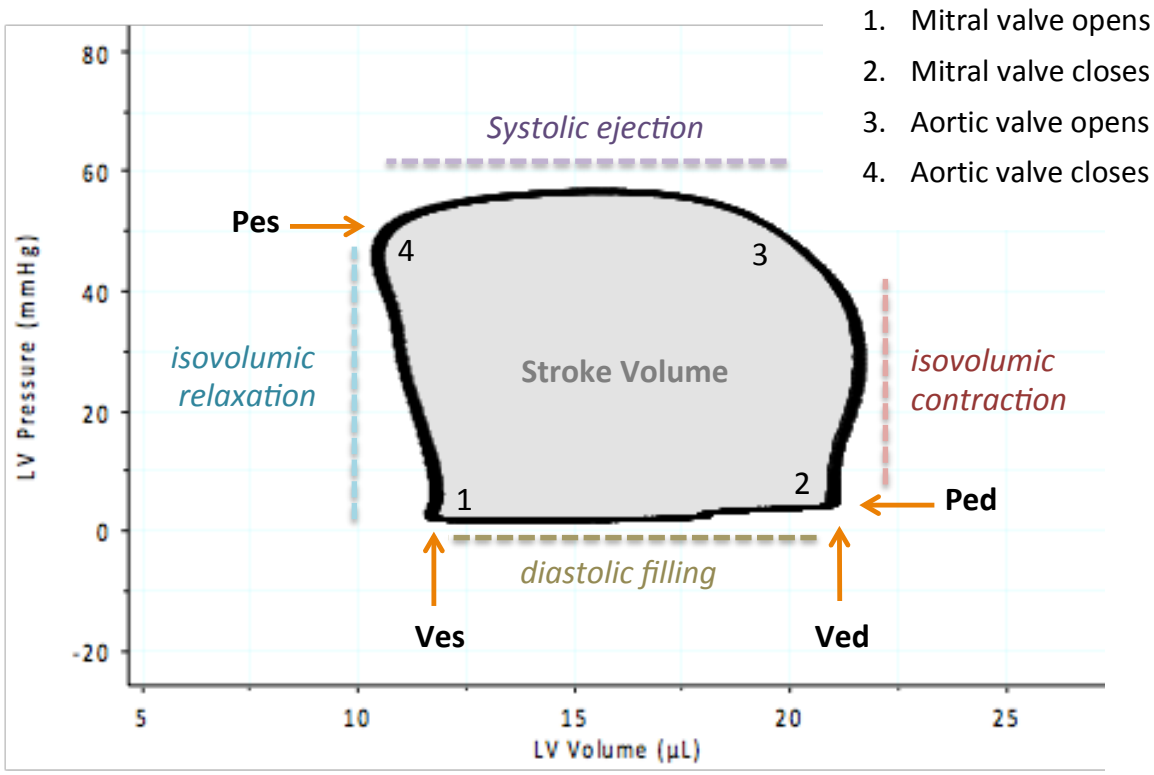

Figure 6: Example of a pressure-volume loop describing each step of a cardiac cycle.
As soon as the mitral valve opens (1), the blood starts to fill the left ventricle passively to reach the end-diastolic volume (Ved), this is the diastolic filling, which ends with the closing of the mitral valve (2). During this filling, the pressure progressively raises up to reach the end-diastolic pressure (Ped). During the isovolumic contraction, the LV starts to contract, and when the LV pressure (Pes) is higher than the aortic pressure, the aortic valve opens (3) and the blood is ejected into the aorta during the systolic ejection. The pressure reached in the aorta is then really high leading to the aortic valve closure (4) followed by isovolumic relaxation. At this stage, the pressure decreases and the LV starts to relax. The amount of blood left in the ventricle is low and represents the end-systolic volume (Ves). A new cardiac cycle can start again. Ped, end-diastolic pressure; Pes, end-systolic pressure; Ved, end-diastolic volume; Ves, end-systolic volume.

The catheter is comprised of one pressure and two conductance sensors. The latter allows an estimation of the blood pool by employing the relationship between electrical conductance and volume using the following formula:[31]

$$V = 1/\alpha \ (\rho \ L^2)(G–Gp)$$

ρ: blood resistivity; L: distance between sensing electrodes; G: conductance (measured as a voltage); Gp: parallel conductance induced by the conductivity of the muscle wall and surrounding tissues; α: gain coefficient (volume correction/calibration factor).

The ventricular pressure-volume loop, as its name suggests, is a loop representing the pressure and volume changes during a cardiac cycle. It is displayed by plotting ventricular pressure (y axis) against ventricular volume (x axis). This loop describes the 4 phases of the cardiac cycle: diastolic filling, isovolumic contraction, systolic ejection and isovolumic relaxation (Figure 6). The opening and closing of the valves depend on the pressure on both sides of them. Due to the pressure gradient, the mitral valve opens (1) and the blood flows from the LA to the LV, this corresponds to the diastolic filling where the cardiac muscle is relaxed. The LV volume attains its maximum; this is the end-diastolic volume (140 ml in human), whereas the pressure is really low (end-diastolic pressure) (2). The LV then contracts, thereby inducing a drastic increase in pressure, this is the isovolumic contraction phase. At the moment that the LV pressure becomes higher than the aortic pressure it causes the aortic valve to open (3). The LV continues to contract and the blood is thus rapidly ejected out of the LV into the aorta driven by the pressure gradient. The pressure remains high due to the still on-going ventricular contraction while the volume decreases rapidly in the LV. The remaining blood volume in the LV is the end-systolic volume (70 ml). The stroke volume corresponds to the volume ejected during one cardiac cycle and represents the width of the pressure-volume loop, in human the SV is equal to 70 ml. Finally, the systole ends, ventricular pressure goes down below aortic pressure leading to the closing of the aortic valve (4), the ventricle relaxes, this corresponds to the isovolumic relaxation phase. A new cardiac cycle can start, the pressure in the LV has fallen to a lower level than in the atria, the mitral valve opens and the blood flows in passively then actively when the atria contracts.

To study cardiac function, it is important to understand a few key words. The afterload is the load against which the heart has to fight during ejection and is determined by the arterial system. Aortic pressure, ejection wall stress, total peripheral resistance and arterial impedance are used to characterize afterload. The velocity of cardiac fiber shortening is maximal when afterload is equal to zero and inversely, it decreases when afterload increases. The preload on the other hand is the load received by the heart at the end of

diastole and results from passive and active emptying of the atrium into the ventricle. The end-diastolic volume and pressure as well as the end-diastolic wall stress give information about the preload. Mitral stenosis or ventricular hypertrophy will affect the preload. The Frank-Starling curve describes the relationship between preload and stroke volume. The Frank-Starling relationship states that "the volume of blood ejected by the ventricle depends on the volume present in the ventricle at the end of the diastole".[32-36] The volume present at the end of the diastole depends on the volume of blood returned to the heart that is to say the venous return. In other words, Frank and Starling demonstrated that an increase in ventricular filling, which is translated by an increased sarcomere length, promotes an increase in the pressure developed during systole, which corresponds to the tension. This relationship is also called length-tension relationship.[14]

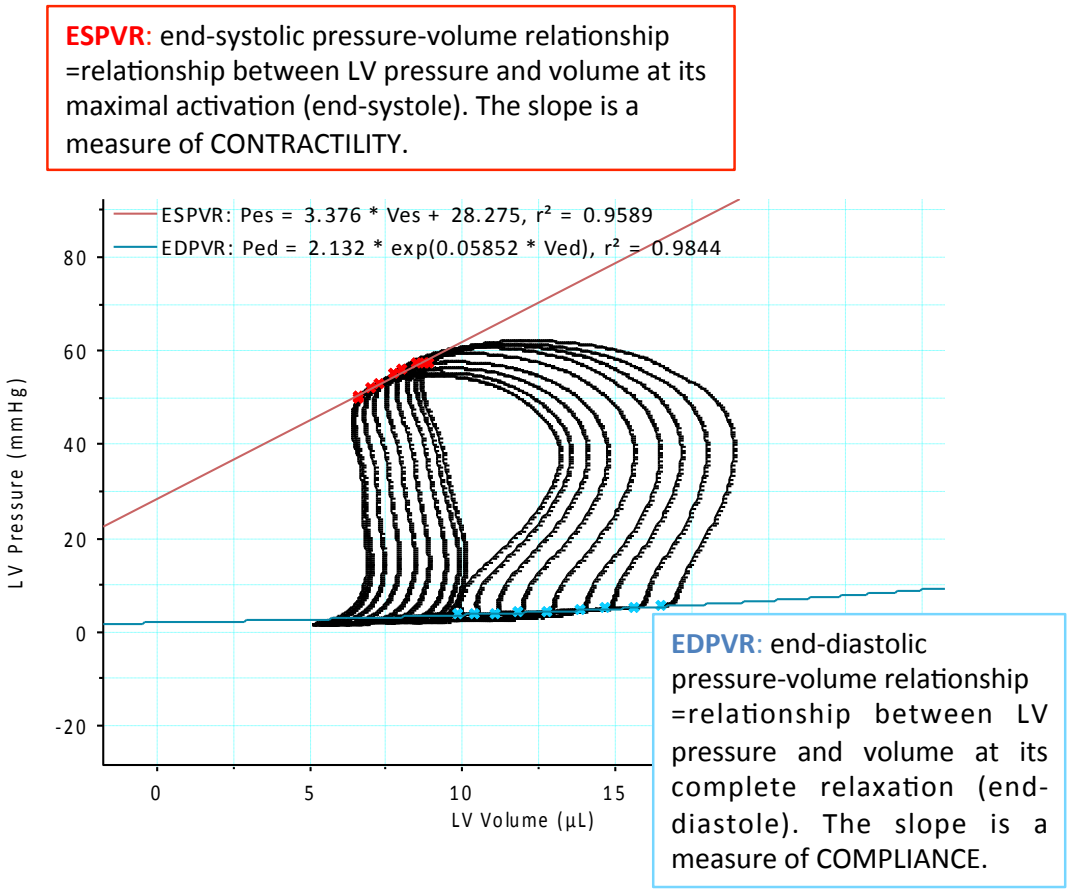

Figure 7: Example of a pressure-volume loop describing the ESPVR and EDPVR.
The venous return is first decreased during vena cava occlusion and then progressively increased which corresponds to increasing the preload, which is demonstrated here by a shift of the loops toward the right side. A group of pressure volume loops linked by a line connecting their intercept is then created at the end-systole point for the end-systolic pressure volume relationship (ESPVR) and at the end-diastole for the the end-diastolic pressure volume relationship (EDPVR). The ESPVR is the relationship between the LV pressure and volume at its maximal activation at the end of the systole. The slope of this relationship corresponds to the dP/dV and represents the elastance, which is used as an index of contractility. The EDPVR is the relationship between the LV pressure and volume at its complete relaxation, the inverse of the slope of this line is used as measure of compliance.

To study the influence of load on cardiac function, additional manipulations can be performed. For instance, occlusion and subsequent opening of the inferior vena cava decreases and increases the venous return, which is translated by decreased and increased preload, respectively. This blood flow occlusion/release method will cause an increase of the stroke volume as the end-diastolic volume increases and consequently the cardiac fibers length (Frank-Starling law). An increase of the afterload can also be visualized on the PV loops. This effect can be due to an increased aortic pressure and will cause a decreased stroke volume since the ventricle is contracting more during the isovolumic contraction to overpass the aortic pressure and trigger the opening of the aortic valves than during the actual ejection contraction. Thus, less blood is ejected and the end-systolic volume increases. Finally, it is possible to increase contractility either intrinsically by using specific experimental stress models, or extrinsically by using pharmacological drugs such as adrenergic agonists. In such cases, the ventricle can develop a greater pressure and tension to eject a larger amount of blood. The stroke volume is increased and the end-systolic volume decreases.

Using this pressure-volume loop technique, many parameters can be measured to evaluate cardiac real-time function. The most commonly used and the most relevant hemodynamic parameters are the end-diastolic and end-systolic pressures and volumes. The end-systolic pressure-volume relationship (ESPVR) is also appreciated to evaluate cardiac elastance as an index of contractility.[37] It corresponds to the relationship between LV pressure and volume at its maximal activation (end-systole). The elastance parameter is obtained by changing the loading conditions.[38] In our experiment we decreased the venous return (preload) via occlusion of the vena cava. A group of PV loops related by a line connecting their intercept is then generated. The slope of this line is expressed as dP/dV and represents the elastance, which is used as index of contractility and describes the strength of the cardiac muscle or ventricle (Figure 7). Similarly, the end-diastolic pressure-volume relationship (EDPVR) is also obtained during the vena cava occlusion, and corresponds to the relationship between LV pressure and volume at its complete relaxation (end-diastole). It is a measure of compliance, which is inversely proportional to the slope of the EDPVR[39] and it describes the diastolic properties of the ventricle, meaning its stiffness (Figure 7).

Other indices of ventricular function can be derived from the PVL technique. The first derivative of the changes in pressure is obtained from the slope of the change in pressure with respect to the change in time. The peak maximal value dP/dt max is a load-independent contractility index,[31] the peak minimal value dP/dt min is used to assess diastolic function.[40] The isovolumic relaxation constant tau also known as time constant is

derived from the time taken by the pressure to fall from the point of dP/dt min to the inverse natural log of that pressure. Tau is a preload-independent measure of diastolic function making it a reliable measurement to assess diastolic dysfunction. This parameter is calculated as follows:

$$P(t) = e^{-t/\tau}$$

P: pressure at a time t; T: relaxation constant Tau

The LV volume during the peak rate of early diastolic filling dV/dt max corresponds to the E-wave visible by Doppler. The volume during the peak rate of ejection is called dV/dt min. These peaks correspond to the steepest tangents to the first part of the early filling curve and the ejection curve respectively (Figure 2). They are expressed in microliters per second.

1.2 Cardiac metabolism

The heart brings nutrients and oxygen supply to the body. Its constant activity makes it a highly energy-demanding organ, which relies mainly on fatty acid (FA) oxidation (FAO). Indeed, under basal conditions and in a healthy heart the maintenance of continuous contraction and relaxation depends for 70% on FAO, whereas 30% of energy is produced through glucose oxidation (GO). In the healthy heart, the glucose transporter GLUT4 (see 1.2.3) and the FA translocase FAT/CD36 (see 1.2.1) are translocated to the cardiomyocyte sarcolemma to increase glucose and FA uptake when cardiac work increases.[41,42] However, glucose metabolism takes over the fatty acid metabolism during a period of stress, such as hypertrophy or infarct event to switch to a more oxygen-efficient energy substrate to meet the increased cardiac work.[43] The vascular system and the heart are closely linked and tightly regulated to maintain a physiological condition. The appearance of disequilibrium is often associated with the onset of a disease. In a fasting state, free fatty acids (FFA) released from adipose tissue (lipolysis) are used for oxidative ATP generation in peripheral tissues and liver where gluconeogenesis will take place to maintain plasma glucose. Inversely, in a fed status ATP will be produced preferentially from GO due to a high and increased availability of glucose; FA synthesis will also be promoted. A high fat diet (HFD) will increase the use of FA for the production of energy. Randle had first depicted this phenomenon in isolated rat heart and diaphragmatic muscle preparations. He described this as a competition between glucose and fatty acid uptake and oxidation.[44] Indeed, glucose and lipids are the main sources of cellular energy, they can compete and interact with each other. Metabolic flexibility is defined as the ability of an organism to adapt its energy use to the energy availability that is to say use preferentially glucose and lipids and to switch rapidly between them when necessary.[45,46] The inability to adapt fuel oxidation to

nutrient availability is often connected to T2DM, ectopic lipid accumulation and mitochondrial dysfunction,[46,47] and is termed metabolic inflexibility.

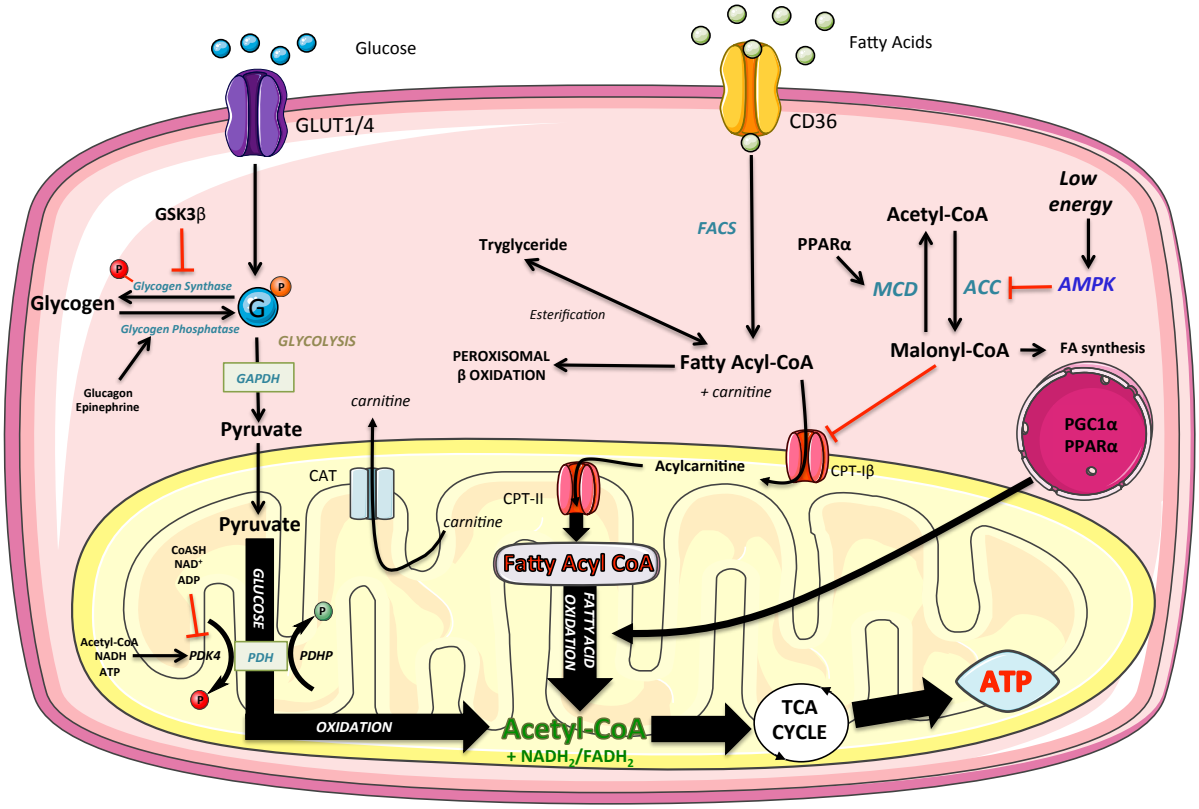

Figure 8: Overview of metabolic pathways in the heart.
Upon insulin stimulation, GLUT4 and CD36 translocate to the sarcolemma to allow glucose and fatty acids to enter the cell. After FA entry into the cytoplasm via the transporter CD36, it is transferred into the mitochondria via a specific transporter CPT-Iβ. Once in the mitochondria it is converted into acetyl-CoA to enter the Krebs cycle. At this stage reducing equivalent $NADH_2$ and $FADH_2$ are released to participate in the production of proton gradient via the electron transport chain. This proton gradient is responsible for the ATP synthesis. PPARα transactivates most of the genes involved in fatty acid utilization. CPT-Iβ can be inhibited in an allosteric way by malonyl CoA. Steady state levels of malonyl CoA are maintained by synthesis via acetyl-CoA carboxylase (ACC) and degradation via malonyl CoA decarboxylase (MCD). ACC is itself inhibited by AMPK protein whereas MCD is activated by PPARα. Glucose metabolism consists of glycolysis and glucose oxidation, which take place in the cytosol and mitochondria, respectively. Glycolysis starts with glucose entry into the cytosol via a glucose transporter (GLUT). Glucose is then phosphorylated into glucose-6-phosphate, finally pyruvate is the last molecule produced during glycolysis. Pyruvate is then transported into the mitochondra where it undergoes oxidative decarboxylation by pyruvate dehydrogenase (PDH) to acetyl-CoA to enter the Krebs cycle. The rest of the cascade is identical to FA oxidation. PDH is the rate-limiting enzyme in glucose oxidation. PDH activity is modulated by its phosphorylation state, which depends on two enzymes: pyruvate dehydrogenase kinase (PDK) inhibits whereas pyruvate dehydrogenase phosphatase (PDHP) enhances it. ACC, acetyl-CoA carboxylase; ATP, adenosine triphosphate; CAT: carnitine acetyl transferase; CPT-I/II, carnitine palmitoyl transferase I/II; FACS, fatty acyl CoA synthetase; $FADH_2$, reduced flavin adenine dinucleotide; G: glucose;GSK3β, glycogen synthase kinase 3β; NADH, nicotinamide adenine dinucleotide; PDH: pyruvate dehydrogenase
(P) inhibitory phosphorylation, (P) activation phosphorylation

The accumulation of these lipids intermediates has been implicated in the development of insulin resistance, cardiac dysfunction and heart failure. CPT-I catalyzes the conversion of long-chain acyl CoA to long-chain acylcarnitine, which is translocated across the inner mitochondrial membrane via the carnitine/acylcarnitine transferase (CT). Once in the matrix, the acylcarnitine is converted back to long-chain acyl CoA by CPT-II, present on the inner mitochondrial membrane. The long-chain acyl CoA produced enters the β-oxidation pathway. Each cycle of β-oxidation involves the production of acetyl-CoA that can enter the TCA cycle. The two dinucletotide flavin adenine dinucleotide ($FADH_2$) and nicotinamide adenine dinucleotide ($NADH_2$) participate in the production of a proton gradient via the electron transport chain that eventually induces ATP synthesis. Figure 8 represents an overview of the main pathways involved in cardiac metabolism.

1.2.1 Fatty acid metabolism: introduction

Fatty acid metabolism is comprised of different steps regrouping FA entering in the cytoplasm, FAO and ATP production in the mitochondria. Free fatty acids derived from albumin and lipoprotein-triacylglycerol (TAG) enter the cytoplasm by passive diffusion or via carriers: the fatty acid translocase FAT/CD36, which takes up 50-60% of the cardiac FA,[48] the plasma membrane isoform of fatty acid binding protein (FABPpm) and fatty acid transport protein (FATP)1/6. In the cytoplasm, FA are converted into long-chain acyl coenzyme A (CoA) esters by the fatty acyl CoA synthetase (FACS), which can serve for synthesis of intracellular lipid intermediates or transfer to carnitine and be taken up into the mitochondria by the carnitine palmitoyltransferase (CPT)-I. Fatty acid can also form complex lipids such as TAG, diacylglycerol, and ceramides.

1.2.2 Fatty acid metabolism: regulation

Fatty acid metabolism is regulated by different players such as insulin, peroxisome-proliferator activated receptor (PPAR), malonyl CoA decarboxylase (MCD), AMP protein activated kinase (AMPK)α, and others. Insulin is a regulator of FA and glucose cellular uptake. Upon insulin binding to its membrane receptor, Akt is activated through PI3K, which in turn will activate the translocation of GLUT4 and CD36 from endosomal compartments towards the cellular membrane.[49]

Peroxisome proliferator-activated receptors are a family of nuclear hormones that function as transcription factors and play a pivotal role in lipid metabolism[50] and inflammatory responses.[51] Three different types exist: α, β/δ, and γ.[52] PPARα is important during prolonged fasting and promotes ketogenesis and FAO, which is associated with increased pyruvate dehydrogenase kinase (PDK) expression. The PPARα agonist WY-14,643 was described as an inducer of both PDK4 mRNA and protein levels in mouse skeletal muscle.[53]

PPARγ is highly expressed in adipose tissue where it regulates adipogenesis and glucose metabolism. The PPARγ agonist rosiglitazone was able to increase the level of PDK4 in adipose tissue but not in the liver or muscle, suggesting a tissue-specific action.[54]

In the heart, PPARα is the most abundant and is present at high levels due to the high energetic demand of the heart, while PPARγ is much less represented.[55] Only little is known about the role of PPARγ in the heart. A specific cardiac deletion of PPARγ in mice caused hypertrophy with preserved cardiac function, and paradoxically using a PPARγ agonist induced the same effect[56] highlighting the complex role of PPARγ in the heart. On the other hand, much more is known about PPARα.[55] PPARα overexpression in mice is responsible for an increased β-oxidation of FA, accumulation of triglycerides and also a decrease in glucose oxidation.[57] Similar results were observed after pharmacologic activation of PPARα.[58] Conversely, PPARα deletion reduced β-oxidation and enhanced glucose oxidation. Mice also presented cardiac fibrosis and an impaired cardiac output while workload was increased.[59,60] PPARα plays a critical role by transactivating most of the genes involved in myocardial fatty acid utilization. Among these, an important regulatory protein is CPT-I, which, as already described under 1.2.1, is involved in lipid uptake into the mitochondria. CPT-Iβ (cardiac isoform) can be inhibited in an allosteric way by the malonyl CoA. Steady level of malonyl CoA is maintained by synthesis via the acetyl-CoA carboxylase (ACC) and by degradation induced by the MCD. ACC is itself inhibited by AMPKα protein whereas the MCD is activated by PPARα. Therefore, malonyl CoA expression is reduced by activation of PPARα or AMPKα, and this will lead to an increased activity of CPT-I.

As already mentioned, in normal conditions the heart uses up to 70% from FAO for its needs. In obesity, when FA supplies increase, the heart switches toward an almost exclusive FA use. This is explained by the fact that insulin resistance, often encountered in diabetes, increases FFA levels since lipolysis in adipocytes is enhanced, which is normally inhibited by insulin.[61] Moreover as insulin is stimulating glucose uptake by inducing GLUT4 transcription and translocation, impaired insulin signaling reduces insulin-stimulated glucose transport.[62]

Another type of FA oxidation is peroxisomal FAO, which is specific for the long-chain FA. Specific enzymes will in this case break down this long-chain FA into shorter ones, which are able to enter the mitochondrion and be processed in the FAO.[63] The excessive activation of the FAO pathway induces the accumulation of lipid metabolic intermediates responsible of cellular damage such as apoptosis, oxidative stress and endoplasmic reticulum (ER) stress. This defense mechanism is known as lipotoxicity and is often associated with cardiac dysfunction. This happens when fat accumulation exceeds the

oxidation rat and induces an ectopic accumulation of lipids in the myocardium, which impairs left ventricle function. This lipid accumulation has been associated with cardiac hypertrophy, dysfunction and apoptosis.[64] In different animal models, the increase in fatty acid uptake is strongly associated with cardiomyopathy.[65,66] However, in human this association between higher FA uptake and cardiomyopathy is not found despite the fact that studies have demonstrated that excess lipid accumulation occurs in obese and insulin-resistance patients.[67,68] Thus obese and T2DM patients affected by heart failure can adapt to the increase circulating lipids and do not exhibit acute myocardial lipotoxicity characteristics.[69] Moreover, humans have been described to be able to reverse lipid accumulation as mechanical unloading corrects metabolic disruption and myocardial lipotoxicity in advanced heart failure and also reverses insulin resistance.[70]

1.2.3 Glucose metabolism: introduction

As mentioned above, in normal conditions glucose counts for 30% of the cardiac energetic supply, but under stress conditions a shift from the fatty acid oxidation towards glucose oxidation is observed to increase ATP production, as glucose oxidation produces more ATP molecules than fatty acid oxidation for the same oxygen use. Glucose metabolism consists of glucose uptake, glycolysis and glucose oxidation,[71] which take place in the cytosol and mitochondrion respectively. Glycolysis is preceded by the glucose uptake into the cytosol via glucose transporters (GLUT). The glucose is then phosphorylated into Glucose-6-phosphate and after different enzymatic reactions pyruvate is generated as final product of glycolysis, with 1 ATP molecule being produced during this process. The pyruvate is then transported into the mitochondrion by a specific transporter named mitochondrial pyruvate carrier (MCP)1 and MCP2,[72,73] where it undergoes oxidative decarboxylation by the pyruvate dehydrogenase (PDH) to Acetyl-CoA to enter the Krebs cycle. The rest of the events in this cascade are similar to those for fatty acid oxidation. The final ATP yield of glucose oxidation is 36 ATP, whereas lipid metabolism is able to produce more ATP depending on the nature of the lipids (for example 106 ATP for palmitate), but glucose oxidation is more effective than FA oxidation as the oxygen needed to produce the same amount of ATP is lower.

Different isoforms of glucose transporters exist. GLUT1 is predominant in the fetal heart while during adulthood more GLUT4 is present.[74] Mice presenting a heterozygous deletion of GLUT4 exhibit a phenotype of human cardiomyopathy, suggesting that decreased glucose utilization is deleterious for the heart.[75] Consistently, increased glucose supply by overexpression of GLUT4 in the db/db obese mouse model has been reported to decrease FA utilization and to be cardioprotective.[75]

1.2.4 Glucose metabolism regulation

Pyruvate dehydrogenase complex

Metabolic flexibility in mammals involves the pyruvate dehydrogenase complex (PDC). PDC is a mitochondrial multi-enzyme complex that catalyzes the oxidative decarboxylation of pyruvate.[76] It ensures the conversion of pyruvate, CoA and NAD^+ into acetyl-CoA, NADH and CO_2.[77] PDC is involved in glucose as well as fatty acid metabolism since the main product of pyruvate decarboxylation, a CoA-activated two-carbon unit, can be condensed with the oxaloacetate during the first reaction of the tricarboxylic acid (TCA) cycle or could be used for fatty acid and cholesterol synthesis.[78] Therefore, PDC links glycolysis with TCA cycle and lipid biosynthesis. PDC is the rate-limiting enzyme complex in glucose oxidation. It consists of 3 enzymes present in multiple copies: pyruvate dehydrogenase (PDH, E1), dihydrolipoamide transacetylase (E2), and dihydrolipoamide dehydrogenase (E3). The E1 enzyme is a tetramer comprised of 2 α and 2 β subunits. The key regulatory subunit of PDH is its E1-α subunit and its activity can be modulated by a family kinase called pyruvate dehydrogenase kinase (PDK). PDKs reversibly phosphorylate PDH at 3 specific serine sites: S232, S293, S300 within the α subunit,[76,79] consequently inactivating its enzymatic activity. On the other hand, PDH activity is increased by pyruvate dehydrogenase phosphatase which dephosphorylates PDH. In the healthy and fed state, PDH is in an activated state but when carbohydrates supply is low, its inhibition is primordial for glucose synthesis.[80] When PDH is inhibited by PDKs, acetyl-CoA levels are decreased and the malonyl-CoA, which inhibits the CPT-Iβ transferase, is reduced.[81] Thus, an upregulation of PDK results indirectly in a facilitated fatty acid oxidation, which is necessary as glucose oxidation is blunted.[82] This mechanism could explain the interaction and competition between these two sources of energy. Additionally, the acetyl-CoA and NADH produced during fatty acid oxidation are able to stimulate PDK activity in skeletal muscle.[83]

Pyruvate dehydrogenase complex kinase

Four isoforms of PDK exist from PDK1 to PDK4, which are expressed in a tissue-specific manner.[84] PDK1 is found in the heart[85] and pancreatic islets.[86] PDK2 is highly expressed in the heart, liver and kidney of humans and rodents,[83] while PDK3 is only found in testis and brain.[84] In the heart, skeletal muscle, lactating mammary gland and liver PDK4 is the most expressed isoform. In starved and insulin-resistant animal models PDK2 and PDK4 are highly expressed in liver, muscle, kidney and heart tissue. Their expression is increased in conditions of reduced insulin levels or impaired insulin signaling. Indeed, in STZ-induced type 1 diabetic rats PDK4 expression was increased in the heart and skeletal muscle.[87,88] Similarly, PDK4 was increased in the skeletal muscle of insulin-resistant human.[89]

An upregulation of PDK decreases PDH activity, which has been observed in metabolic disorders such as diabetes,[90,91] heart disease[92,93] and fatty liver.[94] PDK4 deficiency is responsible for an inhibition of fatty acid oxidation and increased glucose oxidation because of PDH activation. The subsequent increased acetyl-CoA concentration induces increased malonyl CoA levels that will in turn inhibit the rate of fatty acid oxidation.[81] PDKs can be regulated by metabolites and transcription factors such as insulin, glucocorticoids, thyroid hormones and fatty acids depending on the conditions and tissues. PDKs are positively modulated by different stimuli such as high level of acetyl-CoA, NADH, ATP, starvation or nutrient deprivation, whereas pyruvate inhibits its transcription. Indeed, during energy deprivation, the reduced availability of glucose, together with the decreased insulin concentrations, induce a decrease of glucose utilization to conserve it for organs highly dependent on glucose metabolism such as the brain, in favor of the use of long-chain fatty acid oxidation for energy production.[77]

PDKs are regulated by multiple factors at the transcriptional level. Insulin represses its expression via forkhead box O (FOXO) modulation. The human PDK4 gene has three insulin responses sequences (IRSs) that are binding FOXO1 and FOXO3.[95] Overexpression of FOXO1 and FOXO3 increased basal and dexamethasone-induced expression of PDK4 in HepG2 cells, which was abolished by mutation of the IRSs in the PDK4 promoter.[95] In murine muscle and C2C12 cells, FOXO was induced by nutrient deprivation, which mediated upregulation of PDK4 gene expression. [96] In the same cell type, it was described that overexpression of the FA transporter CD36 induced FOXO1 expression and is thus participating in the upregulation of PDK4 expression.[97]

Upregulation of PDK transcription is induced by several nuclear hormone receptors including PPAR, estrogen related receptor (ERR), thyroid hormone receptor, and glucocorticoid receptor, which are activated by starvation or increased fatty acid levels. PDKs are also modulated by other factors such as growth hormone (GH), but its effect on PDKs remains controversial. Some studies showed that GH is able to increase PDH activity in rat myocardium,[98] whereas recent studies demonstrated the inverse effect, namely that GH increased PDK4.[99,100] In the liver of fasting mice, GH has opposite effects to that of insulin since it activates PDK4 expression by stimulating JNK signaling, leading to activation of the STAT5 pathway to increase gluconeogenesis. A clinical study showed that GH was able to promote lipolysis and reduce insulin sensitivity by upregulation of PDK4 mRNA leading to a decrease in PDH activity similar to the effect observed during fasting.[101] Along similar lines, the antidiabetic Metformin inhibits the PDK4 activation by GH via the inhibition of the binding of STAT5 to the PDK4 promoter.[100] Finally, adiponectin and AMPKα

are two others factors involved in PDK regulation. In skeletal muscle, it is known that adiponectin can activate AMPKα and this leads to fatty acid oxidation.[102]

Free fatty acids and derivatives as endogenous PPAR ligands have been implicated in the increased PDK expression observed in fasting states and diabetes. Indeed, long-chain FAs such as palmitate and oleate directly induce PDK4 in skeletal muscle and hepatoma cells.[53,97,103] Additionally, indirectly increased supplies of FAs for example by increased cardiac lipoprotein lipase or hepatic lipase have been shown to increase PDK4 mRNA expression via interaction with PPARα and PPARβ/δ.[104,105]

In healthy individuals, upon insulin stimulation, the skeletal muscle, which is the major site for glucose and fatty acids oxidation, is able to switch from lipid to glucose oxidation and suppresses lipid catabolism in favor of increased glucose uptake, oxidation and storage.[106] However, insulin-resistant obese and T2DM patients had greater rates of lipid oxidation in skeletal muscle than lean individuals during insulin infusion, suggesting that they had metabolic inflexibility.[106] Furthermore, methylation of the PDK4 promoter at specific cytosine sites was reduced in T2DM patients, suggesting that epigenetic modification of mitochondrial genes regulate substrate switching.[107] In the liver, inactivation of PDH by PDKs can downregulate the conversion of pyruvate to acetyl-CoA ending in a shift of pyruvate from TCA cycle toward gluconeogenesis.[108] PDK4 can interact with FAT/CD36, PPARβ/δ and FOXO1.[97] Under fasting conditions, CD36 facilitates fatty acid flux, which activates PPARβ/δ that in turn will activate FOXO and PDK4 transcription to inhibit glucose oxidation. Together with the increase in fatty acid flux, the decreased insulin concentration is responsible of a downregulation of Akt, which induces activation of FOXO1.[109] In skeletal muscle, FOXO1 recruits CD36 to the plasma membrane and activates lipoprotein lipase (hydrolyzes plasmatic triglycerides and lipoproteins) enhancing fatty acid utilization.[97]

In T2DM patients, PDK2 and PDK4 mRNA were found increased in skeletal muscle after overnight fasting, which is coherent with the insulin resistance and metabolic inflexibility of these patients.[107] Moreover, 4h of lipid infusion in humans decreases insulin-stimulated glucose uptake and PI3K in muscle.[110] Similarly, Tsintzas et al. observed in healthy men that lipid infusion during a hyperinsulinemic-euglycemic clamp experiment attenuated the suppression of PDK4 expression induced by insulin, and that this effect was independent of Akt mediated pathway stimulation. This indicates that in healthy conditions the lipid accumulation plays a more important role than insulin stimulation in the regulation of skeletal muscle PDK4 expression.[111] On the contrary, the suppression of PDK4 expression by insulin was independent of insulin's effect on plasma FA levels, indicating that the observed

increased PDK4 expression in starvation and diabetes could be due to insulin deficiency rather than increased levels of FA.[112]

In conclusion, targeting PDK to inhibit its activity would be a promising therapeutic solution for patients suffering from metabolic disease. Indeed, inhibiting PDK would lead to an enhanced PDH activity and would help to restore a normal insulin activity and lower the blood glucose concentration.

1.2.5 From obesity to Type 2 diabetes: mechanisms

Obesity (body mass index >30 kg/m^2) may be associated with several disorders: type 2 diabetes mellitus, hypertension, hypercholesterolemia, hypertriglyceridemia, and non-alcoholic fatty liver disease. Obesity increases the risk of insulin resistance, type 2 diabetes, cancer, dyspnea and other chronic diseases and most weighty cardiovascular diseases.[113,114] During the last decades this disease has become a worldwide health problem and the prevalence numbers are alarming. In 2014, 39% of adults aged 18 years and over were overweight (1.9 billion) and 13% were obese (World Health Organization, WHO, June 2016).

The excess of calories ingested lead to an increase in body weight together with adipose tissue mass. This adiposity and adipocyte malfunction lead to dysregulation of adipose tissue-derived secretory factors called adipokines (e.g. leptin) that can participate in the development of metabolic disease because of their role in glucose and lipid homeostasis and inflammatory responses.[115,116] Among the adipokines secreted by the endocrine adipose tissue are chemokines, cytokines and hormones. In obesity, adipocytes increase the secretion of pro-inflammatory chemokines and cytokines,[117,118] including monocyte chemotactic protein (MCP)-1, tumor necrosis factor α (TNFα), IL (interleukin)-1, IL-6 and IL-8 that promote insulin resistance.[119-121] Macrophages are actually responsible for the release of pro-inflammatory cytokines such as TNFα, and macrophage content correlates positively with adipocyte size and body mass.[122]

It has been described that insulin signaling is blunted in adipose tissue, skeletal muscle and liver in obesity-induced T2DM.[123] One of the consequences is that glucose transport is reduced in these tissues. A major role of insulin in adipose tissue is to inhibit lipolysis. Because of its resistance to insulin and accumulation of fat, the adipose tissue will release free fatty acids, which may participate in the modulation of insulin sensitivity.[124,125] The adipokine adiponectin, known to increase insulin sensitivity, is reduced with increased adiposity. The cause of insulin resistance in skeletal muscle and liver are multiple, and

lipotoxicity is one of them. This is due to an increase in lipid deposits that enhances triglyceride and toxic lipid intermediates such as ceramide and diacylglycerol (DAG).[126]

The increased activation of nutrient-sensing pathways such as the hexosamine synthetic pathway impairs directly the insulin pathway.[127] Free fatty acids can act as ligands for the toll-like receptor (TLR) 4 complex[128] and stimulate macrophages to secrete cytokines.[129] The toll-like receptor and c-Jun N-terminal kinase (JNK) are also known to influence insulin function as they mediate increased inflammation, which impairs the insulin pathway.[130] Moreover, mitochondrial dysfunction has been described in insulin resistant states, without knowing if this phenomenon is directly affecting insulin sensitivity or if it is the consequence of insulin resistance.[131] In the diabetic heart, an impairment in insulin-stimulated glucose utilization was described, however preclinical and clinical studies showed that insulin signaling was maintained, suggesting that some pathway might be upregulated in response to hyperinsulinemia underlying systemic insulin resistance.[132,133]

Peterson et al. described the effect of obesity on cardiac metabolism in women. They noted that myocardial fatty acid uptake, utilization and oxidation as well as myocardial oxygen consumption were increased in proportion to body mass index and glucose intolerance.[134] This suggests that cardiac metabolism is enhanced together with the grade of obesity and glucose intolerance, consistent with the Randle principle.

1.2.6 Obesity and Type 2 diabetes: players

Obesity causes an increase in circulating FA levels, which leads to PPARα activation and in turn increases FAO.[135] As described under 1.2.2, PPARα is regulating genes implicated in fatty acid uptake (FAT, CD36, FATP, and FABP), in the generation of fatty acyl CoA (FACS), as well as mitochondrial fatty acid uptake (CPT-I/II). PPARα also activates the acyl CoA oxidase (ACO), which participates in peroxisomal FAO and enzymes involved in mitochondrial β-oxidation. It has been proposed that the increased FA utilization induced by PPARα is not an early event in obesity since obese mice showed increased fatty acid oxidation already before any changes in PPARα regulated target genes occurred.[136] Additionally, Wright et al. demonstrated that FAO was increased after 2 wks of high fat feeding, and this was not associated with changes in PPARα target genes and was also independent of an increase in circulating FA or triglycerides. In the same study, they described that insulin-stimulated glucose uptake and GLUT4 translocation in the myocardium were impaired and this was accompanied by hyperinsulinemia, while interestingly the Akt pathway upon insulin stimulation was not altered.[133] PPARα target genes were only activated after 5 wks, thus PPARα activation may have a role to sustain this metabolic change but not at early stages

of the pathology, where a defect in glucose transport seems to be happening as a first answer to cardiac metabolic adaptation to high fat diet. Abel proposed that this adaptation where glucose utilization is reduced is the leading cause for a secondary increase in fatty acid oxidation as the Randle cycle describes it.[108] During minor ischemia, FFA are the main source of fuel and glycolysis is still active while glucose is used for lactate production for anaerobic ATP production.[137] Therefore, it would be interesting to use a PDK4 inhibitor such as dichloroacetate to increase ATP production and Ca^{2+} uptake, or an inhibitor of FA oxidation, and also enhance glucose, insulin and potassium levels to increase cardiac efficiency during ischemia.[137]

The increased fatty acid transporter (CD36) translocation to the membrane following Akt activation by the insulin pathway is also participating in the increased use of FA in a diabetic heart as described in a db/db mouse model and in fa/fa Zucker rats, as well as in rats fed with high fat diet.[138-140] Paradoxically, insulin also acutely inhibits FAO, and this phenomenon could be explained by the fact that most of the FAO is using an endogenous pool of triacylglycerol[141] and that in normal conditions, insulin might stimulate the refilling of this pool by increasing the CD36 translocation. As cardiac Akt signaling is intact in obesity, Abel proposed that this effect could participate in the increased cardiac lipotoxicity when hyperinsulinemia is established.[74]

Fatty acid oxidation produces more mitochondrial ROS than pyruvate oxidation. Anderson et al. showed that an attenuation of mitochondrial ROS production completely preserves insulin sensitivity despite high fat feeding in both humans and rodents.[142] They also demonstrated that in mice, overexpression of a mitochondrial catalase reduced ROS production and similarly these mice were protected against insulin resistance after high fat feeding. In vitro studies demonstrated that acetylation of cardiac mitochondria increases ROS production and inhibits pyruvate oxidation, proposing that the acetylation of mitochondrial proteins is implicated in metabolic inflexibility.[143]

1.2.7 Akt and metabolism

Akt, also known as protein kinase B (PKB), is a serine/threonine kinase involved in various cellular mechanisms including protein synthesis, growth, proliferation, survival, metabolism and others.[144] Figure 9 describes the signaling between insulin/Akt and the mammalian target of rapamycin (mTOR) and some of their roles. Akt signaling can be activated by receptor tyrosine kinases, integrins, B and T cell receptors, cytokine receptors, G-protein-coupled receptors and other factors. Insulin pathway activation results in the production of membrane lipid phosphatidylinositol (3,4,5) triphosphates (PIP_3) by the activated

phosphoinositide 3-kinase (PI3K), which allow proteins with PH domains, such as Akt and its upstream activator PDK1, to be recruited at the membrane. PDK1 phosphorylates Akt at T308 its main activity site, whereas mTORC2 phosphorylates Akt at S473 resulting in its maximal activation.[145] Akt can be dephosphorylated by protein phosphatases 2A (PP2A) and the PH-domain leucine rich repeat containing protein phosphatases (PHLPP1/2). Akt signaling can also be inhibited by the tumor suppressor phosphatase and tensin homolog PTEN, which dephosphorylates PIP3.

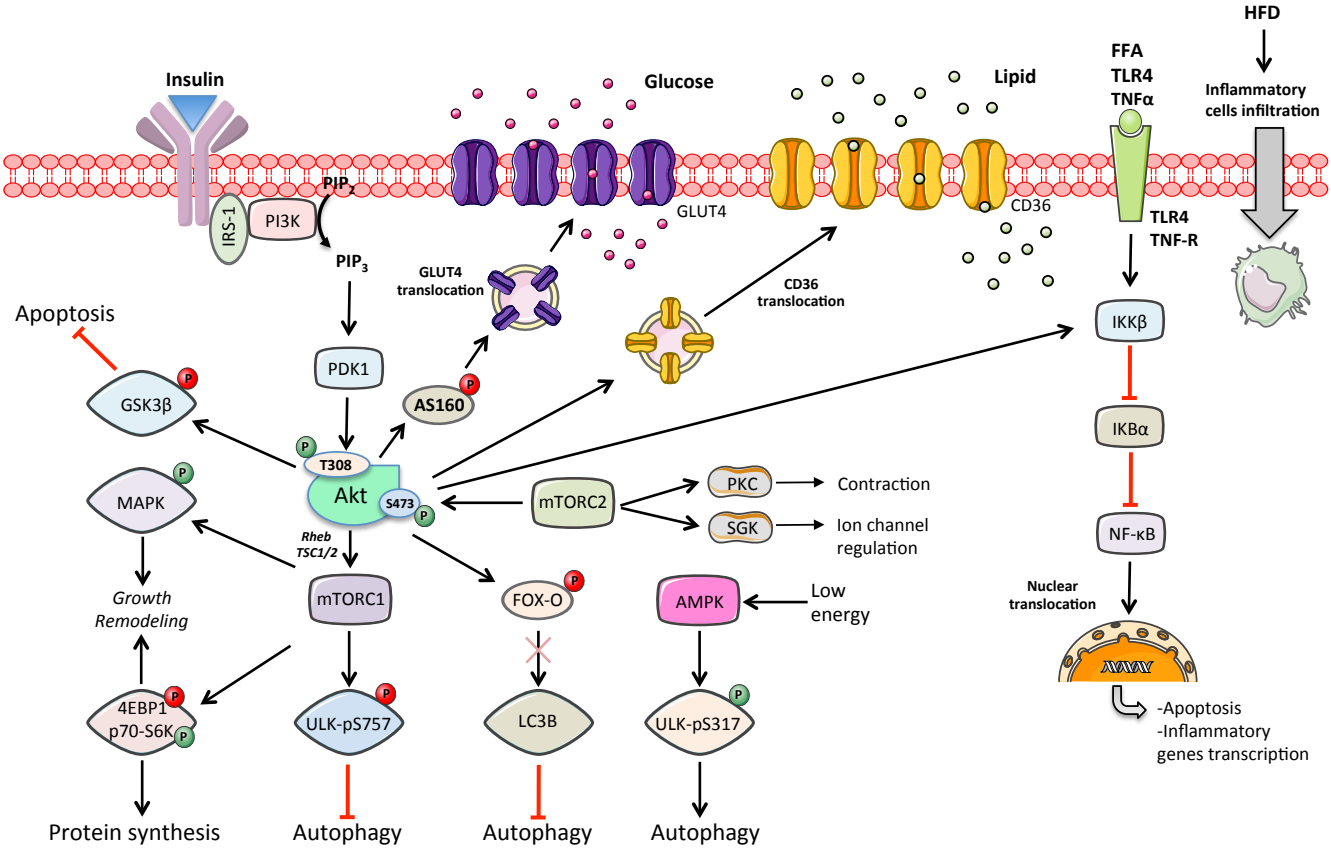

Figure 9: Insulin/Akt/mTOR signaling.
Insulin is the main anabolic hormone in mammals and plays an essential role in metabolic homeostasis. Upon insulin binding to its cell membrane receptor, the insulin receptor substrate-1 (IRS-1) is phosphorylated, which leads to the activation of the phosphatidylinositol 3-kinase (PI3K) and Akt. Activation of the Akt pathway promotes different cellular mechanisms including translocation of the glucose transporter GLUT4 to the cell membrane, activation of mTOR and mitogen-activated protein kinase pathways. Akt also inhibits autophagy via FOXO, and inflammation by activating IKKβ. (P) inhibitory phosphorylation, (P) activation phosphorylation

Upon normal insulin stimulation, Akt gets activated which in turn affects many substrates. Akt increases mTORC1 activation, it induces GLUT4 and CD36 translocation to the membrane, and it inhibits FOXO and GSK3β to downregulate autophagy and apoptosis. Akt controls cell growth through its regulation of mTORC1 signaling, it inhibits by phosphorylation the GTPase activity of tuberous sclerosis complex (TSC) allowing accumulation of GTP-bound Rheb the principal activator of mTORC1 kinase. Akt is involved

in glucose metabolism via its phosphorylation of 160 kDa substrate of the Akt Ser/Thr kinase, known as AS160 or TBC1D4, at many sites. AS160 is a Rab-GTPase that regulates GLUT4 trafficking, its phosphorylation site Thr642 is necessary for GLUT4 translocation to the membrane to allow glucose uptake. Under normal conditions, the Rab-GTPase activating domain of AS160 catalyzes the hydrolysis of Rab-GTP to Rab-GDP, which is bound to the GLUT4 vesicles in the cytoplasm and inhibits its exocytosis. Upon insulin stimulation, AS160 is phosphorylated and Rab-GDP becomes less abundant and releases its inhibition to promote GLUT4 translocation. On the other hand, AMPKα can also phosphorylate AS160 to induce contraction-stimulated translocation of transporter GLUT4. Additionally, Akt is a major mediator of cell survival by its direct inhibition of pro-apoptotic proteins such as Bad or the inhibition of pro-apoptotic signal produced by transcription factor such as FOXO. Akt also inhibits the glycogen synthase kinase (GSK) and AMPK, which result in cardiac glycogen synthesis and accumulation.[146]

1.2.8 mTOR and metabolism

mTOR is a serine/threonine kinase that is responsible for protein synthesis and inhibition of autophagy. mTOR is sensitive to growth factors, nutrient signals, energy levels and stress[147] and is activated under nutrient rich conditions where it will increase cell growth. mTOR forms together with several other proteins 2 different complexes called mTORC1 and mTORC2.[148] mTORC1 is composed of mTOR, RAPTOR, PRAS40, DEPTOR and MLST8. mTORC2 regulates cytoskeleton organization, contraction, ion channels and autophagy through Akt. It is composed of RICTOR, SIN1, PRR5, DEPTOR, and MLST8. Figure 9 shows part of the mTOR signaling cascade induced by insulin. Following Akt activation by PDK1 and mTORC2, Akt activates mTORC1 via inhibition of the TSC1/2 complex, which releases its inhibition on Rheb. GTP bound Rheb then accumulates and eventually activates mTORC1. The two principal downstream targets of mTORC1 are p70 ribosome S6 kinase (p70-S6K) and eukaryotic initiation factor 4E-binding protein 1 (4EBP1) that trigger protein synthesis. mTORC1 also inhibits autophagy via the inhibitory phosphorylation of ULK1. The activation of mTORC1 causes an inhibitory phosphorylation of IRS-1 via p70-S6K1 by a negative feedback loop mechanism, which provokes proteasomal degradation of IRS-1 and leads to insulin-stimulated signaling impairment.[149] It was reported that p70-S6K1 deletion improves insulin sensitivity in mice,[150] and therefore chronic activation of mTORC1 could be related to insulin resistance onset. Additionally, mTORC1 also activates Grb10 protein, which similar to p70-S6K1 negatively regulates the insulin/IGF1 receptor signaling via its inhibition of IRS-1 phosphorylation and the subsequent recruitment of PI3K. [151,152] mTORC2 can be activated by PI3K to regulate actin cytoskeleton organization and cell survival via

protein kinase C (PKC) and Akt activation. Additionally, mTORC2 can activate Rho-GTPases to control cell-cell contacts.

Given its key function in modulating protein turnover and energy metabolism, it is not surprising that many studies suggested a primordial role of mTOR in cardiac function. Zhu et al. recently showed that cardiomyocyte-specific deletion of mTOR is responsible for more than 90% of embryonic lethality.[153] Moreover, Shende et al. found that cardiac-specific deletion of the gene encoding for RAPTOR in adult mice induces severe heart failure accompanied by high mortality 6 wks after the deletion.[154] They showed that the mice developed cardiac dilation and dysfunction accompanied with apoptosis, autophagy and mitochondrial dysfunction. In these mice, a switch from FAO to GO was also observed. Using the same model, the research group also showed that transaortic banding inducing cardiac pressure overload does not lead to adaptive hypertrophy but achieves to the development of heart failure.[154] mTOR is an important player in metabolism regulation in particular mitochondrial metabolism partially via the regulation of PPARγ coactivator (PGC)-1α expression and activation in skeletal muscle and C2C12 cells.[155] In a mouse model, mTOR was described to be involved in cardiac metabolism as cardiac mTOR disruption induced during adulthood decreases FAO and increases GO.[156] This was in line with the decrease expression of FA metabolism genes such as FABP3, medium-chain acyl-CoA dehydrogenase, hydroxyacyl-CoA dehydrogenase/3-ketoacyl-CoA thiolase/enoyl-CoA hydratase (trifunctional protein)-α and β as well as the decrease enzymatic activity of CPT-I/II. These changes were not associated with reduced FAO gene regulator PGC1α.[156] In contrast, cardiac-specific deletion of RAPTOR downregulated ERRα, PGC1α and PPARα. Similarly, glucose use was increased while FAO was decreased together with a reduced CPT-1β and MCD-1 expression levels.[154] These changes were observed when cardiac function was not altered yet. mTOR regulates metabolism but it is also regulated by metabolic dysfunction. mTORC1 is activated during nutritional excess, obesity and metabolic syndrome in liver, skeletal muscle, and adipose tissue.[157-161] The Akt/mTOR pathway activation is increased in the vasculature in HFD-induced obesity and provokes endothelial senescence and increase peripheral ischemia risk. These effects were rescued by rapamycin treatment, proving that mTOR is specifically involved in these effects.[162]

1.3 Metabolic cardiovascular disease and heart failure

Cardiovascular diseases are the leading cause of worldwide death. In Europe, 46% of all deaths (4.1 million in 2013) were attributed to CVD,[163] which affected more women (51%) than men (42%).[163] In Switzerland, in 2010, 181.2 and 80.4 men out of 100 000 died from CVD and coronary heart diseases (CHD), respectively. For women, these rates were lower:

115.9 for CVD and 38.4 for CHD.[164] Men are at higher risk to develop obesity, cardiovascular disease and hypertension than women. However, this tendency inverses in the postmenopausal population meaning that women lose their advantage while ovarian hormone levels decrease.[165,166] The risk factors are multiple and the mechanisms are not fully understood. Among them obesity, diabetes, and hypertension as the most common and important.

Metabolic disorders such as diabetes, insulin resistance and obesity are tightly linked to CVD occurrence. Metabolic syndrome is the most studied disease since it affects a large population. Numerous studies have demonstrated that metabolic syndrome is associated with left ventricle remodeling and dysfunction. The hallmarks of metabolic disease are obesity, insulin resistance, glucose resistance and dyslipidemia. The incidence of obesity and diabetes has increased considerably over the past decades due to a sedentary lifestyle and the excess of ingested calories. The major cause of morbidity and mortality in obese and diabetic patients are cardiovascular events, heart failure is particularly increased even after correction for risk factors such as hypertension or ischemic heart disease.[167] Rubler was the first to describe an association between diabetes and increase heart failure risk without signs of hypertension, myocardial ischemia or valvular heart disease.[168] He named this condition “diabetic cardiomyopathy” and it was defined as a ventricular dysfunction without hypertension or coronary heart disease. Thus, diabetic cardiomyopathy is associated with systemic metabolic disorders such as obesity and sustained diabetes, and is characterized by structural and functional alterations and interstitial fibrosis independently of hypertension or coronary artery disease.[169,170] Heart failure is defined as an insufficient cardiac performance to maintain a blood flow to perfuse all the organs. It is characterized by dyspnea, fatigue and fluid retention. Heart failure can be categorized into two different groups: heart failure with reduced ejection fraction (HFrEF) where both cardiac systolic and diastolic functions are altered and in contrast heart failure with preserved ejection fraction (HFpEF) where only the diastolic function is altered, both are equally distributed.[171] The HFpEF affects a large population and the risk factors include hypertension,[172] older age and female sex,[173,174] which are the most important, and also obesity[175] and diabetes.[176] This pathology involves diastolic dysfunction, characterized by an impaired LV relaxation, decreased LV compliance, longitudinal LV systolic dysfunction, abnormal ventriculo-arterial coupling, and pulmonary hypertension (associated with RV remodeling and dysfunction). Some studies show that both diastolic and systolic function are altered in obese patients with absence of clinical heart disease.[177]

1.3.1 Cardiac changes in obesity and diabetes

Different research groups described that high fat diet-induced metabolic syndrome provokes structural and functional cardiac alterations, since fractional shortening was found decreased, while ventricular wall thickness, left ventricular end-diastolic and systolic pressures were increased.[113,114,178] Cardiomyocyte contractility has also been shown to be impaired as the peak shortening and maximal contraction velocity were decreased, whereas relenghtening time was increased. All these modifications were accompanied by interstitial fibrosis.[113,114]

Diabetic and obese hearts show increases in fatty acid uptake and oxidation, intramyocardial triacylglycerol, while glucose uptake and oxidation as well as malonyl-CoA are decreased due to the activation of malonyl-CoA decarboxylase (MCD).[179] This leads to a decreased cardiac efficiency that could be linked to the low oxygen-efficiency of FAO and increased mitochondrial uncoupling as a consequence of increased FA use. Eventually, this results in a reduction of ATP production despite energy substrate oxidation.[180,181] Therefore, the delivery of reducing equivalents produced from FAO is increased while the oxidative phosphorylation ability of the respiratory chain is decreased leading to higher ROS production. Mitochondrial uncoupling in the long term contributes to the energy deficit as the ratio PCr/ATP is reduced in diabetic hearts.[182] In obese mice, mitochondrial respiration with palmitate as a substrate is preserved, while PDH activity is decreased together with the oxidation of pyruvate in a similar manner as what has been described in diabetes.[183] It was observed that gene expression of the sarcoplasmic reticulum calcium-ATPase 2 (SERCA2), the protein responsible for calcium (Ca^{2+}) reuptake permitting cardiac relaxation, is decreased in the diabetic heart[184,185,186] and this change might be implicated in diastolic dysfunction in diabetic cardiomyopathy.

At a more advanced stage of diabetes, cardiac dysfunction is related to several changes: altered metabolism, reduced contractility, modified calcium handling, dysfunctional mitochondria, ER stress, lipo- and glucotoxicity, necrosis, apoptosis, autophagy, and fibrosis.[179,187-189] At the origin of these changes, cellular mechanisms are thought to be involved such as protein kinases, calcium, ROS and ceramide production, hexosamines and advanced glycation end-products (AGEs).[190]

1.3.2 Cardiac stress markers

Under stress conditions, the adult heart starts to re-express fetal genes that are used to evaluate stress and hypertrophy. For example, sarcomeric proteins such as myosin, actin and titin are changing to their fetal isoform and can be used as markers of stress and hypertrophy. Myosin filaments are formed by α and β subunits. Three different isoforms of

myosin exist in rodents: α-myosin heavy chain (α-MHC), which detains the highest ATPase activity and contractile velocity; the α/β-MHC and the β-MHC form which has the lowest contractile ability.[191] During fetal development of rodents, the β isoform is replaced by the α isoform, which becomes the dominant form at the adult stage.[192] Therefore, a decrease in the α/β ratio is linked to cardiac hypertrophy in rodents.[193] Inversely, in the human adult the β isoform is predominant. Skeletal α-actin is highly expressed in the fetal heart whereas the adult heart expresses cardiac α-actin, which makes the fetal skeletal α-actin a marker used for cardiac dysfunction characterization. Finally, the protein titin also undergoes a switch from the long form N2BA isoform expressed in the embryonic heart towards a higher expression of the shorter N2B isoform in perinatal and adult hearts.[194] Thus an increase of the N2BA isoform is used as cardiac stress marker.

Peptides hormones are also commonly used in detecting cardiac stress. The atrial and brain natriuretic peptides, ANP and BNP respectively, are released by the atria in response to cardiac wall strain.[195] ANP expression is activated by the fetal cardiac transcription factors GATA4 and NKX2-5. Their main effects on the heart are indirect through regulation of natriuresis and reduction of blood pressure. It also has been shown that both inhibit cardiac hypertrophy, fibrosis and activate lipolysis.[196-198] As mentioned above, some transcription factors control the formation of the fetal heart, with the fetal transcription factor GATA4 being one of these. GATA4 is essential for valvular development and activates cardiac genes such as ANP and α-MHC, and is able to induce an increase in β-MHC after pathological hypertrophy. Expression of NKX2-5 protein is exclusively present in the heart, its activation in adult heart is also considered as fetal gene reactivation and has been associated with congestive heart failure.[198]

1.3.3 Inflammation and fibrosis

Hyperglycemia and fatty acids induce metabolic disorder entailing by a low-grade chronic inflammation in metabolically active tissues such as liver, adipocytes and skeletal muscle.[199] Patients suffering from insulin resistance and T2DM have elevated pro-inflammatory cytokines such as IL-6, TNFα and C-reactive protein (CRP).[200] Inflammation affects insulin signaling and sensitivity. The nuclear factor-kB (NF-κB) is a major regulator of the inflammation process, in the heart it induces the expression of pro-inflammatory cytokines such as TNFα, IL-6, IL-1β and IL-18.[169] Moreover, NF-κB was activated after FA or high glucose exposure in cardiomyocytes.[201,202] NF-κB is a dimeric complex comprised of p65 and p50 subunits, bound to the inhibitor protein IκB, NF-κB is sequestrated in the cytoplasm and is inactive. Upon stimulation by cytokines (TNFα, IL-1β) or TLR activation (by LPS), IκBα undergoes a phosphorylation-dependent degradation mediated by the IκBα

kinase complex (IKK), IKK-α, -β, and -γ. The loss of IκBα exposes the nuclear localization motif on the p65 NF-κB subunit allowing its phosphorylation and nuclear translocation where it mediates gene transcription of targets such as IFNγ, IL-6 or TNFα leading to inflammatory responses, cell growth and cell survival. In the heart, NF-κB has also been described as a player in hypertrophic responses in cardiomyocytes[203,204] and in vivo[205] and involves mTOR.[206]

In a mouse model fed with HFD, cardiac hypertrophy, inflammation (upregulation of IL-6, TNFα, MCP-1, and NF-κB p65 mRNA levels), ROS production and AGE accumulation were observed.[207] Additionally, TNFα, IL-6 and FFAs can activate kinases, which phosphorylate IRS-1 with, as a consequence, the inhibition of insulin signaling and insulin resistance.[208] Moreover, free fatty acids are able to activate the TLR4 signaling pathway leading to NF-κB and JNK activation[209] in adipocytes and macrophages.

Cardiac low-grade inflammation is secondary to systemic pro-inflammatory status induced by inflammation in adipocytes and macrophages from adipose tissue and liver.[169,210-212] The cardiac defects observed in obesity-related HFpEF may be induced by alterations of homeostatic, neurohumoral and pro-inflammatory immune responses.[213,214] Diabetes and obesity trigger the secretion of adipokines, which play a role in insulin sensitivity. Palnivel et al. reported that in cardiomyocytes, adiponectin acutely stimulates glucose uptake and oxidation, whereas at long term it increases FA uptake and oxidation and decreases glucose oxidation.[215] Leptin's effect was different since glucose uptake and oxidation as well as insulin signaling were not altered, while fatty acid uptake was increased. However, at short term leptin decreased FAO and resulted in an accumulation of lipids.[216] They also showed that conditioned medium derived from adipocytes of wild type rats increases glucose and FA uptake and oxidation in cardiomyocytes, whereas medium from adipocytes of streptozotocine (STZ)-induced diabetic rats stimulates non-oxidative glucose metabolism and abolishes FA oxidation. These differences were observed along with a different level of adiponectin and leptin secretion from the adipocytes.[217] Together, these results support the theory that adipokines have deleterious effects on the heart.

Estrogen is implicated in inflammatory responses and might decrease the expression of CRP following vascular injury in human endothelial cells via activation of the ERα and upregulation of eNOS.[218] Estrogen also prevents upregulation of intracellular cell adhesion molecule-1 (ICAM-1) induced by angiotensin II.[219] Estrogen receptors (ERs) cross-talk with several intracellular inflammatory signaling pathways by activating TLRs and interleukins.[220] It has been reported that estrogen inhibits NF-κB signaling via ERα and ERβ.[221] Therefore,

estrogen could be a good candidate to modulate inflammatory responses. However, its effects depend on different factors such as the amount, composition, type of stimulus, type of cells and the presence of its receptor.[221,222]

1.3.4 Regulators of cardiac contractility

Calcium is a key player of the excitation-contraction coupling in muscle. Upon stimulatory depolarization, Ca^{2+} enters the cell and promotes the release of more Ca^{2+} from the sarcoplasmic reticulum (SR). A mechanism specific to the heart exists, it is called calcium induced calcium release, whereby the initial entry of calcium via the L-type Ca^{2+} channel induces a further calcium release from the SR.[223,224] The intracellular Ca^{2+} concentration is then 10-fold higher and binds to troponin C which allows the change in conformation of tropomyosin, that rotates and exposes the myosin-actin binding site.[223] Thereby, actin and myosin can bind and interact to trigger cross-bridge cycling where the hydrolysis of ATP induces movements of the myosin along the actin filament through a series of conformational changes.[225]

SERCA is an important regulator of cardiac function, it is a pump that belongs to the P-type ATPase family and is able to transport two Ca^{2+} ions into the SR in exchange of proton.[226,227] Ten different SERCA isoforms exist, SERCA2a is the form expressed in the heart. The various SERCA isoforms are encoded by one of the three SERCA genes: ATP2A1, ATP2A2 and ATP2A3. In human, the ATP2A gene encodes for SERCA2a-c isoforms.[228] Its role is to reuptake Ca^{2+} after contraction to allow cardiac relaxation and therefore it is a critical protein for determining relaxation time and inotropy of contraction.[229] Actually, SERCA is the main responsible protein for calcium uptake following contraction, but other molecules are also involved: the sarcolemmal calcium ATPase, the mitochondrial calcium uniport, and the Na^{+}/Ca^{2+} exchanger.[230] In the mammalian heart, SERCA2a is the primary protein that transport Ca^{2+} to the SR.[230] The percentage of calcium removal done by SERCA2a vary between species: 92%, 75% and 70% removal, in the rat, rabbit and human heart respectively.

SERCA2a is regulated by different mechanisms: transcriptional, protein, hormonal, and post-translational modification. ATP2A2 is regulated by mitochondrial transcription factor A (TFAM) and B2 (TFB2M).[231] Overexpression of these factors in a rat model of myocardial infarction increased SERCA2a transcription and prevented the decrease of SERCA2a mRNA.[231] Inversely, in the diabetic heart and in a heart failure model, TFAM and TFB2M were found reduced. Another important transcription factor important for SERCA transcription is specificity protein 1 (SP1), which can mediate an increase[232,233] but also a

decrease of SERCA transcription in a pressure overload model.[234] The myocyte enhancing factor-2 (MEF2) upregulates SERCA transcription in hypertrophy.[235,236] Diabetic patients with heart failure display decreased MEF2C and SERCA2a protein levels compared to heart failure patients without diabetes.[237]

An alteration of SERCA2a function due to reduced mRNA, protein expression or activity is associated with defects in calcium handling with a decreased calcium uptake into the SR and inefficient energy use.[228,238-240] These features are found in patients with heart failure and lead to systolic and diastolic dysfunction.[228,240,241] Up to a 60% decrease of SERCA2a mRNA has been observed in heart failure patients.[242] In the RV of failing hearts, SERCA2a activity was also found to be affected, since a 50% decrease in calcium reuptake was noticed.[238] In the same manner, diabetic hearts also exhibit decreased SERCA2a expression and activity. In a diabetic mouse model, SERCA2a protein expression and maximal activity were decreased by 21% and 32% respectively, conjointly with diastolic function impairment.[243] In another study, SERCA2a protein and activity were also decreased, but in contrast the PLN/SERCA2a ratio was increased in diabetic hearts.[244] The reason for decreased SERCA2a in diabetic hearts is not clear, but it is thought that decreased activity of silent information regulation (SIRT)1 might be involved as the activation of SIRT1 increased SERCA2 to normal values and improved cardiac functional parameters.[245]

In this context, reestablishing SERCA2a expression could be promising to treat cardiac dysfunction in metabolic cardiac disease and heart failure. In a mouse model of diabetic cardiomyopathy, conditional expression of SERCA2a was able to restore cardiac function.[246] In clinical trials, SERCA2a therapy was beneficial, since overexpression of SERCA2a by adenoviral gene transferrin in cardiomyocytes improved the contraction velocity and cardiac relaxation.[247] Similarly, another clinical trial (CUPID trial) observed that heart failure patients that received intracoronary infusion of SERCA2a had 88% risk reduction in adverse effect occurrence such as LV assistive device implant, heart transplant and death than the ones which did not receive SERCA2a infusion.[248]

Phospholamban (PLN) and sarcolipin regulate SERCA activity. PLN is predominantly present in cardiac muscle, while SLN is abundant in skeletal muscle. PKA can phosphorylate PLN at Ser16 whereas Ca^{2+}-CAMKII phosphorylates it at Thr17, both effects reduce PLN inhibition of SERCA2, which thereby becomes more active and obtains higher affinity for calcium.[249] Mouse models with reduced or ablated PLN showed that PLN is actually an inhibitor of SERCA affinity for calcium and that PLN inhibition is relieved during beta-adrenergic stimulation.[250] Inversely, overexpression of PLN induced SERCA2a inhibition and altered

contractility.[251] In human and experimental heart failure, SERCA was reduced whereas PLN was not changed while its phosphorylation was decreased.[252] Targeting PLN in heart disease appeared appealing as some studies showed that PLN ablation had beneficial effects on cardiac function and remodeling by improving SR calcium cycling. Indeed use of RNA interference of PLN rescued cardiac function in rat model of heart failure.[253] However, others demonstrated that the resulting normalization of myocyte calcium handling after PLN ablation may not improve cardiac function in vivo or reverse cardiac remodeling. Another level of complexity of PLN is added as it can interact with several partners to form multimeric complex.[254] Thus PLN can interact with the anti-apoptotic protein HAX-1 to increase the SERCA inhibition, additionally HAX-1 is able to recruit the heat shock protein (Hsp)90 from the ER to the PLN/SERCA2 complex proposing a link between ER stress signaling and calcium homeostasis. PLN is also able to bind the protein phosphatase-1 (PP1) that de-phosphorylates it to increase its inhibition on SERCA2 when the cytosolic calcium is low.[255] PKA modulates PLN phosphorylation level and consequently SERCA activity through PLN inhibition by phosphorylation during adrenergic activation.

The understanding of PLN in cardiac disease is becoming challenging as two human PLN-null mutations were found in heart failure patients and were associated with opposite subcellular mechanisms or PLN actions. The R9C mutation induced chronic inhibition of SERCA2a and early death in heterozygous carriers,[256] whereas the other mutation, L39stop, which is associated with a loss of PLN function, resulted in dilated cardiomyopathy and premature death in homozygous patients.[257] These effects observed in human did not match what was observed after PLN ablation in mice, which resulted in hyper-dynamic cardiac function highlighting the difference between mouse and human hearts. This might be due to a different role of PLN, or different consequences of PLN mutations in the two species. One other hypothesis suggested that these PLN mutations generate modified PLNs that traffic abnormally, cause cellular damage and associate incorrectly with other proteins in cardiomyocytes. Recently, other PLN mutations have been discovered and were associated with arrhythmogenic cardiomyopathy, although the underlying mechanisms are poorly understood.

1.3.5 Protein degradation by autophagy

Autophagy and apoptosis participate in the regulation of cell homeostasis, and autophagy accounts for a larger part of this role. In tissues from heart failure patients, much more cardiomyocytes showed signs of enhanced autophagy than of apoptosis,[258] suggesting its importance and the relevance of studying autophagy in cardiac disease. Eukaryotic cells

have to maintain a fine equilibrium between protein synthesis and protein degradation to ensure their homeostasis. Autophagy adapts rapidly in response to nutrient and growth factor availability and is responsible for degradation of intracellular organelles and misfolded protein. This makes autophagy essential for protein quality control. Protein degradation also happens via the ubiquitin-proteasome system, but currently the autophagy lysosome pathway is perceived as the most important in the heart.

Autophagy involves degradation of misfolded proteins, large damaged organelles or intracellular pathogens that cannot be degraded by the ubiquitin-proteasome system. Protein degradation is defined to be the key player to the self-renewal of cells by degrading long-lived protein and organelles. This process is essential during all stages of life and is particularly important during stress periods where its rapid activation or inhibition is critical for the maintenance of cell survival. Three different types of autophagy exist according to the cargo delivery way and the selectivity. The chaperone-mediated autophagy is specific to the degradation of soluble protein. Microautophagy and macroautophagy, which commonly refers to autophagy, are meant to degrade large structures. Depending on the selectivity of the cargo, others terms can be used: mitophagy for degradation of mitochondria, ribophagy (ribosomes), pexophagy (peroxisomes), lipophagy (lipids), and reticulopathy (endoplasmic reticulum).[259]

Different steps leading to degradation of the components are needed. First of all, a membrane supposedly coming from the endoplasmic reticulum is isolated to form a phagophore. Then, this membrane starts to elongate thanks to Atg (autophagy related genes) proteins. Proteins and organelles to degrade are sequestrated into this membrane undergoing elongation to create a structure called the autophagosome. The next step is the recruitment of a lysosome containing lysosomal proteases and its fusion with the autophagosome, resulting in the formation of an autolysosome. Finally the content of the autolysosome is degraded, amino acids, fatty acids and other components are released and can be reused by the cells in particular during stress periods such as starvation. All these processes need several molecular players. Beclin-1, VPS34 and VPS15 are essential for phagophore nucleation, while the autophagy proteins Atg-5, -12, and -16 and the microtubule-associated protein 1 light chain 3 beta (LC3B) play a role in its elongation. LC3B exists in two forms: LC3BI is the cytosolic form, which is converted to LC3BII during the formation of autophagosomes. LC3BII is specifically recruited to expanding autophagosomal membranes.[260] The ratio LC3BII/LC3BI is used as a marker of autophagy.[261]

Many proteins regulate autophagy. The Bcl-2 family proteins have an inhibitory effect on autophagy since these proteins can interact with and alter the formation of class III phosphatidylinositol 3-kinase (PI3K) family complex (Beclin1, VPS34, VPS15) which are responsible for phagophore formation. The mTOR pathway inhibits autophagy via inhibition of ULK1, an Atg protein important for autophagosome formation via its action on Beclin1. AMPKα is a primordial player in cell homeostasis as an ultimate energetic sensor of the cell. When the energetic status is low, AMPKα phosphorylates ULK1, Beclin1 and JNK to activate autophagy. It also activates FOXO1/3, which is responsible for the transcription of autophagy genes such as LC3B. Next to AMPKα, mTORC2 is also able to inhibit FOXO1/3 via phosphorylation of Akt at S473 and thus may inhibit autophagy.

Autophagy is a major mechanism of cardiomyocyte survival[262,263] and is thought to play an important role in cardiac remodeling.[262] However, excessive autophagy could results in cell death and cardiac dysfunction.[261,262,264] In a mouse model fed with a high sucrose diet, insulin resistance was associated with enhanced autophagy in cardiomyocytes,[265] as well as in a pig model where HFD increased autophagy and apoptosis.[266] However, Sciaretta et al. found that autophagy flux was reduced in a HFD model, and by restoring autophagy they were able to reduce the infarct size after ischemic injury.[267] Furthermore, by inhibiting mTOR with rapamycin, the infarct size after ischemia was reduced, beclin-1 heterozygous knock-out mice suppressed the protective effect of rapamycin proving that beclin-1 and autophagy were implicated in this beneficial effect.[267] Upregulation of autophagy during acute events such as myocardial infarction is cardioprotective, whereas its downregulation in mouse models of chronic disease such as obesity, diabetes and metabolic syndrome is deleterious and contributes to heart failure development. Indeed, prolonged hyperglycemia downregulates autophagy and thereby leads to an accumulation of misfolded proteins and dysfunctional organelles such as mitochondria, which is responsible for the release of death-promoting factors and results in cardiomyocyte apoptosis. Thus, restoring autophagy can rescue cardiac function in this situation. However, as already mentioned before, many discrepancies appear concerning its role in pathologic conditions. Indeed some studies using animal models showed that autophagy was either unaffected,[268] decreased,[266] or disrupted.[114] These contradictory results could be explained by the animal model, age, gender, time-course, and diet composition chosen for the study.

1.4 Estrogen

1.4.1 Sex hormones

The initiation of sex hormone synthesis is triggered by the gonadotropin-releasing hormone (GnRH) released by the hypothalamus. This hormone will stimulate the release of luteinizing hormone (LH) and follicle-stimulating hormone (FSH) from the pituitary gland into the blood stream. LH will be targeting Leydig cells (testis) in males and theca cells (ovaries) in females. This binding induces an increase of stereoidenogenic acute regulatory protein (StAR), which initiates steroidogenesis in the inner mitochondrial membrane via the uptake of cholesterol. Cholesterol will then be converted to pregnenolone leading to the synthesis of estrogen, progesterone and testosterone through different enzymatic pathways. Estrogen and progesterone are the two main female hormones. Progesterone synthesis initiation takes place in the theca cells and corpus luteum, where LH is stimulating the conversion of pregnenolone to progesterone. Testosterone represents the major male hormone. Its synthesis will go through different steps involving several enzymatic reactions. Pregnenolone is first converted to dehydroepiandrosterone (DHEA), followed by androstenedione, then testosterone. In peripheral tissues (skin, prostate, epididymis), testosterone is converted to dihydrotestosterone (DHT), which is much more potent than testosterone despite its lesser abundance.

Three different estrogen forms exist in females: estrone (E1), estradiol (E2 or 17-β-estradiol) and estriol (E3).[269] E2 is the most abundant and the most potent estrogen during premenopause, whereas E1 is the most important after menopause when it is synthesized in adipose tissue. E3 is the least potent and plays a role during pregnancy when the placenta produces it. They are synthetized from cholesterol in the gonadal organ where they are responsible for the occurrence of the primary and secondary female sexual characteristics and gonadal function. Estrogen has also an important role in extra gonadal tissues including liver, heart, muscle, bone and brain. Together with progesterone, estrogen plays a role in the menstrual cycle, inducing the development of the uterus mucous. Progesterone is released after ovulation to prepare the uterus to an eventual fertilization. Over 90% of the estradiol is produced in the granulosa of the ovaries. The remaining 10% are produced in peripheral tissues (brain, breast, skin, blood vessel, muscle) where FSH can convert it to estradiol.

The circulating level of estrogen is kept by the balance between estrogen synthesis and deactivation. E2 deactivation occurs through estrogen metabolism including the conversion from E2 to the less active form E1 or E3[270] or the formation of E2 sulfation by estrogen

sulfotransferase to form 17-beta-estra-1,3,5-trien-3,17-diol 3-sulfate that cannot interact with the ERs anymore.[271] Studies in female mice described another way of estrogen synthesis regulation implicating lipocalin 2, a novel adipose-derived cytokine which can inhibit E2 synthesis through downregulation of aromatase in adipose tissue.[272] The enzyme aromatase is responsible of the last step in E2 synthesis, this enzyme belongs to the cytochrome P450 superfamily and is widely expressed in many tissues: brain, gonads, blood vessels, liver, bone, skin, adipose tissue and endometrium.[273] Thus, aromatase is expressed in a tissue-specific manner, which depends on three major mechanisms: alternative splicing, tissue-specific promoter and different transcription factors. The different aromatase promoters are specifically regulated in tissues by distinct sets of hormones, cytokines, second messenger signaling pathways and other factors. Aromatase is present in gonads of both gender, it is found only in the granulosa and luteal cells in the female and in the testis and accessory glands in the male where it plays a crucial role for maintaining high level of E2 necessary for normal spermiogenesis, sperm maturation and sperm motility.[274]

Estrogen synthesis is different between reproductive and non-reproductive women. In non-reproductive women (young females and menopausal women), the extra gonadal sites are the main source of estrogen and include kidney, adipose tissue, skin and brain, estrogen acts locally at the site of synthesis and functions as a paracrine/intracrine factor to maintain the function of the tissue. [275] In contrast, in reproductive women, estrogen is produced mostly in the ovaries, which will be mainly released into the bloodstream. In the male, estrogen is produced in the testis and acts locally to regulate normal male gonadal development and spermatogenesis, particularly spermiogenesis.[276] E2 is also produced locally in both genders through the conversion of testosterone by aromatase,[277] the adipose tissue is the major source of circulating E2.[278]

Estrogen binds to nuclear receptors known as estrogen receptor α (ERα) and estrogen receptor beta (ERβ), encoded by ESR1 and ESR2 respectively. They belong to the steroid receptor superfamily and are able to influence transcriptional processes of target genes via binding to the ERE and recruiting co-activators. Thus, estrogen is implicated in the regulation of various genes involved in mitochondrial function, redox homeostasis, carbohydrate metabolism, lipogenesis and extracellular matrix integrity.[279,280] Estrogen receptors (ERs) are also found at the cytosolic and cell membrane level where they exert a rapid non-genomic action,[281] as well as in the nucleus. These receptors are not equally distributed in the body, the heart for example disposes of both receptors whereas in the liver only the ERα is present.[282] In the mid-1990s a new receptor has been identified and cloned from vascular endothelial cells. This receptor is called G protein-coupled estrogen

receptor (GPER)30 and is a 7-transmembrane receptor involved in rapid non-genomic estrogen responses together with the membrane-associated subgroups of ERα and ERβ.[283] GPER has also been localized to the endoplasmic reticulum.[284,285] The first GPER knockout mice appeared in 2008, in this study the authors identified GPER as a player in thymic atrophy. GPER is present on the vasculature[286] and is also highly expressed in cardiac tissue.[287]

1.4.2 Estrogen in the heart: introduction

Cardiovascular disease is the leading cause of death in both female and male. Interestingly it was described that the incidence of CVD is lower in premenopausal female than age-matched male. However, this female advantage gradually disappears after menopause and leads to a CVD risk that is higher in postmenopausal women than age-matched men.[288] Many preclinical studies demonstrated beneficial effects of estrogen on CVD, however, data from the clinical study Heart and Estrogen/Progestin Replacement Study (HERS-I) and the follow-up HERS-II failed to prove the cardioprotective effect of estrogen.[289] Surprisingly, the Women's Health Initiative (WHI) combined estrogen-progestin trial described an increase in risk for coronary heart disease in patients receiving estrogen supplements.[5] This finding could be explained by estrogen formulation, dosing, and administration routes used in these studies.

Recent evidence proved that the aromatase enzyme is present in the heart implying that estrogen is produced locally in the myocardium.[290,291] In the heart, E2 is synthetized endogenously from testosterone by the aromatase enzyme. This presence of testosterone may be the major source of estrogen in postmenopausal women. It was recently reported that a correlation exists between aromatase gene polymorphism and gender-differential mortality risk among patients diagnosed with acute coronary syndromes and patients with stable CVD.[292] Indeed the aromatase variant allele CYP19A1-81371C>T was associated with increase adverse outcomes in men and decreased risk of outcomes in women, suggesting a role of cardiac aromatase in estrogen-mediated cardioprotection.[292]

1.4.3 Estrogen in the heart: role and mechanisms

The three estrogen receptors ERα, ERβ[293] and GPER are present in the adult and neonatal heart and have also been found in ventricular and atrial cells in both genders in mice.[294] In the heart, ERs regulate gene expression and posttranslational modifications through both genomic and non-genomic mechanisms.[295] Several studies demonstrated that the ERs induce anti-apoptotic, anti-inflammatory, anti-atherosclerotic, vasodilatory, pro-hypertrophic and angiogenic effects on the cardiovascular system.[221,295-297] These cardioprotective effects have been associated with direct actions on vascular tone in

cardiac tissue, cell growth, and risks factors such as obesity and hypertension[298] and involve both classical estrogen receptors as well as the GPER.[284,299] Estrogen is cardioprotective during ischemia-reperfusion (IR), since an acute administration of estrogen just before ischemia reduces infarct size.[300] Interestingly, these protective effects disappeared when women reach menopause.[301-303] Female show also a reduced infarct size after IR compared to males.[304-306] A decline in E2 in postmenopausal female may result in dysregulation of lipid and glucose metabolism and an increased risk to develop CVD.

The effects of E2 on cellular mechanisms imply activation of PI3K/Akt pathway which can lead to the phosphorylation and activation of eNOS to increase nitric oxide. E2 can also intervene in the expression and activity of ion channels, as it decreases the mRNA level of potassium channel component Kv4.3 and Kv1.5.[307] In another study, E2 has been related to a decrease in ether-a-go-go-related channel that is linked to QT prolongation syndrome, which is affecting more women.[308] Thus E2 affects cardiac contractility, repolarization and can play a role in arrhythmias. A study performed on monkeys proved that E2 is responsible for the reduction of atherosclerosis.[309] Estrogen has many other effects, including the decrease of hypertrophy in female mice after aortic constriction-induced pressure overload.[310]

Some studies highlight that E2 deficiency may be the trigger for obesity development and result in T2DM, metabolic syndrome and CVD.[311-313] Estrogen plays a primordial role in several metabolic pathways. Indeed, estrogens are implicated in adipocyte activity and fat distribution. The deletion of ERα in female and male mice causes central obesity, insulin resistance and diabetes.[314-316] A mouse model of ovariectomized mice fed with high fat diet has demonstrated that E2 replacement improved glucose and insulin sensitivity in skeletal muscle of wild-type mice but not in knock-out ERα mice, confirming that ERα has an important role in preventing from diet-induced obesity adverse effects and could be a potential target in the treatment of obesity.[317-319]

Devanathan et al, developed a mouse model of cardiomyocyte-specific deletion of ERα to distinguish the systemic effects from cardiac effects induced by estrogen.[280] They characterized the genomic changes by microarray and discovered that 208 genes were modified compared to the wild type mice. Recently, studies were conducted to better understand the role of E2 in cardiac metabolism. It has been shown that administration of estrogen improved myocardial ATP levels and mitochondrial function in the heart.[320] Additionally, ERα and its specific agonist were necessary to maintain glucose uptake in the mouse heart.[321] The use of GPER knockout mice allowed determining the importance of

GPER. These mice exhibit an altered metabolism,[322] an increase in visceral adiposity,[323] obesity[11] and osteoporosis.[322] Indeed, female but not male GPER knockout mice become glucose intolerant at 6 months of age.[322] In another study it has been highlighted that male GPER knockout mice are insulin resistant at 6 months of age and become glucose intolerant at a later life stage.[324] This fact is connected to the observation that GPER is able to improve glucose intolerance and diabetes in female mice by activating insulin secretion from pancreatic β-cells.[325] In addition, administration of the GPER agonist G-1 causes a decrease in fatty acid synthesis and triglyceride accumulation in human and rodent pancreatic β-cells.[326]

Estrogen is known to regulate adiposity.[327] In rodents, it has been shown that the absence of ovarian hormones increases adiposity[328] and that this is prevented by implantation of subcutaneous pellet of E2. The different fat tissues present in the body exert different functions. Indeed, it is thought that abdominal adipose tissue is metabolically and functionally different than the other fat tissues. Removal of abdominal tissue is associated with reduced insulin and glucose levels in human[329] and prevent insulin resistance and glucose intolerance in male rodents whereas the removal of subcutaneous adipose tissue do not show the same effects.[330] Moreover, the transplantation of subcutaneous adipose tissue into the visceral region of a recipient mouse reduced the total amount of fat and ameliorates the glucose homeostasis.[331]

Figure 10 shows the interaction between Akt and estrogen signaling in the heart. Upon insulin binding to its membrane receptor, activation of IRS-1, PI3K and PDK1 result in the phosphorylation of Akt at T308, which in turn will activate multiple signaling pathways. Among them the mTOR pathway is activated to modulate cardiac modeling and performance. In the same way, estrogen can modulate cardiac function and morphology via the regulation of Akt signaling and also via nuclear actions opening to an adjustment of different channel transcription and expression (calcium, potassium channels). Estrogen signaling is complex because of various factors. It has been proven that estrogen receptor expression is differently regulated in a tissue-specific manner and more importantly the three receptors can exhibit different effects, which can be opposed, synergistic or completely independent according to the tissue and time.

Upon stimulation of the estrogen receptor, its translocation into the nucleus and binding on the ERE will regulate transcription of genes according to the co-regulator recruited, which are tissue- and gender-specific. Moreover, the ERs can indirectly bind DNA via transcription factors and can be activated in a ligand-independent way by growth factors

for example, leading to ER phosphorylation and translocation into the nucleus to trigger gene transcription.[332,333] Besides these genomic effects, a non-genomic effect of ER activation exists, indeed ERs are also present in the plasma membrane and can trigger rapid actions such as activation of Src, PI3K, Akt and MAPK. To add another level of complexity, the two estrogen signaling mechanisms, genomic and non-genomic, are able to interact with each other in synergy.[334] This reflects the difficulty to understand estrogen signaling and highlights the need of studies to describe the role of estrogen in particular in the heart, where it appears to be cardioprotective in conditions such as ischemia-reperfusion, myocardial infarction, or chronic heart failure. It was only in the 60s that the membrane delimited action of estrogen was first described.[335] Today it is well accepted that E2 not only acts at the genomic level, but also induces rapid cellular responses via its plasma membrane localization.[336,337] Estrogen receptors have also been localized in organelles such as mitochondria and the reticulum endoplasmic.[338,339] More and more studies are going to this direction aiming to understand better their physiologic role.

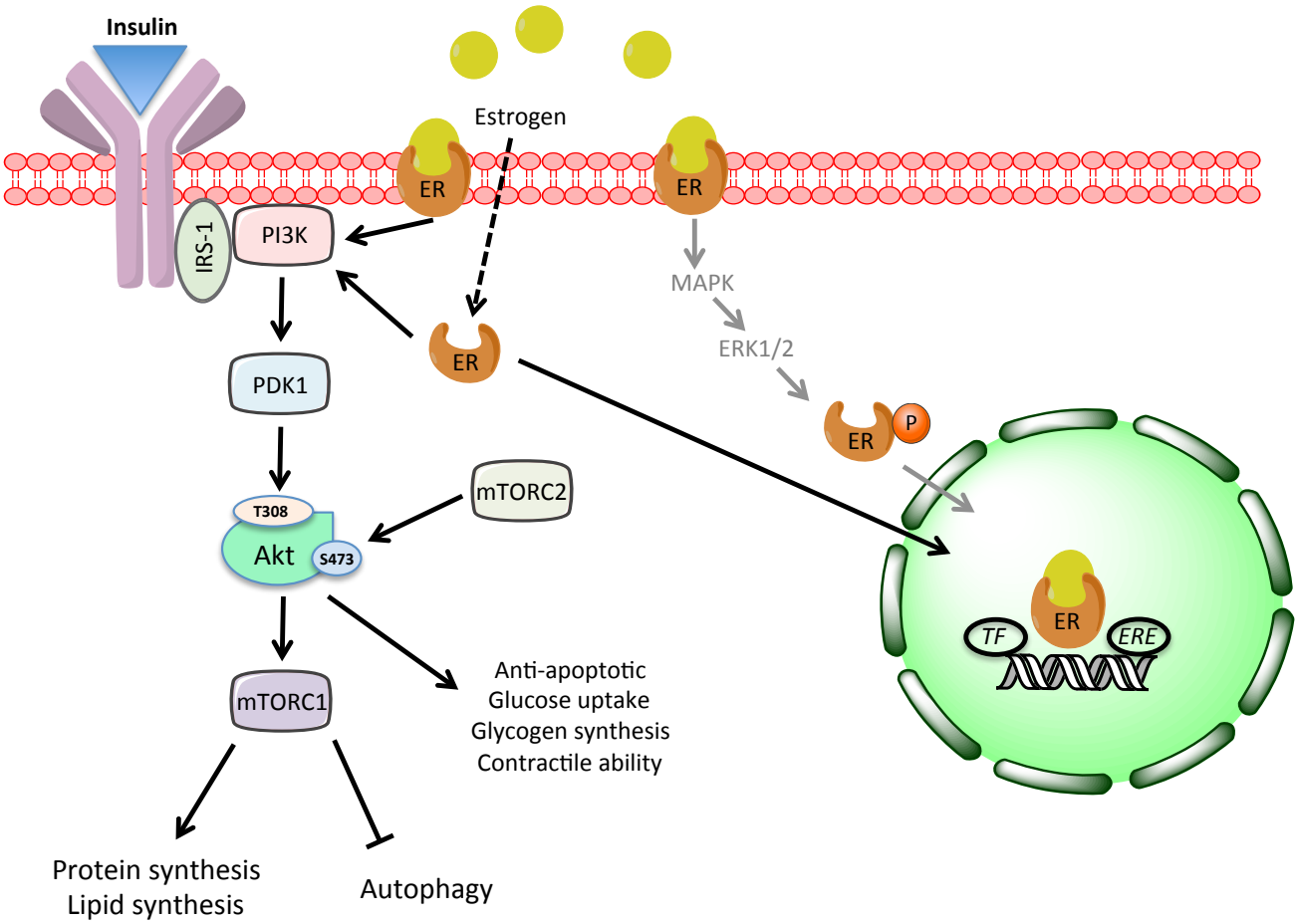

Figure 10: Insulin-estrogen signaling crosstalk in the heart.
Estrogen can bind the 3 different estrogen receptors (ER) ERα, ERβ and GPER, to induce the various physiological responses. Three different ways of binding are known. The classical genomic estrogen signaling involves the dimerization and the translocation of the ERα and ERβ receptors from the

cytosol to the nucleus where it binds directly to consensus estrogen response elements (ERE) in the chromosomal DNA, to initiate changes in gene expression. Co-activators or co-inhibitors are recruited to activate or inhibit genes. ER can also attach indirectly to the DNA via other transcription factors (e.g. API, Sp1). Another way of estrogen signaling activation is called ligand independent activation. In this case ERs are phosphorylated by kinases such as p38, ERK or Akt, which are activated by ERs at the membrane, and leads to DNA binding and gene transcription. The activity and localization of both ER can be influenced by posttranslational modifications.

1.4.4 Estrogen in the heart: gender-specificity

It is clear that menopause is associated with increased obesity, insulin resistance, diabetes and osteoporosis,[340] and this is explained by the important role of estrogen in metabolic effects such as regulation of lipid and glucose metabolism, adiposity, body fat distribution and obesity. Indeed, the estrogen decline in postmenopausal female may result in dysregulation of lipid and glucose metabolism and an increase in the risk to develop CVD. This is due to several metabolic changes: an atherogenic lipid profile with an increase in FFA, small dense low-density lipoprotein particles, triglycerides, lipoprotein and a decrease in HDL2 particles, which are the most cardioprotective.[312] Moreover, this period is also propitious to development of CVD hallmarks such as insulin resistance, disturbed peripheral glucose clearance, increased gluconeogenesis and glucose output of the liver, increased inflammatory markers and decreased fibrinolytic capacity.

Men are at higher risk to develop obesity and cardiovascular disease including hypertension than women. However, this tendency is inversed in postmenopausal population meaning that at this stage, women lost their advantage while ovarian hormone levels decrease.[165,166] This observation is today accepted but the reasons why menopausal women are more susceptible to obesity and so CVD remain unclear, however ovarian hormones appear to be the ideal player involved. It has been described that premenopausal females affected by diabetes are also at higher risk to develop cardiovascular disease compared with age-matched males. Insulin sensitivity has also been described to be involved in the gender-differences observed in insulin signaling. A clinical study suggested that females were less insulin sensitive than males.[287] This was consistent with an experimental study where hearts from female rats were less sensitive to insulin compared to those from male rats.[340] Interestingly however, ovariectomy (OVX) did not alter insulin sensitivity,[341] showing the complexity of the regulation of insulin sensitivity.

1.5 Aim of the study

Cardiovascular diseases are the major cause of death in industrialized countries and postmenopausal women are more affected than their counter part men. Moreover, it has been described that premenopausal females affected by diabetes are also at higher risk to

develop cardiovascular disease compared with age-matched males. Hence, we found it relevant to study gender-specific effects and the role of ovarian hormones in a model of metabolic disease induced by HFD.

High fat diet feeding is an important risk factor for metabolic syndrome occurrence and results in structural and functional cardiac alterations. One hallmark of the metabolic syndrome is obesity, and according to the WHO estimates, more women (14.9%) than men (10.8%) were obese in 2014. However, women are less prone to develop cardiovascular diseases[166] until menopause when this female-advantage disappears, suggesting a role of estrogen hormones. Estrogen has multiple roles in glucose and energy metabolism and has been reported to be involved in the cardiovascular system, as E2 modulates vasculature, inflammatory responses and insulin sensitivity. For example, estrogen administration is able to reduce cardiac infarct size after ischemia-reperfusion.

The number of studies on estrogen signaling is constantly growing but nevertheless, a lot is still not discovered or understood. In this regard, many studies have been performed to evaluate the role of E2 in regulating gene expression and only few have addressed protein expression. It is well known that changes in gene expression do not always reflect the changes observed at the protein level. This is why in this study I aim to reveal potential sex-differences in protein expression by studying male, female, and female mice lacking estrogen. Besides, by mimicking the postmenopausal situation in female, the results obtained with my model could be important for other pathologies such as polycystic ovaries where a defect in ovaries leads to decreased estrogen.

The aims of my study are:
1. to investigate gender-specific effects and the role of ovarian hormones on cardiac function, geometry and cellular mechanisms in a model of obese mice
2. to better understand the cardioprotective effect of female hormones in mice

It has been shown that after 2 wks of western diet, glucose oxidation and glycolysis are reduced while FA oxidation and oxygen consumption are increased in a mouse model,[133] in part due to altered insulin signaling.[342,343] Cardiac dysfunction similar to diabetic cardiomyopathy was observed at a later stage, after 20 wks of diet.[133,344] Hence, the timeline chosen in our study, which also depended on the observation of changes in diastolic function by echocardiography. Hallmarks analyzed include glucose tolerance, blood pressure, cardiac dimension and hemodynamic function, insulin pathway, inflammation, and autophagy. We performed these analyses on male as well as sham- and

OVX-operated female mice before, during and after feeding for 22 wks with a control (CTD) or high sucrose and high fat diet (HFD) that mimics a western diet.

2. Materials and Methods

2.1 Protocol and mouse model

Female and male C57Bl/6N mice were used in this study. Ovariectomy and different tests were performed according to the precise timeline shown in Figure 11. The mice were put on two different diets: a regular chow diet referred to as control diet (CTD, Kliba Nafag) and a high fat diet (HFD, Ssniff) containing 45% calories derived from saturated fat and 17% from sucrose. By choosing this diet rich in fat and sucrose we aimed to mimic the diet used in western countries, which contains a lot of saturated fat and carbohydrates. The study was approved by the Veterinary Office of Canton Basel-Stadt. The mice that suffered from ulcerative dermatitis[345] were excluded from the study and in severe cases mice were immediately euthanized.

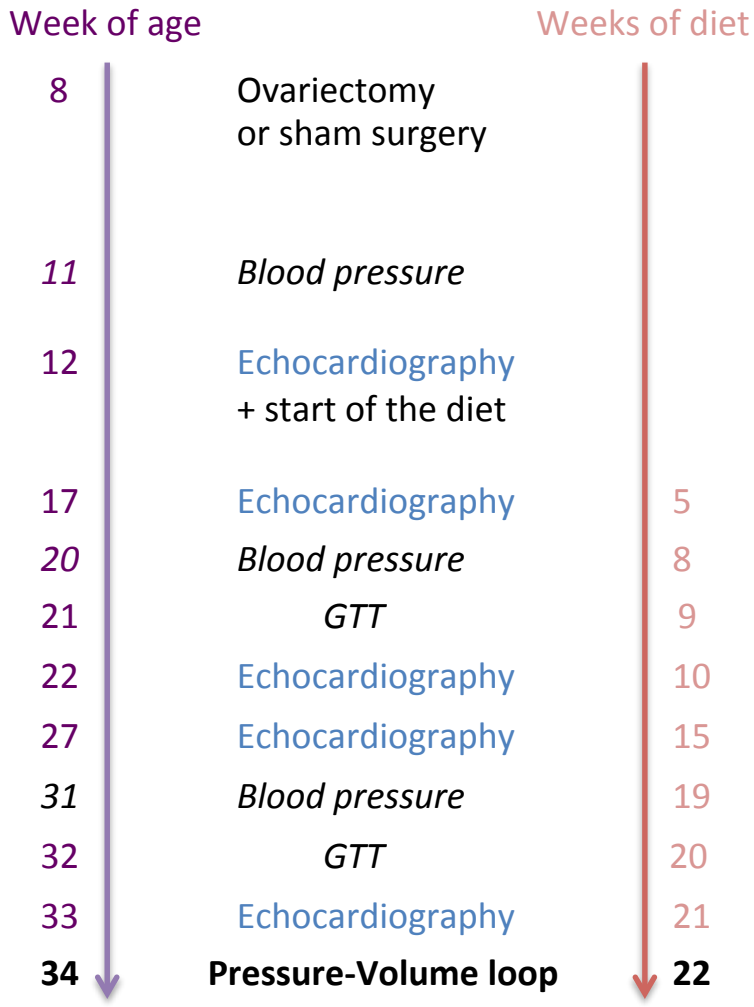

Figure 11: Experimental design of our study.
At 8 weeks of age, all mice underwent ovariectomy or sham surgery. Their blood pressure and cardiac function were assessed by tail-cuff and echocardiography prior to and at different timepoints after start of the diet, as indicated in the figure. Additionally, glucose tolerance tests were realized at 9 and 20 weeks of diet. At 22 wks of diet, cardiac hemodynamics were measured by the pressure-volume loop method.

2.2 Ovariectomy- and sham-surgery

Female and male mice were anesthetized with isoflurane, the surface of interest of the skin was shaved and cleaned with antiseptic agent before a 3 mm incision was made at the back of the mouse, next to the spine 0.5 cm below the rips. The ovaries were localized and either ligated and extracted for the ovariectomized (OVX) mice or not ligated and left intact for the sham-female and male mice. The OVX rodent model is commonly used in research to study the role of E2 in cardiac function, indeed this model closely mimics the sex hormone level of surgical and natural menopause in women.[346]

2.3 Tail-cuff blood pressure measurement

Blood pressures were measured using a non-invasive method, which consists of placing a cuff around the animal's tail to occlude the blood flow. As the cuff inflates and deflates, a sensitive sensor placed distally to the occlusion cuff monitors the blood pressure. To assess blood pressure and pulse, we used the BP-2000 Series II blood pressure analysis system (Visitech Systems, Apex, NC, USA), which relies on photoplethysmography, a light-based technology. Diastolic and systolic blood pressures as well as pulse were measured at baseline (before the beginning of the diet) and at 8 and 19 wks of diet. The measurements were performed in a quiet room during the afternoon at a regular hour and by the same investigator. The mice were first trained for 5 days to allow acclimation to the procedure until reproducible baseline measurements are obtained before to use the data. To avoid any systematic errors, the blood pressure measurement of each mouse was performed on different channels during the week.

2.4 Glucose tolerance test and plasma insulin levels

The glucose tolerance test (GTT) is a widely used and easy procedure important to assess the ability of the body to clear glucose over time, it is susceptible to uncover glucose intolerance. After 6h of fasting, mice were injected intraperitoneally (i.p.) with a glucose solution (2 mg D-glucose/g BW). Blood glucose concentrations were determined before injection and 15, 30, 60, 90, 120 min after injection using the Freestyle Lite glucometer (Abbott, Chicago, IL, USA), to observe glucose clearance from the blood. Each measurement was recorded in duplicate, if the values were too far apart (more than 1 mmol/l), a third or a fourth measure was taken. Insulin was measured in plasma collected during sacrifice using the Multi-array Assay System Mouse/Rat Insulin Kit from Meso Scale Discovery (Rockville, Maryland, USA).

2.5 Echocardiography and pressure-volume loop

Cardiac geometry and function were analyzed by ultrasound under isoflurane anesthesia.[154] Next to routine echo parameters,[154] M-mode imaging was used to evaluate systolic and diastolic dimensions, posterior and anterior wall thickness, fractional shortening and ejection fraction. Pulsed-waved Doppler images in the apical 4-chamber view were used to measure peak early (E) and late (A) mitral valve inflow velocities as a first evaluation of diastolic function. Echocardiography was performed at baseline (before the start of the diet), at 5, 10, 15 wks of diet and before sacrifice, using the Vevo® 2100 System from Visual Sonics. In parallel, one batch of animals was dedicated to pressure-volume loop experiments for real-time cardiac function assessment. To induce an additional cardiac stress, and because LV dysfunction in HFpEF may be revealed better during exercise than in the resting state, the β-adrenergic stimulator dobutamine was infused.

For the realization of the PVL experiment, mice were anesthetized with a mixture of α-chloralose (50 mg/kg) and urethane (1200 mg/kg), intubated with a ventilator to provide oxygen (MiniVent 845, Hugo Sachs/Harvard Apparatus) at a rate of 130 strokes/mi, 7 µL/g BW tidal volume). The body temperature was maintained at 37°C. Mice also received a dose of pancuronium bromide, a neuromuscular blocking agent, which will inhibit spontaneous breathing. While recording the data, the ventilator was briefly stopped preventing the breathing movement that influences the cardiac cycle loops.

Briefly, after calibration a pressure-conductance transducer (1.4 Fr pressure transducer, Mikro-Tip® ultra-miniature, model SPR839, Millar, Houston, TX, USA) was inserted into the right carotid artery and the catheter tip was manipulated across the aortic valve into the left ventricle. After catheter stabilization, hemodynamic parameters were recorded before and after dobutamine infusion through the jugular vein stepwise at different concentrations: 0.3, 1, 3, and 10 µg/ml/kg for 2 min each. To measure LV compliance and elasticity, preload was decreased by occlusion of the inferior vena cava for 5-10 sec to obtain load-independent measurements. The calculated Tau is using the Weiss formula. The conductance was converted into volume by using a cuvette calibration containing several small cylinders with known volumes. The catheter was placed in each of the cylinders and the conductivity of the blood was translated into volume using the formula described under 1.1.5. A calibration curve was thus obtained, which served for obtaining the final volumes.

Data were acquired with ADinstruments PowerLab 8 and processed with LabChart Pro software (ADInstruments, Dunedin, New Zealand). During this procedure, different

hemodynamic parameters were recorded in the LV as well as the aorta, which is also relevant to detect eventual abnormalities.

2.6 Sacrifice and tissue analysis

Mice from the PVL experiment were sacrificed immediately after the β-adrenergic challenge and used for microscopy analysis. To proceed, hearts were harvested and sliced into 3 distinct parts: base, middle and apex, placed into OCT embedding matrix (Cell Path, UK), and frozen into isopentane/liquid nitrogen for later histology analysis.

In addition, another cohort of mice was sacrificed to study molecular mechanisms. For that, mice were fasted 6h during the morning prior sacrifice. They were anesthetized with 3% isoflurane, blood withdrawn from the heart, and tissues (heart, liver, gastrocnemius muscle, visceral fat) were dissected, weighed and snapfrozen in liquid nitrogen for further Western blot and RNA analysis. The fat harvested consisted of mesenteric/epididymal depots of white adipose tissue, and will later be referred to as visceral fat. The uterus was also weighed and served as a readout for successful ovariectomy. Tissue weights were normalized to tibia length. Plasmas were collected to analyze insulin concentration in the different groups, and all tissues collected were stored at -80°C.

2.7 Protein analysis

Total proteins were extracted in RIPA buffer (50 mmol/l Tris-HCl, pH=7.4, 150 mmol/l NaCl, 1% (v/v) NP40, 0.25% (v/v) Na^+-deoxycholate, 5 mmol/l EDTA, 10 mmol/l Na^+-pyrophosphate, 10 mmol/l glycerophosphate, 0.5% (v/v) phosphatase inhibitor cocktail 1 and 2 (Sigma), 1% protease inhibitor cocktail (Sigma) using a Polytron homogenizer. Equal amounts of protein were separated by SDS-PAGE and transferred onto a PVDF membrane (0.2µm, GE healthcare). After 1h of blocking with 5% BSA to mask non-specific sites, membranes were incubated with the primary antibody overnight at 4°C on a shaking platform. The membranes were then washed 3x20 min with TBS-Tween20 0.1% to remove unbound primary antibodies, and blocked again with 5% BSA for 30 min prior to incubation with a HRP-labeled secondary antibody (Jackson Laboratories) for 1h at RT. After 3x20 min of washing, the signal was detected using SuperSignal West Pico Chemiluminescent substrate (Thermo Scientific) and pictures were acquired with the Chemi-Doc (Bio Rad) and analyzed with the Image Lab software (Bio Rad). Antibodies were purchased from different companies (Supplement, Table SI).

2.8 RNA analysis

Tissues were homogenized in Tri-Reagent (Sigma) using a Polytron. RNA was first separated from DNA and proteins using chloroform. After centrifugation, three phases were obtained, an aqueous phase containing the RNA, an interphase containing DNA and a phenolic phase containing proteins. The aqueous phase containing RNA was then transferred into microtubes and precipitated with isopropanol. After centrigugation, the obtained pellet was washed with 70% ethanol, dried, and dissolved in water. It then received DNAse treatment using the DNA-free kit (Ambion) to eliminate any potential genomic DNA contamination. The RNA was then quantified with a spectrophotometer (OD 260 nm), and the purity evaluated by using the ratio OD_{260}/OD_{280}, and stored at –80°C. To check RNA integrity, electrophoresis on an agarose gel was performed: two intact bands should be visible corresponding to the subunit 28s and 18s of the ribosomal RNA.

The reverse transcription process started with denaturation of the RNA, which was then transcribed into cDNA using the High Capacity cDNA Reverse Transcription kit from Applied Biosystems. cDNA was stored at –20°C. Quantitative real-time PCR was performed with the GoTaq qPCR Master Mix kit from Promega. Briefly, forward and reverse specific primers (5 µM) and an equal quantity of cDNA were added to the Master Mix. Each sample was measured in triplicate and a standard curve was made to allow RNA quantification. All PCR primers were bought from Microsynth, (see Supplement, Table SII for primers sequences). To normalize our data different housekeeping genes were tested: GAPDH, myoglobin and lamin B1, all these genes were regulated in our experimental groups. This is why our results were normalized with the only gene that was not regulated, the GLUT4 gene (Supplement, Figure S VIIC).

2.9 Microscopy

Frozen hearts were sectioned at 12 µm thickness with a Leica Cryostat and stored at -80°C. Cryosections were processed for Picrosirius red (PSR) and Oil Red O (ORO) staining to visualize fibrosis and neutral lipids, respectively. For the PSR staining, sections were fixed with MetOH at -20°C for 10 min, incubated with hematoxylin to color the nuclei, stained with Sirius Red F3BA (Polysciences kit) and rinsed with 0.01N HCl. Slides were mounted in an anhydrous mounting medium.

For the ORO staining, sections were allowed to equilibrate at room temperature (RT) for 10 min and were then incubated with the ORO working solution, containing Oil Red O (Sigma) dissolved in isopropyl alcohol, for 5 min. Sections were counterstained with Mayer's

hematoxylin, washed and mounted in a water-soluble mounting medium. For both stains, Pictures were acquired using bright-field on an Olympus BX63 microscope.

Wheat germ agglutinin (WGA) staining, caspase-3, Mac-2, and TGF-βI labelling were detected by immunofluorescence. Cryosections were fixed with 4% paraformaldehyde and permeabilized with Triton X-100 0.3%. After 2 washings with PBS-glycine, sections were treated with $NaBH_4$ to reduce the background. For 2x15 min a solution containing PBS+0.2% gelatin+3% BSA was used to block non-specific sites. Finally, sections were incubated overnight at 4°C with the primary antibody, one section served as a negative control. The second day, the sections were washed with PBS-gelatin and incubated with a secondary antibody (Alexa Fluor-conjugated, Jackson, Molecular Probes) for 1h at RT in a humid chamber. Consecutive to washing, the sections were mounted with a minimal amount of homemade mounting medium. Pictures were acquired with fluorescent light using an Olympus BX63 microscope.

For Transmission Electron Microscopy, mice were perfuse-fixed with 2.5% glutaraldehyde in 0.1 mol/l sodium phosphate for 10-15 min. The heart was isolated and immerged in glutaraldehyde. A small part of the LV free wall was taken out and transferred into tubes containing glutaraldehyde for overnight post-fixation at 4°C on a rotator. Samples were then processed by the Bio-EM lab at the Center for Cellular Imaging and NanoAnalytics from the Biocenter, University of Basel.

2.10 Statistical analysis

Data are presented using a box plot representing the interquartile range and showing the highest and the lowest values as well as the median. Differences in means were evaluated with two-way ANOVA (**P**-values in text), followed by Sidak's multiple comparisons tests (P-values in figures). To discriminate gender-specific effects from effects due to the OVX surgery, data were analyzed into 2 different sets: male vs sham-female and OVX- vs sham-female mice. For multiple measurements of the same mice, repeated-measures ANOVA was used. All statistics were performed with GraphPad Prism 7.0. P-values **<**0.05 were considered statistically significant. Three different symbols were used to compare the conditions: *refers to differences between HFD and CTD, $ refers to male vs female differences and # to the effects of ovarian hormones ablation. The p-values correspond to *p≤0.05, **p<0.01, ***p<0.001, ****p<0.0001 and are identical for the three symbols used.

3. Results

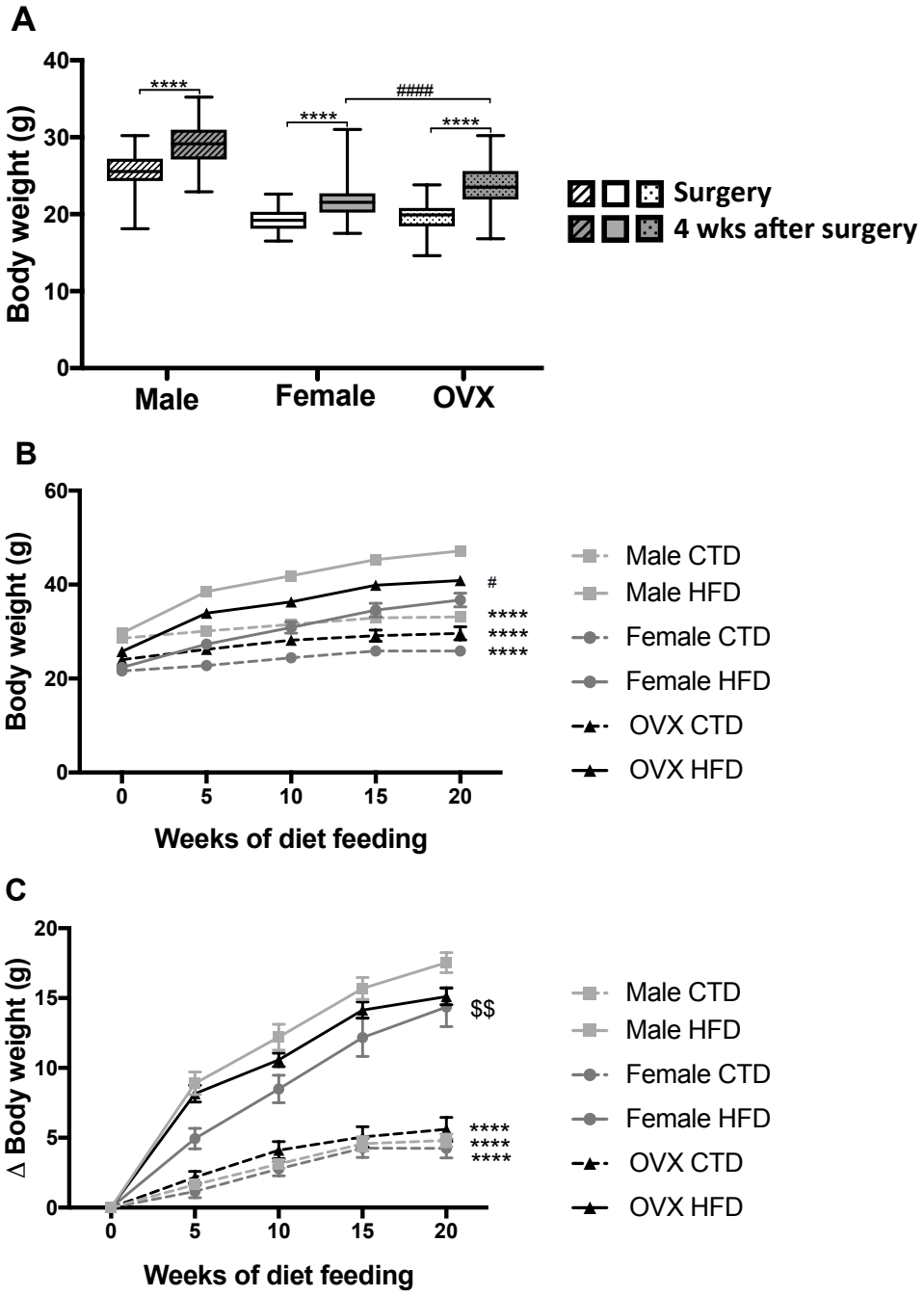

Figure 12: Body weights of female and male mice prior to and after feeding with CTD and HFD.

A: OVX or sham surgery was performed at 8 wks of age and body weights measured at 4 wks after this surgery (N=82-110); B: diet feeding was started at 4 weeks after OVX/sham surgery and body weights were measured at multiple time points afterwards as indicated (N=18-25); C: body weight gain was calculated by subtracting body weight at 0 wks from body weight at the indicated time point (N=18-25). Results are presented with the median, whiskers show the min and max values (A), and mean ± SEM (B+C). * symbol corresponds to CTD vs HFD, # symbol corresponds to OVX vs sham, $ symbol corresponds to male vs female.

3.1 Analysis of body weight over time

Female mice underwent OVX- or sham-surgery at 8 wks of age and feeding with control or high fat diet was started 4 wks later, at 12 wks of age. Male mice underwent sham surgery and diet feeding was started at 12 wks in parallel to the female groups. To evaluate potential differences in weight gain between male, female, and OVX-female mice after feeding with CTD or HFD, body weight was measured on a weekly basis. Body weights were also measured prior to sham/OVX surgery and at start of the diet feeding (referred to as baseline hereafter) to assess the acute effects of OVX on body weight (Figure 12).

First of all, Figure 12A shows that during the 4 wks after surgery prior to the begin of HFD- or CTD-feeding, the OVX mice (n=111) gained 1.7 grams more weight than the sham-operated female mice (n=83, $p<0.0001$). As a consequence, the body weight of the OVX-HFD-group was already 15% higher than that of the sham-female-HFD-group at the time that diet feeding was started (Figure 12B). After 10 wks of HFD feeding, a difference of 15% was still observed between OVX- and sham-female mice, whereas at 20 wks this value dropped to 10%, showing that overtime the difference between OVX and sham-female mice became less (Figure 12B). In fact, the body weight curves of the OVX-HFD and the sham-HFD groups diverged up to 5 wks of feeding, then started to run parallel, and finally during the last weeks of feeding the difference in weight became less (Figure 12B).

Since baseline body weights were different between the groups due to gender (males had higher body weights than age-matched females) and OVX, we calculated the body weight gain compared to baseline for each mouse to evaluate the effects of HFD feeding for the male, sham- and OVX-female groups (Figure 12C). First of all, and as expected, HFD feeding significantly increased body weight gain compared to CTD feeding for the three groups. Overall, the male-HFD group gained most weight followed by the OVX- and sham-female mice. However, when the increase is calculated as percentage of total body weight, the sham-female group gained most weight over time with a 64% increase measured at 20 wks compared to baseline at the beginning of the feeding. The OVX and male HFD groups gained 59% body weight over the same time period. As for the CTD groups, during the 20 wks of feeding, the OVX-group gained somewhat more weight over time, but the differences between the groups were small and not significant.

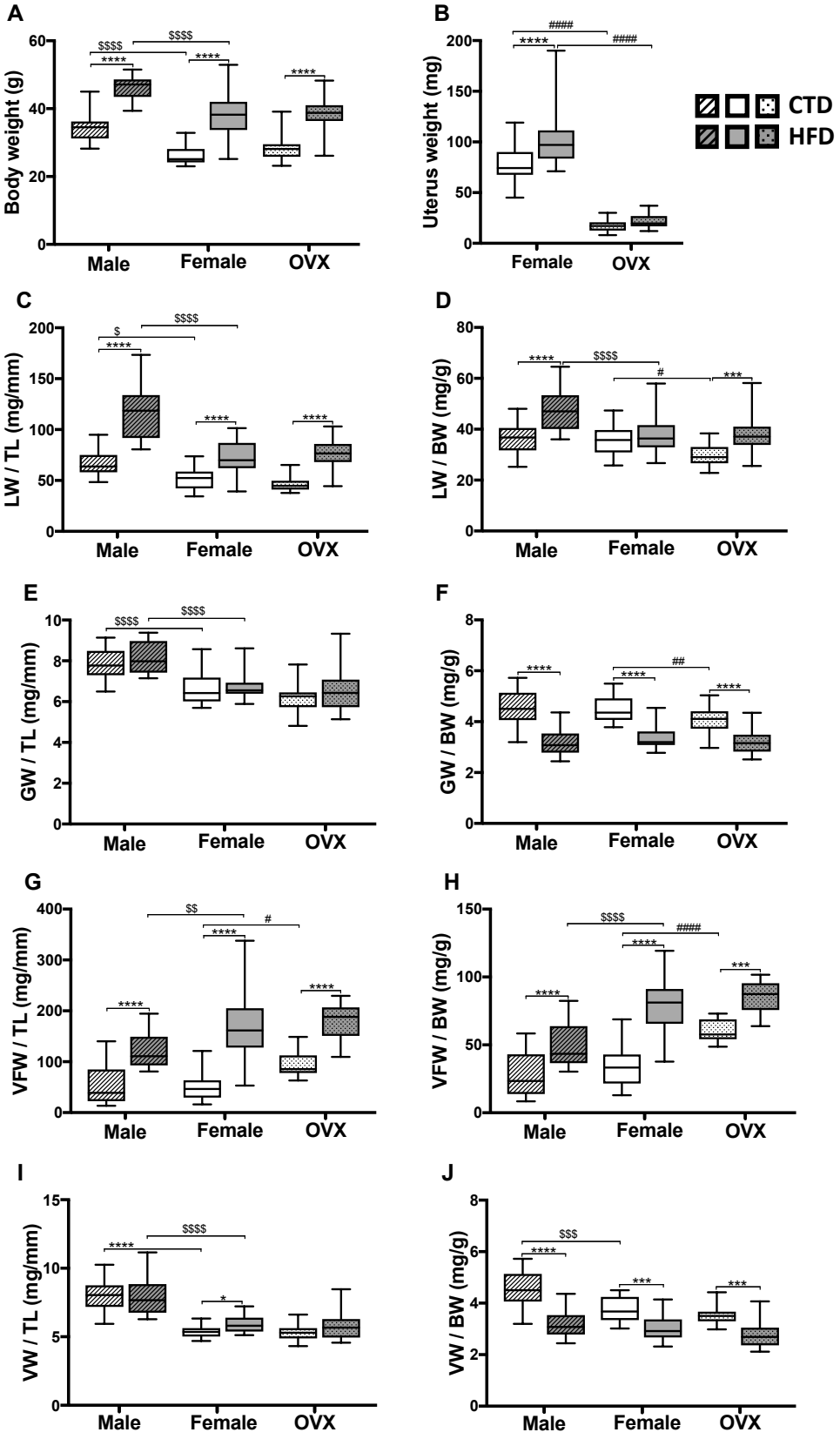

Figure 13: Post-mortem organ weights of male, female and OVX mice fed with CTD or HFD for 22 wks.

Organs were weighed after sacrifice and normalized to tibia length (TL: C, E, G and I) or body weight (BW: D, F, H and J). LW, Liver weight; GW, gastrocnemius weight; VFW, visceral fat weight; VW, ventricle weight. Results are presented with the median, whiskers show the min and max values. *symbol corresponds to CTD vs HFD, # symbol corresponds to OVX vs sham, $ symbol corresponds to male vs female; N=18-24.

3.2 Analysis of organ weights

Body weight measurements done at the day of sacrifice after 22-23 wks of diet gave results similar to those described above under 3.1. For all three groups (sham-females, OVX-females and males), the HFD-fed mice had significantly higher body weights than CTD-fed mice. The males had higher body weights than the females irrespective of the diet that was fed, and no differences were observed between the sham- and OVX-females (Figure 13A). Notably, the OVX mice had a decreased uterus weight compared with the sham-female mice, confirming the successfulness of ovary ablation and the decreased level of estrogen (Figure 13B).

In females as well as males, the HFD increased liver weight, but not the gastrocnemius weight (Figure 13C-F). Moreover, paralleling the higher body weights of males compared to females, the liver and gastrocnemius were heavier in males than in females (Figure 13C, E). In the CTD-fed mice, the gender-related difference in liver and gastrocnemius weight lost significance after normalization to body weight, meaning that the liver and gastrocnemius weight were in proportion to the body weight (Figure 13D, F). However, for the HFD-fed mice, normalization of liver weight to body weight resulted in higher values for males than sham-females, indicating a gender-difference in the liver's response to HFD feeding (Figure 13D). On the other hand, the CTD-fed OVX mice had slightly lower liver/BW ratios than the sham-females, whereas HFD-fed OVX mice had an increased ratio compared to CTD-fed mice (Figure 13D). Thus, compared to CTD, HFD feeding causes an over-proportional increase in liver weight in OVX-females and males, but not in sham-females. These findings suggest that liver hypertrophy develops in a gender-specific manner after HFD feeding. Our data also suggest a role for the ovarian hormones in determining liver weight at least under CTD conditions.

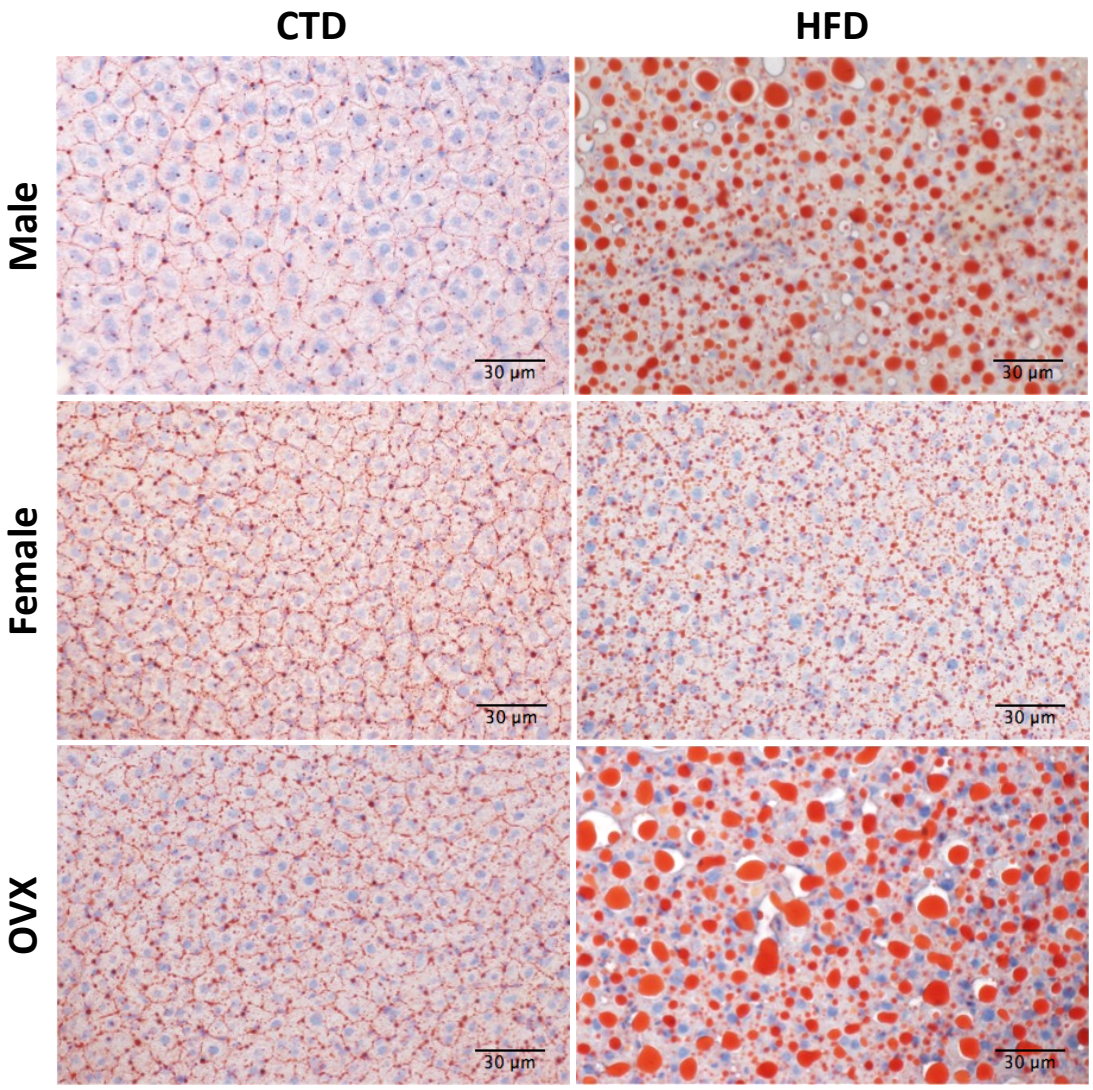

Figure 14: Oil Red O staining to detect neutral lipids in liver sections.
Liver cryosections of male, female and OVX mice (sacrificed at 22 wks) were stained with Oil red O to detect neutral lipids (red) and counterstained with hematoxylin to reveal nuclei (blue). Magnification x20.

To evaluate if the liver from males had a different composition or appearance than the liver from sham-females, liver sections were stained with Oil Red O to detect neutral lipids (Figure 14). The HFD feeding was responsible for an important accumulation of lipids in all groups but the effect was much more pronounced in the OVX-female followed by the male mice. This observation could explain the fact that the livers from these two groups were heavier after HFD. In the sham-female group, the HFD feeding had a smaller effect. The observed low accumulation of lipids after HFD feeding is in line with the fact that liver weight was not increased in this group. In the CTD-fed groups, the OVX-female mice seem to have bigger lipids droplets than the sham-female. It also appeared that in males the intercellular lipids are less abundant than in females after CTD.

The gender-specific differences in weight applied to the liver but not the gastrocnemius. The latter was heavier in males than in females, with no difference between the OVX- and sham-female groups (Figure 13E). No effects of HFD on gastrocnemius weight were observed for any of the groups after normalization to tibia length (Figure 13E). Normalization to body weight resulted in reduced GW/BW ratios in response to HFD for males, females, and OVX-females alike (Figure 13F). These results are explained by a change in body composition after HFD. Muscle mass was stable after the HFD feeding, but fat and liver weight increased and are together responsible for the overall body weight increase, consistent with the GW/BW decrease.

Interestingly, the visceral fat weight showed OVX-related differences (Figure 13G, H). First of all, and as expected, HFD caused an increase in fat weight for all three groups. Moreover, OVX increased visceral fat weight after CTD feeding, but no effect of OVX was noticeable after HFD feeding most likely because the HFD by itself had already maximally increased the fat weight. In other words, HFD increased fat mass in sham-females and OVX did not increase this any further. These effects on fat mass remained significant also after normalization to body weight, indicating an over-proportional increase in body fat. Interestingly, despite the higher BW of the males, fat mass after HFD was lower in males than in females. Thus, HFD-fed males had less fat than the females for a given body weight (Figure 13H).

Immediately after sacrifice by cardiectomy, the hearts were dissected for further analysis. Atria were removed and the ventricles weighed. HFD feeding increased the ventricular weight only in the female and not in the male mice (Supplement, Figure S ID). After normalizing for tibia length, the HFD feeding increased the ventricular weight in the sham-females but not in the males, highlighting the presence of a gender difference (Figure 13I). A small increase observed in the OVX-females was not significant ($p=0.079$), so more mice are needed to draw a conclusion about the role of ovarian hormones on ventricular weight. As expected, the ventricular weights of males were higher than those of females. This was still true after normalizing to body weight. Thus, males have heavier hearts than females and HFD increases ventricular weight in sham-females after 22 wks of feeding.

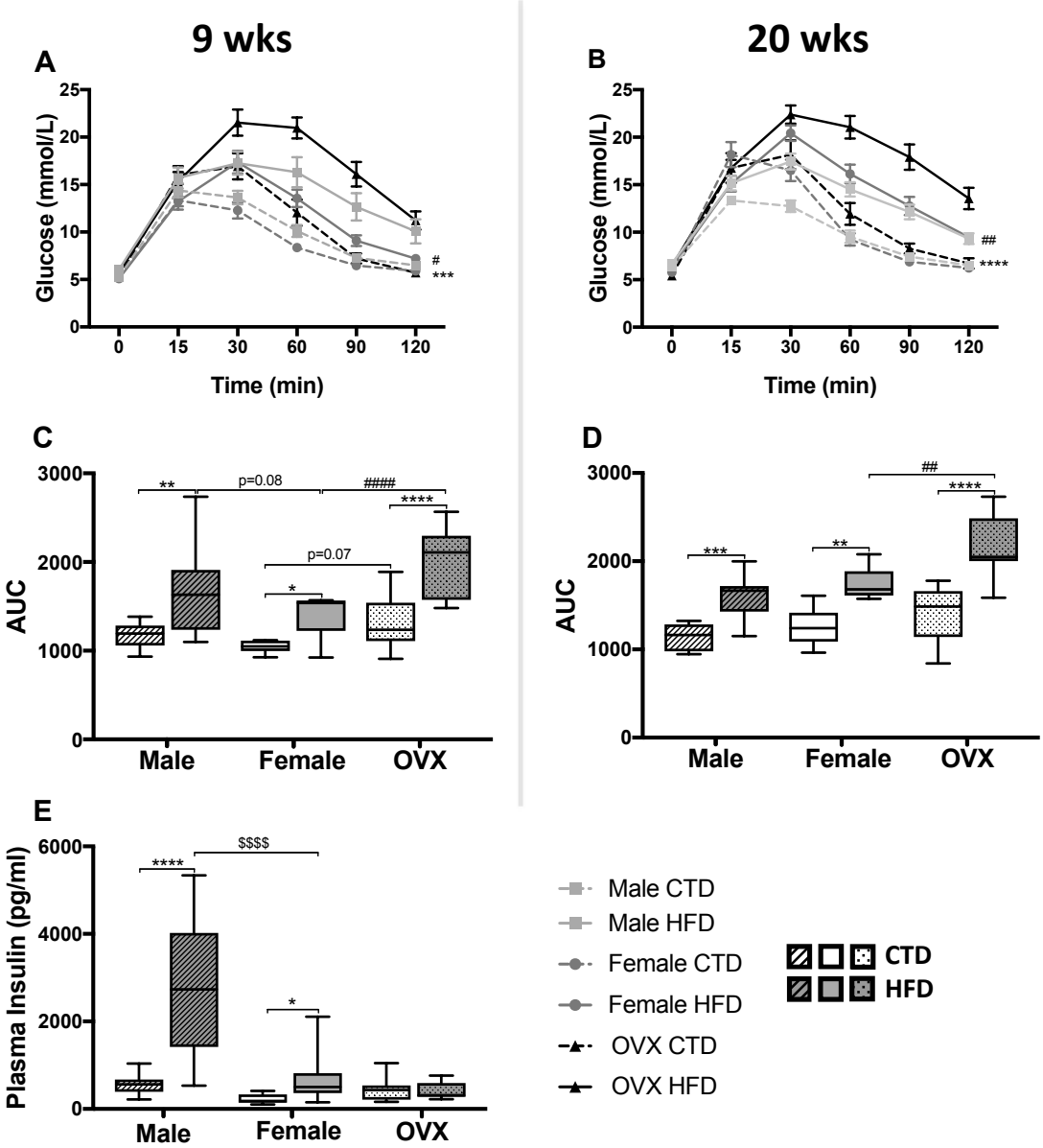

Figure 15: Systemic glucose clearance assessed by glucose tolerance tests at 9 and 20 wks of diet in male, female and OVX mice.

A, B: glucose tolerance tests were performed after 6h of fasting. Glucose clearance was followed prior and 120 min after i.p. glucose injection; C, D: the "area under the curve" (AUC) of A and B was calculated using the trapezoid method; E: plasma insulin was measured as described in the methods section. Results are presented with the median, whiskers show the min and max values (C, D, E), and mean ± SEM (A,B). * symbol corresponds to CTD vs HFD, # symbol corresponds to OVX vs sham, $ symbol corresponds to male vs female; N=18-25.

3.3 Analysis of glucose tolerance and plasma insulin levels

At 9 and 20 wks of CTD- or HFD-feeding, we performed the glucose tolerance test (GTT) to assess the efficiency of systemic glucose clearance in the different groups (Figure 15). The GTT evaluates the body's capability to metabolize glucose and the ability of the liver to store excess glucose as glycogen. After i.p. injection of glucose, its concentration was measured at multiple timepoints (Figure 15A, B). The resulting curve shows the relationship

between glucose concentration and time and is used to calculate the "area under the curve" (AUC) as a measure of glucose clearance (Figure 15C, D). At 9 wks, HFD increased the AUC values in all groups (Figure 15C), indicating decreased glucose tolerance compared to CTD, and this effect was similar at 20 wks (Figure 15D). The effect of HFD feeding was stronger in OVX-females (1.54-fold at 9 and 20 wks) than in sham-females (1.34-fold and 1.38-fold at 9 and 20 wks, respectively). Consistently, the AUC was 1.44- and 1.24-fold higher in OVX- than in sham-females after HFD at 9 wks ($p<0.0001$) and 20 wks and ($p=0.034$) respectively, indicating a role for the ovarian hormones. The effect of OVX after CTD was smaller compared with the HFD feeding. Thus, at 9 wks of diet the OVX-females had a slightly higher AUC than the sham-females ($p=0.07$), whereas at 20 wks there was no effect. No differences were observed between the sham-female and the male mice. The glucose tolerance was reduced by OVX despite equal amounts of adipose tissue in the OVX- and sham-female mice. As it is thought that inflammatory cytokines released from fat (adipokines) may participate in the onset of glucose intolerance, these data suggest that the glucose intolerance observed in the OVX-HFD mice may be independent of adipokines. Inversely, when the mice are fed with CTD, the OVX mice do not exhibit a higher AUC despite an increased fat mass, strengthening the fact that there is no correlation between visceral fat mass and glucose tolerance measured with the GTT method. In conclusion, our data demonstrate that OVX decreases glucose tolerance in HFD-fed female mice and that this effect is most likely independent of the amount of adipose tissue. In our earlier work, we observed similar effects of OVX already at 3 wks of feeding (data not shown).

Fasting glucose concentrations were not changed by HFD in any of our experimental groups, proving that our mice were not yet diabetic at this stage. The difference appeared only at the glucose clearance level after a glucose load, suggesting that after 20 wks of diet the HFD-fed mice and in particular the OVX mice are pre-diabetic. To further investigate this, we analyzed plasma insulin levels. At 22 wks, the mice were sacrificed in the fasted state and blood was collected to measure insulin by ELISA (Figure 15E). Female, OVX-female and male mice were not different after CTD feeding. However, HFD strongly increased the insulin concentration in the male group, indeed, a 5-fold increase was measured compared to CTD ($p<0.0001$). After HFD, the male mice had much higher insulin levels than the sham-female mice. HFD also increased plasma insulin in the sham-females, but the effect (2.9-fold increase) was much smaller than in the males. In contrast, no effect of HFD was visible in the OVX group. In conclusion, 22 wks of HFD feeding rendered the male mice highly hyperinsulemic to attempt to compensate for their insulin resistance. The effect was much weaker in the sham-females and completely absent in the OVX-females, suggesting that these groups are less and not insulin-resistant at all, respectively.

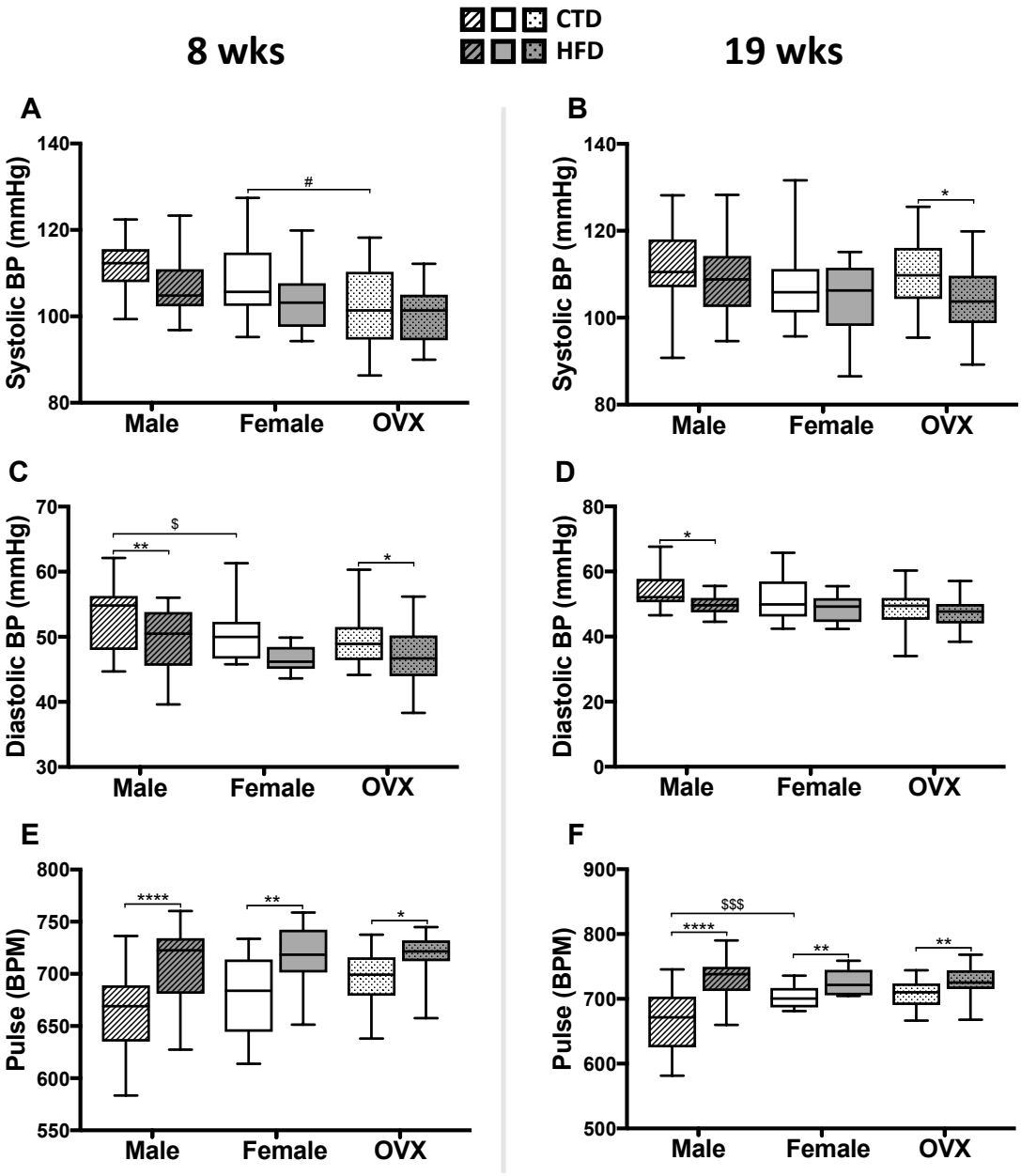

Figure 16: Blood pressure and heart pulse measurements using the tail-cuff method at 8 and 19 wks of diet in male, female and OVX mice.

A, B: systolic blood pressure (BP); C, D: diastolic blood pressure; E, F: heart pulse. Results are presented with the median, whiskers show the min and max values. * symbol corresponds to CTD vs HFD, # symbol corresponds to OVX vs sham, $ symbol corresponds to male vs female. N=14-26

3.4 Blood pressure and pulse measurements

In human, estrogen is known to regulate blood pressure via endothelial[347] and vascular smooth muscle cells.[348] However, in rodent models, blood pressure changes have not been observed in estrogen-deficient states.[349-352] Since blood pressure may influence cardiac functional parameters and hypertrophy, we verified blood pressures at baseline, 8 and 19 wks of feeding, using the non-invasive tail-cuff method. At 8 wks of CTD, OVX mice had lower systolic blood pressures (SBP) than sham-female mice. At 19 wks, HFD decreased the SBP compared with CTD, an effect that was observed only in the OVX mice (Figure 16A, B). Additionally, HFD reduced diastolic blood pressures (DBP) in male mice at both time points and in OVX-female mice at 8 wks of diet (Figure 16C, D). The CTD-fed males had a higher DBP than the diet-matched sham-females at 8 wks. HFD increased the pulse rate in all groups at both timepoints (Figure 16E, F). Moreover, the male fed with CTD had a lower pulse rate than the sham-female at later stage. Therefore, HFD increased the heart rate in all groups, whereas it decreased the diastolic blood pressure in the male mice only, identifying a gender-specific effect.

3.5 Echocardiography

We used echocardiography as non-invasive method to assess cardiac geometry and function. Images were acquired in the parasternal long and short axis view in B-mode and M-mode. Mitral annulus velocity and mitral valve blood flow were assessed by tissue Doppler and pulsed-wave Doppler, respectively. At baseline, none of the parameters obtained by echocardiography were different between the experimental groups (Supplement, Table SIII). Table I (p.86) shows the data recorded after 21 wks of diet. The LV free wall thickness, LV internal diameter, LV mass, FS and E/E' ratio were not affected by gender, OVX or diet. Also, the ejection fraction (EF), which is the percentage of total blood pumped out of the left ventricle during each cardiac cycle, stayed unchanged between the experimental groups.

The parameters that showed significant changes are shown in Figure 17. Importantly, cardiac geometry was altered in some groups. Notably, in the sham-female group, the HFD increased the relative wall thickness during diastole (+9.3%) compared with the CTD group (Figure 17A). The LV posterior wall was also slightly increased by the HFD in the sham-female group (2-way ANOVA p=0.02, post-hoc p=0.06) (Figure 17B). These results suggest that the sham-female mice start to develop cardiac remodeling. Moreover, the HFD increased the LV anterior wall thickness during diastole in the OVX-group, where the effect

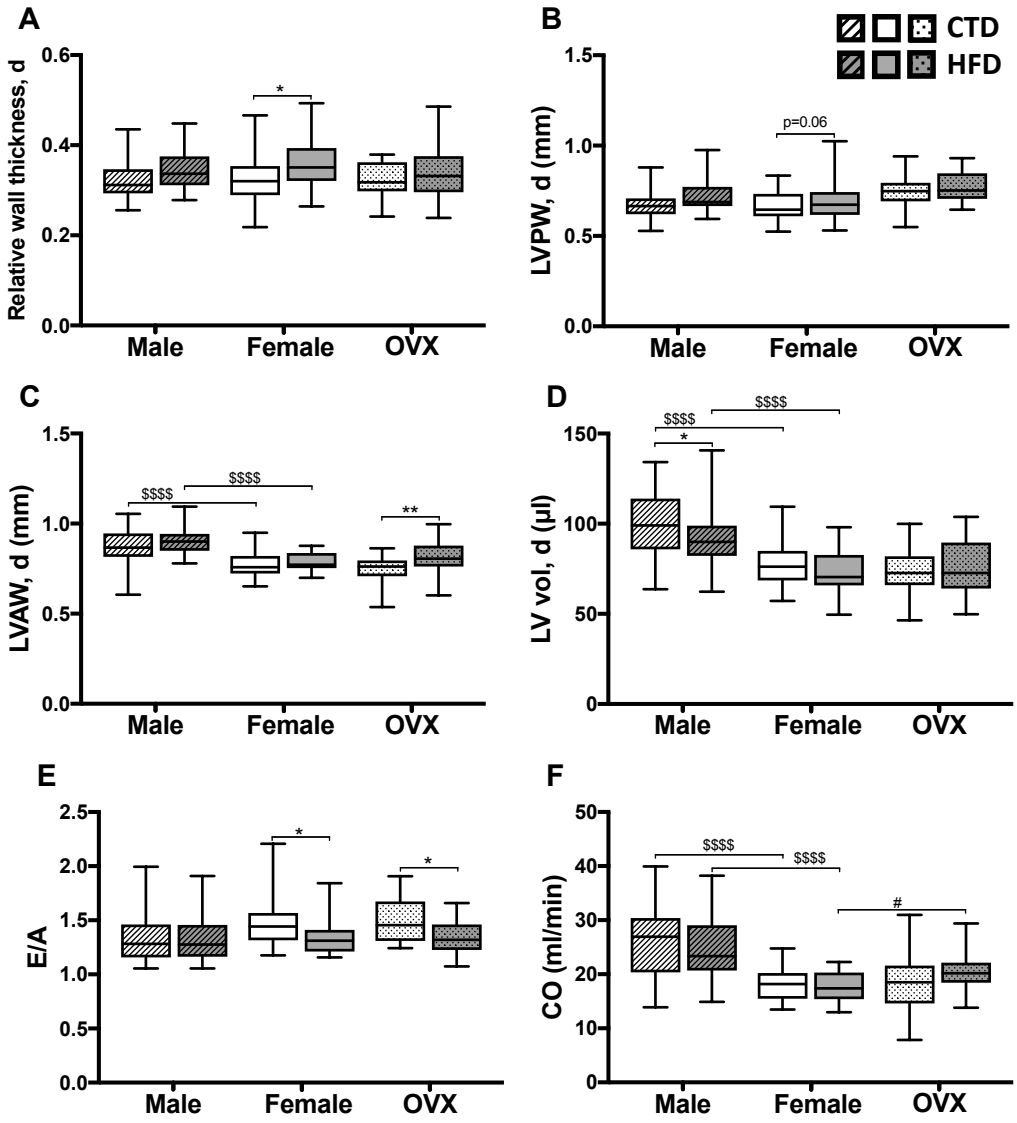

Figure 17: Echocardiographic parameters of male, female and OVX mice evaluated after 21 wks of diet.

A: relative wall thickness during diastole; B: left ventricle anterior wall (LVAW) thickness during diastole; C: left ventricle posterior wall (LVPW) during diastole; D: left ventricle volume (LV vol, d) during diastole; E: E/A ratio, E represents the velocity of the mitral blood flow at early stage and A at late stage; F: cardiac output. Results are presented with the median, whiskers show the min and max values. * symbol corresponds to CTD vs HFD, # symbol corresponds to OVX vs sham, $ symbol corresponds to male vs female. N=22-32.

of HFD was clearly more pronounced than in the other groups (Figure 17C). The HFD had another effect specific to the male mice. Indeed, the LV volume at diastole is lower in the male group after HFD feeding (Figure 17D). Thus, the LV of the HFD-fed males is not able to fill with the same volume of blood as in the CTD-fed males. This observation suggests that the hearts of the HFD-fed male mice present a reduced capability to distend during diastole, which could be linked to a less compliant LV or alternatively, could be the consequence of a beginning concentric hypertrophy that is not detectable yet.

Interestingly, HFD feeding caused a decrease in the E/A ratio in the sham and OVX-female mice (Figure 17E). The E in the E/A ratio corresponds to the E-wave measured by Doppler, which is the peaking of blood velocity in early diastole during the initial filling of the LV after the mitral valve opens. At the end-diastole, the atrium contracts creating the final filling stage of the LV, this is the late filling A-wave. The E/A ratio is therefore used to assess diastolic function. A stiffer LV could be at the origin of a decreased E/A ratio since the LV pressure at the end diastole would increase, slowing down the early filling. On the other hand, the late filling A could also be impaired and increased as a consequence of a stiffer LV walls. A decrease in the E/A ratio can be translated as a decrease of the blood flow velocity during the early filling due to a stiffer heart, which induces an increase of pressure. Our data therefore suggest a defect in diastolic function in the female mice when fed with HFD whereas the males are not affected, pointing to the presence of a gender-specific effect.

Finally, our echocardiographic analysis also revealed that the cardiac output was increased after HFD in the OVX-female compared with the sham-female mice (Figure 17F). The cardiac output is the volume of blood ejected by the heart per minute. Although this effect was small, our results indicate that hearts from OVX mice expel a higher volume of blood per minute than the sham-female mice despite a similar body weight. Moreover, the male mice have a higher CO than the female, as the ejected volume necessary to properly perfuse the organs is higher.

3.6 Pressure-volume loop analysis

Very few studies evaluated gender differences in cardiac hemodynamics after high fat feeding and described the effect of ovariectomy in this context. In our study, we analyzed the influence of diet, gender and ovarian hormones on cardiac hemodynamic function by the pressure-volume loop (PVL) technique. The PVL technique is the gold standard method to accurately measure real-time pressure and volume in the ventricle. To induce an additional stress to the heart, we infused the β-adrenergic agonist dobutamine, which normally increases contractility and heart rate enhancing the energy demand thereby mimicking physical exercise. Table II (p.90) shows the results at baseline without dobutamine infusion, whereas Table S IV shows the results at the highest dobutamine concentration. Most hemodynamic parameters were neither influenced by the diet, nor by the gender or ovariectomy. Concretely, the minimal and maximal pressure, end-systolic pressure, the relaxation constant Tau, and the rate of pressure development and decline (dP/dt max and dP/dt min, respectively) were not changed. Some significant changes were found and will be described in detail hereafter (Figures 18-19).

Table I: Echocardiographic parameters of male, female and OVX mice fed with CTD or HFD for 21 wks.

	MALE		FEMALE		OVX	
Echocardiography, 21 wks of diet	CTD (*n* =28)	HFD (*n* =28)	CTD (*n* =27)	HFD (*n* =22)	CTD (*n* =27)	HFD (*n* = 32)
Heart rate (beats/min)	518±50	529±63	495±40	498±37	502±57	507±42
Left ventricular anteroseptal wall thickness (mm)						
diastole	0.87±0.09	0.90±0.07	0.77±0.07	0.80±0.07	**0.74±0.07**	**0.81±0.09***
systole	1.24±0.16	1.27±0.11	1.10±0.13	1.11±0.12	1.06±0.12	1.14±0.14
Left ventricular free wall thickness (mm)						
diastole	0.74±0.08	0.77±0.08	0.66±0.07	0.72±0.09	0.66±0.07	0.68±0.1
systole	1.04±0.13	1.08±0.16	0.95±0.14	1±0.16	0.97±0.15	1.01±0.15
Left ventricular internal diameter (mm)						
diastole	4.65±0.36	4.47±0.32	4.15±0.26	4.03±0.27	4.10±0.29	4.11±0.33
systole	3.53±0.38	3.33±0.34	3.12±0.34	3.01±0.37	3.04±0.31	3.01±0.42
Relative wall thickness, d						
diastole	0.32±0.04	0.34±0.04	**0.32±0.05**	**0.359±0.06***	0.32±0.03	0.33±0.06
systole	0.59±0.12	0.66±0.15	0.62±0.15	0.68±0.18	0.64±0.14	0.69±0.18
Ejection fraction (%)	47.9±7.11	50±6.72	49.45±8.47	50.5±8.72	50.6±8.97	52.8±8.58
Fraction of shortening (%)	24.2±4.34	25.4±4.27	24.97±5.22	25.6±5.37	25.6±5.48	27.05±5.51
Cardiac Output (ml/min)	25.4±1.15	24.7±1.03	18.32±0.62	**17.67±0.544**	18.956±1.083	**20.15±0.58**$^{\#}$
Left ventricular Volume (µl)						
diastole	**101±0.09**	**91.7±3.04***	77.05±2.28	72.04±2.46	74.83±2.45	75.7±2.59
systole	53±2.51	46.1±2.07	29.28±2	36.22±2.34	36.95±1.80	36.47±2.13
E/A	1.36±0.26	1.34±0.24	1.48±0.24	1.35±0.18	**1.48±0.19**	**1.34±0.14***
E/E'	20±1.38	19.5±1.17	19.3±1.14	19.32±1.32	21.37±1.32	18.71±0.82
Deceleration (mm/s^2)	-27192±1262	-23307±902	**-31155±2077**	**-23858±1484****	-26765±1208	-26387±1074
Body weight (g)	**33.1±2.84***	**47.1±4.1***	**26.2±5.52***	**33.9±5.8***	**27.57±4***	**39.43±5.34***$^{\#}$

* Symbol corresponds to CTD vs HFD, # symbol corresponds to OVX vs sham, $ symbol corresponds to male vs female.

First of all, heart rates were somewhat different between the groups at baseline (p=ns). Heart rates were increased upon administration of increasing doses of dobutamine in all groups independently from the diet, as expected (Supplement, Figure S II).

The end-diastolic pressure (Ped) was affected by the HFD in the sham-female group. Indeed, the HFD-fed sham-female mice had lower end-diastolic pressures than the corresponding CTD-fed mice at baseline (Figure 18A) and at all dobutamine concentrations (Figure 19A shows the highest concentration). In contrast, the OVX-female as well as male mice exhibited similar pressures when fed with CTD or HFD (Figure 18A). Interestingly, the sham-female mice presented slightly higher Ped values than the OVX-females when fed the CTD (p=0.1). As at the highest dose of dobutamine the sham-female but not the OVX-female mice decreased their Ped in response to HFD, the sham-female mice had significantly lower pressures than the OVX mice under these stress conditions (Figure 19A).

Other hemodynamic parameters affected were the peak emptying and filling rates, dV/dt min and dV/dt max, respectively. Both were decreased in the male after HFD compared to CTD at baseline (Figure 18B, C) and at the highest dose of dobutamine (Figure 19B, C). These effects of HFD were not observed in the females with or without OVX. Moreover, these parameters were lower in female mice compared with male mice after CTD feeding, indicating a gender difference. The peak-filling rate is normally reached shortly after opening of the mitral valves whereas the peak-emptying rate happens when the LV contracts actively. This observation therefore suggests that HFD reduces the contraction and relaxation velocity in the male group.

The end-systolic pressure-volume relationship (ESPVR) is the relationship between the LV pressure and the volume when the heart reaches its maximum contraction. This parameter gives an estimation of cardiac contractility capability as it describes how much pressure is developed for a certain volume to be ejected. For example, when the ESPVR is increased (steeper slope) the heart builds more pressure to pump out a certain amount of blood, and this indicates an increased contractility. This value was not altered by diet or gender at baseline and at the maximal infusion of dobutamine (Figure 18D and 19D). A small gender difference was observed in the hearts from HFD-fed mice, with the females having higher values that the males (p=0.059) at high dobutamine concentrations. As for the end-diastolic pressure-volume relationship (EDPVR), which characterizes the compliance of the heart: at baseline the HFD tended to increase it in the OVX group (Figure 18E, p=0.08), suggestive of a less stiff or a more dilated heart. On the other hand, after dobutamine infusion the compliance was not affected by gender, OVX or diet (Figure 19E). To summarize, HFD

decreases emptying and filling peak rates only in male mice, suggesting that male hearts need more time to relax and contract and are more susceptible to this diet-induced effect than female hearts. On the other hand, HFD decreases end-diastolic pressures in sham-female and not in the OVX-female mice, whereas after dobutamine stress HFD-fed OVX mice have higher end-diastolic pressures than sham-female mice.

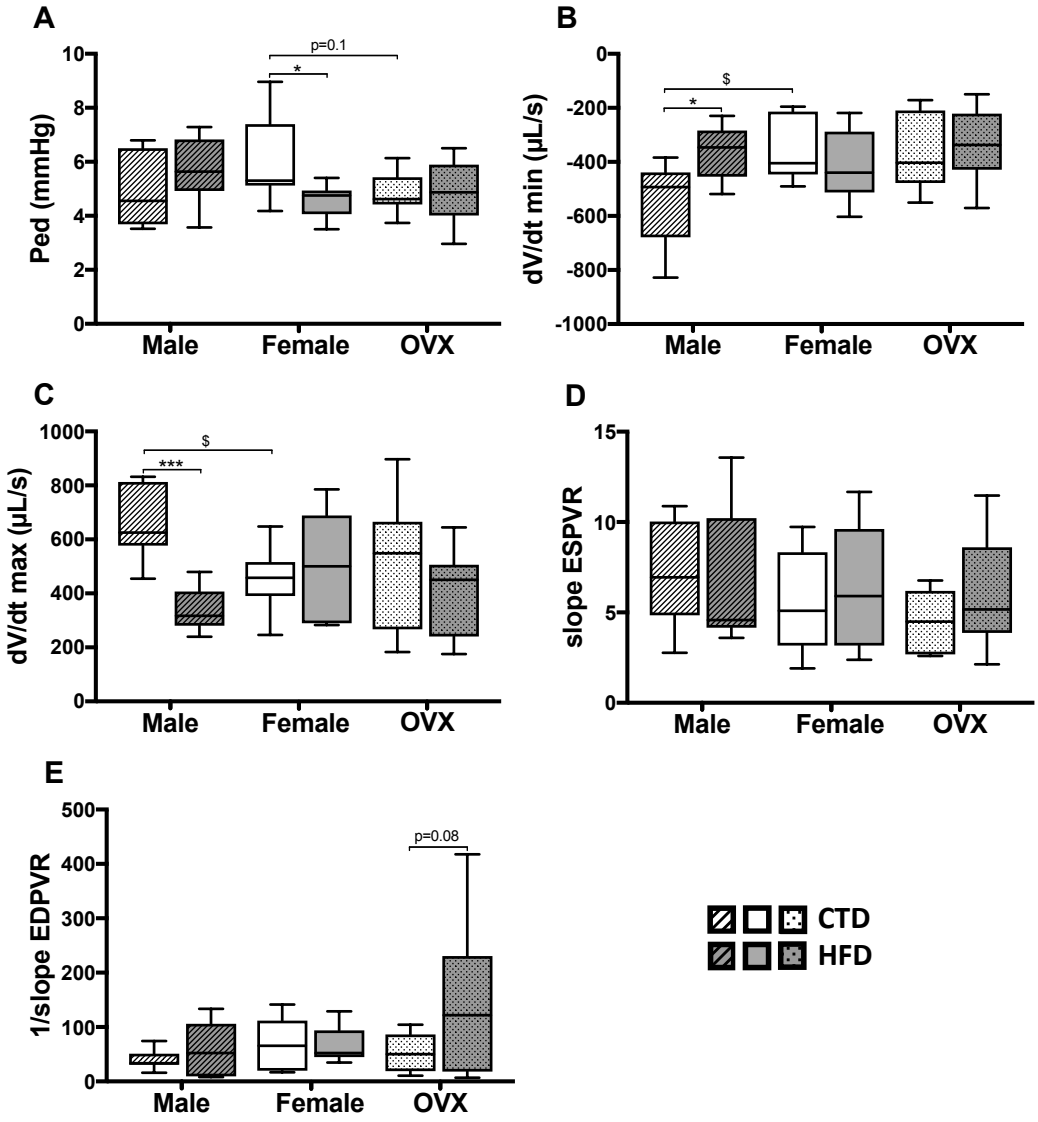

Figure 18: Baseline LV hemodynamic parameters recorded with PVL method in male, female and OVX mice fed with CTD or HFD for 22 wks.

A: end-diastolic pressure (Ped); B: dV/dt min is the emptying peak rate; C: dV/dt max is the filling peak rate; D: the slope of the end-systolic pressure-volume relationship (ESPVR) is a measure of contractility; E: the 1/slope end-diastolic pressure-volume relationship (EDPVR) is a measure of compliance. Results are presented with the median, whiskers show the min and max values. * symbol corresponds to CTD vs HFD, # symbol corresponds to OVX vs sham, $ symbol corresponds to male vs female. N=7-11.

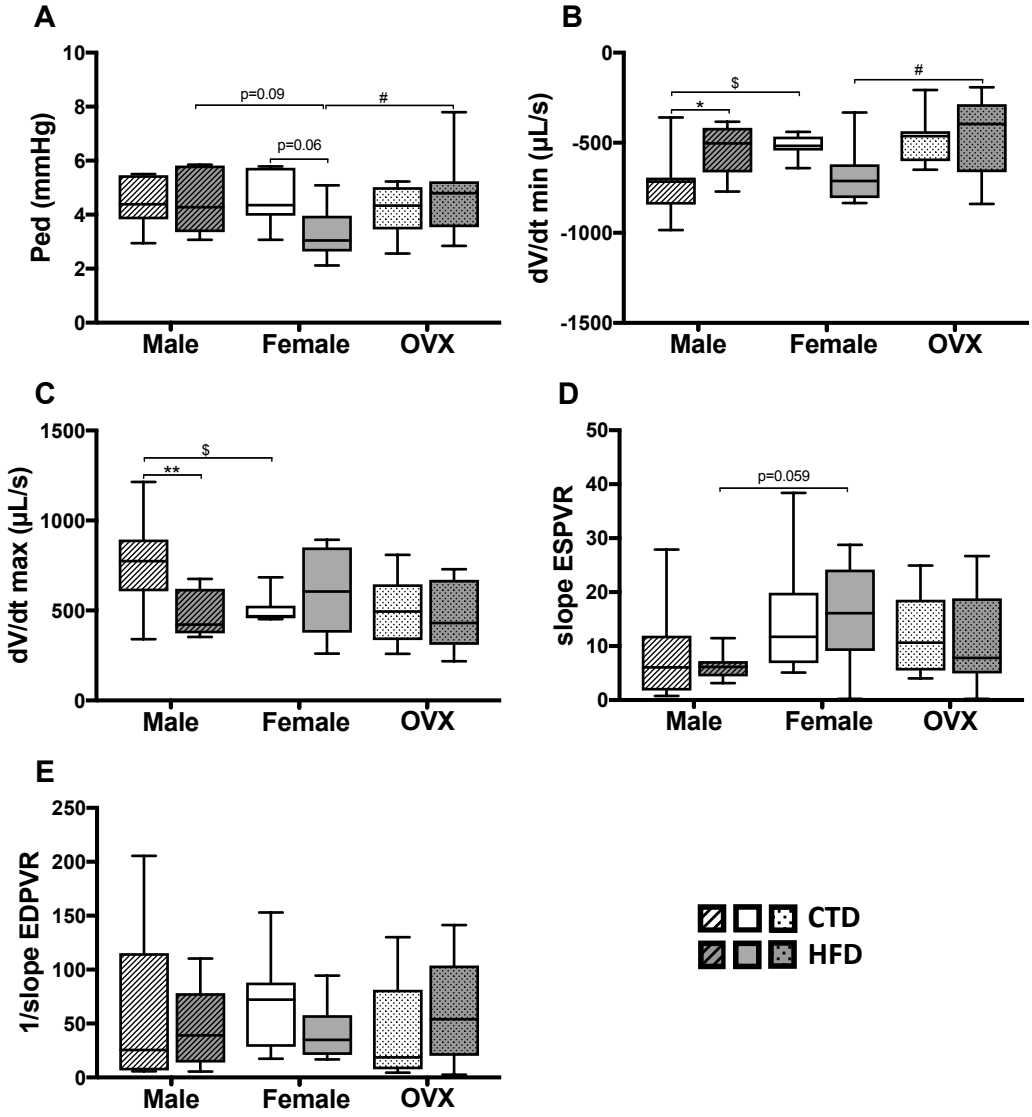

Figure 19: Hemodynamic parameters of male, female and OVX mice recorded with the PVL method after 21 wks of diet with maximal dobutamine infusion.

A: end-diastolic pressure (Ped); B: dV/dt min is the emptying peak rate; C:dV/dt max is the filling peak rate; D: the slope end-systolic pressure-volume relationship (ESPVR) is a measure of contractility; E: the 1/slope end-diastolic pressure-volume relationship (EDPVR) is a measure of compliance. Results are presented with the median, whiskers show the min and max values. * symbol corresponds to CTD vs HFD, # symbol corresponds to OVX vs sham, $ symbol corresponds to male vs female. N=7-11.

Table II: Baseline LV hemodynamic parameters of male, female, and OVX mice recorded with the PV loop method after 21 wks of diet of CTD and HFD.

	Male		Female		OVX	
LV Hemodynamics, Baseline	CTD (*n* =8)	HFD (*n* =8)	CTD (*n* =8)	HFD (*n* =7)	CTD (*n* =8)	HFD (*n* = 9)
Heart rate (beats/min)	527±13	478±19	438±24	485±17	468±21	480±7
Volume (µl)						
End-diastole, Ved	19.5±2.14	15.9±2.43	16.8±2.25	14±1.96	14.2±1.98	14.1±2.5
End-systole, Ves	7.98±0.88	7.78±0.86	8.79±1.52	5.41±1.08	6.51±1.46	6.16±1.62
Minimum Volume, Vmin	7.55±0.88	8.9±1.75	8.78±1.65	5.07±0.99	6.12±1.36	5.83±1.31
Maximal Volume, Vmax	20.2±2.08	16.9±2.28	18.2±2.44	15.3±1.99	15.5±1.96	14.6±2.14
Pressure (mmHg)						
End-diastole, Ped	5.07±0.5	5.67±0.46	6.04±0.62	4.56±0.23	4.85±0.3	4.82±0.35
End-systole, Pes	71.7±5.07	71.6±4.36	65.6±5.02	60±4.4	70.8±3.83	68.5±3.82
Minimum Pressure, Pmin	2.16±0.64	3.37±1.1	3.85±0.54	2.41±0.28	2.12±0.51	2.26±0.31
Maximum Pressure, Pmax	79.4±4.94	78.6±4.87	73.3±4.68	71.2±3.7	78.6±4.83	77±3.7
Peak rate (µL/sec)						
Filling, dV/dt max	**662±47.5$**	**338±28.2*** **	449±47.5	509±78.46	516±84.2	403±44.7
Emptying, dV/dt min	**-544±54.2$**	**-366±35.7***	-354±45.4	-419±49.6	-369±49.4	-339±40.9
Rate of pressure (mmHg/sec)						
Development, dP/dt max	7553±738	6724±946	5580±790	6006±708	7932±1216	6986±670
Decline, dP/dt min	-7086±669	-5716±750	-5556±960	-5426±720	-6863±1015	-5820±578
Time constant of isovolumic relaxation, Tau (msec)	9.41±1.03	11.1±1.67	12.7±1.42	12.5±2.4	10.1±1.47	9.96±0.83
End-diastolic pressure-volume relationship (EDPVR), 1/slope	40.1±7.06	60.7±17.5	68.4±17.9	65.2±12.7	52.6±48.4	148±43.7
End-systolic pressure-volume relationship (ESPVR), slope	7.24±1.14	5.83±1.39	5.34±1.08	6.34±1.2	4.47±0.62	5.92±0.94

* symbol corresponds to CTD vs HFD, $ symbol corresponds to male vs female.

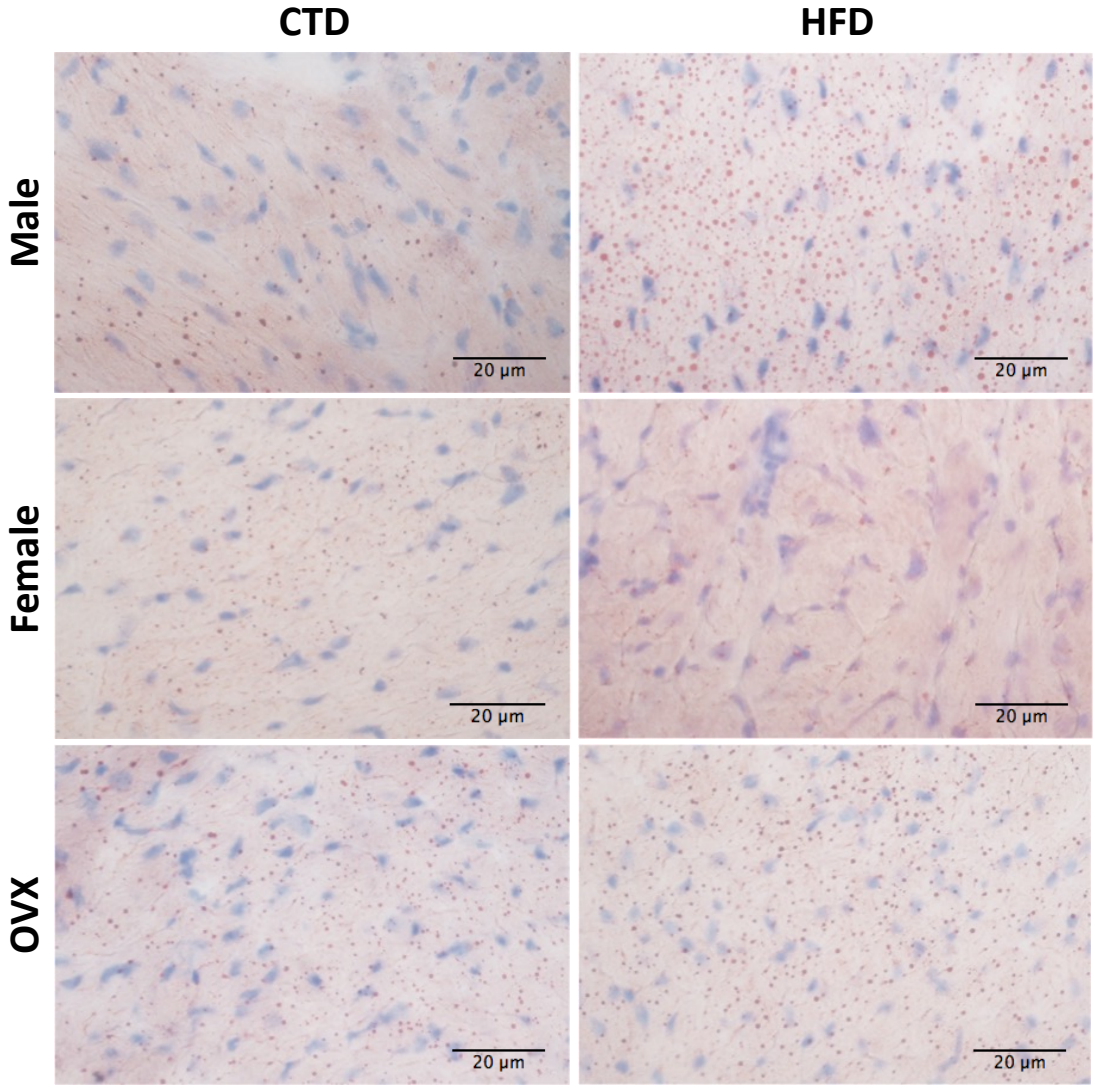

Figure 20: Oil Red O staining to detect neutral lipids on heart sections.
Cryosections of the hearts of male, female and OVX mice (sacrificed at 22 wks) were stained with Oil Red O to detect neutral lipids (red) and counterstained with hematoxylin to reveal nuclei (dark blue). A representative picture of each condition is shown. Magnification x40; N=3.

3.7 Analysis of cardiac lipid deposition and fibrosis

Long-term high fat diet feeding may lead to cardiac lipid accumulation and lipotoxicity, which contributes to cardiac dysfunction. To evaluate the impact of the diets that we used on cardiac lipids, Oil Red O staining was performed to reveal the neutral lipids (in red) (Figure 20). Our results showed that the HFD increased the number of droplets in the male, sham- and OVX-female mice. However, this increase was not equal in the 3 groups. Indeed, the accumulation of lipids induced by HFD was more pronounced in the male group where the droplets appeared numerous and of bigger size compared to the female groups. Moreover, the OVX-female mice have a higher number of droplets than the sham-female mice after HFD as well as CTD. These observations were confirmed by transmission electron microscopy (TEM, Supplement, Figure S III). Thus, the absence of ovarian hormones increases the accumulation of lipid droplets in the heart of females irrespective of the diet. In contrast, the males have larger lipid droplets than the females for both diets. It appears that under CTD conditions, the droplets are fewer in the male mice but an opposite effect was observed when fed with HFD. Along with our earlier observation of decreased filling and emptying LV rates, these data strengthen the view that males are more sensitive to HFD-induced cardiac effects than females. A quantification of the lipid droplets is still necessary to confirm the differences observed between conditions. A technical limitation for proper quantification is that the pictures from the Oil Red O staining present some dirt particles coming from the oil red O powder despite multiple filtrations steps. These small particles would fake the quantification, as they would be counted as lipid droplets.

As fibrosis is an important trigger for cardiac dysfunction development, we analyzed gene expression of collagen I and III in our cardiac tissues. These are the two collagen isoforms that participate in cardiac fibrosis and increase myocardial stiffness by contributing to a more elastic extracellular matrix.[353,354] Although small decreases of collagen I and III mRNA were observed in the HFD-fed OVX-females compared with the CTD group (Supplement, Figure S IVA, B), none of the differences reached significance. Increased ratios of type I to type III collagen have been reported in chronic congestive heart failure[355] and end-stage dilated cardiomyopathy.[356] This ratio was however not changed in our mouse model; only a slight increase was visible in the OVX-female mice (Supplement, Figure S IVC). To further investigate fibrosis, we performed Picrosirius Red staining (Figure 21). The results did not show any striking differences between the three groups. Nevertheless, the HFD seemed to increase the intensity of the staining in all groups. Figure 21 visualizes that the OVX-female mice have higher staining after CTD and that the HFD feeding enhances this effect. Thus, our results suggest that HFD increases the collagen content in the heart and that the absence of ovarian hormones by itself is increasing it as well. It also appeared that more

collagen fibers were detected in the male mice compared to the sham-female mice. These results still require a proper quantification and more mice need to be analyzed to draw conclusions. The Picrosirius Red pictures quantification was problematic, as the automatic quantification planned would not discriminate between collagen surrounding the vessels and the intercellular collagen fibers, which is of interest for evaluation of cardiac collagen content.

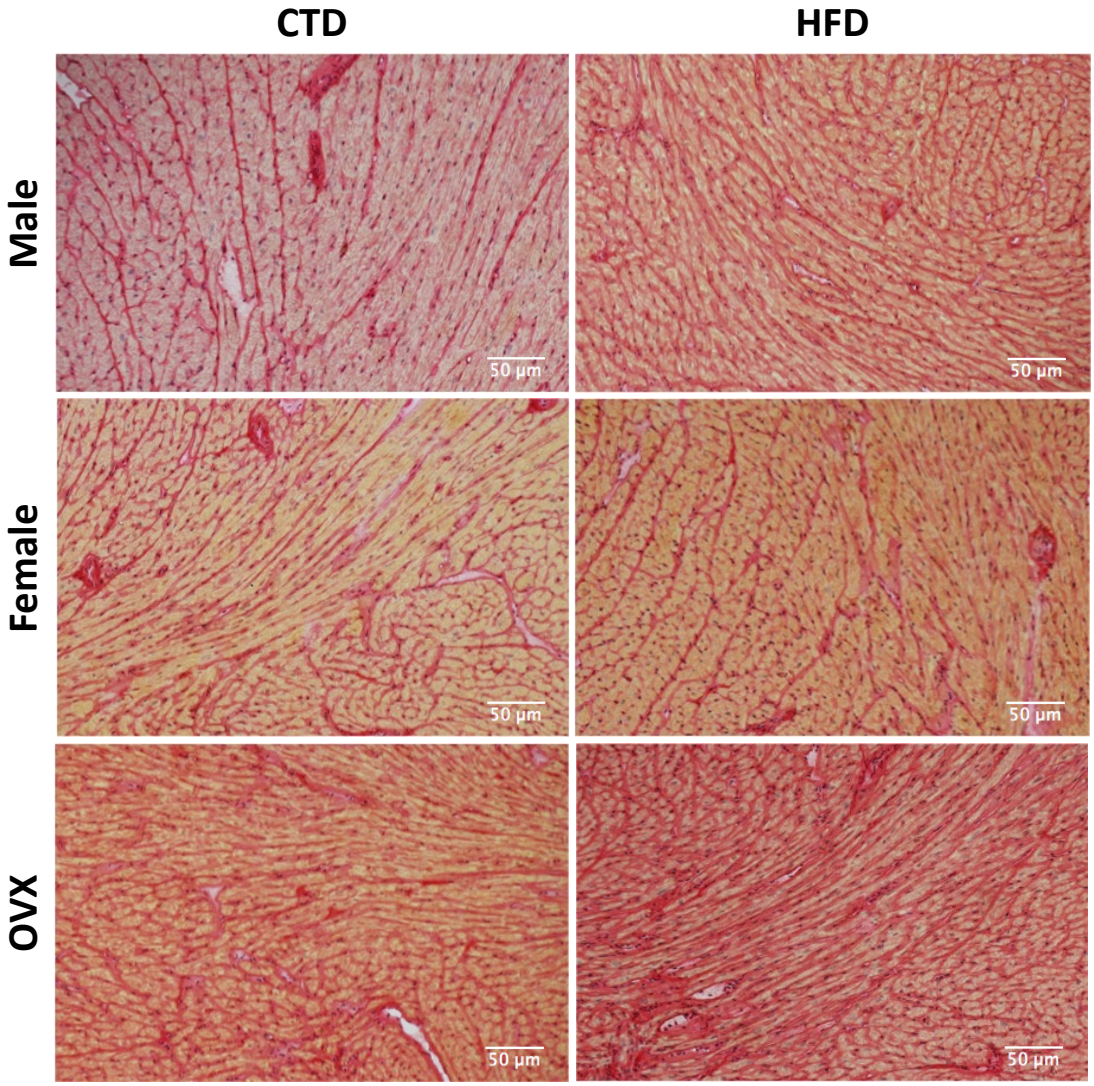

Figure 21: Picrosirius Red staining to detect collagen on heart sections.
Cryosections of the hearts of male, female and OVX mice (sacrificed at 22 wks) were stained with Picrosirius Red to detect collagen fibers (red). A representative picture of each condition is shown. Magnification x10; N=3.

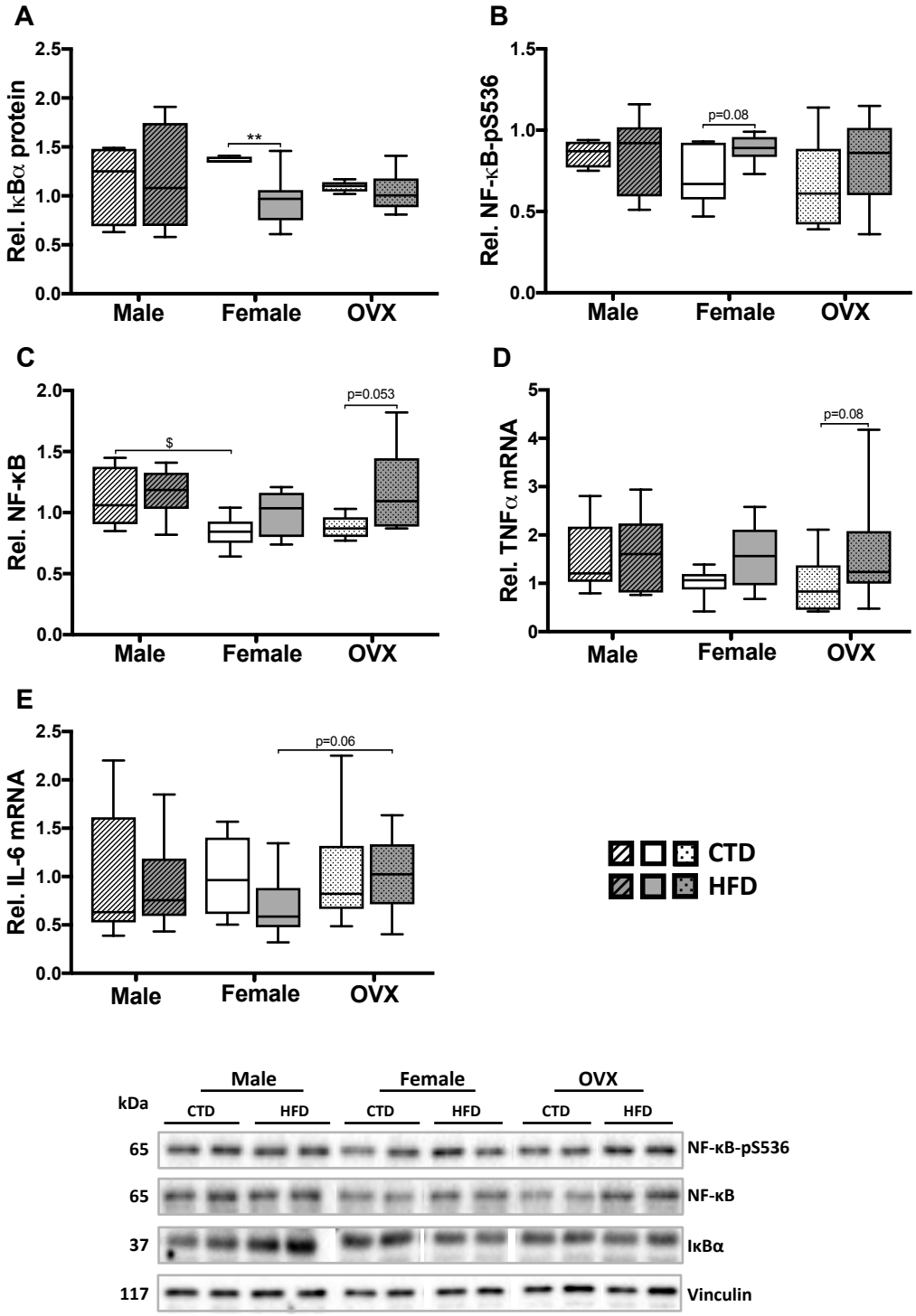

Figure 22: Quantitative real-time PCR and Western-blot analysis of genes and proteins involved in inflammation.

Cardiac muscles from male, female and OVX mice fed with CTD or HFD for 22 wks were used to extract mRNA and protein to evaluate genes and proteins involved in inflammation. Representative examples of Western blots (bottom) and quantification normalized to the corresponding control (top) are shown. The bands visible for each protein belong to the same membrane. A: N=5-7; B, C: N=6-8; D, E: N=8-10. Results are presented with the median, whiskers show the min and max values. * symbol corresponds to CTD vs HFD, # symbol corresponds to OVX vs sham, $ symbol corresponds to male vs female.

3.8 Inflammatory signaling molecules and cytokines

Inflammation is one of the first mechanisms that our organism sets up to defend against pathogens or other stress stimuli. Chronic inflammation can become deleterious and lead to irreversible fibrosis. The onset of this cellular mechanism is characteristic of hearts that in the long term may fail. We had hypothesized that chronic inflammation is present after HFD feeding, but we did not yet find any detectable effects on cardiac fibrosis at this stage. Indeed, we were not able to draw a strong conclusion about the Picrosirius Red staining (Figure 21), similarly collagen expression was not modified by the HFD (Supplement, Figure S IV).

To further evaluate whether diet, gender or ovarian hormones had any effect at all on cardiac inflammation, we analyzed relevant signaling molecules and pro-inflammatory cytokines at the protein or RNA level, including NF-κB, IκBα, TNFα, and IL-6. The protein NF-κB is an important regulator of inflammation. In the unstimulated state, NF-κB is sequestered in the cytoplasm by IκBα inhibitory proteins.[357,358] Upon stimulation by TNFα or other inflammatory signaling molecules, the kinase IKKB is activated and will phosphorylate IκBα, which in turn will release its inhibitory effect on NF-κB p65. The proteasome/ubiquitin pathway will degrade IκBα and NF-κB will migrate into the nucleus where it will activate the transcription of target proteins involved in inflammation,[359-361] such as TNFα.

Figure 22A shows that HFD decreased IκBα expression in the sham-female group ($p=0.0042$) and not in the OVX-female and male groups. It has been reported that upon stimulation with TNFα, NF-κB phosphorylation on the p65 subunit at S536 is increased resulting in the onset of the inflammation process.[362,363] We observed that HFD did not modify NF-κB protein expression although a slight increase was noticeable in the sham-female mice ($p=0.08$, Figure 22B). As for the total form of NF-κB, the sham-females had significantly lower levels than the males when fed with CTD ($p=0.019$), whereas HFD increased NF-κB in the OVX-female ($p=0.053$, Figure 22C).

We also evaluated the cardiac mRNA content of IL-6 and TNFα. Similar to NF-κB, HFD slightly enhanced the level of TNFα in the female groups ($p=0.018$, post-hoc: $p=0.18$ and $p=0.08$ for sham and OVX-female, respectively) (Figure 22D). IL-6 mRNA expression was not changed in our groups, only a slight increase was noticeable in the OVX-female compared to the sham-female mice after HFD feeding ($p=0.06$) (Figure 22E). Together, these observations indicate that female have lower expression of the inflammatory NF-κB than male mice and also that the HFD increases NF-κB and TNFα in the OVX-female mice,

suggesting that the absence of ovarian hormones could accentuate the inflammatory status after HFD.

Additionally, we performed an immunofluorescent staining of macrophages using Mac-2 antibody (Supplement, Figure S VI). We observed that HFD feeding increased macrophages densities in all groups with a more accentuated effect in the OVX-female and male group. Under CTD conditions, no striking differences were observed between the groups. A quantification of Mac-2 positive cells should still be done to reliably evaluate this sign of inflammation in our model. To further test potential differences in cardiac inflammatory responses, we stained cardiac cryosections for TGF-β1, an important player in inflammation, fibrosis and hypertrophy. As shown in Figure S VII, the TGF-β1 signal was homogenous and identically found in all conditions namely at the intercalated disks.

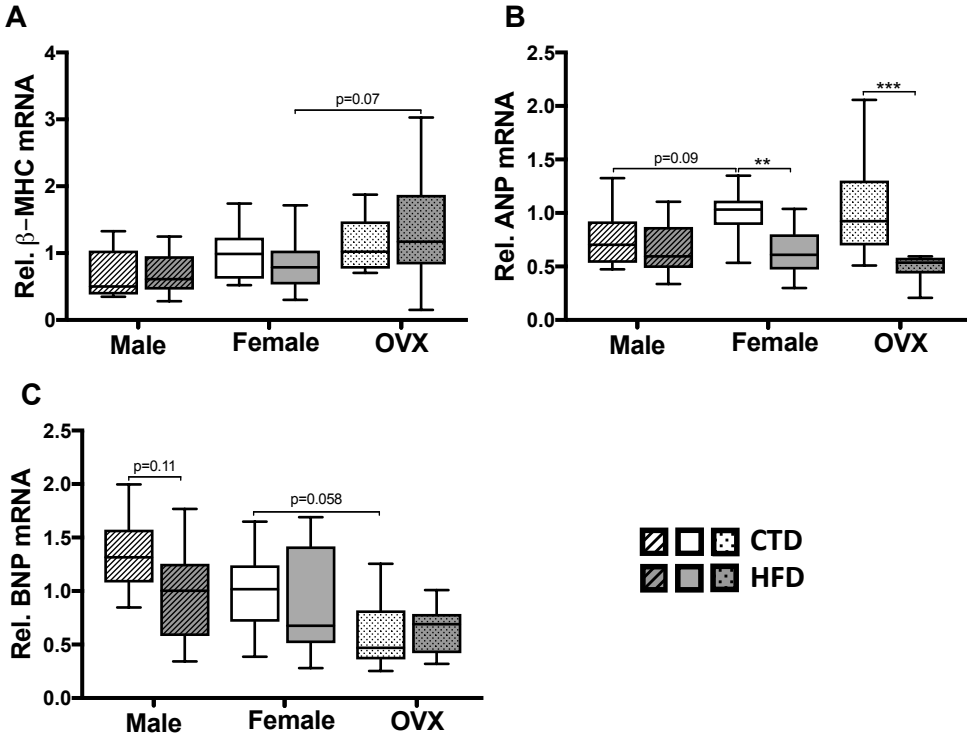

Figure 23: Quantitative real-time PCR analysis of genes involved in cardiac stress.
Cardiac muscles from male, female and OVX mice fed with CTD or HFD for 22 wks were used to extract mRNA evaluate genes involved in cardiac stress. Results are presented with the median, whiskers show the min and max values. * symbol corresponds to CTD vs HFD, # symbol corresponds to OVX vs sham, $ symbol corresponds to male vs female. N=8-10.

3.9 Stress markers

In a failing or hypertrophied heart certain cellular markers called stress markers are upregulated. For instance, a shift from the adult form of MHC, the α-MHC, toward the fetal form β-MHC, as well as increased levels of ANP and BNP, normally involved in arterial pressure reduction, have been described in heart failure. To evaluate the level of cardiac stress, we measured gene expression of β-MHC, ANP and BNP. Figure 23A shows that after HFD, OVX caused slightly higher β-MHC expression levels in females (p=0.07). Interestingly, ANP mRNA was decreased in both female groups after HFD, and the male had slightly lower ANP mRNA than the sham-female (p=0.09) under CTD conditions (Figure 23B). Furthermore, BNP mRNA showed a decrease due to the HFD in the male group (p=0.11) whereas the OVX- had lower BNP than the sham-female group (p=0.058, Figure 23C). We observed that the HFD is decreasing the stress marker ANP in female and BNP in male. A question that must to be asked is if these changes in mRNA expression are direct effects of the HFD and in this case HFD would have a positive effect by reducing these stress markers; or if these effects are a consequence of long-term HFD feeding, and what we observe is a compensatory effect aiming to decrease the level of the cardiac stress. In this regard, it would be interesting to test stress markers at an earlier time point.

3.10 Insulin/Akt/mTOR signaling pathways

With our mouse model, we aimed to mimic cardiometabolic disease and indeed, we observed specific alterations in cardiac geometry and function accompanied by systemic metabolic changes. The metabolic changes were induced primarily by the diet, and to a lesser extent by the absence of estrogen. The next question we wanted to answer is which cardiac molecular mechanisms are affected in our model. Multiple pathways are thought to be actively involved in the pathophysiology of cardiometabolic disease. Insulin-induced Akt/mTOR signaling has been implicated in glucose, lipid and protein metabolism. This pathway regulates different processes including autophagy, inflammation and fibrosis, each of which may contribute to cardiac failure in the long-term.

We analyzed different components of the insulin/Akt/mTOR pathway. IRS-1 is an important adapter protein that transmits the signal from insulin and IGF-1 receptors to PI3K/Akt. Different players interact with IRS-1 to regulate downstream signal transduction proteins. We found effects on total IRS-1 in our model as follows. OVX mice had lower total IRS-1 protein than sham-female mice when fed with CTD and HFD slightly increased IRS-1 protein in the OVX mice (Figure 24B). Notably, the HFD feeding increased IRS-1 protein in the male, the OVX-female, but not in the sham-female group. Consistently, sham-female mice had less IRS-1 protein than male after HFD (Figure 24B, p=0.0002).

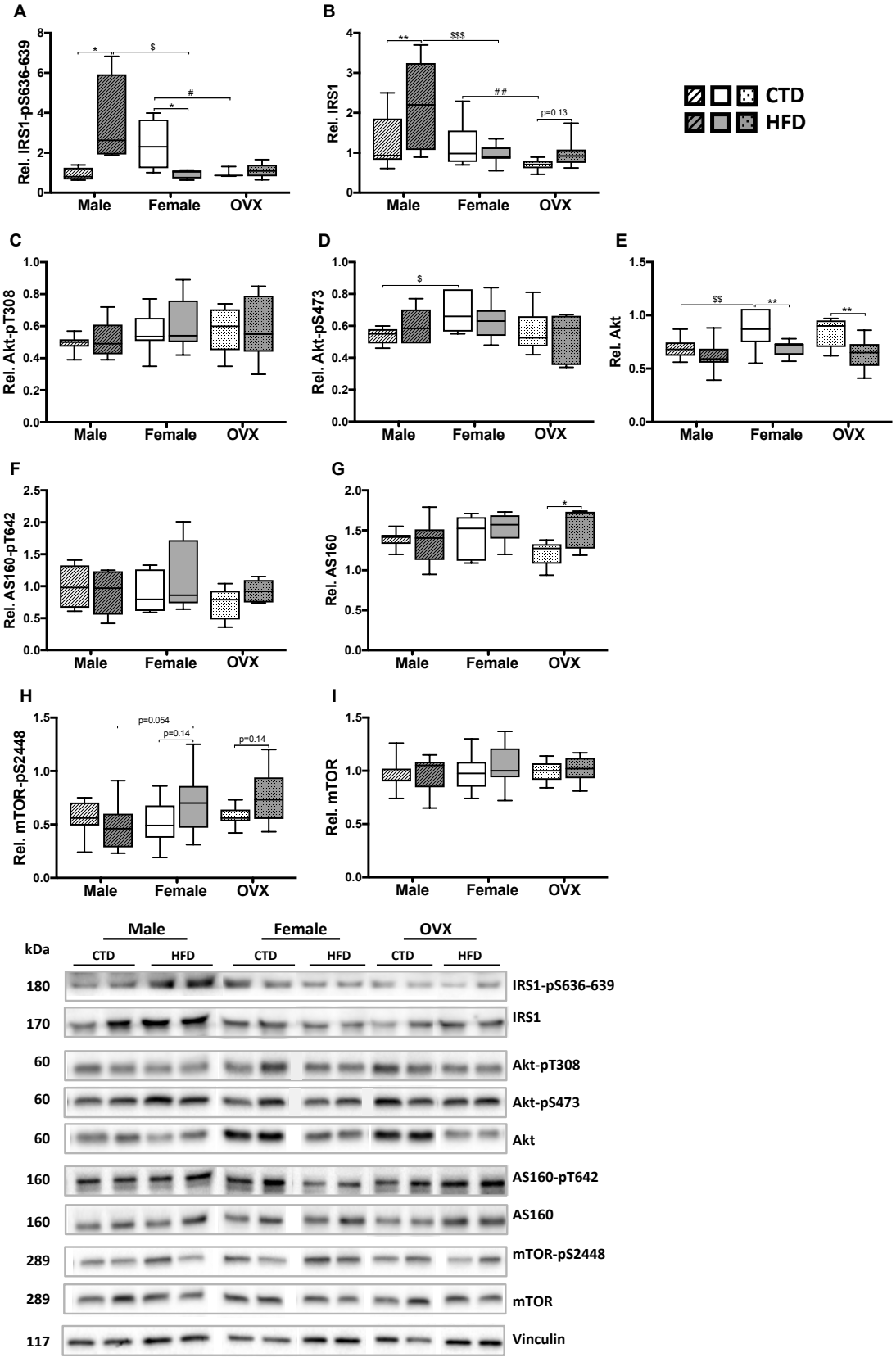

Figure 24: Western-blot analysis of the insulin/Akt/mTOR pathway (1).
Cardiac proteins from male, female and OVX mice fed with CTD or HFD for 22 wks were subjected to SDS-PAGE and probed with antibodies to proteins as indicated. Representative examples of Western blots (bottom) and quantification normalized to the corresponding control (top) are shown. The bands visible for each protein belong to the same membrane. Results are presented with the median, whiskers show the min and max values. * symbol corresponds to CTD vs HFD, # symbol corresponds to OVX vs sham, $ symbol corresponds to male vs female. N=9-12 (A: N=4-5).

Distinct phosphorylation sites on IRS-1 are known to have specific effects. mTOR/p70-S6K activation is key in PI3K/Akt signaling because it causes phosphorylates of IRS-1 at S636-639 to inhibit its activity and decrease Akt signaling as a negative feedback loop. A strong gender difference appeared here: in sham-female mice, HFD feeding decreased IRS-1 phosphorylation, whereas in male mice HFD had the inverse effect as it increased IRS-1 phosphorylation. Consistently, HFD-fed males had higher IRS-1-pS636-639 than sham-females. On the other hand, the sham-female had higher IRS-1-pS636-639 than the OVX-female mice under CTD conditions (Figure 24A).

Association of IRS-1 with the p85α domain of PI3-kinase leads, through PDK1, to activation of Akt. Figure 24C shows that despite the above-described differences in total IRS-1, phosphorylation of Akt at T308 stayed unchanged, suggesting that Akt activity is not altered in our experimental groups. Concerning Akt phosphorylation at the site S473, the female mice had higher phosphorylation of this site than the male mice after CTD feeding (Figure 24D). It is of note that overall the HFD decreased total Akt protein, although post-hoc testing did not reveal significance for the males ($p=0.2$). Moreover, male mice had lower Akt protein levels than both female groups when fed with CTD ($p=0.0015$) (Figure 24E).

To analyze whether the observed lower total Akt levels had consequences for its downstream targets we tested GSK3β (Supplement, Figure S VIIA and B). This protein is involved in apoptosis and glycogen metabolism by inhibiting glycogen synthase. Akt inhibits GSK3β activity by phosphorylating it at S9. HFD slightly increased GSK3β-pS9 in the female whereas no effects were observed in the male group. Total GSK3β followed the same pattern, as the HFD slightly increased it in both female groups ($p=0.12$, $p=0.18$ for the sham- and OVX-female, respectively), but did not affect it in the male group. Nonetheless, these effects did not reach statistical significance. Thus, the reduced Akt levels that we found in the HFD groups were not paralleled by reduced GSK3β phosphorylation, suggesting that this target of Akt is not playing a role in our model.

Another target of Akt is Akt substrate 160 (AS160). Upon insulin stimulation, AS160 is phosphorylated and triggers the translocation of the glucose transporter GLUT4 from the cytoplasm to the membrane to allow glucose entry into the cell and be processed during glycolysis. Figure 24F shows that AS160 phosphorylation at T642 is not affected in any of our experimental groups. In contrast, HFD increased total AS160 protein in the OVX-female group (Figure 24G), which could be linked to the observation that these mice have decreased IRS-1 and Akt protein, which both participate in the insulin pathway activity and lead to GLUT4 translocation through AS160. Our results suggest that AS160 is significantly

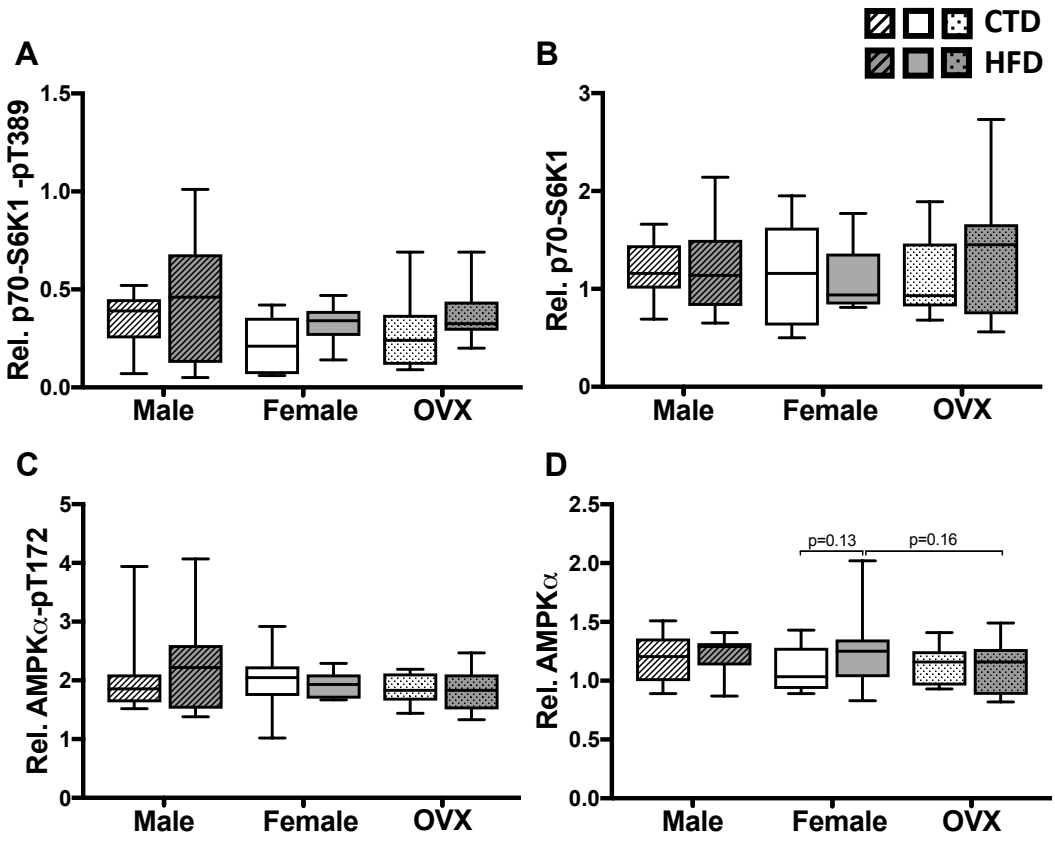

Figure 25: Western-blot analysis of the insulin/Akt/mTOR pathway (2).
Cardiac muscle proteins hearts from male, female and OVX mice fed with CTD or HFD for 22 wks were subjected to SDS-PAGE and probed with antibodies to protein involved in insulin/Akt/mTOR pathway. Results are presented with the median, whiskers show the min and max values. * symbol corresponds to CTD vs HFD, # symbol corresponds to OVX vs sham, $ symbol corresponds to male vs female. N=6-8.

increased to alleviate the decreases in IRS-1 and Akt (Figure 24G). However, unchanged phosphorylation of AS160 suggests that GLUT4 translocation to the membrane is not modified by OVX or gender-specific. GLUT4 mRNA was also not altered by HFD, gender, or estrogen (Supplement, Figure S VIIC).

mTOR is another protein regulated by Akt. It has an essential role in several primordial cellular mechanisms by regulating protein and lipid synthesis as well as autophagy, important in our experimental model. mTOR can undergo phosphorylation at different sites, Akt signaling leads to its phosphorylation at S2448, which activates it. The phosphorylation of this site appears increased by the HFD in both female groups (p=0.01, post-hoc: p=0.15) and decreased in the male (ns) (Figure 24H). The sham-female mice have slightly higher mTOR phosphorylation than the male after HFD (p=0.054). As for the total form of mTOR, it stayed unchanged (Figure 24I). Another phosphorylation site known for mTOR is S2481. In our experimental model, it was not affected by diet, hormonal status or gender (data not shown). We also analyzed p70-S6K1 as one of the downstream targets of mTOR implicated in protein synthesis. Figure 25A shows that its phosphorylation at T389 was increased after HFD (p=0.03 and p=0.08 in 2-way ANOVA for female and male respectively; post-hoc: ns). The effect was the strongest in female mice, in line with increased mTOR activation in the female following HFD feeding. However, total p70-S6K1 protein remained unchanged in all experimental groups (Figure 25B).

Finally, we also measured AMPKα as important regulator that controls cell metabolism in general. This essential protein is an energy sensor that inhibits the mTOR activation when the cell is low in energy (when the ATP/AMP ratio decreases). In other circumstances, it is activated by LKB1, a tumor suppressor that phosphorylates it at its T172 site. Its inhibitory effect on mTOR goes through the activation of the TSC1/TSC2 complex that inhibits mTORC1, but also via a direct inhibition of mTORC1.[364] Additionally, AMPKα is able to phosphorylate ULK1 to initiate its activation and promote autophagy. Our statistical analysis shows that phosphorylation of T172, the activity site of AMPKα, as well as total AMPKα protein were not modified by HFD, OVX or gender. Nevertheless, AMPKα total protein showed trends toward increased levels in the HFD-fed sham-female mice compared to CTD-fed female mice (p=0.13) and to the HFD-fed OVX mice (p=0.16). (Figure 25C, D).

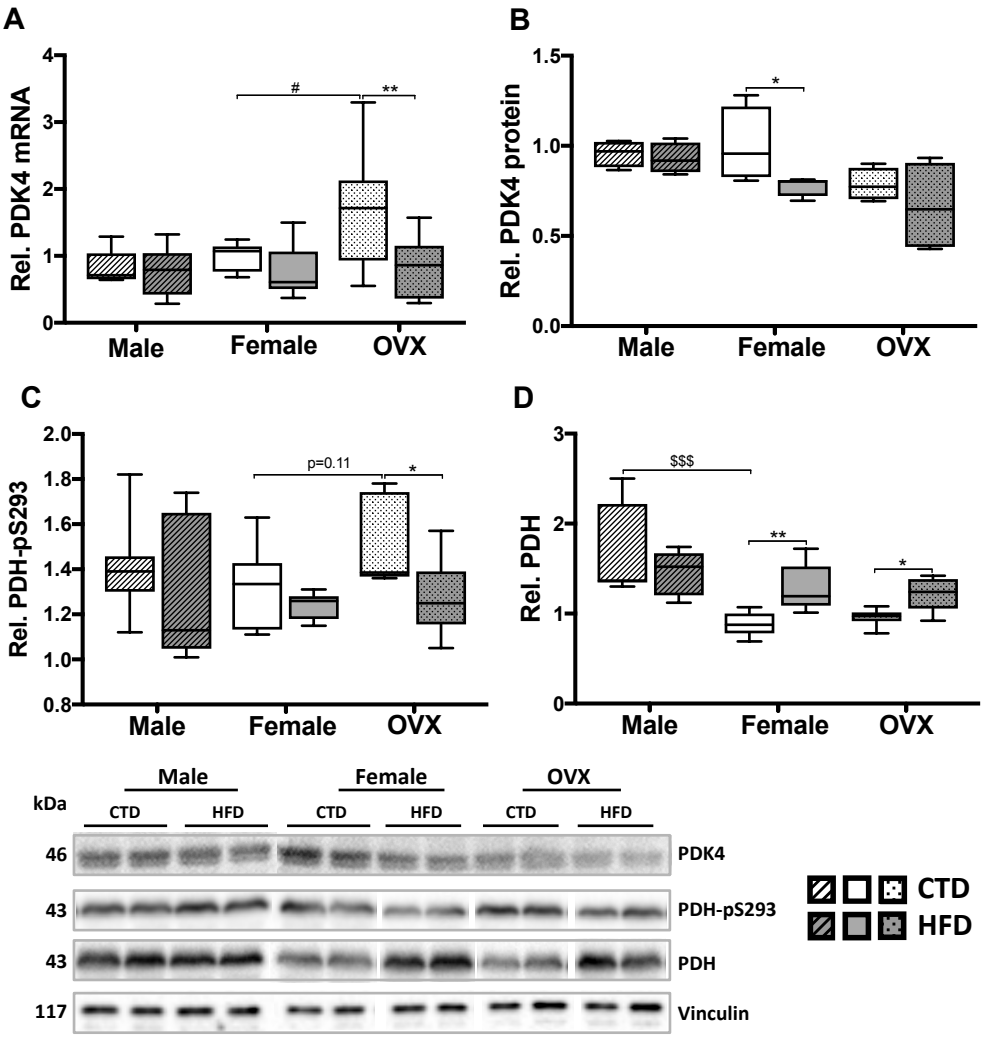

Figure 26: Quantitative real-time and Western-blot analysis of metabolic targets (1).
Cardiac muscles from male, female and OVX mice fed with CTD or HFD for 22 wks were used to extract mRNA and protein to evaluate genes and proteins involved in metabolism.
Representative examples of Western blots (bottom) and quantification normalized to the corresponding control (top) are shown. The bands visible for each protein belong to the same membrane. Results are presented with the median, whiskers show the min and max values.
* symbol corresponds to CTD vs HFD, # symbol corresponds to OVX vs sham, $ symbol corresponds to male vs female. N=6-10.

3.11 Regulators of glucose and fatty acid metabolism

We hypothesized that gender or OVX would modify expression of genes that encode proteins involved in glucose metabolism such as GAPDH and PDK4 in response to HFD feeding. Interestingly, PDK4 mRNA levels increased in the OVX- compared with the sham-female and the male under CTD conditions, and the HFD had a negative effect on its expression in the OVX mice (Figure 26A). The HFD feeding also slightly decreased PDK4 protein expression (p=0.048) in the sham-female mice (Figure 26B).

PDK4 is involved in the phosphorylation of the pyruvate dehydrogenase (PDH) complex, another important player in glucose oxidation because it catalyzes the conversion of pyruvate into acetyl-CoA (see 1.2.4). In our mouse model, HFD decreased the S293 phosphorylation site of PDH, which indicates its inhibition level, in the OVX-female group (p=0.04) (Figure 26C), this is consistent with the observed PDK4 mRNA level decrease. The sham-female mice also exhibited reduced PDK4 mRNA and PDH phosphorylation, but to a much lesser extent (ns, Figure 26A, C). Moreover, the OVX-group had also an increased level of PDH phosphorylation compared to the sham-female group when fed with CTD (Figure 26C). The total form of PDH is increased after HFD in both female groups, and in contrast, it was decreased in the male group in response to HFD. Moreover, male had a higher protein expression of total PDH than both female groups (Figure 26D). Since PDK4 and PDH are involved in glucose oxidation, our results suggest that OVX-female have a decreased glucose oxidation at baseline (CTD) compared with the sham-female mice and that this effect is blunted by HFD feeding as they present less inhibited PDH underlining a possible higher level of glucose oxidation than the sham-female mice. Overall, HFD decreased PDH phosphorylation, and together with the increased total PDH, this is suggestive of increased glucose oxidation in female mice mainly.

Acetyl-CoA-carboxylase (ACC) is a mediator involved in lipid metabolism. ACC activity inhibits FA oxidation; indeed, this enzyme is responsible for the synthesis of malonyl-CoA, which is inhibiting the mitochondrial transporter CPT-I that transfers FA from the cytosol to the mitochondria. Activated AMPKα inhibits ACC when the cellular energy supply is decreasing. Protein analysis of ACC demonstrated that its AMPKα phosphorylation site S79 was not modified in our experimental groups although it appeared that OVX mice have a higher expression than the sham-female after HFD (p=0.2) (Supplement, Figure S VIID). The total form of ACC was also not affected neither; a trend toward an increase was noticeable in the sham-female mice compared with the male mice after CTD (p=0.16) (Supplement, Figure S VIIE). These findings are consistent with the results on AMPKα described above.

As part of glucose metabolism signaling, gene expression of GAPDH was also changed. Indeed, it was decreased after HFD, but this effect was significant only in the sham-female (p=0.007, Figure 27A). Many genes are implicated in mitochondrion metabolism, among them the PGC1α and the PPARs genes. We hypothesized that these metabolic genes would be modified in our study, as they play a major role in controlling glucose and fatty acid oxidation. The mRNA level of PGC1α was not different between our experimental groups (Supplement, Figure S VIIF). The expression of PPARα mRNA, on the other hand, was increased by HFD feeding of the male mice (Figure 27B). Moreover, the sham-female mice

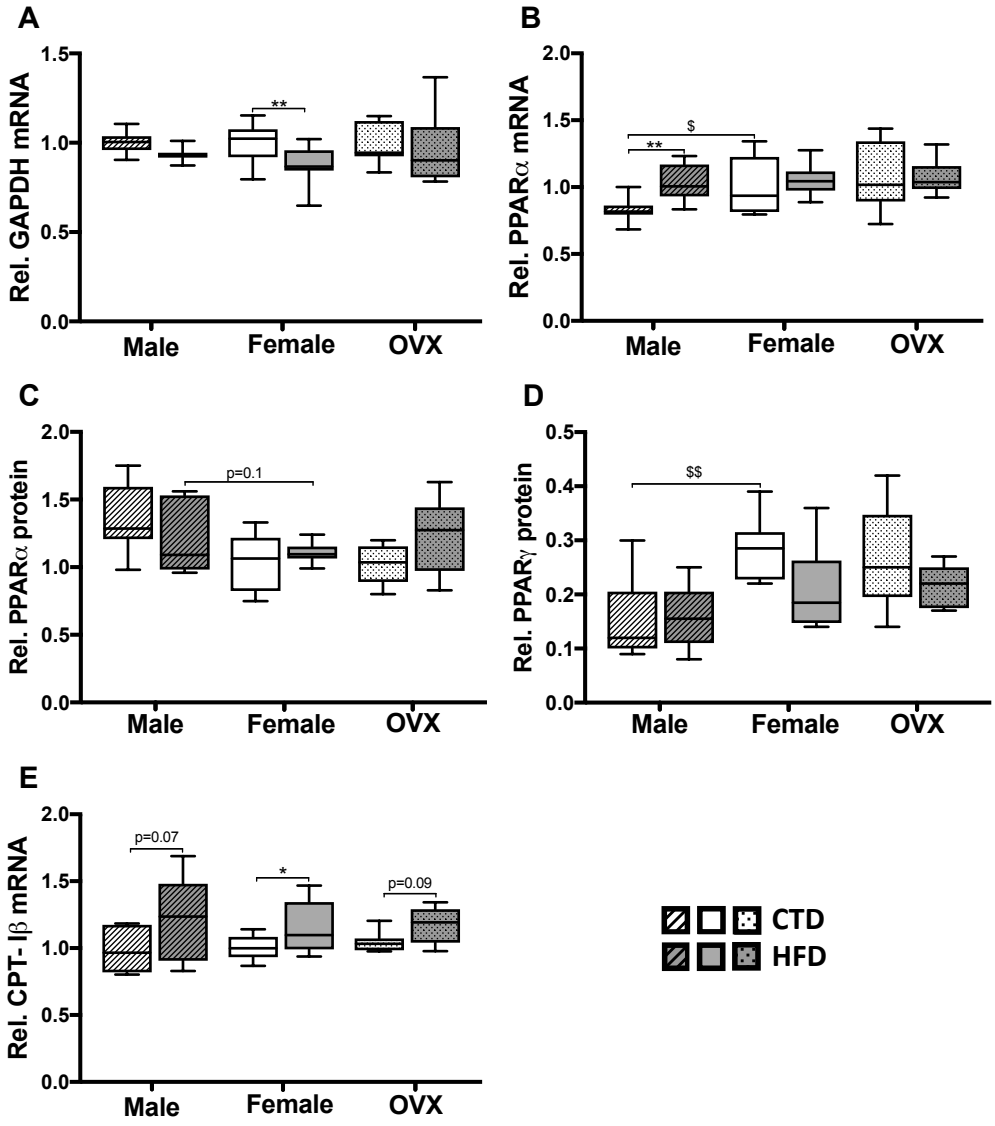

Figure 27: Quantitative real-time and Western-blot analysis of metabolic targets (2).
Cardiac muscles from male, female and OVX mice fed with CTD or HFD for 22 wks were used to extract mRNA and protein to evaluate genes and proteins involved in metabolism.
Results are presented with the median, whiskers show the min and max values. * symbol corresponds to CTD vs HFD, # symbol corresponds to OVX vs sham, $ symbol corresponds to male vs female. N=6-10.

had higher PPARα mRNA expression than the male mice under CTD conditions. Protein expression of PPARα was slightly higher in male mice than in sham-female mice when fed with CTD (p=0.1) (Figure 27C). PPARγ is another member of the PPAR family and its role in the heart stays unclear and controversial. Our analysis showed that HFD decreased its expression in the sham- and OVX-female but not in the male group (p=0.04, post-hoc: ns). Interestingly, both female groups had higher protein levels of PPARγ than the male group (Figure 27D). Finally, HFD increased mRNA levels of CPT-Iβ, a transferase in the outer mitochondrial membrane involved in lipid uptake. Post-hoc testing demonstrated significance in the sham-female group (p=0.04, Figure 27E).

To summarize, in female mice mRNA expression of GAPDH, an enzyme involved in glycolysis was reduced by the HFD and PDK4 protein levels were decreased consistent with decreased phosphorylation of its downstream target PDH. However, total PDH was increased, maybe to increase glucose oxidation. Unlike the molecules involved in glucose metabolism, the lipid transporter CPT-Iβ was increased. Altogether, these data point toward decreased glycolysis and increased glucose oxidation and lipid metabolism. Interestingly, in the male group only the PPARα mRNA was significantly increased by the HFD, proving that female and male mice diverge in their answer to HFD.

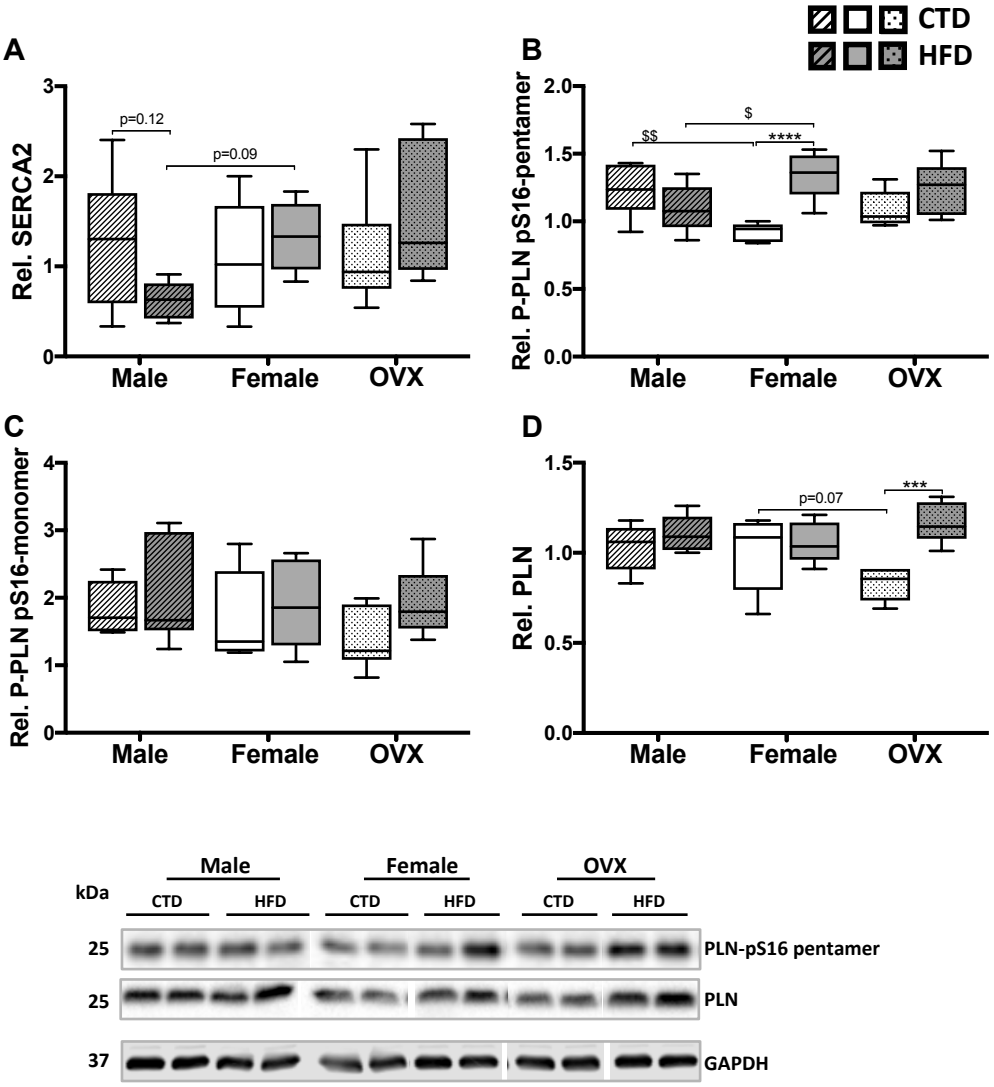

Figure 28: Western-blot analysis of proteins regulating cardiac contractility.
Cardiac muscle proteins from male, female and OVX mice fed with CTD or HFD for 22 wks were subjected to SDS-PAGE and probed with antibodies to protein involved in the regulation of cardiac contractility**.** Representative examples of Western blots (bottom) and quantification normalized to the corresponding control (top) are shown. The bands visible for each protein belong to the same membrane. Results are presented with the median, whiskers show the min and max values.
* symbol corresponds to CTD vs HFD, # symbol corresponds to OVX vs sham, $ symbol corresponds to male vs female. N=6-8.

3.12 Regulators of cardiac contractility

SERCA2a is a calcium pump responsible for the reuptake of calcium into the SR to allow cardiac relaxation. The protein levels of SERCA2 were unchanged under our experimental conditions. Small trends toward decreased SERCA2 in the male group after HFD ($p=0.12$) and toward increased SERCA2 in the sham-female compared to the male mice ($p=0.09$) (Figure 28A) were visible. SERCA2 is regulated by phospholamban (PLN), which exists in two forms: a pentamer and a monomer. At a basal state, it forms a pentamer that will dissociate upon SERCA2a interaction. As a monomer, this protein inhibits SERCA2a, which will lead to a reduced affinity for calcium thus lowering the calcium reuptake into the SR. When phosphorylated at S16, PLN releases its inhibitory action on SERCA2a and consequently enhances calcium re-entry into the SR.

Interestingly, the phosphorylated PLN pS16 pentamer was increased in sham-female mice ($p<0.001$), slightly increased in OVX mice ($p=0.15$), and unchanged or even slightly decreased in the male mice ($p=0.23$) after HFD (Figure 28B). Furthermore, the male mice fed with CTD had significantly higher phosphorylated PLN pentamer compared with the sham-female mice. Inversely, the sham-female mice had a significantly higher level of phosphorylated protein than the male mice after HFD. The monomer form of PLN was not different between our groups (Figure 28C). Concerning the total PLN protein, HFD increased its expression in the OVX mice only ($p<0.001$), while OVX-female fed with CTD had a slightly lower PLN protein expression than the sham-female mice ($p=0.07$) (Figure 28D). The observation that the monomer form of PLN was not changed suggests that calcium re-uptake into the SR was not altered. The fact that HFD increased the pentamer and total form in sham-female and OVX-female mice, respectively, could indicate that PLN upregulation is taking place to increase calcium reuptake and facilitate cardiac relaxation.

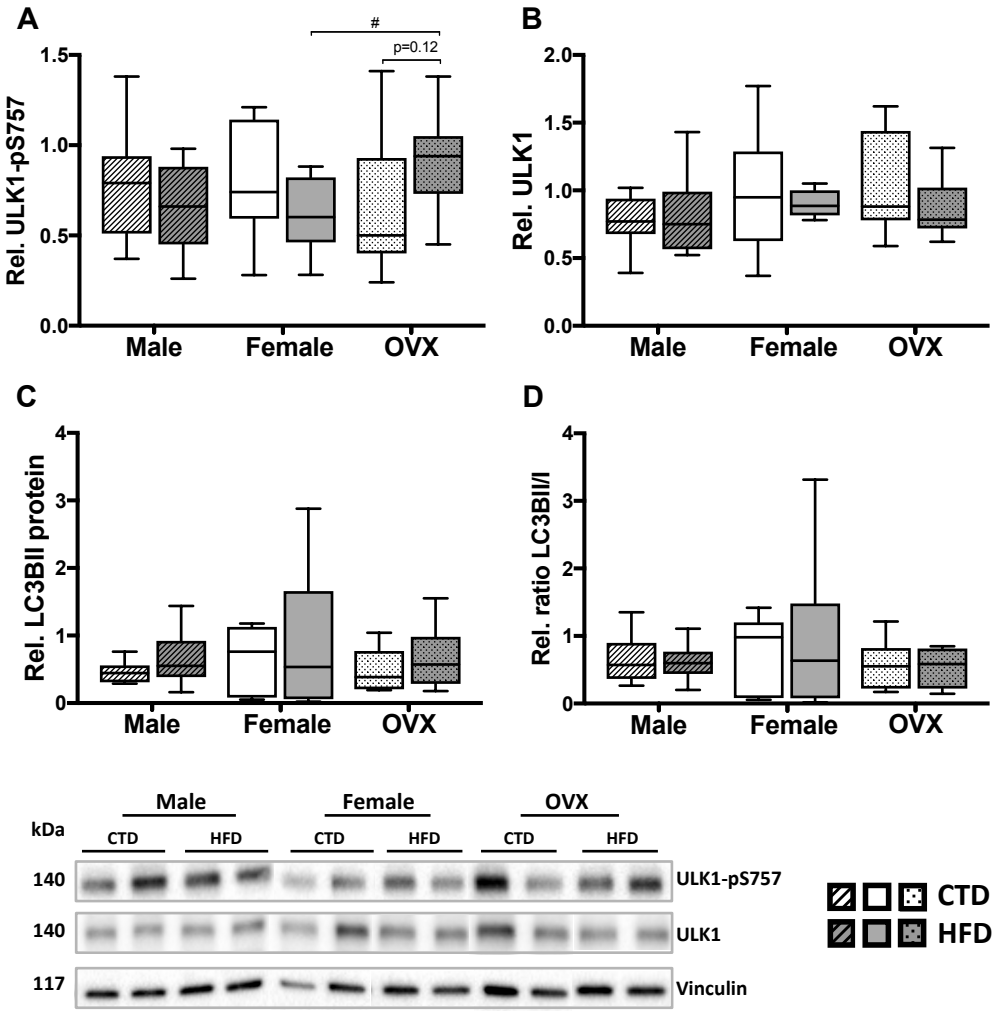

Figure 29: Western-blot analysis of proteins involved in autophagy.
Cardiac muscle proteins from male, female and OVX mice fed with CTD or HFD for 22 wks were subjected to SDS-PAGE and probed with antibodies to proteins involved in autophagy. Representative examples of Western blots (bottom) and quantification normalized to the corresponding control (top) are shown. The bands visible for each protein belong to the same membrane. A, B: N=9-13; C: N=6-8. Results are presented with the median, whiskers show the min and max values. * symbol corresponds to CTD vs HFD, # symbol corresponds to OVX vs sham.

3.13 Autophagy and apoptosis

Kinases such as mTOR and AMPKα tightly regulate autophagy. High levels of glucose allow the activation of mTOR, which in turn phosphorylates the protein ULK1 at S757 to prevent its interaction with AMPKα and its concomitant activation to induce autophagy. In our model, ULK1-pS757 was increased in the OVX- compared to the sham-female mice (Figure 29A). Interestingly, HFD had different effects on ULK1 phosphorylation in the OVX- and sham-female groups. Whereas a slight increase was observed in the OVX-female mice

(p=0.12), the sham-female and male mice experienced a small decrease upon HFD feeding (p=ns). As for total ULK1 protein, its level stayed equal between feeding conditions (Figure 29B). Taken together, our observations suggest that the OVX-female mice have lower autophagy than sham-female mice after HFD feeding.

Akt may change LC3BI/LC3BII expression. In the fed state, activated Akt will inhibit LC3B gene transcription through FOXO inhibition, to eventually block autophagy. LC3BII protein expression did not exhibit differences between the groups (Figure 29C). In the HFD-fed sham-female group, LC3BII showed very high variability with a few animals having very high LC3BII levels, whereas in the CTD group all animals had low levels (Figure 29C). To evaluate autophagy, the ratio LC3BII/LC3BI is essential. In our study, the ratio showed the same as the LC3BII levels by itself (Figure 29D). Our data suggest increased autophagy in some sham-female mice, and no effect of the diet in male and OVX-female mice. We would need to test more mice to prove significance of this gender difference.

Additionally, we studied autophagy by TEM since it is considered as “gold-standard” method to detect morphological and ultrastructural changes associated with autophagy activation.[365] We obtained mitigated results, as it was difficult to detect with certainty the presence of autophagosome or autolysosome (Supplement, Figure S III). Given this, it would be interesting to use chloroquine, an autophagic flux inhibitor, to better evaluate the level of autophagy in our different experimental conditions. We also stained for cleaved-caspase3 on cardiac sections to detect apoptosis, but no obvious differences were observed between our conditions (data not shown). Further experiments are needed to prove that no changes are induced, for instance since apoptosis is a rare event more mice would need to be tested and multiple sections at different levels of the heart would have to be quantified.

4. Discussion

4.1 Introduction

The metabolic syndrome is defined by a combination of pathologies: obesity, hypertension and diabetes, and is associated with a high risk to develop CVD.[366] The prevalence of obesity, diabetes and hypertension is higher in postmenopausal women than in age-matched men and is associated with increased diastolic heart failure.[170,367-369] The causes for this unequal distribution for the genders remain unclear.[370] Several preclinical studies attributed to estrogen a beneficial effect on cardiac function. However, hormone replacement therapy failed to improve cardiac function in advanced menopausal women[371,372] highlighting the complexity of the estrogen system in the heart. Our study therefore aimed to investigate the impact of gender and ovarian hormones on cardiac function in a mouse model of diet-induced obesity, depicting a cardiometabolic disorder.

4.2 Summary of the effects of HFD in male, female and OVX-female mice

Body weight, glucose tolerance, insulin levels and fat weight

1. High fat diet decreased glucose tolerance in male, female and OVX-female mice at 3, 9 and 22 wks of feeding. 2. Male mice gained less weight than female mice and their glucose tolerance was similar to that of the sham-female. HFD induced a much stronger increase of plasma insulin in male than in female mice. Male had less visceral adipose tissue than female mice. 3. OVX-female mice fed with HFD had higher body weights than sham-female mice, but this difference disappeared over time and was absent after 22 wks of feeding. The HFD-fed OVX-females were more glucose intolerant than the corresponding sham-females. Furthermore, in response to HFD, the sham-female mice had slightly increased insulin levels, whereas this HFD-induced increase was absent in the OVX-female mice. The ablation of the ovaries induced an increase in fat content in the female mice fed with CTD, a difference that disappeared when the female mice were fed with HFD. Since glucose uptake mainly takes place in organs such as skeletal muscle, liver and adipose tissue, the observed changes in glucose tolerance are most likely related to these organs. Whether or not the various conditions also affect cardiac glucose uptake remains to be investigated. The first hints came from our analysis of insulin/Akt-signaling in cardiac tissue, which points toward modest effects of HFD, gender and OVX on this pathway that amongst other things regulates glucose uptake in the heart.

Cardiac dimensions and function

Firstly, our analysis by echocardiography demonstrated that HFD had distinct effects in a gender-specific way. 1. It decreased the E/A ratio in the female mice only. 2. The relative wall and posterior wall thicknesses were increased in the sham-female mice. Notably, HFD also increased the ventricle weight measured post-mortem solely in the sham-female mice.

Secondly, HFD had specific effects linked to the absence of ovarian hormone. 1. The LV anterior wall thickness was increased in the OVX group only. 2. The cardiac output was increased in the OVX compared with the sham-female group.

The PVL method showed that 1. HFD decreased the emptying and filling rates dV/dt min and dV/dt max in male respectively. 2. Female had a lower dV/dt min and dV/dt max values than male when fed with CTD diet under conditions of normal work as well as dobutamine-induced increased work. 3. HFD caused a decrease in end-diastolic pressure in sham-female mice. Concerning the effects linked to estrogen deficiency: 1. Following dobutamine infusion, OVX-female had a lower dV/dt min than the sham-female group after HFD. 2. Dobutamine infusion revealed that HFD-fed OVX-female mice have higher end-diastolic pressures than diet-matched sham-female mice.

Cardiac steatosis, inflammation, fibrosis and stress markers

Our evaluation of cardiac steatosis suggests that HFD increased lipid accumulation in the heart, an effect that was more pronounced in male and OVX-female mice than in sham-female mice. Additionally, cardiac signaling pathways implicated in inflammation were changed: 1. After HFD, phosphorylation of NF-κB at S536 was slightly increased in the sham-female group, whereas IκBα was decreased in this same group. 2. Male showed an increased expression of NF-κB compared with the sham-female mice under CTD conditions. 3. NF-κB was also slightly increased in the OVX-female group after HFD. Collagen I and III mRNA levels were not different between our groups at the timepoint of analysis. This was confirmed by Picrosirius Red staining on sections, although it seemed that in the OVX-female mice the staining was more pronounced than in the sham-female and male mice.

To assess the level of cardiac stress induced by HFD in the three groups, we measured ANP, BNP and β-MHC mRNA levels. 1. The HFD decreased ANP gene expression in the female mice, and its level was slightly increased in the sham-female compared with the male group after CTD feeding. 2. BNP was slightly decreased in the OVX-female compared to sham-female in the CTD-fed group.

Cardiac signaling: insulin/Akt/mTOR

Some components of the insulin/Akt/mTOR pathway were modified. 1. HFD increased IRS-pS636-639 in the male whereas it was decreased in the sham-female mice. Male mice, next to having more phosphorylated IRS-1 than sham-female mice, also had higher total IRS-1 protein amounts. 2. HFD strongly decreased Akt protein in both female groups but not in the male group. The sham-female mice had higher Akt expression than the male when fed

with CTD, and similarly the Akt phosphorylation at S473 was higher in the sham-female than in the male. 3. AS160 protein expression and phosphorylation were not importantly altered by the diet or the gender. 4. HFD increased the activation site S2448 of mTOR in the female groups, whereas it was slightly decreased in the male group. As a consequence the female had higher phosphorylated mTOR than the male mice after HFD feeding.

Ablation of ovaries induced the following specific effects: 1. OVX-female had lower levels of phospho- and total IRS-1 than sham-female mice after CTD feeding. 2. Total AS160 was increased in the OVX-female after HFD feeding. 3. ULK1 as a downstream target of mTOR was studied to evaluate autophagy. ULK1 was not much changed, only phosphorylated ULK1 was increased in the OVX-female after HFD compared to the sham-female mice. LC3B protein expression was not affected by the various conditions.

Cardiac metabolic signaling

Reduced GAPDH gene expression was observed in the sham-female mice after HFD feeding. Other genes participating in glucose metabolism were also changed: 1. PDH protein expression was increased after HFD in the female groups, and the sham-female had a lower protein level than the male mice. 2. HFD caused an overall increase in mRNA expression of the lipid transporter CPT-Iβ, an effect that reached significance for the sham-female mice. 3. PPARα gene expression was lower in the male than in the female group under CTD conditions, and HFD increased its expression in the male group. 4. Protein expression of PPARγ was increased in the sham-female compared to the male under CTD conditions. As for the ovarian-hormone-related effects: 1. PDK4 gene expression was higher in the OVX-female than in the sham-female mice under CTD conditions. HFD decreased PDK4 in the OVX group back to levels of the sham group. 2. Similar to PDK4, PDH protein phosphorylation at S293 was higher in the OVX than in the sham-female, and HFD decreased it in the OVX group. Table III shows a summary of the main results obtained in our study.

Table III: Summary of the main results obtained in our study.
Differences and similarities between groups after 19-22 wks of diet.
Additional color code: grey filling: no changes occurred, green filling: higher level, red filling: lower level

		CTD vs HFD			♂ vs ♀		♀ vs OVX	
Comparison between conditions		♂	♀	OVX	CTD	HFD	CTD	HFD
GTT Plasma Insulin	Glucose Tolerance	CTD>HFD	CTD>HFD	CTD>HFD				♀<OVX
	Plasma Insulin	CTD<HFD	CTD<HFD			♂>♀		
Echo-cardio-graphy	Rel. wall tickness		CTD<HFD					
	LVAW, d			CTD<HFD				
	E/A		CTD>HFD	CTD>HFD				
PV loop max. dobuta mine infusion	dV/dt min	CTD>HFD			♂>♀			♀>OVX
	dV/dt max	CTD>HFD			♂>♀			
	Ped							♀<OVX
mRNA	ANP		CTD>HFD	CTD>HFD				
	PPARα	CTD<HFD			♂<♀			
	PDK4			CTD>HFD			♀<OVX	
	CPT-1β	CTD<HFD	CTD<HFD	CTD<HFD				
Protein	Akt-pT308							
	Akt		CTD>HFD	CTD>HFD	♂<♀			
	mTOR-pS2448					♂<♀		
	mTOR							
	PDH-pS293			CTD>HFD				
	PDH		CTD<HFD	CTD<HFD	♂>♀			

4.3 Ovariectomy increases body weight gain, adiposity and glucose intolerance

Postmenopausal women present deteriorated metabolism resulting in increased abdominal adipose tissue and dyslipidemia.[312] Similarly, ovariectomized animals show a weight gain and an altered metabolic state, which is reversed by estrogen replacement.[328] The ablation of ovaries in our mouse model triggered an increase in body weight detectable already 4 wks after the surgery, prior to the start of CTD and HFD feeding. In a pilot study we observed that the food intake between the sham- and OVX-female mice was not different, excluding the possibility that the higher body weight measured in the OVX-female mice was due to higher food consumption. During the 22 wks of regular chow feeding the two female groups maintained similar body weights, a difference remained visible only when the mice were fed with HFD. Indeed, the OVX mice kept their higher body weights up to 15 wks of feeding, indicating that the deficiency of ovarian hormones has more pronounced effects under HFD conditions.

The OVX mice had more visceral fat than the sham-female mice after 5 and 22 wks of feeding, and therefore their higher body weights may be explained by the development of more visceral adipose tissue. Surprisingly, we observed this difference in the amount of adipose tissue after CTD-, but not after HFD-feeding. This may be due to the fact that at 22 wks of HFD feeding a plateau of body and fat weight was reached. A difference in fat weight between sham- and OVX-females may have been present at earlier timepoints, while BW was still increasing. Our results are consistent with earlier rodents studies in which it has been shown that the absence of ovarian hormones increases adiposity[328] and that this is prevented by implantation of subcutaneous pellet of E2, proving that of the different ovarian hormones it is indeed E2 that regulates adiposity.[327] Collectively, the available data support that E2 modulates fat mass in animals that are increasing their body weight.

Is E2 responsible for gender differences in fat mass after HFD feeding? Males have lower E2 than females. We found that males had also lower fat content than females in our mouse model especially after HFD feeding. However, the HFD-fed OVX-female mice had the same amount of visceral fat as the sham-female mice despite the absence of E2. Taken together, this suggests that the observed gender difference in fat accumulation is most likely not directly related to E2. The observed gender difference in fat is in line with studies showing that men have a lower amount of total body-fat, due to a lower fat storage capacity of their adipose tissue.[373] It is however known that a sexual dimorphism exists related to fat distribution. Men have increased central intra-abdominal adipose tissue compared with women, who exhibit more subcutaneous adipose tissue.[374] After menopause, women gain

intra-abdominal fat thus following a male pattern, and this can be improved by estrogen replacement therapy.[375] Accumulation of abdominal fat correlates with a higher risk and mortality caused by diabetes and atherosclerosis.[376]

Interestingly, we found that OVX-female mice became more glucose intolerant after HFD-feeding than sham-female mice suggesting a role of E2 in glucose homeostasis. These two groups had similar amounts of visceral adipose tissue at 22 wks, and the glucose intolerance found in the OVX mice may therefore not be directly related to visceral fat content. It is thought that adipose tissue participates in the onset of insulin resistance via the secretion of adipokines.[119-121,377] In our study, the sham and OVX-female mice had the same amount of fat, thus comparable adipokine levels are expected and should have triggered the same insulin resistance in both groups, which is not the case. These findings suggest that the lack of ovarian hormones modifies glucose tolerance independently of potential endocrine effects of adipose tissue. Indeed, from a batch of mice sacrificed at 5 wks we know that a difference in fat mass and glucose tolerance between sham- and OVX-females was present earlier during the HFD-feeding, which could have caused their more severe glucose intolerance.

Furthermore, fasting glucose was not influenced by the HFD, gender or ovarian hormones after 22 wks of diet, similarly Carbone et al., did not find any increase in fasting glucose in male and female mice fed with a western-diet similar to ours during 8 wks.[378]

4.4 Male mice have higher plasma insulin than female mice after HFD

Diabetes is a progressive disease that takes place according different stages. A hyperglycemic state triggers an overproduction of insulin by the beta pancreatic cells to alleviate this increase of blood glucose. At an early stage, blood glucose levels are brought back to normal thanks to this increased production of insulin. When the hyperglycemic state is sustained, it ensues pancreatic failure: insulin is less, or ultimately not secreted and its blood concentration drops characterizing more advanced diabetes.[379] Insulin resistance is defined as a decreased capacity of the large metabolic organs to respond to insulin. The main metabolic organs (liver, adipose tissue and skeletal muscle) start to be less insulin sensitive, increasing the insulin demand, which leads to hyperinsulinemia.[380] Obesity is a state that importantly contributes to the development of insulin-resistance, which itself is part of diabetic pathophysiology.

Our results demonstrate that 22 wks of HFD feeding resulted in obesity and induced an increase in fasting plasma insulin levels in male and female mice. This increase can be

interpreted as an adaptation to the HFD feeding, which is known to affect insulin sensitivity.[381-383] The increased insulin would be important in the context of our HFD model, in which fatty acid utilization is enhanced. Indeed, to overcome this situation, the increased insulin secretion would be beneficial since it would activate the Akt pathway and increase glucose uptake and utilization to participate in the process of energy production. The question whether this insulin pathway activation is cardioprotective or not in the context of obesity and T2DM still remains open, but activation of the Akt pathway is thought to be beneficial for the heart in certain conditions such as ischemia-reperfusion.[384-386]

Notably, we observed a striking sexual dimorphism with the males having much stronger increases in insulin after HFD feeding than the females. This stronger increase could mean that males are more insulin insensitive and suggests that they are facing a more advanced stage of insulin resistance, hence the overproduction of insulin to cope with the decreased insulin sensitivity. This strong increase in insulin levels could suggest that the male mice start to develop diabetes and are most likely in a pre-diabetic phase, where the pancreas is still able to cope with increased needs of insulin to palliate decreased insulin sensitivity in the liver, adipose tissue and skeletal muscle. Surprisingly however, glucose tolerance was reduced to a similar degree in the female and male groups after HFD. This indicates that male mice may need a lot more insulin to trigger the same glucose clearance than the female mice after HFD. One could hypothesize that with the same insulin level as female, male would be more glucose intolerant than female. Alternatively, it could also be thought that the males exhibit a higher level of adaptation than the sham-female by increasing more their plasma insulin to increase glucose utilization. In our study, no major differences existed between male and female regarding glucose tolerance at 9 and 20 wks of HFD feeding. Only a trend toward lower glucose tolerance appeared in the male compared with the sham-female after 9 wks of HFD ($p=0.08$), suggestive of reduced insulin-sensitivity at this timepoint. Based on all these data, we propose that the males started to develop insulin resistance earlier than females.

Interestingly, the OVX-female mice did not show any plasma insulin increase at all after HFD, this in contrast to the sham-female and the male mice. This absence of increased insulin secretion is in line with the observed decrease in glucose clearance in OVX- compared to sham-female mice. Thus, low plasma insulin level in the OVX mice may cause their glucose intolerance. Moreover, the main difference that separates sham- from OVX-female mice is their different ovarian hormone level, and therefore our result suggests that ovarian hormones are implicated in increasing plasma insulin in response to HFD feeding. However, the male mice that have no ovaries and only low levels of E2 derived from other

tissues are very well able to increase insulin levels, which suggests that this strong effect in the males is due to some E2-independent mechanisms, possibly the male hormones or other features that distinguish males from females. Dandona et al. recently showed that testosterone increases insulin sensitivity in men.[387] Hypogonadal men, presenting a low level of testosterone, were randomized to receive intramuscular injection of testosterone or placebo every two weeks for 24 wks. The men treated with testosterone had an increased insulin sensitivity, lean mass and decreased subcutaneous fat. They also showed a higher expression of genes implicated in insulin signaling such as IR-β, IRS-1, Akt2 and GLUT4 in adipose tissue compared to before testosterone treatment. They observed that low testosterone levels were associated with decreased insulin sensitivity and proposed that low testosterone contributes to T2DM.[387]

Increased adiposity is thought to be implicated in the onset of insulin resistance and diabetes through the secretion of adipokines, which may lead to pancreatic dysfunction. As discussed above (4.3), we noted that the OVX-female mice have a higher adiposity than the sham-female after CTD and during early stages of HFD feeding. On the other hand, we noticed that 22 wks of HFD did not increase plasma insulin in these OVX mice, in contrast to the sham-female and male mice that increased their plasma insulin. This could suggest that at 22 wks of HFD the OVX mice already passed the first stage of diabetes characterized by increased insulin levels or that these OVX mice are not insulin resistant at all at this timepoint. However, their increased glucose intolerance tested by GTT would rather point toward a more advanced diabetes state than the other groups. Another possibility, would be that the absence of ovarian hormones is directly responsible for the absence of overproduction of insulin in response to HFD as the sham-female and male groups do. To further investigate these possibilities, it would be interesting to evaluate the plasma insulin at an earlier timepoint. In a previous study, we observed that the OVX mice have a higher level of visceral fat than the sham-female mice at the early time point of 5 wks of HFD, which could contribute to more severe insulin resistance already at this stage. This observation matches our hypothesis that the absence of ovarian hormones is leading to a premature onset of insulin resistance compared to the female with intact ovaries.

Estrogen has been reported to be involved in insulin secretion from pancreatic beta cell as reviewed in this article.[388] Prossnitz et al. showed that activation of GPER by E2 or the GPER specific agonist G-1 induces insulin secretion from the beta pancreatic cells via the activation of epidermal growth factor (EGF) receptor and ERK pathways. Insulin secretion was inhibited by the GPER antagonist G-15 and absent in the isolated islet from GPER KO mice.[325] Another study demonstrated that both receptors ERα and ERβ are present in

isolated beta pancreatic islets from mice. They observed that long-term exposure to E2 increased beta cell insulin content, insulin expression and insulin release. Using ERα and ERβ agonists and KO mice, they suggested that it is the ERα that induces this effect via the activation of ERK1/2 pathway.[389] Moreover, studies also proved that testosterone acts on the pancreatic beta cells. Male mice with beta cell-selective androgen receptor deficiency (βARKO) showed a decreased glucose-stimulated insulin secretion (GSIS) resulting in glucose intolerance.[390] Mice developed hypoinsulinemia and hyperglycemia after western diet feeding. In cultured male human and mouse islets, testosterone increased GSIS. This effect was absent in the βARKO mice and in human islets treated with the androgen receptor antagonist flutamide, proving that indeed testosterone increases GSIS via direct androgen receptor activation in islet beta cells.[390]

The mechanisms involved in sex differences in glucose clearance are not clear but may be related to insulin secretion from the pancreas. Different studies were performed to assess this question and some discrepancies were reported. In a clinical study, healthy young men and women had similar insulin secretion.[391] Flanagan et al. demonstrated that after glucose infusion, female have higher first phase insulin secretion than age-matched men, suggesting that females were less insulin sensitive than males.[287] This was consistent with an experimental study where female rat hearts were less sensitive to insulin than male hearts.[392] However, other rodent studies show that female have greater insulin sensitivity and lower insulin resistance compared to male fed a high fat diet,[393] which was also confirmed by our own findings as plasma insulin in sham-female mice was only lightly increased after HFD compared to the male group where the effect was much more pronounced. On the other hand, one study showed that OVX in rats did not alter insulin sensitivity,[341] suggesting that ovarian hormones are not implicated and that regulation of insulin sensitivity is complex. Rats fed with HFD for 12 wks gave rise to a similar increase in body weight in both genders, nevertheless only males displayed hyperinsulinemia, hyperglycemia, and reduced ejection fraction, underlining a gender difference.[394] Additionally, it has been shown that in cardiomyocytes from women and men treated with estrogen, the gene profile was different on 36 estrogen-dependent genes, supporting that estrogen effects on the heart are sex-specific.[395]

Estrogen is known to interact with a major player in glucose metabolism, Akt, which might explain its role in regulating insulin sensitivity.[396] Indeed, consistent with our own findings, it has been described that premenopausal women have greater insulin sensitivity than men,[396] and that menopause or OVX is inducing a rapid decline in insulin sensitivity.[397] Although women have a higher body fat content, they have a lower risk to develop insulin

resistance and T2DM than men[398] because of their higher insulin sensitivity and glucose clearance.[399] Nevertheless, postmenopausal women exhibit a lesser insulin sensitivity than age-matched men, underlining the role of E2 in regulating insulin sensitivity in women.[397] Concordantly, OVX mice and rats show insulin-resistance and altered contraction-stimulated glucose uptake into muscle.[400] It has recently been reported that a specific ERα agonist is necessary to maintain a normal cardiac glucose uptake in a mouse model.[321] Moreover, women and female rodents are protected against high fat diet and fatty acid-induced insulin resistance, whereas male rodents fed with a high fat diet showed a decline of 40-50% in insulin-stimulated glucose disposal, indicating reduced insulin sensitivity.[401,402] A mouse model of OVX mice fed with high fat diet had demonstrated that E2 replacement was able to improve glucose and insulin sensitivity in skeletal muscle of wild-type mice but not in knock-out ERα mice, confirming that ERα has an important role in preventing from diet-induced obesity consequences and could be a potential target in the treatment of obesity.[317-319] E2 may also regulate glucose and energy metabolism via the control of glucose transporters GLUT3 and GLUT4.[403-406]

In summary, our analysis of body weight, fat content, glucose tolerance and plasma insulin demonstrates that 1. After HFD feeding, male mice have less adipose tissue, similar glucose tolerance but higher plasma insulin, suggesting that they are less insulin-sensitive than sham-female mice. 2. After HFD-feeding, OVX-female have a similar fat content as sham-female mice but a higher glucose intolerance, suggesting that adipose tissue is not, whereas E2 is implicated in the observed glucose intolerance. 3. The absence of increased plasma insulin after HFD in the OVX-female mice could explain their more pronounced glucose intolerance compared to the sham-female mice. The lacking increase in plasma insulin together with reduced glucose tolerance suggests that OVX female mice may be at a more advanced stage of insulin resistance than the female mice. However, their fasting glucose concentration was still normal, so the OVX mice are not yet diabetic.

4.5 High fat diet increases heart rate

In our model, HFD caused an overall decrease in systolic blood pressures and this decrease was significant in the OVX group after 19 wks of feeding. An initial decrease in the systolic blood pressure of the OVX mice compared with the sham-female was observed at 8 wks of chow diet, this effect may be interpreted as a negative feedback loop to compensate the absence of ovarian hormones, which could have led to an increase in blood pressure. Additionally, the HFD decreased the diastolic blood pressure in the male at 8 and 19 wks of diet, as well as in the OVX-female mice at the 8 wks time point, but not in the sham-female

group. The diastolic blood pressure was higher in the male than in the female after CTD feeding, thus revealing sex-dimorphism.

Several epidemiological studies showed a strong positive correlation between CVD and both systolic and diastolic blood pressures.[407,408] The Framingham Study demonstrated that high SBP rather than high DBP is the best predictor of all-cause and cardiovascular mortality.[409] In this study and in others it was shown that after adjustment of the high SBP, the DBP does not correlate with CVD risk, proving that DBP data used in many clinical studies are not sensitive enough to determine CVD risk.[409,410] Maybe the decreased systolic blood pressures observed in our obesity mouse model can therefore be seen as beneficial adaptation? Or are the reduced pressures related to a general less active state of the obese mice and a reduced ejected volume during cardiac systole? Against this latter possibility speaks our echocardiography data, which did not reveal any reduced ejected volumes.

Further investigations are required to assess the reason for the reduced pressures. For example, measurements of peripheral resistance could be done, because increased resistance elevates DBP. Also the large arteries condition could be investigated, because their stiffening can induce a decrease in DBP.[411,412] A study by Witteman et al. demonstrated that in women, a decrease in DBP during a nine-year follow-up was associated with a progression of atherosclerotic lesions of the aorta, and thus suggested that the DBP could be a marker of atherosclerosis.[413] Based on these clinical studies, the decrease in DBP observed in our male and OVX-female mice at 8 wks of diet could be due to a stiffening of large arteries, however, it would be difficult to verify this hypothesis in our mouse model, because this effect was observed as early as 8 wks of diet, and at a later stage this effect is less pronounced. Thus, we cannot draw any conclusion on the significance of this small decrease observed after HFD.

In the metabolic syndrome, obesity is often associated with increased blood pressures[414] and therefore we were initially surprised to find decreased pressures. However, many experimental rodent models have failed to detect spontaneous hypertension under after a high fat diet.[415,416] Generally, an additional hypertension inducer such as genetic[417] and environmental factors (e.g. high-salt diet[418]), hormones (e.g. angiotensin II)[419-421] or renal abnormalities[422] are needed to trigger hypertension in rodents. Moreover, blood pressure changes are not observed in rodents lacking of estrogen, consistent to our findings.[349-352]

Our non-invasive tail-cuff blood pressure measurements also revealed changes in heart rates, which were systematically increased after HFD in all three groups. This could be

explained by the fact that HFD feeding importantly increased the body weight, and therefore the need for body oxygenation should in this case be larger than in the mice fed with CTD. Thus, to sufficiently perfuse the organs of a bigger mouse, the heart has to pump faster. This may also help to reach sufficient output with lower systolic pressures. It is noteworthy however that the tail-cuff measurement method to assess blood pressures is not the most reliable technique although it has the advantage to evaluate blood pressures of wake animals. To obtain more precise and reliable results the use of a direct blood pressure measurement method such as radio-telemetry would have been preferred.

4.6 High fat diet alters cardiac function and geometry

Ejection fractions and fractional shortening were not altered by HFD, gender or ovariectomy, indicating that systolic function was preserved. We used the E/A ratio to evaluate diastolic function. Whereas the male mice did not exhibit any change at 22 wks, the female mice fed with HFD had decreased E/A ratios, suggesting diastolic dysfunction. Thus, female and male mice respond differently to the HFD with the females developing diastolic dysfunction irrespective of their ovarian hormone levels. It is known that the E/A ratio evolves along with the pathology development. First the ratio is elevated when diastolic dysfunction is mild and then it decreases revealing severe diastolic dysfunction.[423] Therefore, our data suggest more advanced diastolic dysfunction in female mice, whereas male mice present normal function after 22 wks of HFD.

Interestingly, cardiac geometry was modified in sham-female mice by HFD, as the HFD increased the relative wall thickness and also caused a trend toward increased LVPW during diastole ($p=0.06$) compared with CTD. The increased relative wall thickness together with the unchanged LV mass does not point toward a hypertrophic LV, but to simple concentric LV remodeling.[24] On the other hand, the diastolic LV anteroseptal wall thickness was increased only in the OVX-female after HFD compared to CTD. These distinct increases in wall thickness may reflect cardiac remodeling as an adaptation to the HFD in both female groups, albeit different parts of the ventricular wall were affected. No increase in ventricular mass was measured between CTD- and HFD-fed sham- and OVX-female mice, and this absence of hypertrophy was confirmed by the WGA staining, which did not reveal any major differences in cross-sectional area between our different experimental groups (Supplement, Figure S VIII). The effects on wall thickness were maybe too small to be revealed as a weight change in the whole ventricle. Alternatively, as the effect was only significant during diastole, it may indicate reduced relaxation. In that case, the end-diastolic diameter and volume is expected to be smaller. In fact, HFD reduced end-diastolic LV volume only in the male group. This moderately decreased filling volume may, besides

reduced relaxation, also be related to a beginning of thickening of the wall in the male group. Indeed, there were some small increases in wall thickness after HFD in the male group, but these did not reach significance.

To summarize, the E/A ratio, which was decreased in the female groups after HFD, points toward diastolic dysfunction, however the absence of impaired cardiac relaxation or increased stiffness do not further corroborate for this conclusion. Moreover, the pathophysiological explanation of diastolic dysfunction relies on the fact that filling of the ventricles and cardiac output take place normally to the detriment of abnormal elevation of cardiac filling pressures.[424] Our PVL results showed no elevated pressures, strengthening the view that our experimental model does not exhibit a high level of cardiac stress. Taken together, our data suggest that our female mice exhibit mild diastolic dysfunction.

Our results obtained with the pressure-volume loop technique showed significant changes in hemodynamic parameters. The peak-filling rate dV/dt max represents the active cardiac relaxation and is translated as the speed of transition between the contracted and dilated state. This parameter is closely linked to the calcium reuptake in the sarcoplasmic reticulum. Noteworthy, the HFD feeding in males caused a strong decrease of the peak-filling rate, suggesting that their ventricular relaxation was slower. This could be explained by a lack of LV elasticity or by a slower reuptake of calcium into the SR. The emptying peak rate dV/dt min was also decreased in the male group after HFD. This parameter is related to the rate of contraction and could be affected by calcium storage in the SR. Thus, our observation that HFD reduces the contractility rate in males suggests a decrease in calcium or a slower release of calcium via the ryanodine receptors to enable contraction. SERCA2 and phospholamban are two proteins regulating contractility. When phosphorylated by PKA, phospholamban releases its inhibition on SERCA2, which becomes activated to allow calcium reuptake into the SR. In this regard, these regulatory proteins could play a role in the calcium reuptake rate, which is linked to the peak filling rate dV/dt min and the calcium availability, which is related to the filling rate dV/dt max. Our protein analysis shows that SERCA2 and phospholamban expression were not regulated by HFD in the male group, suggesting that other players should be involved in the observed changes in dV/dt min and dV/dt max. A change in heart rate could also have explained the difference of relaxation and contraction, indeed a lower heart rate would lead to a lower relaxation and contraction rates. However, heart rate was not different between male fed with CTD and HFD.

Whereas in the male group the dV/dt min and dV/dt max were negatively affected by HFD, in the sham-female group these two parameters were already lower than in the male

under CTD conditions, and were not affected by the HFD, highlighting a gender difference in the rate of cardiac relaxation and contraction. Thus, the males reached the relaxation and contraction stage more rapidly than the female under normal diet conditions. Our western blotting analysis showed that these differences were associated with decreased phospho-PLN pentamer, whereas SERCA2, PLN monomer or cardiac contraction rates were not changed. This suggests that different protagonists are involved in the decreased dV/dt min and dV/dt max differences. Finally, increasing cardiac work with dobutamine was necessary to uncover an effect of OVX. At the highest dose of dobutamine, the peak emptying rate dV/dt min was lower in the OVX- than the sham-female mice after HFD. The heart rate in this case could have been implicated, only a trend was observed toward a reduced heart rate in the OVX-female mice after HFD ($p=0.08$) during PVL measurements. In conclusion, males have faster filling and emptying rates than females, but these rates are reduced after HFD in males (reaching values similar to those observed in females) whereas HFD has no such effects in females. The absence of ovarian hormones decreases emptying peak rates in females, but only after HFD feeding and under conditions of high cardiac work.

At baseline, the HFD-fed sham-female mice had a lower end-diastolic pressure than their control fed with CTD, this effect of HFD was not observed in the OVX neither in the male groups highlighting a specific role of ovarian hormones and a gender-specificity. As for the end-diastolic pressure changes under dobutamine stress conditions, similarly the HFD-fed sham-female mice had a trend towards decreased end-diastolic pressures. Again this effect was not observed after OVX and in the male group. Additionally, we observed that the infusion of dobutamine decreased even more the end-diastolic pressure in the sham-female and not in the OVX-female mice creating a difference between the sham and OVX mice, the latter having a higher end-diastolic pressure.

In the sham-female group, HFD caused lower end-diastolic pressures than CTD, suggesting their ability to adapt. Knowing the deleterious effect of HFD, we propose that the sham-female mice adapt to this harmful situation by decreasing their end-diastolic pressure to limit or compensate for the expected increase of pressure due to the HFD.[378] Concerning the male, the end-diastolic pressure was not changed by the diet and was not different compared with the female. This is suggesting that female mice and not male nor OVX are able to decrease their end-diastolic pressure as a protective mechanism in response to HFD and dobutamine. Thus our results indicate a role of the ovarian hormones and the presence of a gender difference. The end-diastolic pressure is an important parameter to evaluate diastolic function. Menopause induces a higher risk of diastolic dysfunction,[425,426] at

baseline no differences were observed between sham and OVX-female mice at least at this stage.

The end-systolic pressure volume relationship, ESPVR, is a measure of contractility. The diet, the gender and the absence of ovarian hormones did not affect ESPVR in our mouse model after 22 wks of diet. Similarly, the end-diastolic pressure volume relationship, EDPVR, was not modified under our conditions. This variable is a direct indicator of LV compliance, the slope of this curve is inversely related to compliance, so when the slope is increased, the compliance is decreased and the stiffness increased and vice versa. Our data shows that the slope is not affected by diet, OVX or gender. Others groups have reported that HFD induces cardiac hypertrophy[427,428] and that this could have an influence on the end-diastolic pressure volume relationship. The absence of striking hypertrophy is thus matching the absence of defect in contractility and compliance. These two parameters ESPVR and EDPVR were determined by occluding the vena cava to increase the venous return. This method is well accepted to study cardiac contractility and compliance but was sometimes difficult to perform due to the presence of considerable amounts of white adipose tissue. This difficulty could explain the high variability observed in our experimental groups, which masks possible effects.

Diastolic dysfunction is characterized by an abnormal myocardial relaxation and filling of the ventricle and is associated with obesity, diabetes, renal disease and hypertension. This preclinical stage precedes systolic dysfunction in which the heart adapts to these changes by increasing left atrial pressure to load the LV with an adequate volume before contraction.[424] Our model showed that females exhibit moderate diastolic dysfunction and that males are more sensitive than females to develop defects in cardiac cycle dynamics in response to HFD feeding.

Several other groups worked on describing and understanding gender-differences related to the cardiovascular impact of obesity. Louwe et al. described that after 12 wks of HFD, cardiac function was defective only in male but not in female mice, independently of enhanced plasma lipids that occurred in both genders.[394] More precisely, male exhibited an increased end-diastolic volume after 6 wks of HFD and after 12 wks, end-systolic volume was also increased, while ejection fraction was decreased, whereas female did not exhibit any differences in cardiac function. Our own echocardiography data show that ejection fractions stayed unchanged, suggesting no alteration of the systolic function in any of the groups consistent with the preserved contractility (PVL experiment) and cardiac output. Other studies demonstrated that male rats fed with high fat and high sucrose exhibited

systolic dysfunction reflected by reduced fractional shortening and ejection fractions.[140,429] However, this phenomenon was not found in male mice where ejection fractions were unchanged after 18 wks of HFD.[430] The same authors described the presence of enhanced LV posterior wall and interventricular septum thickness in HFD- compared to CTD-fed mice, suggesting an adaptive answer to HFD. Brainard et al. demonstrated that HFD does not influence heart structure and function in male mice after 6 months of diet[431] whereas Park et al. showed a significant alteration of cardiac function after 20 wks of diet in male.[432] Therefore, different opinions are found concerning the effect of HFD on cardiac function and geometry. In our mouse model, no changes in ejection fraction were visible in the male, female and OVX mice, suggesting that gender and ovarian hormones are not implicated in the regulation of systolic function. Cardiac geometry was not modified in the male group but only in the female after HFD, perhaps due to the ability to the female to adapt. These discrepancies between studies suggest that duration of feeding, the model that was used, and gender are major factors for the different results obtained.

4.7 Male and ovariectomized female mice have increased cardiac steatosis

In our model, high fat diet feeding induced a body weight gain associated with increased visceral fat in all groups. The detection of lipids in the cardiac tissue revealed that after HFD feeding, the male developed more severe cardiac steatosis than the sham-female mice. After CTD feeding, the lipid droplets visible in the male group were less numerous but of a bigger size than in the sham-female group. Previous studies have demonstrated that diet-induced obesity induces an abnormal accumulation of triglycerides in cardiomyocytes, i.e. steatosis, and results in impaired cardiac function characterized by an increase in left ventricle end-diastolic diameter and altered contractile performance.[433,434] It is thought that cardiac dysfunction develops because cardiac steatosis is associated with the production of lipotoxic intermediates such as ceramides, which produce reactive oxygen, and may lead to apoptosis.[433] Cardiac geometry and function were similar between male and female after 21 wks of diet, however in female mice the HFD decreased the E/A ratio and induced an increase in the relative wall thickness and LVPW as well as a reduced end-diastolic pressure. These effects of HFD feeding were not present in the male mice. Whether our observation of a gender difference in steatosis is directly related to cardiac dysfunction is not clear at this moment.

In our study, the ablation of estrogen triggered a more pronounced cardiac accumulation of lipids than in the sham-female already when fed with CTD, and the HFD marked this difference even further. Indeed, the increased number of lipid droplets associated with HFD feeding was more important in the OVX- group than in the sham-female group and this

observation might be linked to the fact that OVX induces an increase in total adiposity suggesting the presence of a larger amount of free fatty acid. It will be interesting to evaluate the level of lipotoxic intermediates, reactive oxygen species and apoptotic cells in this context.

4.8 Effects of gender and ovariectomy on cardiac inflammation

The early stage of metabolic cardiomyopathy is associated with the onset of cellular abnormalities such as oxidative stress, mitochondrial dysfunction, ER stress, and defective calcium handling leading to impaired cardiac relaxation, however no structural or functional changes are detected at this stage. At a more advanced stage of the pathology, these abnormalities are enhanced and are accompanied by infiltration of inflammatory cells and neurohumoral activation, together causing cardiomyocyte apoptosis and cardiac fibrosis and leading to diastolic and systolic dysfunction.[212,435] The signs of diastolic dysfunction that we observed in our model went along with small changes in the mRNA levels of different important players of inflammation and fibrosis such as IL-6, TNFα, collagen I and collagen III. However, none of these changes reached significance at this stage of the experiment regardless the conditions. Only small trends appeared toward increased IL-6 mRNA expression in the OVX-female compared to the sham-female mice after HFD, while TNFα increased in the OVX group after HFD. However, the NF-κB inhibitory protein IκBα was decreased in the sham-female group after HFD indicating increased NF-κB activity. Consistently, we observed a small increase in phosphorylated NF-κB, suggesting an increased cardiac inflammatory response due to the HFD feeding in these sham-female mice. In obese mice, it has been described that TGF-β-Smad signaling is over-activated in the heart,[436] which is known to be triggered by inflammation and is thought to cause fibrosis. Moreover, it has been reported that HFD-induced obese mice have high protein levels of TLR4 and macrophage infiltration in the heart.[437] In line with this literature, in our mouse model the Mac-2 staining revealed increased macrophage infiltration in the heart of HFD-fed mice along with the signs of fibrosis that we observed.

Diastolic dysfunction associated with obesity has previously been related to enhanced inflammation and collagen deposition.[438-440] Consistent with the slightly increased inflammation, our preliminary results of the Picrosirius red staining also did not reveal any obvious difference between the groups, although a proper quantification still remains to be done. It has been suggested that a hypertensive stimulus is needed for the development of fibrosis in obesity,[441] hence the possible reason of our minor effects of HFD and OVX on cardiac inflammation and fibrosis. Indeed, a model of hypertensive OVX rats showed LV remodeling associated with increased collagen deposition and hypertrophy, which was

reversed by the administration of GPER agonist G-1.[442] This implies an important role of estrogen in fibrosis. These results were partially in line with our own results as IL-6 was increased in the OVX-female compared to the sham-female mice after HFD. Moreover, NF-κB and TNFα were also enhanced in the OVX female and not in the sham-female mice after HFD. Thus, it would be of interest to further investigate the effect of OVX and HFD in our model and to appropriately quantify the histology result of the Picrosirius Red staining. Moreover, given the fact that collagen deposition is not always associated with changes in collagen and pro-fibrotic genes expression, it will be worthy to evaluate other molecules involved in extracellular matrix changes such as the matrix metalloproteinase (MMP) or the tissue inhibitor of metalloproteinase (TIMP).[443]

Taken together, our results show signs of inflammation and fibrosis in line with mild effects of HFD and OVX on cardiac geometry and function as measured by echocardiography and PVL analysis, and are suggestive of diastolic dysfunction. Moreover, our results indicate that E2 may be implicated in the maintenance of anti-inflammatory effects in the heart.

4.9 High fat diet decreases the cardiac stress marker ANP in female mice

BNP levels are often used as prognostic marker of heart failure and in animal models both ANP and BNP are used as markers of cardiac stress and hypertrophy.[444,445] Our mouse model showed unexpected results concerning these markers. First of all, the HFD strongly decreased ANP levels in both female groups, but not in the male group. A possible interpretation is that the hemodynamic stress or hypertrophy induced by HFD (we found only small effects on wall thickness, see above) was not sufficient to increase the expression of ANP. It was even decreased in the females, suggesting that their hearts are less stressed. The decreased levels in both female groups may however also be harmful, because ANP exerts beneficial effects through its natriuretic action, by which it reduces blood pressure. In our study, any changes in blood pressure that may have happened were below detection level. It has been shown that deregulation of the endogenous cardiac ANP and its receptor might provoke cardiomyocyte hypertrophy.[444-446] Similar to our study, Nilsson et al. found that in female mice, cardiac ANP gene expression was decreased after a low carbohydrate and high fat diet despite any changes in cardiac hypertrophy evaluated by echocardiography.[447] Recently, it has also been reported that decreased ANP expression coincides with an increase of its receptor NPR-A, and was associated with metabolic dysfunction.[446] This observation was similar to our results, we also showed a decrease in ANP and cardiac metabolic alterations (see below).

The absence of increased ANP expression in our model is not surprising as it is in line with the mild effects on cardiac function and geometry due to HFD and OVX. Indeed, our mouse model did not develop strong cardiac hypertrophy as only small increases of the LV posterior and anterior walls, as well as the relative wall thickness were observed in the female mice. Overall, our model showed only a moderate level of stress, which was also confirmed by the small increased level of inflammation. At first sight, the decrease in ANP observed in our study could be deleterious, since ANP acts to decrease blood pressure, and this decrease would lead to an increase in pressure. However, increased pressures were not seen in our model, which makes the interpretation of this result complex: no strong hypertrophy nor effects on pressures were observed but ANP was modified. We could hypothesize that the ANP decrease is preceding the usually seen increase of ANP in cardiac stress and hypertrophy, and that at a later timepoint we could have detected a higher level of ANP in the mice fed with HFD. Alternatively, we will need to evaluate the expression of ANP at the protein level, as mRNA levels do not always reflect protein levels. It would also be interesting to analyze NPR-A receptor expression in the heart.

4.10 High fat diet and ovariectomy modify metabolic signaling pathways

4.10.1 Ovariectomy reduces IRS-1 protein level after high fat diet feeding

To better understand the functioning of the glucose intolerance observed in the OVX-female mice and to check if regulators of glucose metabolism were altered in the heart, we analyzed different targets at the protein level. IRS-1 is part of the insulin pathway, it is an adapter protein that transduces the signal from the insulin receptor to PI3K. OVX resulted in decreased IRS-1 protein amounts under CTD conditions, but this decrease did not occur after HFD feeding. The lower IRS-1 protein in the CTD-fed OVX-female suggests that ovarian hormones regulate the balance of IRS-1 protein synthesis and degradation, with a shift towards more degradation when these hormones are missing.

Next to this effect of OVX, we observed a gender difference because the male had a higher IRS-1 than the sham-female mice after HFD, which could be a consequence of their higher insulin resistance as deducted from their very high plasma insulin. Indeed, the high IRS-1 observed after HFD could indicate that males are trying to compensate their insulin resistance by increasing IRS-1 protein. In line with this high insulin resistance, IRS phosphorylation at S636-639 was increased in the HFD-fed male group, a site that is thought to cause the degradation of IRS-1.[448-451] Interestingly, sham-female mice showed a decrease of IRS-1-pS636-639 phosphorylation, which suggests better insulin responsiveness than in males. The gender-specific effects of HFD on IRS-1-phosphorylation matched the

total IRS-1 protein levels. Both IRS-1 and IRS-1 phosphorylation are decreased in OVX-female compared to the sham-female mice, suggesting good insulin responsiveness with a higher IRS-1 protein degradation or turnover. However, the OVX mice are more glucose intolerant, so it will be interesting to evaluate for example the activity of upstream targets, the insulin receptor and downstream targets of IRS-1, PI3K.

4.10.2 High fat diet decreases total Akt protein

We found no effects of gender, OVX and diet on the phosphorylation of Akt at the T308 site, which indicates that Akt activity was not affected. Given the increased plasma insulin, which was particularly high in the male and also elevated in the females after HFD, this highlights that the heart is not affected by these differently elevated plasma insulin levels. In this regard, it would be worthy to analyze the effect of insulin on skeletal muscle, an important organ responsible for glucose clearance. Consistently, downstream of Akt phosphorylation of AS160, a protein involved in glucose transporter translocation, was not increased in any of the groups after HFD. We would need to perform an ex-vivo working heart experiment to test if glucose uptake is indeed unchanged in the heart of OVX mice after HFD and to conclusively prove changes in the cardiac responses to insulin.

Our findings that Akt-pT308 and AS160-pT642 were not influenced by the diet at 22 wks are consistent with the results from Abel's group, which showed that phosphorylation of Akt and its downstream targets were not affected by HFD.[452] However, another study found reduced Akt phosphorylation after 1.5 wks of HFD.[432] It is not clear how glucose intolerance and insulin resistance are initiated, but several studies suggest the implication of ectopic lipid accumulation, endoplasmic reticulum stress activation, and inflammation responses through adipokines and cytokines.[453] Despite the fact that estrogen is involved in insulin/Akt signaling in cardiac muscle,[454-456] the phosphorylation of Akt at T308 showed no changes after HFD in the OVX mice. In line with the absence of any effects on Akt signaling in our own study, Wright et al. demonstrated that insulin stimulated glucose uptake and GLUT4 translocation in the myocardium are impaired without any Akt pathway alterations even after insulin stimulation.[133]

Interestingly, total Akt protein expression was significantly decreased by HFD in both female groups. Despite this decrease in total Akt, phosphorylation levels remained similar to those in the mice fed with CTD. Since Akt activation is thought to act as a protective mechanism, this could suggest that despite decreased total Akt due to the HFD, Akt is acting normally to conserve a normal physiological condition in the heart. In this context, it would be interesting to evaluate the activity of Akt at a later stage and observe if this

implementation of a protective pathway is still present. Furthermore, our study reveals that the total form of AS160 is increased in the OVX mice after HFD, but the phosphorylated form was unchanged, which again reflects unmodified activity. To the best of our knowledge, our study is the first to describe this gender difference and to show that ovarian hormones are not implicated.

The protein mTOR is next to AS160 another downstream effector of Akt. Akt-induced mTOR phosphorylation at S2448 displayed small increases due to the HFD in the female groups, as opposed to the male group, in which this phosphorylation was slightly reduced. In contrast, other studies described increased cardiac mTORC1 activity in the male heart after HFD.[457,458] In our own study, the sham-female mice had higher mTOR phosphorylation than the male after HFD feeding, indicating a gender difference. This suggests that female mice are able to induce an adaptive mechanism in response to HFD, which the male mice are not able to do, at least at the timepoint that the animals were sacrificed. As the mice fed with HFD are bigger than the others, it would make sense that the heart has to grow bigger, and that mTOR could be more activated to support this necessary growth. The fact that the males did not demonstrate increased mTOR phosphorylation suggests a lack of cardiac adaptation. There were indeed no differences in cardiac weight and function due to HFD in the male group. We found slightly increased raw ventricle weight as well as increased wall thickness in females, which may be related to the modest mTOR-pS2448 changes. Possibly, the lack of clear effects on mTOR phosphorylation may be due to the impaired activation of this pathway under HFD conditions. Alternatively, the absence of increased mTOR activity, which we confirmed at the level of its direct target p70-S6K1, could be beneficial, because recent studies showed that mTOR inhibition could be protective. Indeed, rapamycin was shown to enhance cardiac function and improve metabolic disorders linked to T2DM and obesity including reduction in oxidative stress and a correction in contractile performance.[459]

4.10.3 High fat diet increases PDH in female mice

The pyruvate dehydrogenase lipoamide kinase isozyme 4 (PDK4) is a mitochondrial enzyme implicated in glucose oxidation. This enzyme phosphorylates and inactivates the PDH complex, which transforms the pyruvate into acetyl-CoA that can then enter the TCA cycle. Thus, PDK4 activity results in a decreased glucose oxidation. First of all, our data show that the OVX mice had higher mRNA expression of PDK4 than the sham-female mice. Secondly, the HFD significantly decreased the OVX-induced increase in PDK4 mRNA. Notably, the differences in PDK4 gene expression were not mirroring its protein expression. Thus, OVX increased only PDK4 mRNA but not PDK4 protein. Only the sham-female group had a

decrease in PDK4 protein expression after HFD. The discrepancies between mRNA and protein expression emphasize the need for analyzing regulation at both levels. PDK4 is highly expressed in hearts of fasted and insulin-resistant animal models. In a streptozotocin-induced type 1 diabetic rat model, PDK4 mRNA was increased in the heart and skeletal muscle.[87,88] In human, insulin resistant patients also exhibit a high PDK4 level in skeletal muscle.[89] It has been reported that insulin represses PDK2 and PDK4 through phosphorylation of FOXO via the PI3K/Akt signaling pathway. The negative regulation of insulin on PDK4 mRNA expression was impaired in an acute insulin resistant mouse model, proposing that insulin resistance increases PDK4 expression.[460] Indeed, this is confirmed by the fact that insulin treatment reversed the increase of PDK4 and PDK2 in liver and skeletal muscle induced by dexamethasone.[88,89] In a mouse model fed with HFD for 10 days, cardiac PDK4 was upregulated with a concomitant decrease in carbohydrate oxidation as a result of PDH activity suppression.[461] This short-term feeding is contrasting with our study, where we observed that PDK4 mRNA was decreased together with phosphorylated PDH protein after 22 wks of feeding. It could be speculated that at short-term, PDK4 is first upregulated and is decreasing glucose oxidation and that at longer term it gets downregulated to favor glucose oxidation at the expense of decreased fatty acid oxidation. Moreover, in our model, the mice were not diabetic yet, insulin was probably still able to decrease PDK4 expression in the heart to induce increased PDH activity and glucose oxidation. Altogether, our results propose that after 22 wks of diet OVX decreases glucose oxidation, and HFD reverses this effect.

As PDK4 is known to inhibit PDH activity, we analyzed PDH expression and phosphorylation. Overall, HFD decreased PDH phosphorylation suggestive of increased glucose oxidation. Inversely to our observation, in the skeletal muscle HFD induces a downregulation of PDH activity via PDK4 to inhibit pyruvate entry in the TCA cycle and the subsequent glucose oxidation.[462] Post-hoc testing showed that OVX caused a trend toward higher PDH-pS293 under CTD conditions and HFD significantly decreased this phosphorylation, mirroring the changes observed in PDK4. Taken together these data suggest that ovarian hormones are increasing glucose oxidation. In the absence of ovarian hormones, HFD abolishes the decrease in glucose oxidation. The total form of PDH was increased in response to the HFD in the female while it was not changed in the male mice, this maybe represents a counter regulatory effect in order to upregulate glucose oxidation.

In another type of study, Kim et al. used a rat model to induce acute insulin resistance by constant infusion of Intralipid (a fat emulsion) and lactate for 5h in fasted animals. This resulted in 2- to 3-fold higher PDK4 expression in skeletal muscle after insulin infusion,

indicating that insulin was not able to suppress PDK4 and proposing that the rats were insulin resistant. This infusion also suppressed the phosphorylation of Akt and FOXO1 highlighting the resulting insulin resistance.[460] Our own results showed again different effects, as HFD induced an overall decrease of PDK4 mRNA. One interpretation of this difference could be that the acute insulin resistance does not induce similar effects as chronic resistance induced by long-term HFD feeding, and that skeletal and heart muscle react in a different manner to this acute insulin resistance.

Many studies related to the understanding of PDK4 have been performed on skeletal muscle but very little is known about its activity in the heart. It was observed that metabolic inflexibility correlates with cardiomyopathy occurrence especially during ischemia and could cause heart failure.[137] In this context, the reason for reduced cardiac efficiency is linked to the inability to use carbohydrates to meet energy demands. Indeed, a cardiac specific overexpression of PDK4 causes a loss of metabolic flexibility and exacerbates cardiomyopathy, which is associated with decreased glucose catabolism and increased FA oxidation.[463]

The mRNA level of GAPDH was decreased in all HFD groups, suggesting that glycolysis may be decreased after HFD, consistent with the known literature. This possible inhibition of glycolysis after HFD could explain the decreased PDH inhibitory phosphorylation and the increased total PDH, which would increase glucose oxidation as a compensatory feed-back effect. This is explained by the fact that under normal conditions the heart preferentially uses FA oxidation as first source of energy, with glucose oxidation being a second energy source. However, when fed with high fat diet this phenomenon is exacerbated and the heart switches toward an almost exclusive FA use.[464] Hence the observed decrease in glucose metabolism genes and increase in FA oxidation genes such as CPT-Iβ.

4.10.4 High fat diet increases PPARα in male mice

We observed HFD-induced increases in PPARα gene expression in the male mice and a similar trend was seen in the sham-female, but not in the OVX mice. PPARα regulates several genes implicated in fatty acid uptake into the cytoplasm and mitochondria as well as genes involved in the generation of fatty acyl CoA. Our results therefore suggest that the males mainly have an increased use of FA, which could be the consequence of the inability of the heart to use glucose as a result of insulin resistance. The OVX-female mice do not show this increase of PPARα, suggesting that their FA metabolism is not increased at this stage after HFD. Our results are similar to those obtained by others after a shorter period of HFD feeding.[452] The authors of this study showed that PPARα target genes and PPARα itself

were increased after 5 wks of HFD. PPARα activation may therefore have a role to sustain the metabolic change toward fatty acid use. At the early stage of the cardiomyopathy pathology, a defect in glucose transport seems to be happening as a first cardiac metabolic adaptation to high fat diet. Abel proposed that this adaptation where glucose utilization is reduced is the main cause for a secondary increase in fatty acid oxidation as the Randle cycle describes it.[465]

4.10.5 Ovariectomy modifies ULK1

We aimed to elucidate if gender and ovarian hormones play a role in regulating autophagy in our obesity model. Our western blot analysis shows that HFD induced an increase in ULK1-pS757 in the OVX-female mice, whereas in sham-female and male mice no increases were observed. As ULK1-pS757 is known to inhibit autophagy,[466,467] these results suggest that the ovarian hormones increase autophagy under HFD conditions. Our analysis of the LC3BII/I ratio did not allow us to confirm this conclusion. No differences were observed due to high variability, which made the autophagy analysis difficult. To conclude about the implication of autophagy further experiments have to be performed such as immunofluorescence or inducing an in-vivo blockage of autophagy to measure autophagy flux, which is more relevant since autophagy is a dynamic process.

The regulation of autophagy is highly complex and in diabetic cardiomyopathy it is not clear if either upregulation or downregulation of autophagy can help the heart. In such conditions, it has been documented that autophagy is suppressed and that this could be assigned to an inhibition of the AMPKα pathway, accompanied by an increase of mTOR activity.[468,469] It has been reported that Beclin 1 knockout, which leads to diminished autophagy, is cardioprotective in a mouse model of type I diabetes by improving cardiac function, reducing oxidative stress level, interstitial fibrosis and myocyte apoptosis.[470] On the other hand, inducing autophagy by stimulating AMPKα leads to an improved cardiac situation by preventing high glucose-induced apoptosis in cardiomyocytes.[471]

These contradictory results lead to the question whether autophagy inhibition in the diabetic heart is a maladaptive or an adaptive response. The answer is not clear and seems to depend on the specific stress condition. Many studies have been performed to elucidate this question and many conclusions were drawn. Thus, decreased autophagy was reported to limit cardiac injury in a mouse model of type 1 diabetes,[472] whereas He et al. showed that increased cardiac autophagy is cardioprotective in diabetes.[473] In a model of diet induced obesity and metabolic syndrome, Sciaretta et al. found that autophagy was suppressed in the heart through deregulation of the Rheb/mTORC1 activation, suggesting

that mTORC1 participates in the cardiac growth observed in obesity and metabolic disorders.[474] Some studies described that autophagosome formation or autophagic flux was impaired in hearts of obese and diabetic animals and it was associated with decreased mTORC1 activity and cardiac dysfunction. Indeed, in a swine model of metabolic syndrome, a decreased autophagosome formation was observed and was associated with decreased mTOR activity, increased apoptosis, decreased mitochondrial function and abnormalities in cardiac structure and function.[475] In another model of HFD-induced obesity, cardiac autophagosome formation was also found reduced, mTOR activity was increased and cardiac function was altered, effects which were rescued by rapamycin.[476] In obese mice, deregulated cardiac Akt2 perturbed the autophagic flux.[477] Similarly, in STZ-induced diabetes, cardiac autophagosome formation and autophagic flux were impaired and associated with increased mTOR activity.[472] In the kidney and liver of obese mice, inhibition of autophagosome formation involved mTORC1 activation.[478,479]

In the context of our diet-induced obesity model, two theories can be proposed. Autophagy is downregulated during periods of energy abundance obtained by HFD feeding because renewal of metabolic precursors such as amino acids and fatty acids is not needed. Conversely, since HFD feeding exerts a deleterious effect on cellular metabolism resulting in accumulation of damaged mitochondria, lipids droplet, misfolded or aggregated proteins (ER stress), autophagy has to be upregulated to counteract this situation and bring cardiomyocytes back to a physiological status. The question whether or not autophagy is harmful or protective is always a topical question. In this regard, our results can be interpreted in two different manners. Either the OVX mice, unlike the sham-female and the male mice, failed to eliminate the damaged organelles and lipids droplets as a consequence of their reduced autophagy, or their reduced autophagy may have been beneficial. Given the observed increase lipids droplet accumulation in the OVX-HFD group, we think that the first interpretation might be correct.

4.11 Limitations

By using the ovariectomized model, we aimed to mimic the phenomenon observed in menopausal women where a decline of ovarian hormones, mainly estrogen, is present. Our goal was to study the role of estrogen in the maintenance of cardiac structure and function. This model is widely used as it closely resembles surgical and natural menopause in humans.[480] However, the model has some limitations. First of all, the ablation of ovaries triggers a sudden loss of ovarian hormones which is not seen in natural menopause as the hormone level decreases progressively; indeed a transition from perimenopause to menopause exists in reality.[480,481] It was reported that the response to OVX is more robust and faster in young rodents (2-6 months) with regular estrous cycles than in aged rats.

Indeed, one week after OVX, young rats have very low or undetectable concentrations of circulating ovarian hormones,[482-484] whereas middle-aged (9-14 months) or old (18-30 months) rats still have detectable circulating level of estrogen and progestin for weeks or months after OVX.[482,483] Thus, to get closer to what is observed in humans, it would be more precise to use female rodents at a more advanced age. Thus, the ablation of ovaries can be done at different stages of the animal's life and this is not always matching the age where menopause is observed in human. In preclinical studies, the ablation of the ovaries could be performed at 2-6 months, which corresponds to the period of the regular estrous cycle, 11 months, corresponding to the beginning of acyclicity, or 18 months where a constant estrous starts to appear where ovaries contain big follicles that secrete large quantities of estrogen.[480,485] Additionally, age-specific effects are present and influence the interpretation of the results, but these effects are also important to understand the age-related factors.[480,485] The different age at which OVX is performed may explain the discrepancies observed between the studies, for example young and old rats do not respond the same way to OVX and hormone replacement.[486] Thus, ideally one should perform OVX at the rodent's chronologically equivalent of middle age.

The pressure-volume loop technique is an appreciated method to evaluate intra-cardiac pressure and volume, however we obtained some negative values for the volume data, making them less reliable because of specific constraints: 1) The parallel conductance varies according to the position of the probe, for some mice the heart orientation or anatomy did not allow a proper penetration and orientation of the catheter into the LV, the parallel conductance is not reliable in this case. 2) Blood is used for the volume calibration at the end of the experiment and the blood temperature is critically influencing the calibration itself, thus artifacts can appear at this stage and may explain the negative volume values obtained. 3) Finally, to obtain trustable volume values, one should combine different methods, indeed it is recommended to use MRI for example to obtain the α value used to calculate volume from conductance (see formula 1.1.5). This α is the gain coefficient and corresponds to the volume correction or calibration factor and is important for volume calculation. Unfortunately, we were not able to determine this value. Altogether, these reasons make it necessary to use the volume data obtained via the PVL method with caution. Nevertheless, our analysis showed differences in LV volume between our conditions, but the results are not shown and discussed, for the reasons outlined here.

5. Conclusions and Perspectives

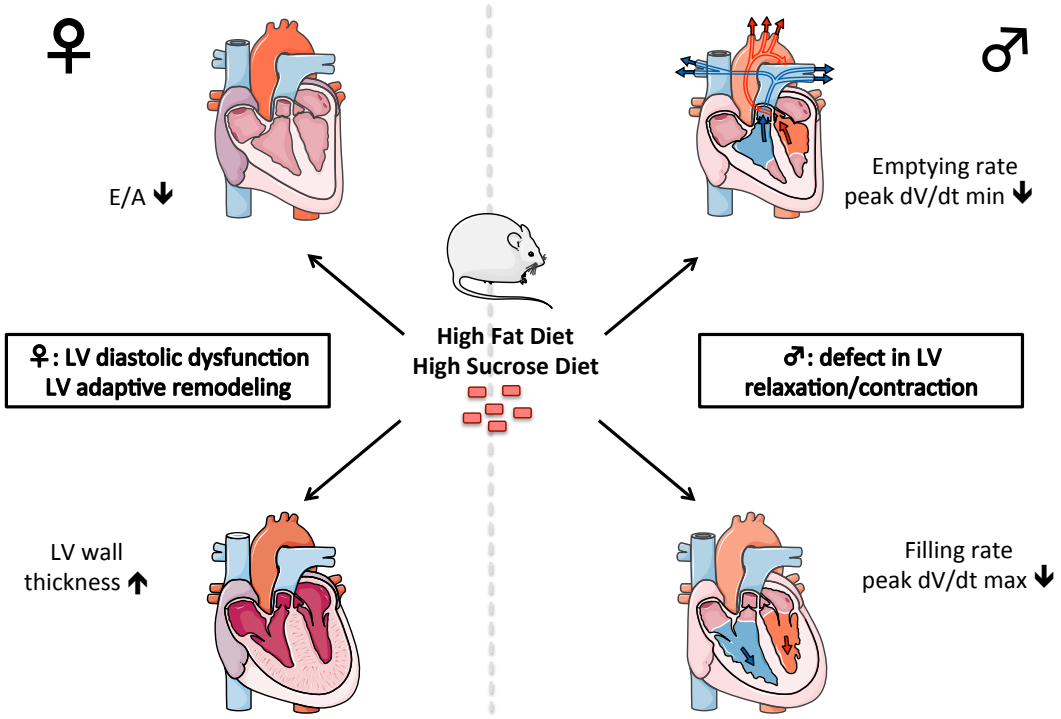

Figure 30: Gender-specific effects of HFD on cardiac function and geometry.
♂, male mice; ♀, female mice; E2, estrogen. Arrows represent an increased or decreased parameter.

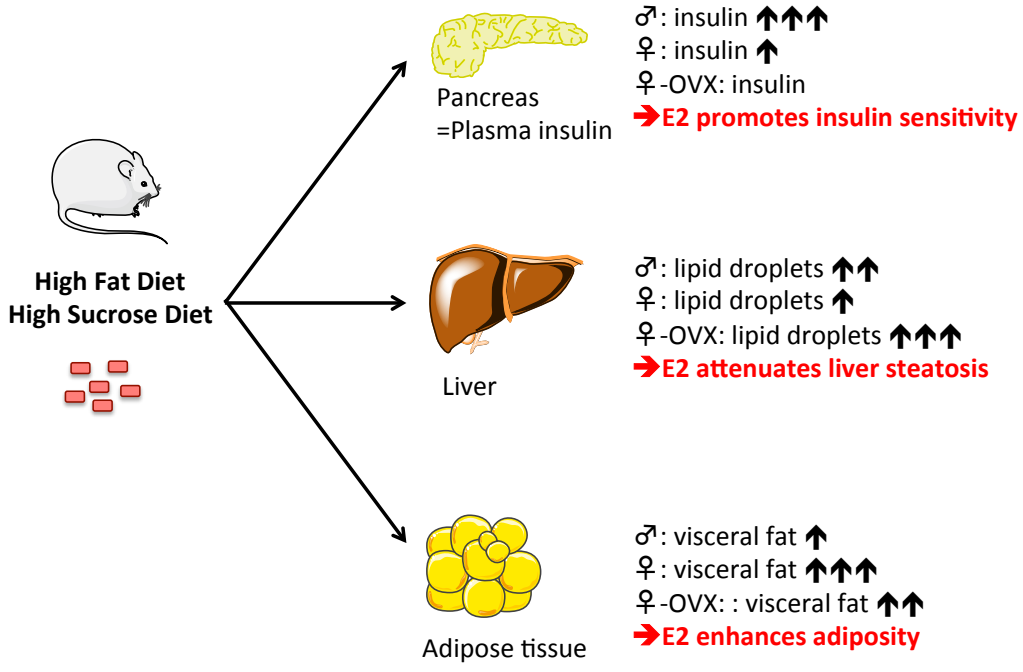

Figure 31: Systemic effects of HFD feeding in our mouse model.
♂, male mice; ♀, female mice; OVX, ovariectomized mice; E2, estrogen. Arrows represent an increased parameter.

Women are less prone to be affected by cardiovascular disease compared to age-matched men. Nevertheless, this female advantage is gradually lost when they reach menopause. This raises the question to know why and how this phenomenon occurs. Many studies suggested that estrogens are cardioprotective, but some of them showed that they could also be deleterious in certain conditions. Hence the need to characterize and better understand the mechanisms underlying the effects of estrogen in the cardiovascular system. In this context, we aimed at describing gender- and ovarian hormone-specific consequences of obesity in the heart. Thus, we analyzed the effect of HFD, gender and ovariectomy on cardiac function and structure and investigated the mechanisms involved.

We demonstrated that high sucrose and fat feeding causes the following gender-specific changes (Figure 30-31):
1. stronger increases of plasma insulin in male than in female mice, suggestive of higher insulin sensitivity in the female mice.
2. strong decreases of the peak filling and emptying rates in male mice only, suggesting that their ventricular relaxation is impaired.
3. decreased E/A ratios in the female mice only, suggesting mild diastolic dysfunction
4. moderate wall thickness increases in the female only, suggestive of cardiac remodeling.

As for the role of female hormones, we demonstrated that (Figure32):
1. Ovarian hormones are implicated in increasing plasma insulin and maintaining glucose tolerance in response to HFD, since OVX abolished the increase in insulin and decreased glucose tolerance.
2. After dobutamine infusion, OVX mice had higher end-diastolic pressure than the sham-female mice after HFD, suggesting that estrogens are implicated in the adaptation to increased cardiac work.
3. OVX mice had a higher expression of PDK4 and its downstream target PDH, suggesting that ovarian hormones are important for preserving a normal glucose oxidation.

In conclusion, our mice showed signs of diabetic cardiomyopathy since they presented overweight, hyperglycemia, insulin resistance, hyperinsulinemia, and altered cardiac contraction and relaxation velocities without blood pressure changes. Moreover, we demonstrated that female and male mice are not affected by HFD in the same way, and only female mice are able to implement a cardiac adaptation to counteract harmful effects of the high fat diet. The ovarian hormones are playing a role in maintaining physiological cardiac function. Our study helps to better understand diastolic dysfunction and may in the

future be translated to the situation of postmenopausal women, a population particularly affected by cardiovascular disease.

Hypertension is a major cardiovascular risk, and therefore it will be interesting to induce an additional stress to trigger hypertension in our mouse model. This will possibly help to achieve a complete diastolic dysfunction phenotype. Once this state is reached, hormonal replacement therapy could be applied to reverse the cardiac dysfunction. More precisely, a specific GPER agonist, G-1, would help to evaluate the short and long-term benefits of estrogen signaling activation via the GPER. Similar to the present study, cardiac function would be assessed by echocardiography and pressure-volume loop techniques. The effects of HFD, gender and ovarian hormones would be assessed at the macroscopic level and the underlying mechanisms at the protein and RNA levels, by studying insulin/Akt/mTOR pathways, inflammation, autophagy and apoptosis. For further investigations, a Langendorff isolated heart model should be used to assess the direct effect of estrogen pathway stimulation on cardiac function, contractility, and conduction.

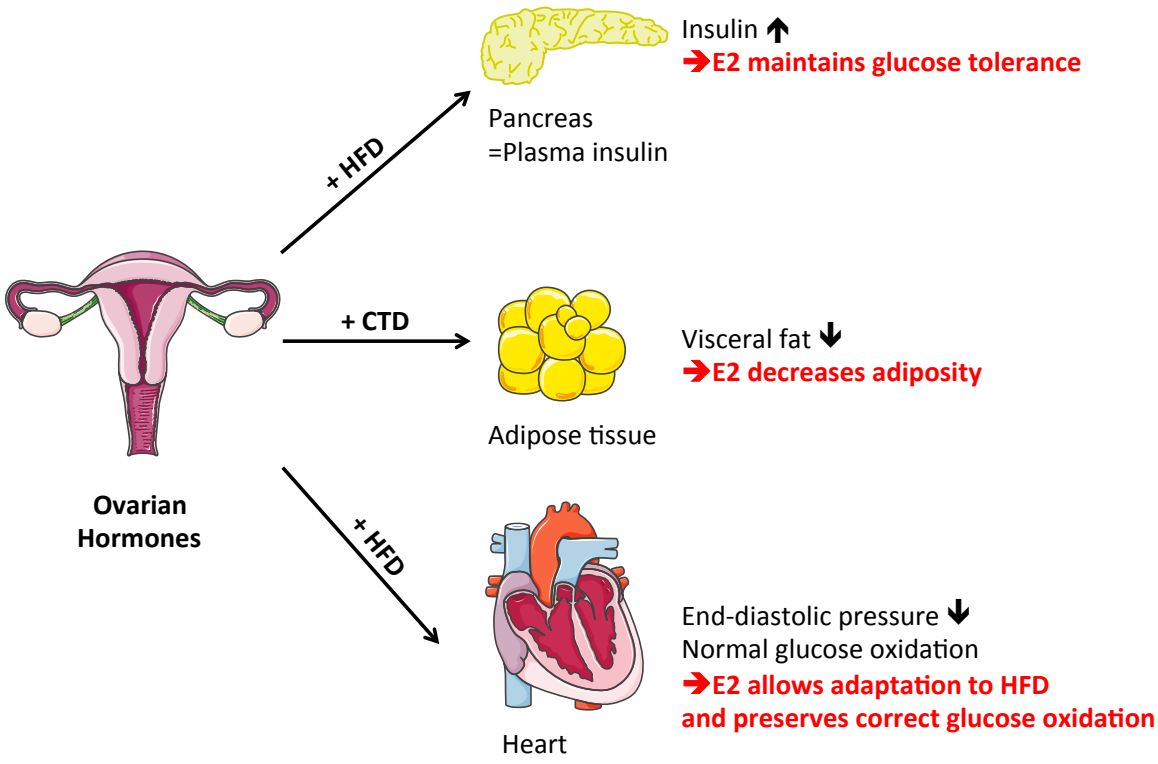

Figure 32: Ovarian hormones - specific effects on the pancreas, adipose tissue and heart.
E2, estrogen. Arrows represent an increased or decreased parameter.

6. References

1 Alberti, K. G. M. M. *et al.* Harmonizing the Metabolic Syndrome A Joint Interim Statement of the International Diabetes Federation Task Force on Epidemiology and Prevention; National Heart, Lung, and Blood Institute; American Heart Association; World Heart Federation; International Atherosclerosis Society; and International Association for the Study of Obesity. *Circulation* **120**, 1640-1645, doi:10.1161/Circulationaha.109.192644 (2009).

2 Kannel, W. B. & McGee, D. L. Diabetes and cardiovascular disease. The Framingham study. *JAMA* **241**, 2035-2038 (1979).

3 Schonfelder, G. The biological impact of estrogens on gender differences in congestive heart failure. *Cardiovascular Research* **67**, 573-574, doi:10.1016/j.cardiores.2005.06.017 (2005).

4 Mercuro, G. *et al.* Evidence of a role of endogenous estrogen in the modulation of autonomic nervous system. *American Journal of Cardiology* **85**, 787-+, doi:Doi 10.1016/S0002-9149(99)00865-6 (2000).

5 Rossouw, J. E. *et al.* Risks and benefits of estrogen plus progestin in healthy postmenopausal women: principal results From the Women's Health Initiative randomized controlled trial. *JAMA* **288**, 321-333 (2002).

6 Grady, D. *et al.* Cardiovascular disease outcomes during 6.8 years of hormone therapy: Heart and Estrogen/progestin Replacement Study follow-up (HERS II). *JAMA* **288**, 49-57 (2002).

7 Harman, S. M. *et al.* Arterial imaging outcomes and cardiovascular risk factors in recently menopausal women: a randomized trial. *Ann Intern Med* **161**, 249-260, doi:10.7326/M14-0353 (2014).

8 Manson, J. E. *et al.* Menopausal hormone therapy and health outcomes during the intervention and extended poststopping phases of the Women's Health Initiative randomized trials. *JAMA* **310**, 1353-1368, doi:10.1001/jama.2013.278040 (2013).

9 Kannel, W. B. & Wilson, P. W. Risk factors that attenuate the female coronary disease advantage. *Arch Intern Med* **155**, 57-61 (1995).

10 Hu, G., Jousilahti, P., Qiao, Q., Katoh, S. & Tuomilehto, J. Sex differences in cardiovascular and total mortality among diabetic and non-diabetic individuals with or without history of myocardial infarction. *Diabetologia* **48**, 856-861, doi:10.1007/s00125-005-1730-6 (2005).

11 Kappert, K. *et al.* Impact of sex on cardiovascular outcome in patients at high cardiovascular risk: analysis of the Telmisartan Randomized Assessment Study in ACE-Intolerant Subjects With Cardiovascular Disease (TRANSCEND) and the Ongoing Telmisartan Alone and in Combination With Ramipril Global End Point Trial (ONTARGET). *Circulation* **126**, 934-941, doi:10.1161/CIRCULATIONAHA.111.086660 (2012).

12 Lam, C. S. & Little, W. C. Sex and cardiovascular risk: are women advantaged or men disadvantaged? *Circulation* **126**, 913-915, doi:10.1161/CIRCULATIONAHA.112.121582 (2012).

13 Juutilainen, A. *et al.* Gender difference in the impact of type 2 diabetes on coronary heart disease risk. *Diabetes Care* **27**, 2898-2904 (2004).

14 Costanzo, L. S. Physiology. (2014).

15 *HANDBOOK OF CARDIAC ANATOMY, PHYSIOLOGY, AND DEVICES*. (SPRINGER, 2016).

16 Gardin, J. M., Siri, F. M., Kitsis, R. N., Edwards, J. G. & Leinwand, L. A. Echocardiographic Assessment of Left-Ventricular Mass and Systolic Function in Mice. *Circulation Research* **76**, 907-914 (1995).

17 Tanaka, N. *et al.* Transthoracic echocardiography in models of cardiac disease in the mouse. *Circulation* **94**, 1109-1117 (1996).

18 Gardin, J. M. Echocardiography Practice Issues - Reimbursement, Quality-Control, Training, and Credentialing. *Echocardiogr-J Card* **12**, 147-151, doi:DOI 10.1111/j.1540-8175.1995.tb00534.x (1995).

19 Syed, F., Diwan, A. & Hahn, H. S. Murine echocardiography: A practical approach for phenotyping genetically manipulated and surgically modeled mice. *J. Am. Soc. Echocardiogr.* **18**, 982-990, doi:10.1016/j.echo.2005.05.001 (2005).

20 Tsujita, Y., Kato, T. & Sussman, M. A. Evaluation of left ventricular function in cardiomyopathic mice by tissue Doppler and color M-mode Doppler echocardiography. *Echocardiogr-J Card* **22**, 245-253, doi:DOI 10.1111/j.0742-2822.2005.04014.x (2005).

21 Lang, R. M. *et al.* Recommendations for Cardiac Chamber Quantification by Echocardiography in Adults: An Update from the American Society of Echocardiography and the European Association of Cardiovascular Imaging. *J. Am. Soc. Echocardiogr.* **28**, 1-U170, doi:10.1016/j.echo.2014.10.003 (2015).

22 Cohn, J. N., Ferrari, R., Sharpe, N. & Remodeling, I. F. C. Cardiac remodeling-concepts and clinical implications: A consensus paper from an international forum on cardiac remodeling. *J. Am. Coll. Cardiol.* **35**, 569-582, doi:Doi 10.1016/S0735-1097(99)00630-0 (2000).

23 Frohlich, E. D. & Susic, D. Pressure Overload. *Heart failure clinics* **8**, 21-+, doi:10.1016/j.hfc.2011.08.005 (2012).

24 Koren, M. J., Devereux, R. B., Casale, P. N., Savage, D. D. & Laragh, J. H. Relation of Left-Ventricular Mass and Geometry to Morbidity and Mortality in Uncomplicated Essential-Hypertension. *Ann. Intern. Med.* **114**, 345-352 (1991).

25 Diez, J. Towards a New Paradigm About Hypertensive Heart Disease. *Med. Clin. North Am.* **93**, 637-+, doi:10.1016/j.mcna.2009.02.002 (2009).

26 Ohno, M., Cheng, C. P. & Little, W. C. Mechanism of Altered Patterns of Left-Ventricular Filling during the Development of Congestive-Heart-Failure. *Circulation* **89**, 2241-2250 (1994).

27 Du, J. F. *et al.* Impaired relaxation is the main manifestation in transgenic mice expressing a restrictive cardiomyopathy mutation, R193H, in cardiac TnI. *American Journal of Physiology-Heart and Circulatory Physiology* **294**, H2604-H2613, doi:10.1152/ajpheart.91506.2007 (2008).

28 Armstrong, W. F. & Ryan, T. Feigenbaum's Echocardiography. (2015).

29 Solomon, S. D. & Bulwer, B. Essential Echocardiography a Practical Handbook With DVD. (2007).

30 Gao, S., Ho, D., Vatner, D. E. & Vatner, S. F. Echocardiography in Mice. *Current protocols in mouse biology* **1**, 71-83, doi:10.1002/9780470942390.mo100130 (2011).

31 Pacher, P., Nagayama, T., Mukhopadhyay, P., Batkai, S. & Kass, D. A. Measurement of cardiac function using pressure-volume conductance catheter technique in mice and rats. *Nature protocols* **3**, 1422-1434, doi:10.1038/nprot.2008.138 (2008).

32 Frank, O. On the Dynamics of Cardiac Muscle. *Am. Heart J.* **58**, 282-317, doi:Doi 10.1016/0002-8703(59)90345-X (1959).

33 Knowlton, F. P. & Starling, E. H. The influence of variations in temperature and blood-pressure on the performance of the isolated mammalian heart. *J Physiol* **44**, 206-219 (1912).

34 Markwalder, J. & Starling, E. H. On the constancy of the systolic output under varying conditions. *J Physiol* **48**, 348-356 (1914).

35 Patterson, S. W. & Starling, E. H. On the mechanical factors which determine the output of the ventricles. *J Physiol-London* **48**, 357-379 (1914).

36 Patterson, S. W., Piper, H. & Starling, E. H. The regulation of the heart beat. *The Journal of physiology* **48**, 465-513 (1914).

37 Taylor, R. R., Covell, J. W. & Ross, J. Volume-Tension Diagrams of Ejecting and Isovolumic Contractions in Left Ventricle. *American Journal of Physiology* **216**, 1097- & (1969).

38 Suga, H., Sagawa, K. & Shoukas, A. A. Load Independence of Instantaneous Pressure-Volume Ratio of Canine Left Ventricle and Effects of Epinephrine and Heart-Rate on Ratio. *Circulation Research* **32**, 314-322 (1973).

39 Loushin, M. K., Quill, J. L. & Iaizzo, P. A. Mechanical Aspects of Cardiac Performance. (2015).

40 Kreulen, T. H., Bove, A. A., McDonough, M. T., Sands, M. J. & Spann, J. F. The evaluation of left ventricular function in man. A comparison of methods. *Circulation* **51**, 677-688 (1975).

41 Abel, E. D. Insulin signaling in heart muscle: lessons from genetically engineered mouse models. *Curr Hypertens Rep* **6**, 416-423 (2004).

42 Stanley, W. C., Recchia, F. A. & Lopaschuk, G. D. Myocardial substrate metabolism in the normal and failing heart. *Physiological Reviews* **85**, 1093-1129, doi:DOI 10.1152/physrev.00006.2004 (2005).

43 Klionsky, D. J. *et al.* A comprehensive glossary of autophagy-related molecules and processes. *Autophagy* **6**, 438-448 (2010).

44 Randle, P. J. Regulatory interactions between lipids and carbohydrates: the glucose fatty acid cycle after 35 years. *Diabetes. Metab. Rev.* **14**, 263-283 (1998).

45 Storlien, L., Oakes, N. D. & Kelley, D. E. Metabolic flexibility. *Proc. Nutr. Soc.* **63**, 363-368, doi:10.1079/Pns2004349 (2004).

46 Galgani, J. E., Moro, C. & Ravussin, E. Metabolic flexibility and insulin resistance. *Am J Physiol-Endoc M* **295**, E1009-E1017, doi:10.1152/ajpendo.90558.2008 (2008).

47 Sugden, M. C., Zariwala, M. G. & Holness, M. J. PPARs and the orchestration of metabolic fuel selection. *Pharmacol. Res.* **60**, 141-150, doi:10.1016/j.phrs.2009.03.014 (2009).

48 Kuang, M., Febbraio, M., Wagg, C., Lopaschuk, G. D. & Dyck, J. R. B. Fatty acid translocase/CD36 deficiency does not energetically or functionally compromise hearts before or after ischemia. *Circulation* **109**, 1550-1557, doi:10.1161/01.Cir.0000121730.41801.12 (2004).

49 Chabowski, A. *et al.* Insulin stimulates fatty acid transport by regulating expression of FAT/CD36 but not FABPpm. *Am J Physiol-Endoc M* **287**, E781-E789, doi:10.1152/ajpendo.00573.2003 (2004).

50 Lee, C. H., Olson, P. & Evans, R. M. Minireview: lipid metabolism, metabolic diseases, and peroxisome proliferator-activated receptors. *Endocrinology* **144**, 2201-2207, doi:10.1210/en.2003-0288 (2003).

51 Staels, B. & Fruchart, J. C. Therapeutic roles of peroxisome proliferator-activated receptor agonists. *Diabetes* **54**, 2460-2470 (2005).

52 Kulkarni, A. A. *et al.* Emerging PPARgamma-Independent Role of PPARgamma Ligands in Lung Diseases. *PPAR research* **2012**, 705352, doi:10.1155/2012/705352 (2012).

53 Wu, P. F., Inskeep, K., Bowker-Kinley, M. M., Popov, K. M. & Harris, R. A. Mechanism responsible for inactivation of skeletal muscle pyruvate dehydrogenase complex in starvation and diabetes. *Diabetes* **48**, 1593-1599, doi:DOI 10.2337/diabetes.48.8.1593 (1999).

54 Cadoudal, T. *et al.* Pyruvate dehydrogenase kinase 4 - Regulation by thiazolidinediones and implication in glyceroneogenesis in adipose tissue. *Diabetes* **57**, 2272-2279, doi:10.2337/db08-0477 (2008).

55 Barger, P. M. & Kelly, D. P. PPAR signaling in the control of cardiac energy metabolism. *Trends Cardiovasc Med* **10**, 238-245 (2000).

56 Duan, S. Z., Ivashchenko, C. Y., Russell, M. W., Milstone, D. S. & Mortensen, R. M. Cardiomyocyte-specific knockout and agonist of peroxisome proliferator-activated receptor-gamma both induce cardiac hypertrophy in mice. *Circ Res* **97**, 372-379, doi:10.1161/01.RES.0000179226.34112.6d (2005).

57 Finck, B. N. *et al.* The cardiac phenotype induced by PPARalpha overexpression mimics that caused by diabetes mellitus. *J Clin Invest* **109**, 121-130, doi:10.1172/JCI14080 (2002).

58 Hafstad, A. D. *et al.* Cardiac peroxisome proliferator-activated receptor-alpha activation causes increased fatty acid oxidation, reducing efficiency and post-ischaemic functional loss. *Cardiovascular Research* **83**, 519-526, doi:10.1093/cvr/cvp132 (2009).

59 Panagia, M., Gibbons, G. F., Radda, G. K. & Clarke, K. PPAR-alpha activation required for decreased glucose uptake and increased susceptibility to injury during ischemia. *Am J Physiol Heart Circ Physiol* **288**, H2677-2683, doi:10.1152/ajpheart.00200.2004 (2005).

60 Campbell, F. M. *et al.* A role for peroxisome proliferator-activated receptor alpha (PPARalpha) in the control of cardiac malonyl-CoA levels: reduced fatty acid oxidation rates and increased glucose oxidation rates in the hearts of mice lacking PPARalpha are associated with higher concentrations of malonyl-CoA and reduced expression of malonyl-CoA decarboxylase. *J Biol Chem* **277**, 4098-4103, doi:10.1074/jbc.M106054200M106054200 [pii] (2002).

61 Nishino, N., Tamori, Y. & Kasuga, M. Insulin efficiently stores triglycerides in adipocytes by inhibiting lipolysis and repressing PGC-1alpha induction. *Kobe J Med Sci* **53**, 99-106 (2007).

62 Reaven, G. M. Banting Lecture 1988. Role of insulin resistance in human disease. 1988. *Nutrition* **13**, 65; discussion 64, 66 (1997).

63 Lazarow, P. B. & Deduve, C. Fatty Acyl-Coa Oxidizing System in Rat-Liver Peroxisomes - Enhancement by Clofibrate, a Hypolipidemic Drug. *Proc. Natl. Acad. Sci. U. S. A.* **73**, 2043-2046, doi:DOI 10.1073/pnas.73.6.2043 (1976).

64 van de Weijer, T., Schrauwen-Hinderling, V. B. & Schrauwen, P. Lipotoxicity in type 2 diabetic cardiomyopathy. *Cardiovasc Res* **92**, 10-18, doi:10.1093/cvr/cvr212 (2011).

65 Chiu, H. C. *et al.* Transgenic expression of fatty acid transport protein 1 in the heart causes lipotoxic cardiomyopathy. *Circ Res* **96**, 225-233, doi:10.1161/01.RES.0000154079.20681.B9 (2005).

66 Yagyu, H. *et al.* Lipoprotein lipase (LpL) on the surface of cardiomyocytes increases lipid uptake and produces a cardiomyopathy. *J Clin Invest* **111**, 419-426, doi:10.1172/JCI16751 (2003).

67 Sharma, S. *et al.* Intramyocardial lipid accumulation in the failing human heart resembles the lipotoxic rat heart. *Faseb J* **18**, 1692-1700, doi:10.1096/fj.04-2263com (2004).

68 Marfella, R. *et al.* Myocardial lipid accumulation in patients with pressure-overloaded heart and metabolic syndrome. *J. Lipid Res.* **50**, 2314-2323, doi:10.1194/jlr.P900032-JLR200 (2009).

69 Nielsen, R. *et al.* Failing heart of patients with type 2 diabetes mellitus can adapt to extreme short-term increases in circulating lipids and does not display features of acute myocardial lipotoxicity. *Circulation. Heart failure* **6**, 845-852, doi:10.1161/CIRCHEARTFAILURE.113.000187 (2013).

70 Chokshi, A. *et al.* Ventricular assist device implantation corrects myocardial lipotoxicity, reverses insulin resistance, and normalizes cardiac metabolism in patients with advanced heart failure. *Circulation* **125**, 2844-2853, doi:10.1161/CIRCULATIONAHA.111.060889 (2012).

71 Chiu, H. C. *et al.* A novel mouse model of lipotoxic cardiomyopathy. *J Clin Invest* **107**, 813-822, doi:10.1172/JCI10947 (2001).

72 Bricker, D. K. *et al.* A Mitochondrial Pyruvate Carrier Required for Pyruvate Uptake in Yeast, Drosophila, and Humans. *Science* **337**, 96-100, doi:10.1126/science.1218099 (2012).

73 Herzig, S. *et al.* Identification and Functional Expression of the Mitochondrial Pyruvate Carrier. *Science* **337**, 93-96, doi:10.1126/science.1218530 (2012).

74 Abel, E. D. Glucose transport in the heart. *Front Biosci* **9**, 201-215 (2004).

75 Stenbit, A. E. *et al.* GLUT4 heterozygous knockout mice develop muscle insulin resistance and diabetes. *Nat Med* **3**, 1096-1101 (1997).

76 Gudi, R., Bowkerkinley, M. M., Kedishvili, N. Y., Zhao, Y. & Popov, K. M. Diversity of the Pyruvate-Dehydrogenase Kinase Gene Family in Humans. *Journal of Biological Chemistry* **270**, 28989-28994 (1995).

77 Sugden, M. C. & Holness, M. J. Mechanisms underlying regulation of the expression and activities of the mammalian pyruvate dehydrogenase kinases. *Arch. Physiol. Biochem.* **112**, 139-149, doi:10.1080/13813450600935263 (2006).

78 Strumilo, S. Short-term regulation of the mammalian pyruvate dehydrogenase complex. *Acta Biochim. Pol.* **52**, 759-764 (2005).

79 Sugden, M. C. & Holness, M. J. Interactive regulation of the pyruvate dehydrogenase complex and the carnitine palmitoyltransferase system. *FASEB J* **8**, 54-61 (1994).

80 Sugden, M. C. PDK4: A factor in fatness? *Obes. Res.* **11**, 167-169, doi:10.1038/oby.2003.26 (2003).

81 Foster, D. W. Malonyl-CoA: the regulator of fatty acid synthesis and oxidation. *J Clin Invest* **122**, 1958-1959 (2012).

82 Sugden, M. C., Kraus, A., Harris, R. A. & Holness, M. J. Fibre-type specific modification of the activity and regulation of skeletal muscle pyruvate dehydrogenase kinase (PDK) by prolonged starvation and refeeding is associated with targeted regulation of PDK isoenzyme 4 expression. *Biochem J* **346 Pt 3**, 651-657 (2000).

83 Holness, M. J. & Sugden, M. C. Regulation of pyruvate dehydrogenase complex activity by reversible phosphorylation. *Biochem Soc Trans* **31**, 1143-1151, doi:10.1042/ (2003).

84 Bowker-Kinley, M. M., Davis, W. I., Wu, P. F., Harris, R. A. & Popov, K. M. Evidence for existence of tissue-specific regulation of the mammalian pyruvate dehydrogenase complex. *Biochem J* **329**, 191-196 (1998).

85 Abel, E. D. Obesity stresses cardiac mitochondria even when you are young. *J Am Coll Cardiol* **57**, 586-589, doi:10.1016/j.jacc.2010.09.039 (2011).

86 Sugden, M. C., Bulmer, K., Augustine, D. & Holness, M. J. Selective modification of pyruvate dehydrogenase kinase isoform expression in rat pancreatic islets elicited by starvation and activation of peroxisome proliferator-activated receptor-alpha - Implications for glucose-stimulated insulin secretion. *Diabetes* **50**, 2729-2736, doi:DOI 10.2337/diabetes.50.12.2729 (2001).

87 Wu, P. *et al.* Starvation and diabetes increase the amount of pyruvate dehydrogenase kinase isoenzyme 4 in rat heart. *Biochem J* **329 (Pt 1)**, 197-201 (1998).

88 Stavinoha, M. A. *et al.* Diurnal variations in the responsiveness of cardiac and skeletal muscle to fatty acids. *Am J Physiol Endocrinol Metab* **287**, E878-887, doi:10.1152/ajpendo.00189.2004 (2004).

89 Rosa, G. *et al.* Reduced PDK4 expression associates with increased insulin sensitivity in postobese patients. *Obes. Res.* **11**, 176-182, doi:10.1038/oby.2003.28 (2003).

90 Kikuchi, A. *et al.* Moyamoya syndrome following childhood acute lymphoblastic leukemia. *Pediatric blood & cancer* **48**, 268-272, doi:10.1002/pbc.20837 (2007).

91 Peters, S. J., Harris, R. A., Heigenhauser, G. J. F. & Spriet, L. L. Muscle fiber type comparison of PDH kinase activity and isoform expression in fed and fasted rats. *Am J Physiol-Reg I* **280**, R661-R668 (2001).

92 Kong, S. W. *et al.* Genetic expression profiles during physiological and pathological cardiac hypertrophy and heart failure in rats. *Physiol Genomics* **21**, 34-42, doi:10.1152/physiolgenomics.00226.2004 (2005).

93 Klionsky, D. J. *et al.* Guidelines for the use and interpretation of assays for monitoring autophagy. *Autophagy* **8**, 445-544 (2012).

94 Hwang, B. & Harris, R. A. Pyruvate dehydrogenase kinase 4 (PDK4) deficiency attenuates the long-term negative effects of a high-saturated fat diet. *Faseb J* **23** (2009).

95 Kwon, H. S., Huang, B., Unterman, T. G. & Harris, R. A. Protein kinase B-alpha inhibits human pyruvate dehydrogenase kinase-4 gene induction by dexamethasone through inactivation of FOXO transcription factors. *Diabetes* **53**, 899-910, doi:DOI 10.2337/diabetes.53.4.899 (2004).

96 Furuyama, T., Kitayama, K., Yamashita, H. & Mori, N. Forkhead transcription factor FOX01 (FKHR)-dependent induction of PDK4 gene expression in skeletal muscle during energy deprivation. *Biochemical Journal* **375**, 365-371, doi:Doi 10.1042/Bj20030022 (2003).

97 Nahle, Z. *et al.* CD36-dependent regulation of muscle FoxO1 and PDK4 in the PPAR delta/beta-mediated adaptation to metabolic stress. *J Biol Chem* **283**, 14317-14326, doi:10.1074/jbc.M706478200 (2008).

98 Seiva, F. R. *et al.* Energy expenditure, lipid profile, oxidative stress, and cardiac energy metabolism after growth hormone treatment in obese young rats. *Horm Metab Res* **42**, 496-501, doi:10.1055/s-0030-1249651 (2010).

99 White, U. A., Coulter, A. A., Miles, T. K. & Stephens, J. M. The STAT5A-mediated induction of pyruvate dehydrogenase kinase 4 expression by prolactin or growth hormone in adipocytes. *Diabetes* **56**, 1623-1629, doi:10.2337/db06-1286 (2007).

100 Kim, Y. D. *et al.* Metformin Inhibits Growth Hormone-Mediated Hepatic PDK4 Gene Expression Through Induction of Orphan Nuclear Receptor Small Heterodimer Partner. *Diabetes* **61**, 2484-2494, doi:10.2337/db11-1665 (2012).

101 Nellemann, B. *et al.* Growth hormone-induced insulin resistance in human subjects involves reduced pyruvate dehydrogenase activity. *Acta Physiol (Oxf)* **210**, 392-402, doi:10.1111/apha.12183 (2014).

102 Yamauchi, T. *et al.* Adiponectin stimulates glucose utilization and fatty-acid oxidation by activating AMP-activated protein kinase. *Nature Medicine* **8**, 1288-1295, doi:10.1038/nm788 (2002).

103 Huang, B. L., Wu, P. F., Bowker-Kinley, M. M. & Harris, R. A. Regulation of pyruvate dehydrogenase kinase expression by peroxisome proliferator-activated receptor-alpha ligands, glucocorticoids, and insulin. *Diabetes* **51**, 276-283 (2002).

104 Augustus, A. *et al.* Cardiac-specific knock-out of lipoprotein lipase alters plasma lipoprotein triglyceride metabolism and cardiac gene expression. *Journal of Biological Chemistry* **279**, 25050-25057, doi:10.1074/jbc.M401028200 (2004).

105 Brown, J. D., Oligino, E., Rader, D. J., Saghatelian, A. & Plutzky, J. VLDL Hydrolysis by Hepatic Lipase Regulates PPAR delta Transcriptional Responses. *Plos One* **6**, doi:ARTN e2120910.1371/journal.pone.0021209 (2011).

106 Kelley, D. E. & Mandarino, L. J. Fuel selection in human skeletal muscle in insulin resistance: a reexamination. *Diabetes* **49**, 677-683 (2000).

107 Kulkarni, S. S. *et al.* Mitochondrial regulators of fatty acid metabolism reflect metabolic dysfunction in type 2 diabetes mellitus. *Metabolism* **61**, 175-185, doi:10.1016/j.metabol.2011.06.014 (2012).

108 Randle, P. J. Fuel selection in animals. *Biochem Soc Trans* **14**, 799-806 (1986).

109 Gross, D. N., van den Heuvel, A. P. & Birnbaum, M. J. The role of FoxO in the regulation of metabolism. *Oncogene* **27**, 2320-2336, doi:10.1038/onc.2008.25 (2008).

110 Dresner, A. *et al.* Effects of free fatty acids on glucose transport and IRS-1-associated phosphatidylinositol 3-kinase activity. *Journal of Clinical Investigation* **103**, 253-259, doi:Doi 10.1172/Jci5001 (1999).

111 Tsintzas, K. *et al.* Elevated free fatty acids attenuate the insulin-induced suppression of PDK4 gene expression in human skeletal muscle: Potential role of intramuscular long-chain acyl-coenzyme a. *J. Clin. Endocrinol. Metab.* **92**, 3967-3972, doi:10.1210/jc.2007-1104 (2007).

112 Lee, F. N., Zhang, L. H., Zheng, D., Choi, W. S. & Youn, J. H. Insulin suppresses PDK-4 expression in skeletal muscle independently of plasma FFA. *Am J Physiol-Endoc M* **287**, E69-E74, doi:10.1152/ajpendo.00461.2003 (2004).

113 Hua, Y. *et al.* Cathepsin K knockout mitigates high-fat diet-induced cardiac hypertrophy and contractile dysfunction. *Diabetes* **62**, 498-509, doi:10.2337/db12-0350 (2013).

114 Xu, X., Hua, Y., Nair, S., Zhang, Y. & Ren, J. Akt2 knockout preserves cardiac function in high-fat diet-induced obesity by rescuing cardiac autophagosome maturation. *Journal of molecular cell biology* **5**, 61-63, doi:10.1093/jmcb/mjs055 (2013).

115 Hauner, H. Secretory factors from human adipose tissue and their functional role. *Proc. Nutr. Soc.* **64**, 163-169, doi:10.1079/Pns2005428 (2005).

116 Halberg, N., Wernstedt-Asterholm, I. & Scherer, P. E. The Adipocyte as an Endocrine Cell. *Endocrinol. Metab. Clin. North Am.* **37**, 753-+, doi:10.1016/j.ecl.2008.07.002 (2008).

117 Jernas, M. *et al.* Separation of human adipocytes by size: hypertrophic fat cells display distinct gene expression. *Faseb Journal* **20**, 1540-+, doi:10.1096/fj.05-5678fje (2006).

118 Skurk, T., Alberti-Huber, C., Herder, C. & Hauner, H. Relationship between adipocyte size and adipokine expression and secretion. *J. Clin. Endocrinol. Metab.* **92**, 1023-1033, doi:10.1210/jc.2006-1055 (2007).

119 Hotamisligil, G. S., Shargill, N. S. & Spiegelman, B. M. Adipose Expression of Tumor-Necrosis-Factor-Alpha - Direct Role in Obesity-Linked Insulin Resistance. *Science* **259**, 87-91, doi:DOI 10.1126/science.7678183 (1993).

120 Amrani, A. *et al.* Interleukin-1 effect on glycemia in the non-obese diabetic mouse at the pre-diabetic stage. *J. Endocrinol.* **148**, 139-148, doi:DOI 10.1677/joe.0.1480139 (1996).

121 Sartipy, P. & Loskutoff, D. J. Monocyte chemoattractant protein 1 in obesity and insulin resistance. *Proc. Natl. Acad. Sci. U. S. A.* **100**, 7265-7270, doi:10.1073/pnas.1133870100 (2003).

122 Weisberg, S. P. *et al.* Obesity is associated with macrophage accumulation in adipose tissue. *Journal of Clinical Investigation* **112**, 1796-1808, doi:10.1172/Jci200319246 (2003).

123 Martyn, J. A. J., Kaneki, M. & Yasuhara, S. Obesity-induced insulin resistance and hyperglycemia - Etiologic factors and molecular mechanisms. *Anesthesiology* **109**, 137-148 (2008).

124 Perseghin, G., Ghosh, S., Gerow, K. & Shulman, G. I. Metabolic defects in lean nondiabetic offspring of NIDDM parents - A cross-sectional study. *Diabetes* **46**, 1001-1009, doi:DOI 10.2337/diabetes.46.6.1001 (1997).

125 Boden, G. Obesity and Free Fatty Acids. *Endocrinol. Metab. Clin. North Am.* **37**, 635-+, doi:10.1016/j.ecl.2008.06.007 (2008).

126 Wende, A. R. & Abel, E. D. Lipotoxicity in the heart. *Bba-Mol Cell Biol L* **1801**, 311-319, doi:10.1016/j.bbalip.2009.09.023 (2010).

127 Yang, X. Y. *et al.* Phosphoinositide signalling links O-GlcNAc transferase to insulin resistance. *Nature* **451**, 964-U961, doi:10.1038/nature06668 (2008).

128 Shi, H. *et al.* TLR4 links innate immunity and fatty acid-induced insulin resistance. *Journal of Clinical Investigation* **116**, 3015-3025, doi:10.1172/Jci28898 (2006).

129 Suganami, T., Nishida, J. & Ogawa, Y. A paracrine loop between adipocytes and macrophages aggravates inflammatory changes - Role of free fatty acids and tumor necrosis factor alpha. *Arterioscl Throm Vas* **25**, 2062-2068, doi:10.1161/01.Atv.0000183883.72263.13 (2005).

130 Kirk, E. P. & Klein, S. Pathogenesis and Pathophysiology of the Cardiometabolic Syndrome. *J. Clin. Hypertens.* **11**, 761-765, doi:10.1111/j.1559-4572.2009.00054.x (2009).

131 Pagel-Langenickel, I., Bao, J. J., Pang, L. Y. & Sack, M. N. The Role of Mitochondria in the Pathophysiology of Skeletal Muscle Insulin Resistance. *Endocr. Rev.* **31**, 25-51, doi:10.1210/er.2009-0003 (2010).

132 Cook, S. A. *et al.* Abnormal myocardial insulin signalling in type 2 diabetes and left-ventricular dysfunction. *European heart journal* **31**, 100-111, doi:10.1093/eurheartj/ehp396 (2010).

133 Wright, J. J. *et al.* Mechanisms for increased myocardial fatty acid utilization following short-term high-fat feeding. *Cardiovascular research* **82**, 351-360, doi:10.1093/cvr/cvp017 (2009).

134 Peterson, L. R. *et al.* Effect of obesity and insulin resistance on myocardial substrate metabolism and efficiency in young women. *Circulation* **109**, 2191-2196, doi:10.1161/01.Cir.0000127959.28627.F8 (2004).

135 Stienstra, R., Duval, C., Muller, M. & Kersten, S. PPARs, Obesity, and Inflammation. *PPAR research*, doi:Artn 9597410.1155/2007/95974 (2007).

136 Buchanan, J. *et al.* Reduced cardiac efficiency and altered substrate metabolism precedes the onset of hyperglycemia and contractile dysfunction in two mouse models of insulin resistance and obesity. *Endocrinology* **146**, 5341-5349, doi:10.1210/en.2005-0938 (2005).

137 Roche, T. E. & Hiromasa, Y. Pyruvate dehydrogenase kinase regulatory mechanisms and inhibition in treating diabetes, heart ischemia, and cancer. *Cell Mol Life Sci* **64**, 830-849, doi:10.1007/s00018-007-6380-z (2007).

138 Schwenk, R. W., Luiken, J. J. F. P., Bonen, A. & Glatz, J. F. C. Regulation of sarcolemmal glucose and fatty acid transporters in cardiac disease. *Cardiovascular Research* **79**, 249-258, doi:10.1093/cvr/cvn116 (2008).

139 Carley, A. N. & Severson, D. L. What are the biochemical mechanisms responsible for enhanced fatty acid utilization by perfused hearts from type 2 diabetic db/db mice? *Cardiovasc. Drugs Ther.* **22**, 83-89, doi:10.1007/s10557-008-6088-9 (2008).

140 Ouwens, D. M. *et al.* Cardiac contractile dysfunction in insulin-resistant rats fed a high-fat diet is associated with elevated CD36-mediated fatty acid uptake and esterification. *Diabetologia* **50**, 1938-1948, doi:10.1007/s00125-007-0735-8 (2007).

141 Banke, N. H. *et al.* Preferential Oxidation of Triacylglyceride-Derived Fatty Acids in Heart Is Augmented by the Nuclear Receptor PPAR alpha. *Circulation Research* **107**, 233-241, doi:10.1161/Circresaha.110.221713 (2010).

142 Anderson, E. J. *et al.* Mitochondrial H2O2 emission and cellular redox state link excess fat intake to insulin resistance in both rodents and humans. *Journal of Clinical Investigation* **119**, 573-581, doi:10.1172/Jci37048 (2009).

143 Vadvalkar, S. S. *et al.* Metabolic inflexibility and protein lysine acetylation in heart mitochondria of a chronic model of type 1 diabetes. *Biochem J* **449**, 253-261, doi:10.1042/BJ20121038 (2013).

144 Hers, I., Vincent, E. E. & Tavare, J. M. Akt signalling in health and disease. *Cell. Signal.* **23**, 1515-1527, doi:10.1016/j.cellsig.2011.05.004 (2011).

145 Moore, S. F., Hunter, R. W. & Hers, I. mTORC2 protein-mediated protein kinase B (Akt) serine 473 phosphorylation is not required for Akt1 activity in human platelets (vol 286, pg 24553, 2011). *Journal of Biological Chemistry* **286**, 31062-31062, doi:10.1074/jbc.A110.202341 (2011).

146 Kovacic, S. *et al.* Akt activity negatively regulates phosphorylation of AMP-activated protein kinase in the heart. *Journal of Biological Chemistry* **278**, 39422-39427, doi:10.1074/jbc.M305371200 (2003).

147 Zhang, Y., Xu, X. & Ren, J. MTOR overactivation and interrupted autophagy flux in obese hearts: a dicey assembly? *Autophagy* **9**, 939-941, doi:10.4161/auto.24398 (2013).

148 Laplante, M. & Sabatini, D. M. mTOR signaling at a glance. *J Cell Sci* **122**, 3589-3594, doi:10.1242/jcs.051011 (2009).

149 Hiratani, K. *et al.* Roles of mTOR and JNK in serine phosphorylation, translocation, and degradation of IRS-1. *Biochem Bioph Res Co* **335**, 836-842, doi:10.1016/j.bbrc.2005.07.152 (2005).
150 Selman, C. *et al.* Ribosomal Protein S6 Kinase 1 Signaling Regulates Mammalian Life Span. *Science* **326**, 140-144, doi:10.1126/science.1177221 (2009).
151 Hsu, P. P. *et al.* The mTOR-Regulated Phosphoproteome Reveals a Mechanism of mTORC1-Mediated Inhibition of Growth Factor Signaling. *Science* **332**, 1317-1322, doi:10.1126/science.1199498 (2011).
152 Yu, Y. H. *et al.* Phosphoproteomic Analysis Identifies Grb10 as an mTORC1 Substrate That Negatively Regulates Insulin Signaling. *Science* **332**, 1322-1326, doi:10.1126/science.1199484 (2011).
153 Zhu, Y. *et al.* Mechanistic target of rapamycin (Mtor) is essential for murine embryonic heart development and growth. *PLoS One* **8**, e54221, doi:10.1371/journal.pone.0054221 (2013).
154 Shende, P. *et al.* Cardiac raptor ablation impairs adaptive hypertrophy, alters metabolic gene expression, and causes heart failure in mice. *Circulation* **123**, 1073-1082,doi:CIRCULATIONAHA.110.977066 [pii]10.1161/CIRCULATIONAHA.110.977066 (2011).
155 Cunningham, J. T. *et al.* mTOR controls mitochondrial oxidative function through a YY1-PGC-1alpha transcriptional complex. *Nature* **450**, 736-740, doi:nature06322 [pii]10.1038/nature06322 (2007).
156 Zhu, Y. *et al.* Regulation of fatty acid metabolism by mTOR in adult murine hearts occurs independently of changes in PGC-1 alpha. *Am J Physiol-Heart C* **305**, H41-H51, doi:10.1152/ajpheart.00877.2012 (2013).
157 Wullschleger, S., Loewith, R. & Hall, M. N. TOR signaling in growth and metabolism. *Cell* **124**, 471-484 (2006).
158 Laplante, M. & Sabatini, D. M. mTOR signaling in growth control and disease. *Cell* **149**, 274-293, doi:10.1016/j.cell.2012.03.017 (2012).
159 Laplante, M. & Sabatini, D. M. Regulation of mTORC1 and its impact on gene expression at a glance. *Journal of Cell Science* **126**, 1713-1719, doi:10.1242/jcs.125773 (2013).
160 Johnson, S. C., Rabinovitch, P. S. & Kaeberlein, M. mTOR is a key modulator of ageing and age-related disease. *Nature* **493**, 338-345, doi:10.1038/nature11861 (2013).
161 Um, S. H., D'Alessio, D. & Thomas, G. Nutrient overload, insulin resistance, and ribosomal protein S6 kinase 1, S6K1. *Cell metabolism* **3**, 393-402, doi:10.1016/j.cmet.2006.05.003 (2006).
162 Wang, C. Y. *et al.* Obesity Increases Vascular Senescence and Susceptibility to Ischemic Injury Through Chronic Activation of Akt and mTOR. *Science Signaling* **2**, doi:ARTN ra1110.1126/scisignal.2000143 (2009).
163 Nichols, M., Townsend, N., Scarborough, P. & Rayner, M. Cardiovascular disease in Europe: epidemiological update. *Eur Heart J* **34**, 3028-3034, doi:10.1093/eurheartj/eht356 (2013).
164 Nichols, M., Townsend, N., Scarborough, P. & Rayner, M. Cardiovascular disease in Europe 2014: epidemiological update. *Eur Heart J*, doi:10.1093/eurheartj/ehu299 (2014).
165 Dubey, R. K., Oparil, S., Imthurn, B. & Jackson, E. K. Sex hormones and hypertension. *Cardiovasc Res* **53**, 688-708 (2002).

166 Meyer, M. R., Haas, E. & Barton, M. Gender differences of cardiovascular disease: new perspectives for estrogen receptor signaling. *Hypertension* **47**, 1019-1026, doi:10.1161/01.HYP.0000223064.62762.0b (2006).

167 Matheus, A. S. *et al.* Impact of diabetes on cardiovascular disease: an update. *Int J Hypertens* **2013**, 653789, doi:10.1155/2013/653789 (2013).

168 Rubler, S. *et al.* New Type of Cardiomyopathy Associated with Diabetic Glomerulosclerosis. *Am J Cardiol* **30**, 595-&, doi:Doi 10.1016/0002-9149(72)90595-4 (1972).

169 Fuentes-Antras, J., Ioan, A. M., Tunon, J., Egido, J. & Lorenzo, O. Activation of Toll-Like Receptors and Inflammasome Complexes in the Diabetic Cardiomyopathy-Associated Inflammation. *International journal of endocrinology*, doi:Artn 84782710.1155/2014/847827 (2014).

170 Witteles, R. M. & Fowler, M. B. Insulin-resistant cardiomyopathy. *J. Am. Coll. Cardiol.* **51**, 93-102, doi:10.1016/j.jacc.2007.10.021 (2008).

171 Borlaug, B. A. The pathophysiology of heart failure with preserved ejection fraction. *Nat Rev Cardiol* **11**, 507-515, doi:10.1038/nrcardio.2014.83 (2014).

172 Vasan, R. S. & Levy, D. The role of hypertension in the pathogenesis of heart failure - A clinical mechanistic overview. *Arch. Intern. Med.* **156**, 1789-1796, doi:DOI 10.1001/archinte.156.16.1789 (1996).

173 Fonarow, G. C. *et al.* Characteristics, treatments, and outcomes of patients with preserved systolic function hospitalized for heart failure - A report from the OPTIMIZE-HF registry. *J. Am. Coll. Cardiol.* **50**, 768-777, doi:10.1016/j.jacc.2007.04.064 (2007).

174 Vasan, R. S., Benjamin, E. J. & Levy, D. Prevalence, Clinical-Features and Prognosis of Diastolic Heart-Failure - an Epidemiologic Perspective. *J. Am. Coll. Cardiol.* **26**, 1565-1574, doi:Doi 10.1016/0735-1097(95)00381-9 (1995).

175 Kenchaiah, S. *et al.* Obesity and the risk of heart failure. *N. Engl. J. Med.* **347**, 305-313, doi:DOI 10.1056/NEJMoa020245 (2002).

176 Fang, Z. Y., Prins, J. B. & Marwick, T. H. Diabetic cardiomyopathy: Evidence, mechanisms, and therapeutic implications. *Endocrine Reviews* **25**, 543-567, doi:10.1210/er.2003-0012 (2004).

177 Wong, C. Y. *et al.* Alterations of left ventricular myocardial characteristics associated with obesity. *Circulation* **110**, 3081-3087, doi:10.1161/01.CIR.0000147184.13872.0F (2004).

178 Ceylan-Isik, A. F. *et al.* Apelin administration ameliorates high fat diet-induced cardiac hypertrophy and contractile dysfunction. *J Mol Cell Cardiol* **63**, 4-13, doi:10.1016/j.yjmcc.2013.07.002 (2013).

179 Lopaschuk, G. D., Ussher, J. R., Folmes, C. D., Jaswal, J. S. & Stanley, W. C. Myocardial fatty acid metabolism in health and disease. *Physiol Rev* **90**, 207-258, doi:10.1152/physrev.00015.2009 (2010).

180 Burkhoff, D. *et al.* Influence of metabolic substrate on rat heart function and metabolism at different coronary flows. *Am J Physiol* **261**, H741-750 (1991).

181 Cole, M. A. *et al.* A high fat diet increases mitochondrial fatty acid oxidation and uncoupling to decrease efficiency in rat heart. *Basic Res Cardiol* **106**, 447-457, doi:10.1007/s00395-011-0156-1 (2011).

182 Scheuermann-Freestone, M. *et al.* Abnormal cardiac and skeletal muscle energy metabolism in patients with type 2 diabetes. *Circulation* **107**, 3040-3046, doi:10.1161/01.CIR.0000072789.89096.10 (2003).

183 Boudina, S. *et al.* Reduced mitochondrial oxidative capacity and increased mitochondrial uncoupling impair myocardial energetics in obesity. *Circulation* **112**, 2686-2695, doi:10.1161/CIRCULATIONAHA.105.554360 (2005).

184 Maalouf, R. M. *et al.* Nox4-derived reactive oxygen species mediate cardiomyocyte injury in early type 1 diabetes. *Am J Physiol Cell Physiol* **302**, C597-604, doi:10.1152/ajpcell.00331.2011 (2012).

185 Zhong, Y., Ahmed, S., Grupp, I. L. & Matlib, M. A. Altered SR protein expression associated with contractile dysfunction in diabetic rat hearts. *Am J Physiol Heart Circ Physiol* **281**, H1137-1147 (2001).

186 Abe, T. *et al.* Left ventricular diastolic dysfunction in type 2 diabetes mellitus model rats. *Am J Physiol Heart Circ Physiol* **282**, H138-148 (2002).

187 Mandavia, C. H., Aroor, A. R., Demarco, V. G. & Sowers, J. R. Molecular and metabolic mechanisms of cardiac dysfunction in diabetes. *Life Sci* **92**, 601-608, doi:10.1016/j.lfs.2012.10.028 (2013).

188 Boudina, S. & Abel, E. D. Diabetic cardiomyopathy, causes and effects. *Rev Endocr Metab Disord* **11**, 31-39, doi:10.1007/s11154-010-9131-7 (2010).

189 Stanley, W. C., Dabkowski, E. R., Ribeiro, R. F., Jr. & O'Connell, K. A. Dietary fat and heart failure: moving from lipotoxicity to lipoprotection. *Circ Res* **110**, 764-776, doi:10.1161/CIRCRESAHA.111.253104 (2012).

190 Battiprolu, P. K. *et al.* Diabetic cardiomyopathy and metabolic remodeling of the heart. *Life Sci* **92**, 609-615, doi:10.1016/j.lfs.2012.10.011 (2013).

191 Gustafson, T. A., Bahl, J. J., Markham, B. E., Roeske, W. R. & Morkin, E. Hormonal regulation of myosin heavy chain and alpha-actin gene expression in cultured fetal rat heart myocytes. *J Biol Chem* **262**, 13316-13322 (1987).

192 Lyons, G. E., Schiaffino, S., Sassoon, D., Barton, P. & Buckingham, M. Developmental regulation of myosin gene expression in mouse cardiac muscle. *J Cell Biol* **111**, 2427-2436 (1990).

193 Hui, H. P. *et al.* [Adeno-associated viral gene transfer of SERCA2a improves heart function in chronic congestive heart failure rats]. *Zhonghua Xin Xue Guan Bing Za Zhi* **34**, 357-362 (2006).

194 Opitz, C. A. & Linke, W. A. Plasticity of cardiac titin/connectin in heart development. *J Muscle Res Cell Motil* **26**, 333-342, doi:10.1007/s10974-005-9040-7 (2005).

195 Dietz, J. R. Mechanisms of atrial natriuretic peptide secretion from the atrium. *Cardiovasc Res* **68**, 8-17, doi:10.1016/j.cardiores.2005.06.008 (2005).

196 Patel, J. B. *et al.* Cardiac-specific attenuation of natriuretic peptide A receptor activity accentuates adverse cardiac remodeling and mortality in response to pressure overload. *American Journal of Physiology-Heart and Circulatory Physiology* **289**, H777-H784, doi:10.1152/ajpheart.00117.2005 (2005).

197 Kishimoto, I., Rossi, K. & Garbers, D. L. A genetic model provides evidence that the receptor for atrial natriuretic peptide (guanylyl cyclase-A) inhibits cardiac ventricular myocyte hypertrophy. *Proc. Natl. Acad. Sci. U. S. A.* **98**, 2703-2706, doi:DOI 10.1073/pnas.051625598 (2001).

198 Holtwick, R. *et al.* Pressure-independent cardiac hypertrophy in mice with cardiomyocyte-restricted inactivation of the atrial natriuretic peptide receptor guanylyl cyclase-A. *Journal of Clinical Investigation* **111**, 1399-1407, doi:10.1172/Jci200317061 (2003).

199 Hotamisligil, G. S. & Erbay, E. Nutrient sensing and inflammation in metabolic diseases. *Nature Reviews Immunology* **8**, 923-934, doi:10.1038/nri2449 (2008).

200 Faulds, M. H., Zhao, C. Y., Dahlman-Wright, K. & Gustafsson, J. A. The diversity of sex steroid action: regulation of metabolism by estrogen signaling. *J Endocrinol* **212**, 3-12, doi:10.1530/Joe-11-0044 (2012).

201 Nan, W. Q., Shan, T. Q. & Qian, X. PPAR alpha agonist prevented the apoptosis induced by glucose and fatty acid in neonatal cardiomyocytes (vol 34, pg 271, 2010). *J. Endocrinol. Invest.* **34**, 654-654 (2011).

202 Min, W., Bin, Z. W., Bin Quan, Z., Hui, Z. J. & Sheng, F. G. The signal transduction pathway of PKC/NF-kappa B/c-fos may be involved in the influence of high glucose on the cardiomyocytes of neonatal rats. *Cardiovascular diabetology* **8**, doi:Artn 810.1186/1475-2840-8-8 (2009).

203 Yamamoto, K., Ohki, R., Lee, R. T., Ikeda, U. & Shimada, K. Peroxisome proliferator-activated receptor gamma activators inhibit cardiac hypertrophy in cardiac myocytes. *Circulation* **104**, 1670-1675, doi:DOI 10.1161/hc4001.097186 (2001).

204 Pagani, F. D. *et al.* Autologous skeletal myoblasts transplanted to ischemia-damaged myocardium in humans - Histological analysis of cell survival and differentiation. *J. Am. Coll. Cardiol.* **41**, 879-888, doi:10.1016/S0735-1097(03)00081-0 (2003).

205 Li, Y. H. *et al.* NF-kappa B activation is required for the development of cardiac hypertrophy in vivo. *American Journal of Physiology-Heart and Circulatory Physiology* **287**, H1712-H1720, doi:10.1152/ajpheart.00124.2004 (2004).

206 Ha, T. Z. *et al.* Attenuation of cardiac hypertrophy by inhibiting both mTOR and NF kappa B activation in vivo. *Free Radic. Biol. Med.* **39**, 1570-1580, doi:10.1016/j.freeradbiomed.2005.08.002 (2005).

207 Tikellis, C. *et al.* Cardiac inflammation associated with a Western diet is mediated via activation of RAGE by AGEs. *Am J Physiol-Endoc M* **295**, E323-E330, doi:10.1152/ajpendo.00024.2008 (2008).

208 Bluher, M. Adipose tissue inflammation: a cause or consequence of obesity-related insulin resistance? *Clin. Sci.* **130**, 1603-1614, doi:10.1042/Cs20160005 (2016).

209 Watanabe, Y., Nagai, Y. & Takatsu, K. Activation and Regulation of the Pattern Recognition Receptors in Obesity-Induced Adipose Tissue Inflammation and Insulin Resistance. *Nutrients* **5**, 3757-3778, doi:10.3390/nu5093757 (2013).

210 Jung, U. J. & Choi, M. S. Obesity and Its Metabolic Complications: The Role of Adipokines and the Relationship between Obesity, Inflammation, Insulin Resistance, Dyslipidemia and Nonalcoholic Fatty Liver Disease. *International journal of molecular sciences* **15**, 6184-6223, doi:10.3390/ijms15046184 (2014).

211 Palomer, X., Salvado, L., Barroso, E. & Vazquez-Carrera, M. An overview of the crosstalk between inflammatory processes and metabolic dysregulation during diabetic cardiomyopathy. *Int. J. Cardiol.* **168**, 3160-3172, doi:10.1016/j.ijcard.2013.07.150 (2013).

212 Jia, G. H., DeMarco, V. G. & Sowers, J. R. Insulin resistance and hyperinsulinaemia in diabetic cardiomyopathy. *Nature Reviews Endocrinology* **12**, 144-153, doi:10.1038/nrendo.2015.216 (2016).

213 Loffredo, F. S., Nikolova, A. P., Pancoast, J. R. & Lee, R. T. Heart failure with preserved ejection fraction: molecular pathways of the aging myocardium. *Circ Res* **115**, 97-107, doi:10.1161/CIRCRESAHA.115.302929 (2014).

214 De Keulenaer, G. W. & Brutsaert, D. L. Systolic and diastolic heart failure are overlapping phenotypes within the heart failure spectrum. *Circulation* **123**, 1996-2004; discussion 2005, doi:10.1161/CIRCULATIONAHA.110.981431 (2011).

215 Palanivel, R. *et al.* Globular and full-length forms of adiponectin mediate specific changes in glucose and fatty acid uptake and metabolism in cardiomyocytes. *Cardiovasc Res* **75**, 148-157, doi:10.1016/j.cardiores.2007.04.011 (2007).

216 Palanivel, R., Eguchi, M., Shuralyova, I., Coe, I. & Sweeney, G. Distinct effects of short- and long-term leptin treatment on glucose and fatty acid uptake and metabolism in HL-1 cardiomyocytes. *Metabolism* **55**, 1067-1075, doi:10.1016/j.metabol.2006.03.020 (2006).

217 Palanivel, R., Vu, V., Park, M., Fang, X. & Sweeney, G. Differential impact of adipokines derived from primary adipocytes of wild-type versus streptozotocin-induced diabetic rats on glucose and fatty acid metabolism in cardiomyocytes. *J Endocrinol* **199**, 389-397, doi:10.1677/JOE-08-0336 (2008).

218 Chakrabarti, S., Lekontseva, O., Peters, A. & Davidge, S. T. 17 beta-Estradiol induces protein S-nitrosylation in the endothelium. *Cardiovasc Res* **85**, 796-805, doi:10.1093/cvr/cvp368 (2010).

219 Masood, D. E. N., Roach, E. C., Beauregard, K. G. & Khalil, R. A. Impact of Sex Hormone Metabolism on the Vascular Effects of Menopausal Hormone Therapy in Cardiovascular Disease. *Curr Drug Metab* **11**, 693-714, doi:Doi 10.2174/138920010794233477 (2010).

220 Ablorh, N. A. & Thomas, D. D. Phospholamban phosphorylation, mutation, and structural dynamics: a biophysical approach to understanding and treating cardiomyopathy. *Biophys Rev* **7**, 63-76, doi:10.1007/s12551-014-0157-z (2015).

221 Barnabas, O., Wang, H. & Gao, X. M. Role of estrogen in angiogenesis in cardiovascular diseases. *Journal of geriatric cardiology : JGC* **10**, 377-382, doi:10.3969/j.issn.1671-5411.2013.04.008 (2013).

222 Leichman, J. G. *et al.* Dramatic reversal of derangements in muscle metabolism and left ventricular function after bariatric surgery. *Am J Med* **121**, 966-973, doi:10.1016/j.amjmed.2008.06.033 (2008).

223 Bers, D. M. Cardiac excitation-contraction coupling. *Nature* **415**, 198-205, doi:DOI 10.1038/415198a (2002).

224 Fabiato, A. Calcium-Induced Release of Calcium from the Cardiac Sarcoplasmic-Reticulum. *American Journal of Physiology* **245**, C1-C14 (1983).

225 Lodish, H. *Molecular cell biology 4.0*. (W. H. Freeman, 2000).

226 Olesen, C. *et al.* The structural basis of calcium transport by the calcium pump. *Nature* **450**, 1036-1042, doi:10.1038/nature06418 (2007).

227 Toyoshima, C. & Mizutani, T. Crystal structure of the calcium pump with a bound ATP analogue. *Nature* **430**, 529-535, doi:10.1038/nature02680 (2004).

228 Kawase, Y. & Hajjar, R. J. The cardiac sarcoplasmic/endoplasmic reticulum calcium ATPase: a potent target for cardiovascular diseases. *Nat Clin Pract Card* **5**, 554-565, doi:10.1038/ncpcardio1301 (2008).

229 Hamm, N. C. *et al.* Regulation of Cardiac Sarco(endo)plasmic Reticulum Calcium-ATPases (SERCA2a) in Response to Exercise. *Adv Biochem Health D* **14**, 187-206, doi:10.1007/978-3-319-24780-9_11 (2016).

230 Bers, D. M. Ca transport during contraction and relaxation in mammalian ventricular muscle. *Basic Research in Cardiology* **92**, 1-10, doi:Doi 10.1007/Bf00794062 (1997).

231 Watanabe, A. *et al.* Mitochondrial transcription factors TFAM and TFB2M regulate Serca2 gene transcription. *Cardiovascular Research* **90**, 57-67, doi:10.1093/cvr/cvq374 (2011).

232 Baker, D. L., Dave, V., Reed, T. & Periasamy, M. Multiple Sp1 binding sites in the cardiac slow twitch muscle sarcoplamsic reticulum Ca2+-ATPase gene promoter are required for expression in Sol8 muscle cells. *Journal of Biological Chemistry* **271**, 5921-5928 (1996).

233 Flesch, M. On the trail of cardiac specific transcription factors. *Cardiovascular Research* **50**, 3-6, doi:Doi 10.1016/S0008-6363(01)00218-8 (2001).

234 Takizawa, T. *et al.* Transcription factor Sp1 regulates SERCA2 gene expression in pressure-overloaded hearts: a study using in vivo direct gene transfer into living myocardium. *Journal of Molecular and Cellular Cardiology* **35**, 777-783, doi:10.1016/S0022-2828(03)00122-6 (2003).

235 Vlasblom, R. *et al.* Contractile arrest reveals calcium-dependent stimulation of SERCA2a mRNA expression in cultured ventricular cardiomyocytes. *Cardiovascular Research* **63**, 537-544, doi:10.1016/j.cardiores.2004.04.005 (2004).

236 Zhang, Z. Y., Liu, X. H., Hu, W. C., Rong, F. & Wu, X. D. The calcineurin-myocyte enhancer factor 2c pathway mediates cardiac hypertrophy induced by endoplasmic reticulum stress in neonatal rat cardiomyocytes. *American Journal of Physiology-Heart and Circulatory Physiology* **298**, H1499-H1509, doi:10.1152/ajpheart.00980.2009 (2010).

237 Razeghi, P., Young, M. E., Cockrill, T. C., Frazier, H. & Taegtmeyer, H. Downregulation of myocardial myocyte enhancer factor 2C and myocyte enhancer factor 2C regulated gene expression in diabetic patients with non-ischemic heart failure. *Circulation* **106**, 263-263 (2002).

238 Arai, M., Alpert, N. R., Maclennan, D. H., Barton, P. & Periasamy, M. Alterations in Sarcoplasmic-Reticulum Gene-Expression in Human Heart-Failure - a Possible Mechanism for Alterations in Systolic and Diastolic Properties of the Failing Myocardium. *Circulation Research* **72**, 463-469 (1993).

239 Mercadier, J. J. *et al.* Altered Sarcoplasmic-Reticulum Ca-2+-Atpase Gene-Expression in the Human Ventricle during End-Stage Heart-Failure. *Journal of Clinical Investigation* **85**, 305-309, doi:Doi 10.1172/Jci114429 (1990).

240 Park, W. J. & Oh, J. G. SERCA2a: a prime target for modulation of cardiac contractility during heart failure. *Bmb Rep* **46**, 237-243, doi:10.5483/BMBRep.2013.46.5.077 (2013).

241 Aronson, D. & Krum, H. Novel therapies in acute and chronic heart failure. *Pharmacology & Therapeutics* **135**, 1-17, doi:10.1016/j.pharmthera.2012.03.002 (2012).

242 Hasenfuss, G. Alterations of calcium-regulatory proteins in heart failure. *Cardiovascular Research* **37**, 279-289, doi:Doi 10.1016/S0008-6363(97)00277-0 (1998).

243 Epp, R. A. *et al.* Exercise training prevents the development of cardiac dysfunction in the low-dose streptozotocin diabetic rats fed a high-fat diet. *Can. J. Physiol. Pharmacol.* **91**, 80-89 (2013).

244 Vasanji, Z., Dhalla, N. S. & Netticadan, T. Increased inhibition of SERCA2 by phospholamban in the type I diabetic heart. *Mol. Cell. Biochem.* **261**, 245-249, doi:Doi 10.1023/B:Mcbi.0000028762.97754.26 (2004).

245 Sulaiman, M. *et al.* Resveratrol, an activator of SIRT1, upregulates sarcoplasmic calcium ATPase and improves cardiac function in diabetic cardiomyopathy. *American Journal of Physiology-Heart and Circulatory Physiology* **298**, H833-H843, doi:10.1152/ajpheart.00418.2009 (2010).

246 Suarez, J., Scott, B. & Dillmann, W. H. Conditional increase in SERCA2a protein is able to reverse contractile dysfunction and abnormal calcium flux in established diabetic cardiomyopathy. *American Journal of Physiology-Regulatory Integrative and Comparative Physiology* **295**, R1439-R1445, doi:10.1152/ajpregu.00736.2007 (2008).

247 del Monte, F. *et al.* Restoration of contractile function in isolated cardiomyocytes from failing human hearts by gene transfer of SERCA2a. *Circulation* **100**, 2308-2311 (1999).

248 Jessup, M. *et al.* Calcium Upregulation by Percutaneous Administration of Gene Therapy in Cardiac Disease (CUPID) A Phase 2 Trial of Intracoronary Gene Therapy of Sarcoplasmic Reticulum Ca2+-ATPase in Patients With Advanced Heart Failure. *Circulation* **124**, 304-U113, doi:10.1161/Circulationaha.111.022889 (2011).

249 Simmerman, H. K. B. & Jones, L. R. Phospholamban: Protein structure, mechanism of action, and role in cardiac function. *Physiol. Rev.* **78**, 921-947 (1998).

250 Luo, W. S. *et al.* Targeted Ablation of the Phospholamban Gene Is Associated with Markedly Enhanced Myocardial-Contractility and Loss of Beta-Agonist Stimulation. *Circulation Research* **75**, 401-409 (1994).

251 Kadambi, V. J. *et al.* Cardiac-specific overexpression of phospholamban alters calcium kinetics and resultant cardiomyocyte mechanics in transgenic mice. *Journal of Clinical Investigation* **97**, 533-539, doi:Doi 10.1172/Jci118446 (1996).

252 Meyer, M. *et al.* Alterations of Sarcoplasmic-Reticulum Proteins in Failing Human Dilated Cardiomyopathy. *Circulation* **92**, 778-784 (1995).

253 Suckau, L. *et al.* Long-Term Cardiac-Targeted RNA Interference for the Treatment of Heart Failure Restores Cardiac Function and Reduces Pathological Hypertrophy. *Circulation* **119**, 1241-1252, doi:10.1161/Circulationaha.108.783852 (2009).

254 Kranias, E. G. & Hajjar, R. J. Modulation of Cardiac Contractility by the Phopholamban/SERCA2a Regulatome. *Circulation Research* **110**, 1646-1660, doi:10.1161/Circresaha.111.259754 (2012).

255 Nicolaou, P., Hajjar, R. J. & Kranias, E. G. Role of protein phosphatase-1 inhibitor-1 in cardiac physiology and pathophysiology. *Journal of Molecular and Cellular Cardiology* **47**, 365-371, doi:10.1016/j.yjmcc.2009.05.010 (2009).

256 Schmitt, J. P. *et al.* Dilated cardiomyopathy and heart failure caused by a mutation in phospholamban. *Science* **299**, 1410-1413, doi:DOI 10.1126/science.1081578 (2003).

257 Haghighi, K. *et al.* Human phospholamban null results in lethal dilated cardiomyopathy revealing a critical difference between mouse and human. *Journal of Clinical Investigation* **111**, 869-876, doi:10.1172/Jci200317892 (2003).

258 Kostin, S. *et al.* Myocytes die by multiple mechanisms in failing human hearts. *Circulation Research* **92**, 715-724, doi:10.1161/01.Res.0000067471.95890.5c (2003).

259 Goldman, S. J., Zhang, Y. & Jin, S. Autophagic degradation of mitochondria in white adipose tissue differentiation. *Antioxid Redox Signal* **14**, 1971-1978, doi:10.1089/ars.2010.3777 (2011).

260 Lavandero, S. *et al.* Cardiovascular autophagy Concepts, controversies, and perspectives. *Autophagy* **9**, 1455-1466, doi:10.4161/auto.25969 (2013).

261 Mizushima, N., Levine, B., Cuervo, A. M. & Klionsky, D. J. Autophagy fights disease through cellular self-digestion. *Nature* **451**, 1069-1075, doi:nature06639 [pii]10.1038/nature06639 (2008).

262 Nishida, K. & Otsu, K. Autophagy during cardiac remodeling. *Journal of Molecular and Cellular Cardiology* **95**, 11-18, doi:10.1016/j.yjmcc.2015.12.003 (2016).

263 Nakai, A. *et al.* The role of autophagy in cardiomyocytes in the basal state and in response to hemodynamic stress. *Nature Medicine* **13**, 619-624, doi:10.1038/nm1574 (2007).

264 Zhang, X. *et al.* Valsartan Regulates Myocardial Autophagy and Mitochondrial Turnover in Experimental Hypertension. *Hypertension* **64**, 87-93, doi:10.1161/Hypertensionaha.113.02151 (2014).

265 Mellor, K. M., Bell, J. R., Young, M. J., Ritchie, R. H. & Delbridge, L. M. Myocardial autophagy activation and suppressed survival signaling is associated with insulin resistance in fructose-fed mice. *J Mol Cell Cardiol* **50**, 1035-1043, doi:10.1016/j.yjmcc.2011.03.002 (2011).

266 Li, Z. L. *et al.* Transition from obesity to metabolic syndrome is associated with altered myocardial autophagy and apoptosis. *Arterioscler Thromb Vasc Biol* **32**, 1132-1141, doi:10.1161/ATVBAHA.111.244061 (2012).

267 Sciarretta, S. *et al.* Rheb is a critical regulator of autophagy during myocardial ischemia: pathophysiological implications in obesity and metabolic syndrome. *Circulation* **125**, 1134-1146, doi:10.1161/CIRCULATIONAHA.111.078212 (2012).

268 Lancel, S. *et al.* Carbon monoxide improves cardiac function and mitochondrial population quality in a mouse model of metabolic syndrome. *PLoS One* **7**, e41836, doi:10.1371/journal.pone.0041836 (2012).

269 Nelson, L. R. & Bulun, S. E. Estrogen production and action. *J. Am. Acad. Dermatol.* **45**, S116-124 (2001).

270 Birkhauser, M. Treatment of pain in estrogen deficiency. *Arch. Gynecol. Obstet.* **259**, S74-S79 (1996).

271 Kotov, A., Falany, J. L., Wang, J. & Falany, C. N. Regulation of estrogen activity by sulfation in human Ishikawa endometrial adenocarcinoma cells. *J. Steroid Biochem. Mol. Biol.* **68**, 137-144, doi:Doi 10.1016/S0960-0760(99)00022-9 (1999).

272 Guo, H. *et al.* Lipocalin 2 Deficiency Alters Estradiol Production and Estrogen Receptor Signaling in Female Mice. *Endocrinology* **153**, 1183-1193, doi:10.1210/en.2011-1642 (2012).

273 Santen, R. J., Brodie, H., Simpson, E. R., Siiteri, P. K. & Brodie, A. History of Aromatase: Saga of an Important Biological Mediator and Therapeutic Target. *Endocr. Rev.* **30**, 343-375, doi:10.1210/er.2008-0016 (2009).

274 Carreau, S., de Vienne, C. & Galeraud-Denis, I. Aromatase and estrogens in man reproduction: a review and latest advances. *Advances in medical sciences* **53**, 139-144, doi:10.2478/v10039-008-0022-z (2008).

275 Inoue, T. *et al.* Sex steroid synthesis in human skin in situ: The roles of aromatase and steroidogenic acute regulatory protein in the homeostasis of human skin. *Mol. Cell. Endocrinol.* **362**, 19-28, doi:10.1016/j.mce.2012.05.005 (2012).

276 Carreau, S., Bouraima-Lelong, H. & Delalande, C. Estrogen, a female hormone involved in spermatogenesis. *Advances in medical sciences* **57**, 31-36, doi:10.2478/v10039-012-0005-y (2012).

277 Simpson, E. R. *et al.* Aromatase expression in health and disease. *Recent Progress in Hormone Research, Proceedings of the 1996 Conference, Vol 52* **52**, 185-214 (1997).

278 Nelson, L. R. & Bulun, S. E. Estrogen production and action. *J Am Acad Dermatol* **45**, S116-S124, doi:10.1067/mjd.2001.117432 (2001).

279 O'Lone, R. *et al.* Estrogen receptors alpha and beta mediate distinct pathways of vascular gene expression, including genes involved in mitochondrial electron transport and generation of reactive oxygen species. *Molecular Endocrinology* **21**, 1281-1296, doi:10.1210/me.2006-0497 (2007).

280 Devanathan, S. *et al.* An animal model with a cardiomyocyte-specific deletion of estrogen receptor alpha: functional, metabolic, and differential network analysis. *PLoS One* **9**, e101900, doi:10.1371/journal.pone.0101900 (2014).

281 Chen, Z. *et al.* Estrogen receptor alpha mediates the nongenomic activation of endothelial nitric oxide synthase by estrogen. *Journal of Clinical Investigation* **103**, 401-406, doi:Doi 10.1172/Jci5347 (1999).

282 Nilsson, S. & Gustafsson, J. A. Estrogen receptors: therapies targeted to receptor subtypes. *Clin. Pharmacol. Ther.* **89**, 44-55, doi:10.1038/clpt.2010.226 (2011).

283 Prossnitz, E. R. & Barton, M. The G-protein-coupled estrogen receptor GPER in health and disease. *Nature reviews. Endocrinology* **7**, 715-726, doi:10.1038/nrendo.2011.122 (2011).

284 Prossnitz, E. R., Revankar, C. M., Arterburn, J. B. & Sklar, L. A. Estrogen receptors and cell signaling - Response. *Science* **310**, 52-53 (2005).

285 Nadal, A. *et al.* Nongenomic actions of estrogens and xenoestrogens by binding at a plasma membrane receptor unrelated to estrogen receptor alpha and estrogen receptor beta. *Proc. Natl. Acad. Sci. U. S. A.* **97**, 11603-11608, doi:DOI 10.1073/pnas.97.21.11603 (2000).

286 Takada, Y., Kato, C., Kondo, S., Korenaga, R. & Ando, J. Cloning of cDNAs encoding G protein-coupled receptor expressed in human endothelial cells exposed to fluid shear stress. *Biochemical and Biophysical Research Communications* **240**, 737-741, doi:DOI 10.1006/bbrc.1997.7734 (1997).

287 Flanagan, D. E. *et al.* Gender differences in the insulin-like growth factor axis response to a glucose load. *Acta Physiol (Oxf)* **187**, 371-378, doi:10.1111/j.1748-1716.2006.01581.x (2006).

288 Reckelhoff, J. F. & Maric, C. Sex and gender differences in cardiovascular-renal physiology and pathophysiology. *Steroids* **75**, 745-746, doi:10.1016/j.steroids.2010.05.020 (2010).

289 Hulley, S. *et al.* Randomized trial of estrogen plus progestin for secondary prevention of coronary heart disease in postmenopausal women. *Jama-J Am Med Assoc* **280**, 605-613, doi:DOI 10.1001/jama.280.7.605 (1998).

290 Grohe, C., Kahlert, S., Lobbert, K. & Vetter, H. Expression of oestrogen receptor alpha and beta in rat heart: role of local oestrogen synthesis. *J. Endocrinol.* **156**, R1-R7, doi:DOI 10.1677/joe.0.156R001 (1998).

291 Jazbutyte, V. *et al.* Aromatase Inhibition Attenuates Desflurane-Induced Preconditioning against Acute Myocardial Infarction in Male Mouse Heart In Vivo. *Plos One* **7**, doi:ARTN e4203210.1371/journal.pone.0042032 (2012).

292 Beitelshees, A. L. *et al.* Aromatase Gene Polymorphisms Are Associated with Survival among Patients with Cardiovascular Disease in a Sex-Specific Manner. *Plos One* **5**, doi:ARTN e1518010.1371/journal.pone.0015180 (2010).

293 Grohe, C. *et al.* Cardiac myocytes and fibroblasts contain functional estrogen receptors. *FEBS Lett* **416**, 107-112 (1997).

294 Lizotte, E., Grandy, S. A., Tremblay, A., Allen, B. G. & Fiset, C. Expression, distribution and regulation of sex steroid hormone receptors in mouse heart. *Cell. Physiol. Biochem.* **23**, 75-86, doi:10.1159/000204096 (2009).

295 Knowlton, A. A. & Lee, A. R. Estrogen and the cardiovascular system. *Pharmacol Ther* **135**, 54-70, doi:10.1016/j.pharmthera.2012.03.007 (2012).

296 Bowling, M. R. *et al.* Estrogen effects on vascular inflammation are age dependent: role of estrogen receptors. *Arterioscler Thromb Vasc Biol* **34**, 1477-1485, doi:10.1161/ATVBAHA.114.303629 (2014).

297 Holm, A. & Nilsson, B. O. Identification and characterization of new mechanisms in vascular oestrogen signalling. *Basic & clinical pharmacology & toxicology* **113**, 287-293, doi:10.1111/bcpt.12118 (2013).

298 Miller, V. M. & Duckles, S. P. Vascular actions of estrogens: Functional implications. *Pharmacol. Rev.* **60**, 210-241, doi:10.1124/pr.107.08002 (2008).

299 Alexander, S. P. H., Mathie, A. & Peters, J. A. Guide to Receptors and Channels (GRAC), 4th edition. *Br. J. Pharmacol.* **158**, S1-S239 (2009).

300 Lagranha, C. J., Deschamps, A., Aponte, A., Steenbergen, C. & Murphy, E. Sex differences in the phosphorylation of mitochondrial proteins result in reduced production of reactive oxygen species and cardioprotection in females. *Circ Res* **106**, 1681-1691, doi:10.1161/CIRCRESAHA.109.213645 (2010).

301 Dubey, R. K., Oparil, S., Imthurn, B. & Jackson, E. K. Sex hormones and hypertension. *Cardiovascular research* **53**, 688-708, doi:Pii S0008-6363(01)00527-2Doi 10.1016/S0008-6363(01)00527-2 (2002).

302 Leichman, J. G. *et al.* Improvements in systemic metabolism, anthropometrics, and left ventricular geometry 3 months after bariatric surgery. *Surgery for obesity and related diseases : official journal of the American Society for Bariatric Surgery* **2**, 592-599, doi:10.1016/j.soard.2006.09.005 (2006).

303 Barton, M. & Meyer, M. R. Postmenopausal Hypertension Mechanisms and Therapy. *Hypertension* **54**, 11-18, doi:10.1161/Hypertensionaha.108.120022 (2009).

304 Gabel, S. A. *et al.* Estrogen receptor beta mediates gender differences in ischemia/reperfusion injury. *J Mol Cell Cardiol* **38**, 289-297, doi:10.1016/j.yjmcc.2004.11.013 (2005).

305 Cross, H. R., Murphy, E. & Steenbergen, C. Ca(2+) loading and adrenergic stimulation reveal male/female differences in susceptibility to ischemia-reperfusion injury. *Am J Physiol Heart Circ Physiol* **283**, H481-489, doi:10.1152/ajpheart.00790.2001 (2002).

306 Chi, P. *et al.* Laparoscopic Transabdominal Approach Partial Intersphincteric Resection for Low Rectal Cancer: Surgical Feasibility and Intermediate-Term Outcome. *Ann. Surg. Oncol.*, doi:10.1245/s10434-014-4085-8 (2014).

307 Saito, T. *et al.* Estrogen contributes to gender differences in mouse ventricular repolarization. *Circ Res* **105**, 343-352, doi:10.1161/CIRCRESAHA.108.190041 (2009).

308 Kurokawa, J. *et al.* Acute effects of oestrogen on the guinea pig and human IKr channels and drug-induced prolongation of cardiac repolarization. *J Physiol* **586**, 2961-2973, doi:10.1113/jphysiol.2007.150367 (2008).

309 Adams, M. R. *et al.* Inhibition of coronary artery atherosclerosis by 17-beta estradiol in ovariectomized monkeys. Lack of an effect of added progesterone. *Arteriosclerosis* **10**, 1051-1057 (1990).

310 van Eickels, M. *et al.* 17beta-estradiol attenuates the development of pressure-overload hypertrophy. *Circulation* **104**, 1419-1423. (2001).

311 Clegg, D. J. Minireview: the year in review of estrogen regulation of metabolism. *Mol Endocrinol* **26**, 1957-1960, doi:10.1210/me.2012-1284 (2012).

312 Carr, M. C. The emergence of the metabolic syndrome with menopause. *J Clin Endocrinol Metab* **88**, 2404-2411, doi:10.1210/jc.2003-030242 (2003).

313 Mauvais-Jarvis, F. Estrogen and androgen receptors: regulators of fuel homeostasis and emerging targets for diabetes and obesity. *Trends Endocrinol Metab* **22**, 24-33, doi:10.1016/j.tem.2010.10.002 (2011).

314 Park, C. J. *et al.* Genetic rescue of nonclassical ERalpha signaling normalizes energy balance in obese Eralpha-null mutant mice. *J Clin Invest* **121**, 604-612, doi:10.1172/JCI41702 (2011).

315 Kumar, R. & McEwan, I. J. Allosteric modulators of steroid hormone receptors: structural dynamics and gene regulation. *Endocr Rev* **33**, 271-299, doi:10.1210/er.2011-1033 (2012).

316 Lu, X., Peng, L., Lv, M. & ding, K. Recent advance in the design of small molecular modulators of estrogen-related receptors. *Curr. Pharm. Des.* **18**, 3421-3431 (2012).

317 Riant, E. *et al.* Estrogens protect against high-fat diet-induced insulin resistance and glucose intolerance in mice. *Endocrinology* **150**, 2109-2117, doi:10.1210/en.2008-0971 (2009).

318 Barros, R. P., Gabbi, C., Morani, A., Warner, M. & Gustafsson, J. A. Participation of ERalpha and ERbeta in glucose homeostasis in skeletal muscle and white adipose tissue. *Am J Physiol Endocrinol Metab* **297**, E124-133, doi:10.1152/ajpendo.00189.2009 (2009).

319 Naaz, A. *et al.* Effect of ovariectomy on adipose tissue of mice in the absence of estrogen receptor alpha (ERalpha): a potential role for estrogen receptor beta (ERbeta). *Horm Metab Res* **34**, 758-763, doi:10.1055/s-2002-38259 (2002).

320 Chen, Y. *et al.* 17beta-estradiol prevents cardiac diastolic dysfunction by stimulating mitochondrial function: A preclinical study in a mouse model of a human hypertrophic cardiomyopathy mutation. *J. Steroid Biochem. Mol. Biol.* **147**, 92-102, doi:10.1016/j.jsbmb.2014.12.011 (2015).

321 Arias-Loza, P. A. *et al.* The estrogen receptor-alpha is required and sufficient to maintain physiological glucose uptake in the mouse heart. *Hypertension* **60**, 1070-1077, doi:10.1161/HYPERTENSIONAHA.111.190389 (2012).

322 Martensson, U. E. A. *et al.* Deletion of the G Protein-Coupled Receptor 30 Impairs Glucose Tolerance, Reduces Bone Growth, Increases Blood Pressure, and Eliminates Estradiol-Stimulated Insulin Release in Female Mice. *Endocrinology* **150**, 687-698, doi:10.1210/en.2008-0623 (2009).

323 Meyer, M. R., Prossnitz, E. R. & Barton, M. The G protein-coupled estrogen receptor GPER/GPR30 as a regulator of cardiovascular function. *Vascular pharmacology* **55**, 17-25, doi:10.1016/j.vph.2011.06.003 (2011).

324 Sharma, G. *et al.* GPER deficiency in male mice results in insulin resistance, dyslipidemia, and a proinflammatory state. *Endocrinology* **154**, 4136-4145, doi:10.1210/en.2013-1357 (2013).

325 Sharma, G. & Prossnitz, E. R. Mechanisms of estradiol-induced insulin secretion by the G protein-coupled estrogen receptor GPR30/GPER in pancreatic beta-cells. *Endocrinology* **152**, 3030-3039, doi:10.1210/en.2011-0091 (2011).

326 Miranda, P. J., DeFronzo, R. A., Califf, R. M. & Guyton, J. R. Metabolic syndrome: definition, pathophysiology, and mechanisms. *Am. Heart J.* **149**, 33-45, doi:10.1016/j.ahj.2004.07.013 (2005).

327 Geary, N., Asarian, L., Korach, K. S., Pfaff, D. W. & Ogawa, S. Deficits in E2-dependent control of feeding, weight gain, and cholecystokinin satiation in ER-alpha null mice. *Endocrinology* **142**, 4751-4757, doi:10.1210/endo.142.11.8504 (2001).

328 Wallen, W. J., Belanger, M. P. & Wittnich, C. Sex hormones and the selective estrogen receptor modulator tamoxifen modulate weekly body weights and food intakes in adolescent and adult rats. *J Nutr* **131**, 2351-2357 (2001).

329 Thorne, A., Lonnqvist, F., Apelman, J., Hellers, G. & Arner, P. A pilot study of long-term effects of a novel obesity treatment: omentectomy in connection with adjustable gastric banding. *Int J Obes Relat Metab Disord* **26**, 193-199, doi:10.1038/sj.ijo.0801871 (2002).

330 Gabriely, I. *et al.* Removal of visceral fat prevents insulin resistance and glucose intolerance of aging: an adipokine-mediated process? *Diabetes* **51**, 2951-2958 (2002).

331 Tran, T. T., Yamamoto, Y., Gesta, S. & Kahn, C. R. Beneficial effects of subcutaneous fat transplantation on metabolism. *Cell metabolism* **7**, 410-420, doi:10.1016/j.cmet.2008.04.004 (2008).

332 Curtis, S. W. *et al.* Physiological coupling of growth factor and steroid receptor signaling pathways: estrogen receptor knockout mice lack estrogen-like response to epidermal growth factor. *Proc Natl Acad Sci U S A* **93**, 12626-12630 (1996).

333 Thomas, R. S., Sarwar, N., Phoenix, F., Coombes, R. C. & Ali, S. Phosphorylation at serines 104 and 106 by Erk1/2 MAPK is important for estrogen receptor-alpha activity. *J. Mol. Endocrinol.* **40**, 173-184, doi:10.1677/Jme-07-0165 (2008).

334 Menazza, S. & Murphy, E. The Expanding Complexity of Estrogen Receptor Signaling in the Cardiovascular System. *Circ Res* **118**, 994-1007, doi:10.1161/CIRCRESAHA.115.305376 (2016).

335 Szego, C. M. & Davis, J. S. Adenosine 3',5'-Monophosphate in Rat Uterus - Acute Elevation by Estrogen. *Proc. Natl. Acad. Sci. U. S. A.* **58**, 1711-&, doi:DOI 10.1073/pnas.58.4.1711 (1967).

336 Bondar, G., Kuo, J., Hamid, N. & Micevych, P. Estradiol-induced estrogen receptor-alpha trafficking. *J Neurosci* **29**, 15323-15330, doi:10.1523/JNEUROSCI.2107-09.2009 (2009).

337 Pedram, A., Razandi, M. & Levin, E. R. Nature of functional estrogen receptors at the plasma membrane. *Molecular Endocrinology* **20**, 1996-2009, doi:10.1210/me.2005-0525 (2006).

338 Chambliss, K. L. *et al.* Estrogen receptor alpha and endothelial nitric oxide synthase are organized into a functional signaling module in caveolae. *Circulation Research* **87**, E44-E52 (2000).

339 Revankar, C. M., Cimino, D. F., Sklar, L. A., Arterburn, J. B. & Prossnitz, E. R. A transmembrane intracellular estrogen receptor mediates rapid cell signaling. *Science* **307**, 1625-1630, doi:10.1126/science.1106943 (2005).

340 Vital, P., Larrieta, E. & Hiriart, M. Sexual dimorphism in insulin sensitivity and susceptibility to develop diabetes in rats. *J Endocrinol* **190**, 425-432, doi:10.1677/joe.1.06596 (2006).

341 Galipeau, D., Verma, S. & McNeill, J. H. Female rats are protected against fructose-induced changes in metabolism and blood pressure. *Am J Physiol Heart Circ Physiol* **283**, H2478-2484, doi:10.1152/ajpheart.00243.2002 (2002).

342 Belke, D. D. *et al.* Insulin signaling coordinately regulates cardiac size, metabolism, and contractile protein isoform expression. *Journal of Clinical Investigation* **109**, 629-639, doi:10.1172/Jci200213946 (2002).

343 Boudina, S. *et al.* Contribution of Impaired Myocardial Insulin Signaling to Mitochondrial Dysfunction and Oxidative Stress in the Heart. *Circulation* **119**, 1272-U1111, doi:10.1161/Circulationaha.108.792101 (2009).

344 Bugger, H. & Abel, E. D. Rodent models of diabetic cardiomyopathy. *Dis Model Mech* **2**, 454-466, doi:10.1242/dmm.001941 (2009).

345 Neuhaus, B. *et al.* Experimental analysis of risk factors for ulcerative dermatitis in mice. *Exp. Dermatol.* **21**, 712-713, doi:10.1111/j.1600-0625.2012.01558.x (2012).

346 Maffucci, J. & Gore, A. in *Handbook of Models for Human Aging* (ed Conn MP) 533-552 (Elsevier, 2006).

347 Guo, X., Razandi, M., Pedram, A., Kassab, G. & Levin, E. R. Estrogen induces vascular wall dilation: mediation through kinase signaling to nitric oxide and estrogen receptors alpha and beta. *J Biol Chem* **280**, 19704-19710, doi:10.1074/jbc.M501244200 (2005).

348 Mendelsohn, M. E. & Karas, R. H. The protective effects of estrogen on the cardiovascular system. *N. Engl. J. Med.* **340**, 1801-1811 (1999).

349 Chen, Y. F. & Meng, Q. C. Sexual Dimorphism of Blood-Pressure in Spontaneously Hypertensive Rats Is Androgen Dependent. *Life Sci.* **48**, 85-96, doi:Doi 10.1016/0024-3205(91)90428-E (1991).

350 Harrison-Bernard, L. M. & Raij, L. Post ovariectomy (OVX) hypertension (HTN) is linked to upregulation of renal angiotensin II type I (AT1) receptors and increased salt-sensitivity. *Hypertension* **34**, 336-336 (1999).

351 Reckelhoff, J. F., Zhang, H. M. & Granger, J. P. Testosterone exacerbates hypertension and reduces pressure-natriuresis in male spontaneously hypertensive rats. *Hypertension* **31**, 435-439 (1998).

352 Wassmann, S. *et al.* Endothelial dysfunction and oxidative stress during estrogen deficiency in spontaneously hypertensive rats. *Circulation* **103**, 435-441 (2001).

353 Lund, L. H., Benson, L., Dahlstrom, U. & Edner, M. Association Between Use of Renin-Angiotensin System Antagonists and Mortality in Patients With Heart Failure and Preserved Ejection Fraction. *Jama-J Am Med Assoc* **308**, 2108-2117, doi:10.1001/jama.2012.14785 (2012).

354 Zhang, J. D. & Crowley, S. D. The Role of Type 1 Angiotensin Receptors on T Lymphocytes in Cardiovascular and Renal Diseases. *Current Hypertension Reports* **15**, 39-46, doi:10.1007/s11906-012-0318-z (2013).

355 Bishop, J. E., Greenbaum, R., Gibson, D. G., Yacoub, M. & Laurent, G. J. Enhanced Deposition of Predominantly Type-I Collagen in Myocardial-Disease. *Journal of Molecular and Cellular Cardiology* **22**, 1157-1165, doi:Doi 10.1016/0022-2828(90)90079-H (1990).

356 Marijianowski, M. M. H., Teeling, P., Mann, J. & Becker, A. E. Dilated Cardiomyopathy Is Associated with an Increase in the Type-I/Type-Iii Collagen Ratio - a Quantitative Assessment. *J. Am. Coll. Cardiol.* **25**, 1263-1272, doi:Doi 10.1016/0735-1097(94)00557-7 (1995).

357 Haskill, S. *et al.* Characterization of an Immediate-Early Gene Induced in Adherent Monocytes That Encodes I-Kappa-B-Like Activity. *Cell* **65**, 1281-1289, doi:Doi 10.1016/0092-8674(91)90022-Q (1991).

358 Thompson, J. E., Phillips, R. J., Erdjumentbromage, H., Tempst, P. & Ghosh, S. I-Kappa-B-Beta Regulates the Persistent Response in a Biphasic Activation of Nf-Kappa-B. *Cell* **80**, 573-582, doi:Doi 10.1016/0092-8674(95)90511-1 (1995).

359 Traenckner, E. B. M. *et al.* Phosphorylation of Human I-Kappa-B-Alpha on Serine-32 and Serine-36 Controls I-Kappa-B-Alpha Proteolysis and Nf-Kappa-B Activation in Response to Diverse Stimuli. *EMBO J.* **14**, 2876-2883 (1995).

360 Scherer, D. C., Brockman, J. A., Chen, Z. J., Maniatis, T. & Ballard, D. W. Signal-Induced Degradation of I-Kappa-B-Alpha Requires Site-Specific Ubiquitination. *Proc. Natl. Acad. Sci. U. S. A.* **92**, 11259-11263, doi:DOI 10.1073/pnas.92.24.11259 (1995).

361 Chen, Z. J., Parent, L. & Maniatis, T. Site-specific phosphorylation of IkappaBalpha by a novel ubiquitination-dependent protein kinase activity. *Cell* **84**, 853-862 (1996).

362 Sasaki, C. Y., Barberi, T. J., Ghosh, P. & Longo, D. L. Phosphorylation of RelA/p65 on serine 536 defines an I kappa B alpha-independent NF-kappa B pathway. *Journal of Biological Chemistry* **280**, 34538-34547, doi:10.1074/jbc.M504943200 (2005).

363 Sakurai, H., Chiba, H., Miyoshi, H., Sugita, T. & Toriumi, W. I kappa B kinases phosphorylate NF-kappa B p65 subunit on serine 536 in the transactivation domain. *Journal of Biological Chemistry* **274**, 30353-30356, doi:DOI 10.1074/jbc.274.43.30353 (1999).

364 Gwinn, D. M. *et al.* AMPK phosphorylation of raptor mediates a metabolic checkpoint. *Molecular cell* **30**, 214-226, doi:10.1016/j.molcel.2008.03.003 (2008).

365 Wang, W. *et al.* Augmentation of autophagy by atorvastatin via Akt/mTOR pathway in spontaneously hypertensive rats. *Hypertens. Res.* **38**, 813-820, doi:10.1038/hr.2015.85 (2015).

366 Zimmet, P., Alberti, K. G. M. M. & Rios, M. S. A new International Diabetes Federation worldwide definition of the metabolic syndrome: The rationale and the results. *Rev. Esp. Cardiol.* **58**, 1371-1376, doi:Doi 10.1016/S0300-8932(05)74065-3 (2005).

367 Maas, A. H. E. M. *et al.* Red alert for women's heart: the urgent need for more research and knowledge on cardiovascular disease in women. *European Heart Journal* **32**, 1362-U1389, doi:10.1093/eurheartj/ehr048 (2011).

368 Fliegner, D. *et al.* Female sex and estrogen receptor-beta attenuate cardiac remodeling and apoptosis in pressure overload. (vol 298, pg R1597, 2010). *American Journal of Physiology-Regulatory Integrative and Comparative Physiology* **299**, R981-R981, doi:10.1152/ajpregu.zh6-7341-corr.2010 (2010).

369 Rosamond. Heart Disease and Stroke Statistics-2007 Update: A Report From the American Heart Association Statistics Committee and Stroke Statistics Subcommittee (vol 115, pg e69, 2007). *Circulation* **122**, E9-E9, doi:10.1161/CIR.0b013e3181e65a91 (2010).

370 Borlaug, B. A. Sex, Load, and Relaxation Are Women More Susceptible to Load-Dependent Diastolic Dysfunction? *Journal of the American College of Cardiology* **57**, 1234-1236, doi:10.1016/j.jacc.2010.10.033 (2011).

371 Rossouw, J. E. *et al.* Risks and benefits of estrogen plus progestin in healthy postmenopausal women - Principal results from the Women's Health Initiative randomized controlled trial. *Jama-J Am Med Assoc* **288**, 321-333 (2002).

372 Anderson, G. L. *et al.* Effects of conjugated, equine estrogen in postmenopausal women with hysterectomy - The women's health initiative randomized controlled trial. *Jama-J Am Med Assoc* **291**, 1701-1712 (2004).

373 Priego, T., Sanchez, J., Pico, C. & Palou, A. Sex-differential expression of metabolism-related genes in response to a high-fat diet. *Obesity* **16**, 819-826, doi:10.1038/oby.2007.117 (2008).

374 Enzi, G. *et al.* Subcutaneous and visceral fat distribution according to sex, age, and overweight, evaluated by computed tomography. *Am J Clin Nutr* **44**, 739-746 (1986).

375 Gambacciani, M. *et al.* Body weight, body fat distribution, and hormonal replacement therapy in early postmenopausal women. *J Clin Endocrinol Metab* **82**, 414-417, doi:10.1210/jcem.82.2.3735 (1997).

376 Wajchenberg, B. L. Subcutaneous and visceral adipose tissue: their relation to the metabolic syndrome. *Endocr Rev* **21**, 697-738, doi:10.1210/edrv.21.6.0415 (2000).

377 Rotter, V., Nagaev, I. & Smith, U. Interleukin-6 (IL-6) induces insulin resistance in 3T3-L1 adipocytes and is, like IL-8 and tumor necrosis factor-alpha, overexpressed in human fat cells from insulin-resistant subjects. *Journal of Biological Chemistry* **278**, 45777-45784, doi:10.1074/jbc.M301977200 (2003).

378 Carbone, S. *et al.* A high-sugar and high-fat diet impairs cardiac systolic and diastolic function in mice. *Int. J. Cardiol.* **198**, 66-69, doi:10.1016/j.ijcard.2015.06.136 (2015).

379 Muoio, D. M. & Newgard, C. B. Mechanisms of disease:Molecular and metabolic mechanisms of insulin resistance and beta-cell failure in type 2 diabetes. *Nat Rev Mol Cell Biol* **9**, 193-205, doi:10.1038/nrm2327 (2008).

380 Shanik, M. H. *et al.* Insulin Resistance and Hyperinsulinemia Is hyperinsulinemia the cart or the horse? *Diabetes Care* **31**, S262-S268, doi:10.2337/dc08-s264 (2008).

381 Liu, H. Y. *et al.* Increased basal level of Akt-dependent insulin signaling may be responsible for the development of insulin resistance. *Am J Physiol-Endoc M* **297**, E898-E906, doi:10.1152/ajpendo.00374.2009 (2009).

382 Johnson, A. M. F. & Olefsky, J. M. The Origins and Drivers of Insulin Resistance. *Cell* **152**, 673-684, doi:10.1016/j.cell.2013.01.041 (2013).

383 Lee, Y. S. *et al.* Inflammation Is Necessary for Long-Term but Not Short-Term High-Fat Diet Induced Insulin Resistance. *Diabetes* **60**, 2474-2483, doi:10.2337/db11-0194 (2011).

384 Wolfrum, S. *et al.* Inhibition of Rho-kinase leads to rapid activation of phosphatidylinositol 3-kinase protein kinase Akt and cardiovascular protection. *Arterioscl Throm Vas* **24**, 1842-1847, doi:10.1161/01.Atv.0000142813.33538.82 (2004).

385 Bao, W. K. *et al.* Inhibition of Rho-kinase protects the heart against ischemia/reperfusion injury. *Cardiovascular Research* **61**, 548-558, doi:10.1016/j.cardiores.2003.12.004 (2004).

386 Hu, P., Han, Z., Couvillon, A. D. & Exton, J. H. Critical role of endogenous Akt/IAPs and MEK1/ERK pathways in counteracting endoplasmic reticulum stress-induced cell death. *Journal of Biological Chemistry* **279**, 49420-49429, doi:10.1074/jbc.M407700200 (2004).

387 Dhindsa, S. *et al.* Insulin Resistance and Inflammation in Hypogonadotropic Hypogonadism and Their Reduction After Testosterone Replacement in Men With Type 2 Diabetes. *Diabetes Care* **39**, 82-91, doi:10.2337/dc15-1518 (2016).

388 Mauvais-Jarvis, F. Role of Sex Steroics in beta Cell Function, Grovv-h, and Survival. *Trends Endocrin Met* **27**, 844-855, doi:10.1016/j.tem.2016.08.008 (2016).

389 Alonso-Magdalena, P. *et al.* Pancreatic insulin content regulation by the estrogen receptor ER alpha. *PLoS One* **3**, e2069, doi:10.1371/journal.pone.0002069 (2008).

390 Navarro, G. *et al.* Extranuclear Actions of the Androgen Receptor Enhance Glucose-Stimulated Insulin Secretion in the Male. *Cell metabolism* **23**, 837-851, doi:10.1016/j.cmet.2016.03.015 (2016).

391 Basu, R. *et al.* The effects of age and gender on glucose tolerance: Contribution of differences in insulin secretion, insulin clearance and insulin action. *Faseb Journal* **15**, A751-A751 (2001).

392 Galipeau, D. M., Yao, L. F. & McNeill, J. H. Relationship among hyperinsulinemia, insulin resistance, and hypertension is dependent on sex. *American Journal of Physiology-Heart and Circulatory Physiology* **283**, H562-H567, doi:10.1152/ajpheart.00238.2002 (2002).

393 Corsetti, J. P., Sparks, J. D., Peterson, R. G., Smith, R. L. & Sparks, C. E. Effect of dietary fat on the development of non-insulin dependent diabetes mellitus in obese Zucker diabetic fatty male and female rats. *Atherosclerosis* **148**, 231-241, doi:Doi 10.1016/S0021-9150(99)00265-8 (2000).

394 Louwe, M. C. *et al.* Gender-dependent effects of high-fat lard diet on cardiac function in C57Bl/6J mice. *Appl Physiol Nutr Metab* **37**, 214-224, doi:10.1139/h11-153 (2012).

395 Kararigas, G. *et al.* Transcriptome characterization of estrogen-treated human myocardium identifies myosin regulatory light chain interacting protein as a sex-specific element influencing contractile function. *J Am Coll Cardiol* **59**, 410-417, doi:10.1016/j.jacc.2011.09.054 (2012).

396 Park, Y. W. *et al.* The metabolic syndrome: prevalence and associated risk factor findings in the US population from the Third National Health and Nutrition Examination Survey, 1988-1994. *Arch Intern Med* **163**, 427-436 (2003).

397 Sites, C. K. *et al.* Menopause-related differences in inflammation markers and their relationship to body fat distribution and insulin-stimulated glucose disposal. *Fertil Steril* **77**, 128-135 (2002).

398 Neigh, G. Sex Differences in Physiology. (2016).

399 Frias, J. P. *et al.* Decreased susceptibility to fatty acid-induced peripheral tissue insulin resistance in women. *Diabetes* **50**, 1344-1350, doi:DOI 10.2337/diabetes.50.6.1344 (2001).

400 Campbell, S. E. & Febbraio, M. A. Effect of the ovarian hormones on GLUT4 expression and contraction-stimulated glucose uptake. *Am J Physiol Endocrinol Metab* **282**, E1139-1146, doi:10.1152/ajpendo.00184.2001 (2002).

401 Choi, C. S. *et al.* Overexpression of uncoupling protein 3 in skeletal muscle protects against fat-induced insulin resistance. *J Clin Invest* **117**, 1995-2003, doi:10.1172/JCI13579 (2007).

402 Hevener, A., Reichart, D., Janez, A. & Olefsky, J. Female rats do not exhibit free fatty acid-induced insulin resistance. *Diabetes* **51**, 1907-1912 (2002).

403 Stirone, C., Boroujerdi, A., Duckles, S. P. & Krause, D. N. Estrogen receptor activation of phosphoinositide-3 kinase, akt, and nitric oxide signaling in cerebral blood vessels: rapid and long-term effects. *Mol Pharmacol* **67**, 105-113, doi:10.1124/mol.104.004465 (2005).

404 Abel, E. D. *et al.* Regulation of insulin-responsive aminopeptidase expression and targeting in the insulin-responsive vesicle compartment of glucose transporter isoform 4-deficient cardiomyocytes. *Mol Endocrinol* **18**, 2491-2501, doi:10.1210/me.2004-0175 (2004).

405 Cheng, C. M., Cohen, M., Wang, J. & Bondy, C. A. Estrogen augments glucose transporter and IGF1 expression in primate cerebral cortex. *FASEB J* **15**, 907-915 (2001).

406 Stirone, C., Duckles, S. P., Krause, D. N. & Procaccio, V. Estrogen increases mitochondrial efficiency and reduces oxidative stress in cerebral blood vessels. *Mol Pharmacol* **68**, 959-965, doi:10.1124/mol.105.014662 (2005).

407 Kannel, W. B., Gordon, T. & Schwartz, M. J. Systolic Versus Diastolic Blood Pressure and Risk of Coronary Heart Disease - Framingham Study. *American Journal of Cardiology* **27**, 335-&, doi:Doi 10.1016/0002-9149(71)90428-0 (1971).

408 Collins, R. *et al.* Blood-Pressure, Stroke, and Coronary Heart-Disease .2. Short-Term Reductions in Blood-Pressure - Overview of Randomized Drug Trials in Their Epidemiologic Context. *Lancet* **335**, 827-838, doi:Doi 10.1016/0140-6736(90)90944-Z (1990).

409 Kannel, W. B., Dawber, T. R. & Mcgee, D. L. Perspectives on Systolic Hypertension - the Framingham-Study. *Circulation* **61**, 1179-1182 (1980).

410 Darne, B., Girerd, X., Safar, M., Cambien, F. & Guize, L. Pulsatile Versus Steady Component of Blood-Pressure - a Cross-Sectional Analysis and a Prospective Analysis on Cardiovascular Mortality. *Hypertension* **13**, 392-400 (1989).

411 Nichols, W. W., ORourke, M. F. & Vlachopoulos, C. McDonald's Blood Flow in Arteries: Theoretical, Experimental and Clinical Principles, 6th Edition. *Mcdonald's Blood Flow in Arteries: Theoretical, Experimental and Clinical Principles, 6th Edition*, 1-741 (2011).

412 Fang, J., Madhavan, S., Cohen, H. & Alderman, M. H. Measures of Blood-Pressure and Myocardial-Infarction in Treated Hypertensive Patients. *J. Hypertens.* **13**, 413-419 (1995).

413 Witteman, J. C. M. *et al.* J-Shaped Relation between Change in Diastolic Blood-Pressure and Progression of Aortic Atherosclerosis. *Lancet* **343**, 504-507, doi:Doi 10.1016/S0140-6736(94)91459-1 (1994).

414 Rosamond, W. *et al.* Heart disease and stroke statistics - 2007 update - A report from the American Heart Association Statistics Committee and Stroke Statistics Subcommittee. *Circulation* **115**, E69-E171, doi:10.1161/Circulationaha.106.179918 (2007).

415 Roberts, N. W. *et al.* Successful metabolic adaptations leading to the prevention of high fat diet-induced murine cardiac remodeling. *Cardiovascular diabetology* **14**, 127, doi:10.1186/s12933-015-0286-0 (2015).

416 Calligaris, S. D. *et al.* Mice long-term high-fat diet feeding recapitulates human cardiovascular alterations: an animal model to study the early phases of diabetic cardiomyopathy. *PLoS One* **8**, e60931, doi:10.1371/journal.pone.0060931 (2013).

417 Mullins, J. J., Peters, J. & Ganten, D. Fulminant Hypertension in Transgenic Rats Harboring the Mouse Ren-2 Gene. *Nature* **344**, 541-544, doi:DOI 10.1038/344541a0 (1990).

418 Yu, Q. *et al.* Characterization of high-salt and high-fat diets on cardiac and vascular function in mice. *Cardiovasc Toxicol* **4**, 37-46 (2004).

419 Zhan, Y. M. *et al.* Ets-1 is a critical regulator of Ang II-mediated vascular inflammation and remodeling. *Journal of Clinical Investigation* **115**, 2508-2516, doi:10.1172/Jci24403 (2005).

420 Vecchione, C. *et al.* Protection from angiotensin II-mediated vasculotoxic and hypertensive response in mice lacking PI3K gamma. *J. Exp. Med.* **201**, 1217-1228, doi:10.1084/jem.20040995 (2005).

421 Francois, H., Athirakul, K., Mao, L., Rockman, H. & Coffman, T. M. Role for thromboxane receptors in angiotensin-II-Induced hypertension. *Hypertension* **43**, 364-369, doi:10.1161/01.Hyp.0000112225.27560.24 (2004).

422 Wiesel, P., Mazzolai, L., Nussberger, J. & Pedrazzini, T. Two-kidney, one clip and one-kidney, one clip hypertension in mice. *Hypertension* **29**, 1025-1030 (1997).

423 Galderisi, M. Diastolic dysfunction and diabetic cardiomyopathy: evaluation by Doppler echocardiography. *J Am Coll Cardiol* **48**, 1548-1551, doi:10.1016/j.jacc.2006.07.033 (2006).

424 Ho, C. Y. Echocardiographic Assessment of Diastolic Function. (2007).

425 Owan, T. E. *et al.* Trends in prevalence and outcome of heart failure with preserved ejection fraction. *N. Engl. J. Med.* **355**, 251-259, doi:DOI 10.1056/NEJMoa052256 (2006).

426 Regitz-Zagrosek, V., Oertelt-Prigione, S., Seeland, U. & Hetzer, R. Sex and Gender Differences in Myocardial Hypertrophy and Heart Failure. *Circulation Journal* **74**, 1265-1273, doi:10.1253/circj.CJ-10-0196 (2010).

427 Hafstad, A. D. *et al.* High- and moderate-intensity training normalizes ventricular function and mechanoenergetics in mice with diet-induced obesity. *Diabetes* **62**, 2287-2294, doi:10.2337/db12-1580 (2013).

428 Fang, C. X. *et al.* Hypertrophic cardiomyopathy in high-fat diet-induced obesity: role of suppression of forkhead transcription factor and atrophy gene transcription. *Am J Physiol Heart Circ Physiol* **295**, H1206-H1215, doi:10.1152/ajpheart.00319.2008 (2008).

429 Vasanji, Z., Cantor, E. J., Juric, D., Moyen, M. & Netticadan, T. Alterations in cardiac contractile performance and sarcoplasmic reticulum function in sucrose-fed rats is associated with insulin resistance. *Am J Physiol Cell Physiol* **291**, C772-780, doi:10.1152/ajpcell.00086.2005 (2006).

430 Alfarano, C. *et al.* Transition from metabolic adaptation to maladaptation of the heart in obesity: role of apelin. *Int J Obes (Lond)*, doi:10.1038/ijo.2014.122 (2014).

431 Brainard, R. E. *et al.* High fat feeding in mice is insufficient to induce cardiac dysfunction and does not exacerbate heart failure. *PLoS One* **8**, e83174, doi:10.1371/journal.pone.0083174 (2013).

432 Park, S. Y. *et al.* Unraveling the temporal pattern of diet-induced insulin resistance in individual organs and cardiac dysfunction in C57BL/6 mice. *Diabetes* **54**, 3530-3540 (2005).

433 Zhou, Y. T. *et al.* Lipotoxic heart disease in obese rats: implications for human obesity. *Proc Natl Acad Sci U S A* **97**, 1784-1789 (2000).

434 Christoffersen, C. *et al.* Cardiac lipid accumulation associated with diastolic dysfunction in obese mice. *Endocrinology* **144**, 3483-3490, doi:10.1210/en.2003-0242 (2003).

435 Schilling, J. D., Machkovech, H. M., Kim, A. H. J., Schwedwener, R. & Schaffer, J. E. Macrophages modulate cardiac function in lipotoxic cardiomyopathy. *American Journal of Physiology-Heart and Circulatory Physiology* **303**, H1366-H1373, doi:10.1152/ajpheart.00111.2012 (2012).

436 Cavalera, M., Wang, J. & Frangogiannis, N. G. Obesity, metabolic dysfunction, and cardiac fibrosis: pathophysiological pathways, molecular mechanisms, and therapeutic opportunities. *Translational research : the journal of laboratory and clinical medicine* **164**, 323-335, doi:10.1016/j.trsl.2014.05.001 (2014).

437 Ko, H. J. *et al.* Nutrient Stress Activates Inflammation and Reduces Glucose Metabolism by Suppressing AMP-Activated Protein Kinase in the Heart. *Diabetes* **58**, 2536-2546, doi:10.2337/db08-1361 (2009).

438 Whaley-Connell, A. *et al.* Overnutrition and the Cardiorenal Syndrome: Use of a Rodent Model to Examine Mechanisms. *Cardiorenal Med* **1**, 23-30, doi:10.1159/000322827 (2011).

439 Wang, C. Y. & Liao, J. K. A Mouse Model of Diet-Induced Obesity and Insulin Resistance. *Mtor: Methods and Protocols* **821**, 421-433, doi:10.1007/978-1-61779-430-8_27 (2012).

440 DeMarco, V. G. *et al.* Obesity-Related Alterations in Cardiac Lipid Profile and Nondipping Blood Pressure Pattern during Transition to Diastolic Dysfunction in Male db/db Mice. *Endocrinology* **154**, 159-171, doi:10.1210/en.2012-1835 (2013).

441 van Bilsen, M. *et al.* Hypertension Is a Conditional Factor for the Development of Cardiac Hypertrophy in Type 2 Diabetic Mice. *Plos One* **9**, doi:ARTN e8507810.1371/journal.pone.0085078 (2014).

442 Wang, H. *et al.* Characterization of the cardiac renin angiotensin system in oophorectomized and estrogen-replete mRen2.Lewis rats. *PLoS One* **8**, e76992, doi:10.1371/journal.pone.0076992 (2013).

443 Zibadi, S., Vazquez, R., Moore, D., Larson, D. F. & Watson, R. R. Myocardial lysyl oxidase regulation of cardiac remodeling in a murine model of diet-induced metabolic syndrome. *Am J Physiol-Heart C* **297**, H976-H982, doi:10.1152/ajpheart.00398.2009 (2009).

444 D'Souza, S. P., Davis, M. & Baxter, G. F. Autocrine and paracrine actions of natriuretic peptides in the heart. *Pharmacology & Therapeutics* **101**, 113-129, doi:10.1016/j.pharmthera.2003.11.011 (2004).

445 Nishikimi, T., Maeda, N. & Matsuoka, H. The role of natriuretic peptides in cardioprotection. *Cardiovascular Research* **69**, 318-328, doi:10.1016/j.cardiores.2005.10.001 (2006).

446 Bartels, E. D., Nielsen, J. M., Bisgaard, L. S., Goetze, J. P. & Nielsen, L. B. Decreased Expression of Natriuretic Peptides Associated with Lipid Accumulation in Cardiac Ventricle of Obese Mice. *Endocrinology* **151**, 5218-5225, doi:10.1210/en.2010-0355 (2010).

447 Nilsson, J. *et al.* A low-carbohydrate high-fat diet decreases lean mass and impairs cardiac function in pair-fed female C57BL/6J mice. *Nutr. Metab.* **13**, doi:ARTN 7910.1186/s12986-016-0132-8 (2016).

448 Harrington, L. S. *et al.* The TSC1-2 tumor suppressor controls insulin-PI3K signaling via regulation of IRS proteins. *J. Cell Biol.* **166**, 213-223, doi:10.1083/jcb.200403069 (2004).

449 Shah, O. J., Wang, Z. & Hunter, T. Inappropriate activation of the TSC/Rheb/mTOR/S6K cassette induces IRS1/2 depletion, insulin resistance, and cell survival deficiencies. *Curr Biol* **14**, 1650-1656, doi:10.1016/j.cub.2004.08.026 (2004).

450 Xu, X. *et al.* The CUL7 E3 ubiquitin ligase targets insulin receptor substrate 1 for ubiquitin-dependent degradation. *Mol Cell* **30**, 403-414, doi:10.1016/j.molcel.2008.03.009 (2008).

451 Harrington, L. S., Findlay, G. M. & Lamb, R. F. Restraining PI3K: mTOR signalling goes back to the membrane. *Trends Biochem Sci* **30**, 35-42, doi:10.1016/j.tibs.2004.11.003 (2005).

452 Wright, J. J. *et al.* Mechanisms for increased myocardial fatty acid utilization following short-term high-fat feeding. *Cardiovasc Res* **82**, 351-360, doi:cvp017 [pii]10.1093/cvr/cvp017 (2009).

453 Samuel, V. T. & Shulman, G. I. Mechanisms for insulin resistance: common threads and missing links. *Cell* **148**, 852-871, doi:10.1016/j.cell.2012.02.017 (2012).

454 Huang, A. & Kaley, G. Gender-specific regulation of cardiovascular function: Estrogen as key player. *Microcirculation* **11**, 9-38, doi:10.1080/10739680490266162 (2004).

455 Patten, R. D. *et al.* 17beta-estradiol reduces cardiomyocyte apoptosis in vivo and in vitro via activation of phospho-inositide-3 kinase/Akt signaling. *Circ Res* **95**, 692-699, doi:10.1161/01.RES.0000144126.57786.89 (2004).

456 Pedram, A., Razandi, M., Aitkenhead, M. & Levin, E. R. Estrogen inhibits cardiomyocyte hypertrophy in vitro - Antagonism of calcineurin-related hypertrophy through induction of MCIP1. *Journal of Biological Chemistry* **280**, 26339-26348, doi:10.1074/jbc.M414409200 (2005).

457 Sung, M. M. *et al.* Increased CD36 expression in middle-aged mice contributes to obesity-related cardiac hypertrophy in the absence of cardiac dysfunction. *J Mol Med (Berl)* **89**, 459-469, doi:10.1007/s00109-010-0720-4 (2011).

458 Turdi, S. *et al.* Deficiency in AMP-activated protein kinase exaggerates high fat diet-induced cardiac hypertrophy and contractile dysfunction. *J Mol Cell Cardiol* **50**, 712-722, doi:10.1016/j.yjmcc.2010.12.007 (2011).

459 Das, A. *et al.* Mammalian target of rapamycin (mTOR) inhibition with rapamycin improves cardiac function in type 2 diabetic mice: potential role of attenuated oxidative stress and altered contractile protein expression. *J Biol Chem* **289**, 4145-4160, doi:10.1074/jbc.M113.521062 (2014).

460 Kim, Y. I., Lee, F. N., Choi, W. S., Lee, S. & Youn, J. H. Insulin regulation of skeletal muscle PDK4 mRNA expression is impaired in acute insulin-resistant states. *Diabetes* **55**, 2311-2317, doi:10.2337/db05-1606 (2006).

461 Zhang, L., Mori, J., Wagg, C. & Lopaschuk, G. D. Activating cardiac E2F1 induces up-regulation of pyruvate dehydrogenase kinase 4 in mice on a short term of high fat feeding. *FEBS Lett* **586**, 996-1003, doi:10.1016/j.febslet.2012.02.027 (2012).

462 Rinnankoski-Tuikka, R. *et al.* Effects of high-fat diet and physical activity on pyruvate dehydrogenase kinase-4 in mouse skeletal muscle. *Nutr. Metab.* **9**, doi:Artn 5310.1186/1743-7075-9-53 (2012).

463 Zhao, G. *et al.* Overexpression of pyruvate dehydrogenase kinase 4 in heart perturbs metabolism and exacerbates calcineurin-induced cardiomyopathy. *Am J Physiol Heart Circ Physiol* **294**, H936-943, doi:10.1152/ajpheart.00870.2007 (2008).

464 Bayeva, M., Sawicki, K. T. & Ardehali, H. Taking diabetes to heart--deregulation of myocardial lipid metabolism in diabetic cardiomyopathy. *Journal of the American Heart Association* **2**, e000433, doi:10.1161/JAHA.113.000433 (2013).

465 Abel, E. D. Free fatty acid oxidation in insulin resistance and obesity. *Heart and metabolism : management of the coronary patient* **48**, 5-10 (2010).

466 Jung, C. H. *et al.* ULK-Atg13-FIP200 Complexes Mediate mTOR Signaling to the Autophagy Machinery. *Mol Biol Cell* **20**, 1992-2003, doi:10.1091/mbc.E08-12-1249 (2009).

467 Noda, T. & Ohsumi, Y. Tor, a phosphatidylinositol kinase homologue, controls autophagy in yeast. *Journal of Biological Chemistry* **273**, 3963-3966, doi:DOI 10.1074/jbc.273.7.3963 (1998).

468 Zou, M. H. & Xie, Z. Regulation of interplay between autophagy and apoptosis in the diabetic heart: new role of AMPK. *Autophagy* **9**, 624-625, doi:10.4161/auto.23577 (2013).

469 Xie, Z., He, C. & Zou, M. H. AMP-activated protein kinase modulates cardiac autophagy in diabetic cardiomyopathy. *Autophagy* **7**, 1254-1255, doi:10.4161/auto.7.10.16740 (2011).

470 Xu, X. *et al.* Diminished autophagy limits cardiac injury in mouse models of type 1 diabetes. *J Biol Chem* **288**, 18077-18092, doi:10.1074/jbc.M113.474650 (2013).

471 He, C., Zhu, H., Li, H., Zou, M. H. & Xie, Z. Dissociation of Bcl-2-Beclin1 complex by activated AMPK enhances cardiac autophagy and protects against cardiomyocyte apoptosis in diabetes. *Diabetes* **62**, 1270-1281, doi:10.2337/db12-0533 (2013).

472 Xu, X. M. *et al.* Diminished Autophagy Limits Cardiac Injury in Mouse Models of Type 1 Diabetes. *Journal of Biological Chemistry* **288**, 18077-18092, doi:10.1074/jbc.M113.474650 (2013).

473 He, C. Y., Zhu, H. P., Li, H., Zou, M. H. & Xie, Z. L. Dissociation of Bcl-2-Beclin1 Complex by Activated AMPK Enhances Cardiac Autophagy and Protects Against Cardiomyocyte Apoptosis in Diabetes. *Diabetes* **62**, 1270-1281, doi:10.2337/db12-0533 (2013).

474 Sciarretta, S. *et al.* Markers of inflammation and fibrosis are related to cardiovascular damage in hypertensive patients with metabolic syndrome. *Am. J. Hypertens.* **20**, 784-791, doi:10.1016/j.amjhyper.2007.01.023 (2007).

475 Li, Z. L. *et al.* Transition From Obesity to Metabolic Syndrome Is Associated With Altered Myocardial Autophagy and Apoptosis. *Arterioscl Throm Vas* **32**, 1132-+, doi:10.1161/Atvbaha.111.244061 (2012).

476 Guo, R., Zhang, Y. M., Turdi, S. & Ren, J. Adiponectin knockout accentuates high fat diet-induced obesity and cardiac dysfunction: Role of autophagy. *Bba-Mol Basis Dis* **1832**, 1136-1148, doi:10.1016/j.bbadis.2013.03.013 (2013).

477 Xu, X. H., Hua, Y. N., Nair, S., Zhang, Y. M. & Ren, J. Akt2 knockout preserves cardiac function in high-fat diet-induced obesity by rescuing cardiac autophagosome maturation (vol 5, pg 61, 2013). *Journal of molecular cell biology* **5**, 212-212, doi:10.1093/jmcb/mjt008 (2013).

478 Yamahara, K. *et al.* Obesity-Mediated Autophagy Insufficiency Exacerbates Proteinuria-induced Tubulointerstitial Lesions. *J. Am. Soc. Nephrol.* **24**, 1769-1781, doi:10.1681/Asn.2012111080 (2013).

479 Yang, L., Li, P., Fu, S. N., Calay, E. S. & Hotamisligil, G. S. Defective Hepatic Autophagy in Obesity Promotes ER Stress and Causes Insulin Resistance. *Cell metabolism* **11**, 467-478, doi:10.1016/j.cmet.2010.04.005 (2010).

480 Maffucci, J. A. & Gore, A. C. Age-related Changes in Hormones and Their Receptors in Animal Models of Female Reproductive Senescence-43. (2006).

481 Frye, J. B. *et al.* Modeling Perimenopause in Sprague-Dawley Rats by Chemical Manipulation of the Transition to Ovarian Failure. *Comparative Med* **62**, 193-202 (2012).

482 Shaar, C. J., Euker, J. S., Riegle, G. D. & Meites, J. Effects of Castration and Gonadal Steroids on Serum Luteinizing-Hormone and Prolactin in Old and Young-Rats. *J. Endocrinol.* **66**, 45-51, doi:DOI 10.1677/joe.0.0660045 (1975).

483 Huang, H. H., Marshall, S. & Meites, J. Capacity of Old Versus Young Female Rats to Secrete Lh, Fsh and Prolactin. *Biol. Reprod.* **14**, 538-543, doi:DOI 10.1095/biolreprod14.5.538 (1976).

484 Steger, R. W., Huang, H. H., Chamberlain, D. S. & Meites, J. Changes in Control of Gonadotropin-Secretion in the Transition Period between Regular Cycles and Constant Estrus in Aging Female Rats. *Biol. Reprod.* **22**, 595-603 (1980).

485 Smith, C. C., Vedder, L. C., Nelson, A. R., Bredemann, T. M. & McMahon, L. L. Duration of estrogen deprivation, not chronological age, prevents estrogen's ability to enhance hippocampal synaptic physiology. *Proc. Natl. Acad. Sci. U. S. A.* **107**, 19543-19548 (2010).

486 Chappell, M. C., Westwood, B. M. & Yamaleyeva, L. M. Differential effects of sex steroids in young and aged female mRen2.Lewis rats: A model of estrogen and salt-sensitive hypertension. *Gender Med* **5**, S65-S75, doi:10.1016/j.genm.2008.03.007 (2008).

487 Sanders, D., Dudley, M. & Groban, L. Diastolic dysfunction, cardiovascular aging, and the anesthesiologist. *Anesthesiology clinics* **27**, 497-517, doi:10.1016/j.anclin.2009.07.008 (2009).

488 Palmiero, P. *et al.* Left ventricular diastolic function in hypertension: methodological considerations and clinical implications. *J Clin Med Res* **7**, 137-144, doi:10.14740/jocmr2050w (2015).

7. Supplementary Figures and Tables

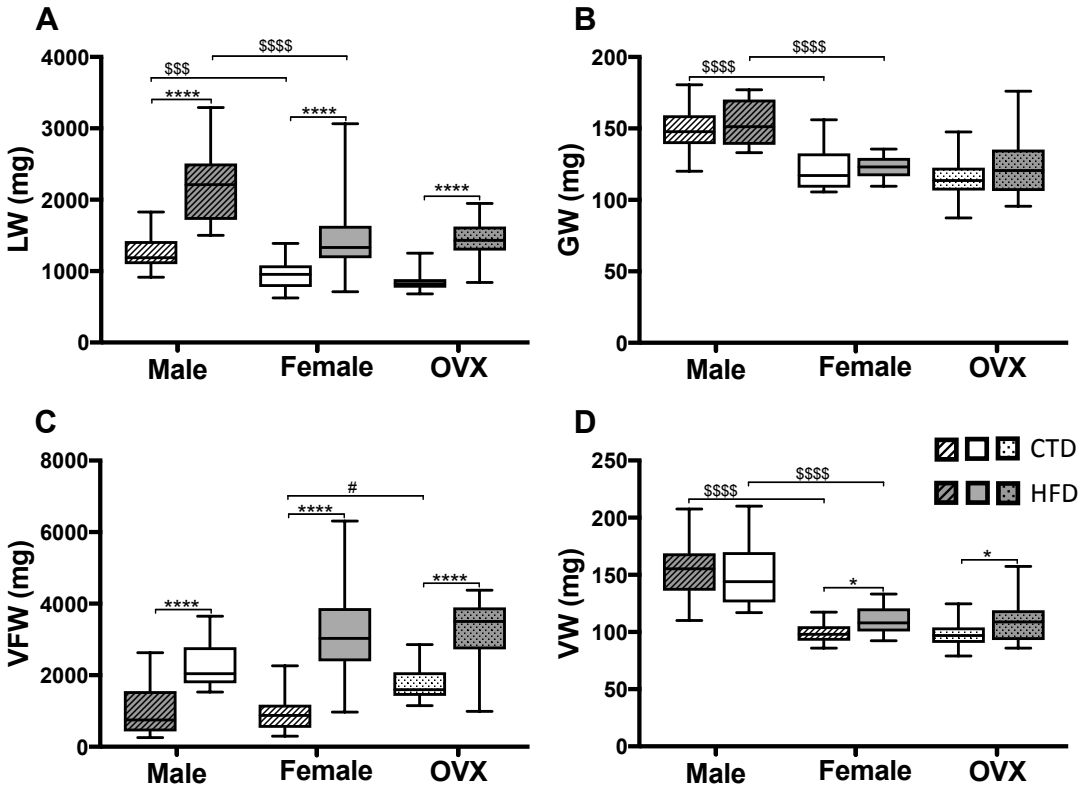

Figure S I: Post-mortem organ weights of male, female and OVX mice fed with CTD or HFD for 22 wks.

Organs were weighed after sacrifice. Non-normalized values are shown. LW, Liver weight; GW, gastrocnemius weight; VFW, visceral fat weight; VW, ventricle weight. Results are presented with the median, whiskers show the min and max values. * Symbol corresponds to CTD vs HFD, # symbol corresponds to OVX vs sham, $ symbol corresponds to male vs female. N=18-24.

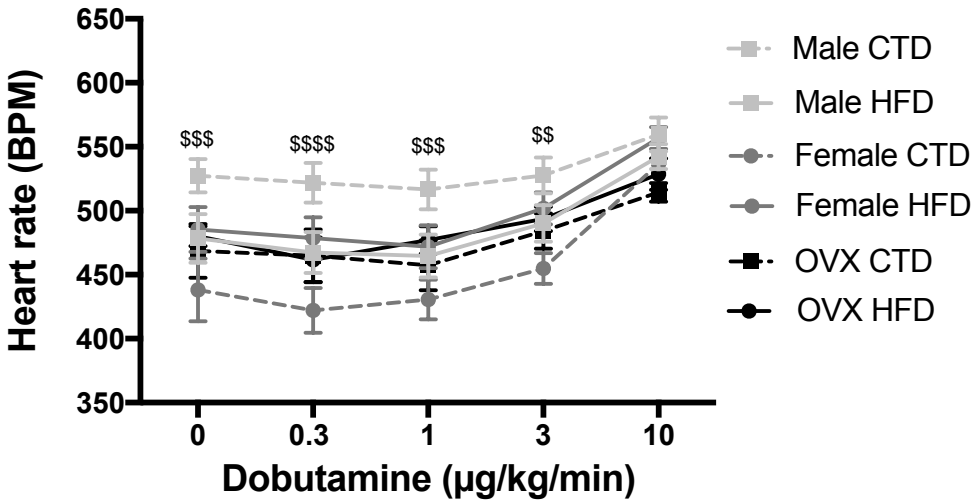

Figure S II: Effect of dobutamine on heart rate during PVL experiment in male, female and OVX mice fed with CTD or HFD for 22 wks.

Heart rates significantly increase with the increased dobutamine infusion dose in all groups.
Under CTD, male mice have a higher heart rate than the female from baseline to 3 µg/kg/min dobutamine infusion. Results are presented mean ± SEM. $ symbol corresponds to male vs female; N=7-11.

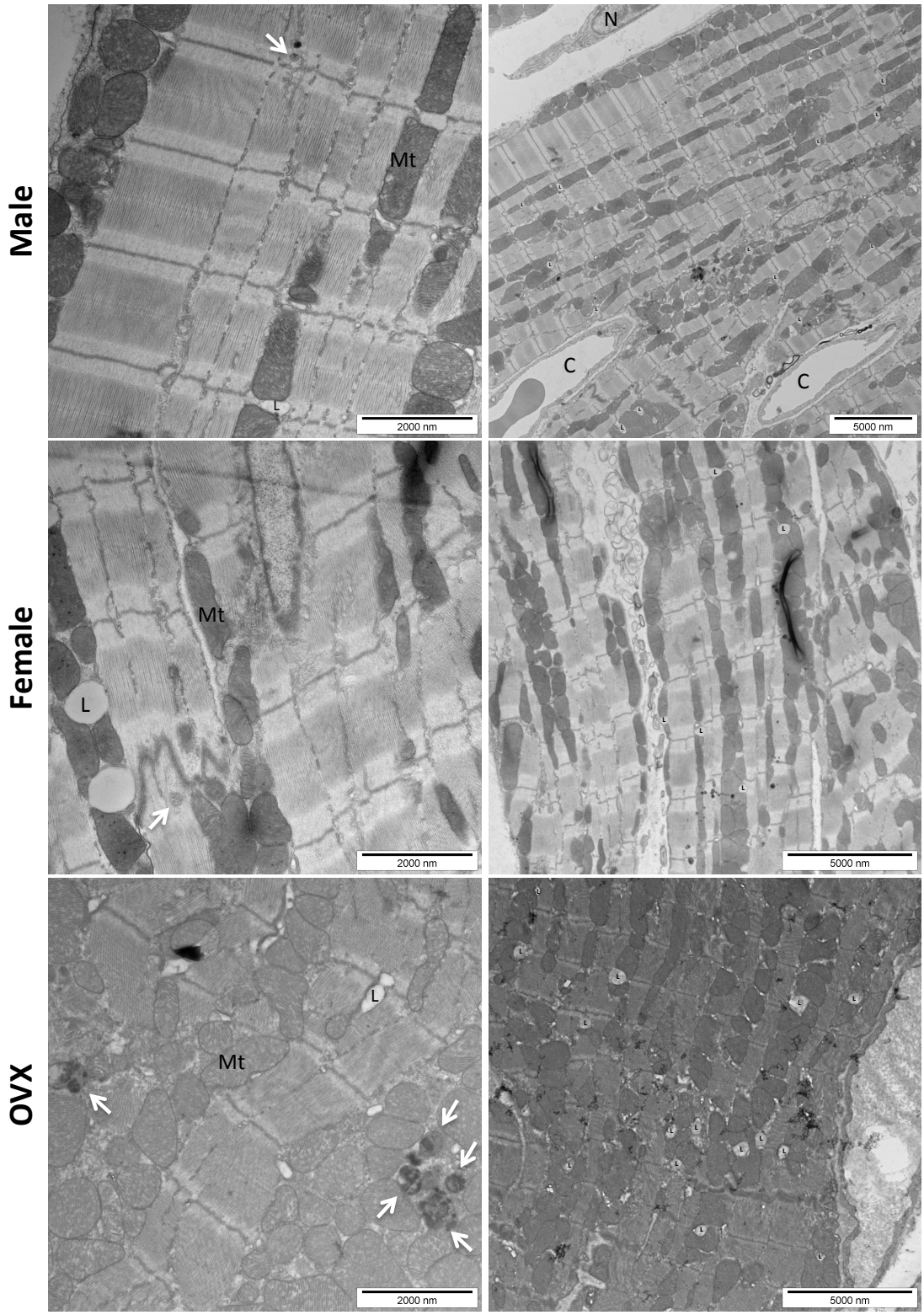

Figure S III: Electron micrographs of hearts to detect autophagy.
Hearts of male, female and OVX mice (sacrificed at 22 wks) were stained to detect autophagy.
C: capillaries; L: lipid droplet; M: mitochondria; N: nucleus. Arrows point to possible autophagic vacuoles. N=2

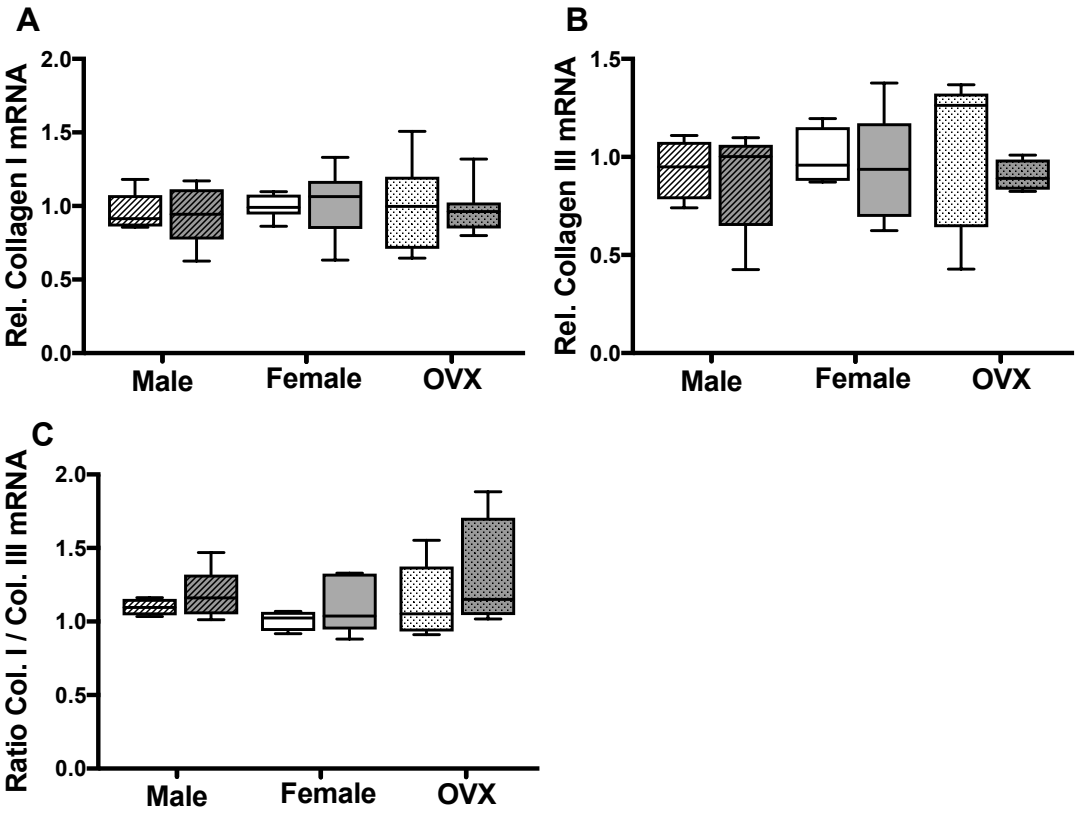

Figure S IV: Quantitative real-time PCR analysis in hearts from male, female and OVX mice fed with CTD or HFD for 22 wks.

mRNA from cardiac muscle was extracted to evaluate mRNA levels of collagen genes. Results are presented with the median, whiskers show the min and max values. * Symbol corresponds to CTD vs HFD, # symbol corresponds to OVX vs sham, $ symbol corresponds to male vs female. N=8-10.

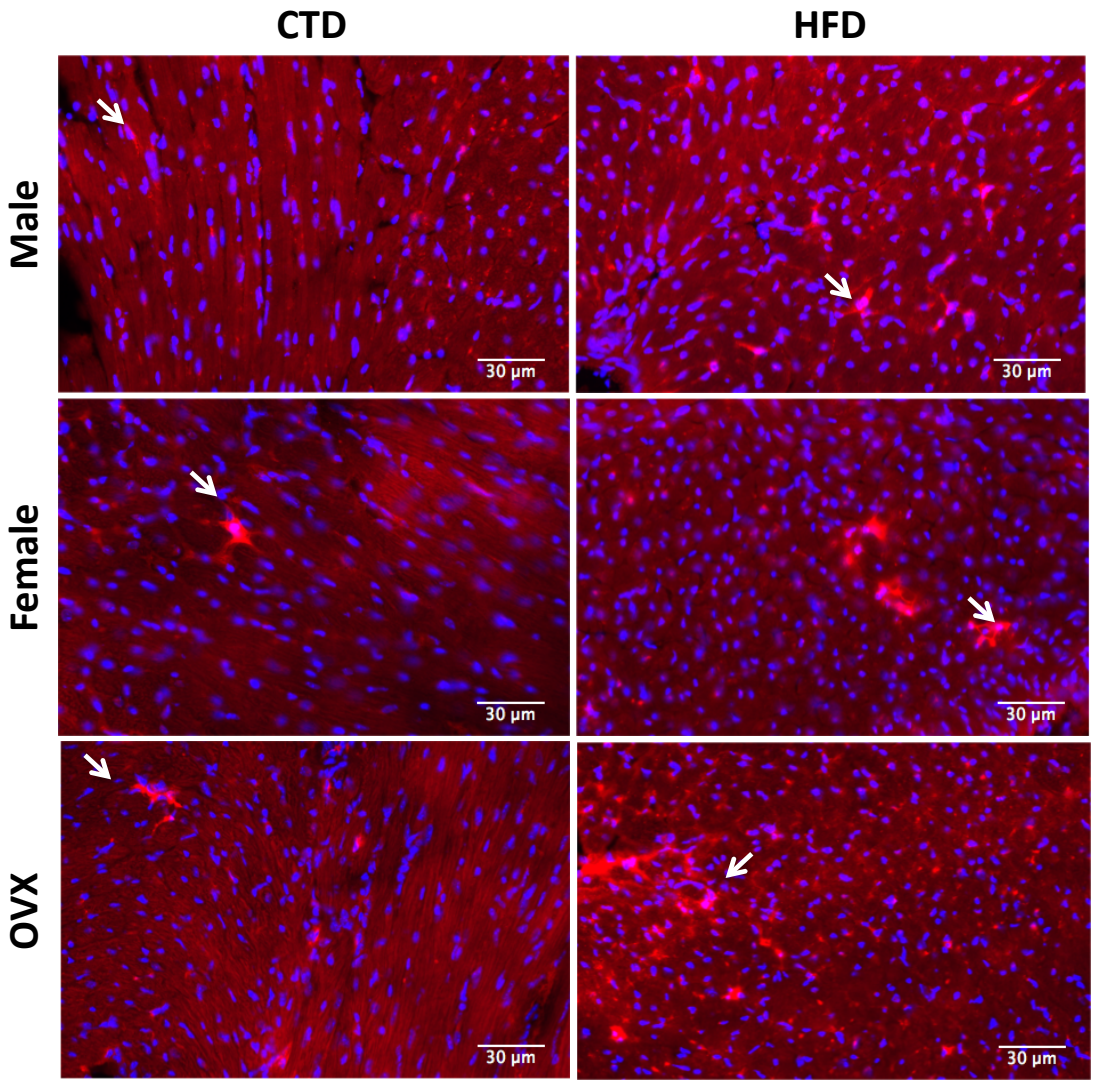

Figure S V: Mac-2 staining to detect macrophages on heart sections.
Cryosections of the hearts of male, female and OVX mice (sacrificed at 22 wks) were stained with Mac-2 and TRITC-labeled secondary antibodies to detect macrophages (arrows), Dapi dye was used to reveal nuclei (blue). A representative picture of each condition is shown. Magnification x20. N=3.

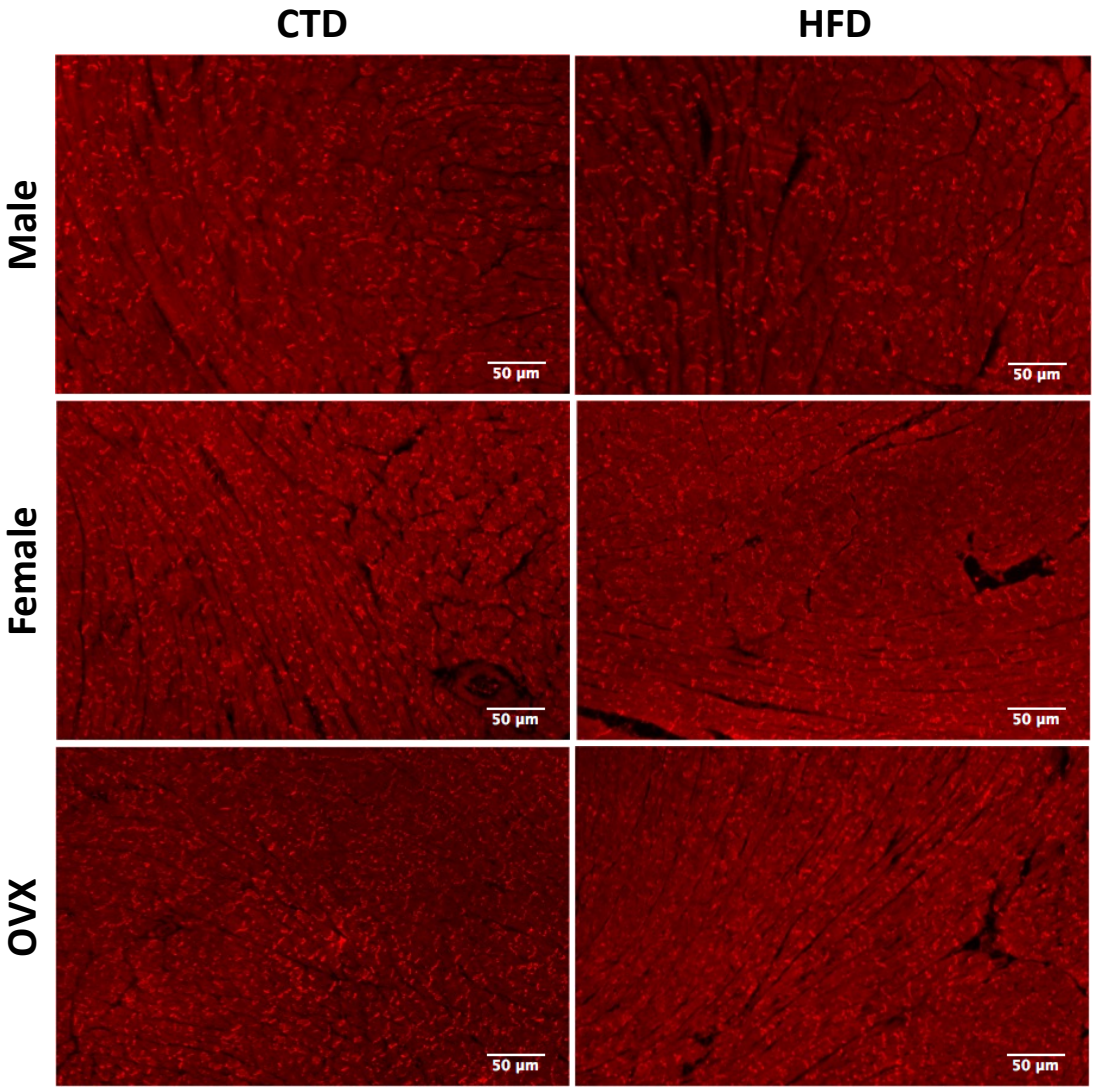

Figure S VI: TGF-β1 staining to detect signs of fibrosis on heart sections.
Cryosections of the hearts of male, female and OVX mice (sacrificed at 22 wks) were stained with TGF-β1 and TRITC-labeled secondary antibodies. A representative picture of each condition is shown. Magnification x10. N=3.

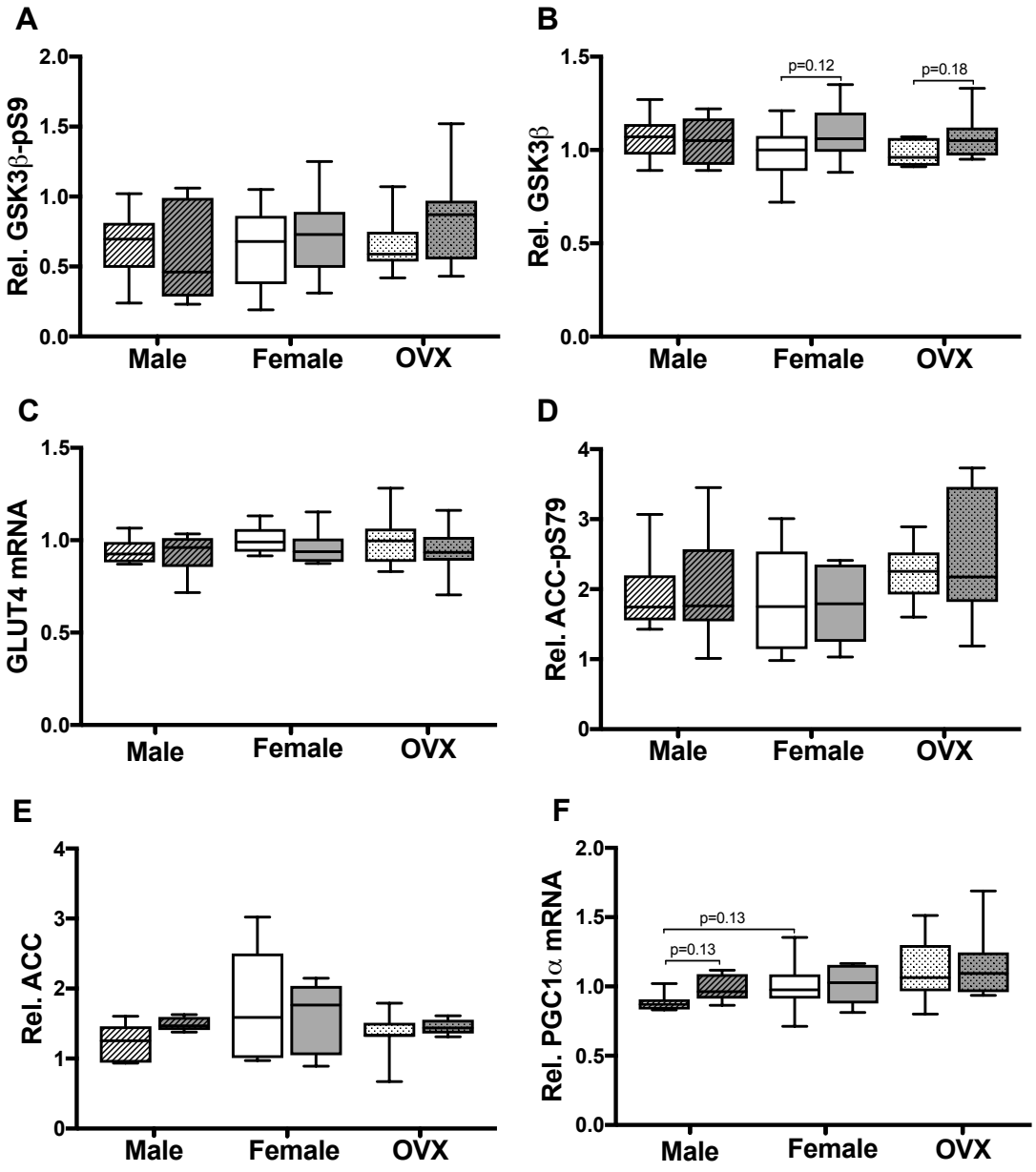

Figure S VII: Quantitative real-time PCR and Western-blot analysis of hearts from male, female and OVX mice fed with CTD or HFD for 22 wks.

Cardiac muscle was used to extract mRNA and protein to evaluate genes and proteins involved in metabolism. Graphs represent quantification normalized to the corresponding control. Results are presented with the median, whiskers show the min and max values. * Symbol corresponds to CTD vs HFD, # symbol corresponds to OVX vs sham, $ symbol corresponds to male vs female; N=8-10.

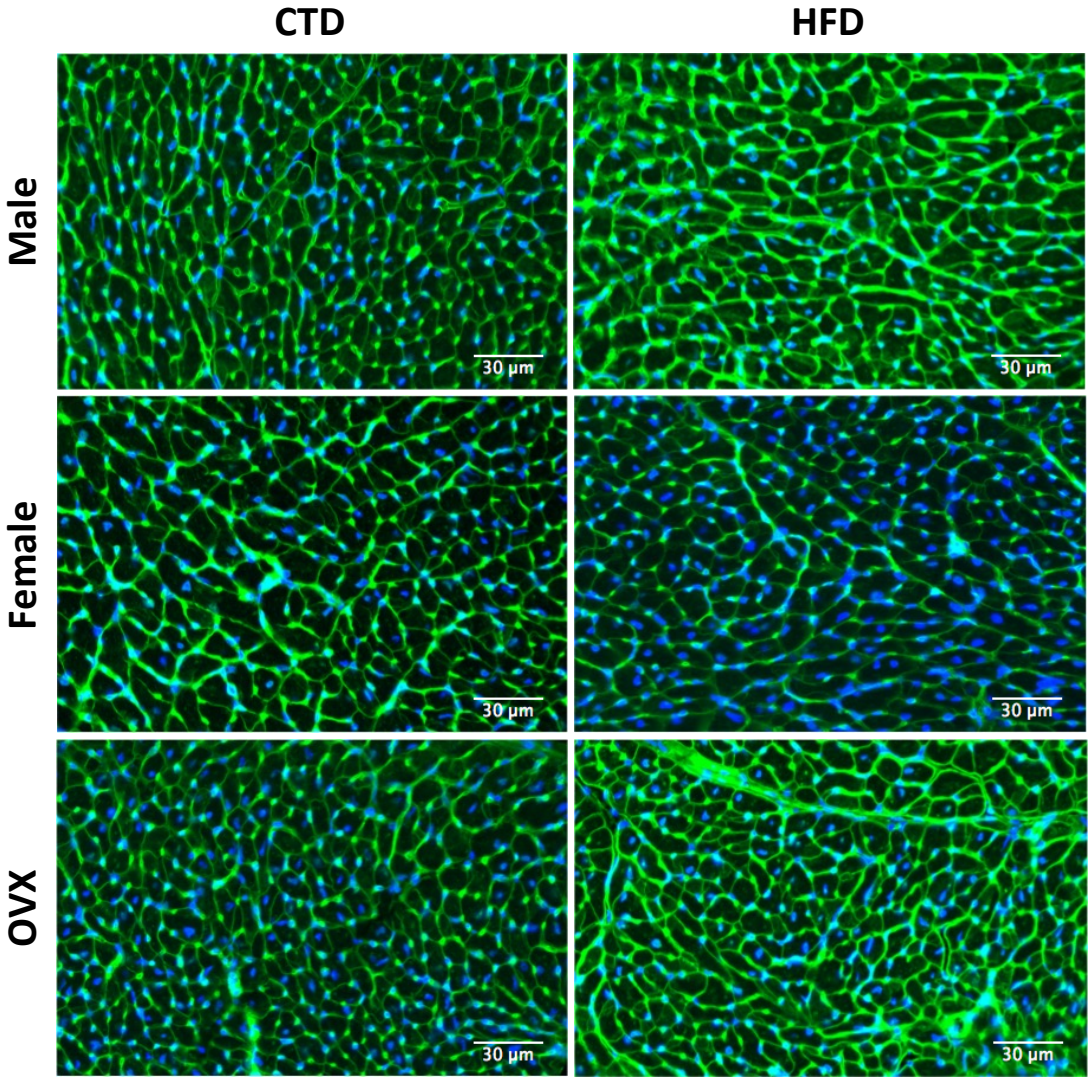

Figure S VIII: WGA staining to evaluate cardiomyocyte cross-sectional area.
Cryosections of the hearts of male, female and OVX mice (sacrificed at 22 wks) were stained with WGA and TRITC-labeled secondary antibodies, DAPI dye was used to reveal nuclei (blue). A representative picture of each condition is shown. Magnification x10. N=3.

Table S I: Antibodies used for biochemistry and histology analysis.

Antibodies	Company	References
Anti-p70-S6K1	Cell Signaling	9202
Anti-ACC	Cell Signaling	3676
Anti-Akt	Cell Signaling	9272
Anti-AMPKα	Cell Signaling	2532
Anti-Atg1/ULK1	Sigma	A-7481
Anti-GSK3β	Cell Signaling	9315
Anti-IRS-1	Santa Cruz	sc-559
Anti-LC3B	Cell Signaling	3868
Anti-Mac-2	BioLegend	125402
Anti-mTOR	Cell Signaling	2972
Anti-NF-κB	Santa Cruz	sc-109
Anti-PDK4	AbCam	ab38242
Anti-PPARγ	Santa Cruz	sc-7273
Anti-SERCA2	Santa Cruz	sc-8095
Anti-Atg1/ULK1	Sigma	A-7481
Anti-P-Lamban	Thermofisher	MA3-922
Anti-PDH E1 (8D10E6)	AbCam	ab110334
Anti-TGF-β1	Santa Cruz	sc-146 P
Anti-p70 S6K-pT389	Cell Signaling	9205
Anti-ACC-pS79	Cell Signaling	3661
Anti-Akt-pT308	Cell Signaling	9275
Anti-Akt-pS473	Cell Signaling	9271
Anti-AMPKα-T172	Cell Signaling	2535
Anti-AS160-pT642	Millipore	ABS271
Anti-GSK3β-S9	Cell Signaling	9336
Anti-IRS-1-pS636/639	Cell Signaling	2388
Anti-mTOR-pS2448	Cell Signaling	2971
Anti-NF-κB p65-pS536	Cell Signaling	3033
Anti-PDH-pS293	AbCam	ab92696
Anti-ULK1-pS757	Cell Signaling	6888

Table S II: Sequence of the primers used to quantify the cardiac expression of targets genes by RT-PCR.

Gene	Forward primer	Reverse primer
ANP	5'-TGG GAC CCC TCC GAT AGA TC-3'	5'-TCG TGA TAG ATG AAG GCA GGA A-3'
BNP	5'-TTC CAA GAT GGC ACA TAG TTC AA-3'	5'-ACA ACC TCA GCC CGT CAC A-3'
β-MHC	5'-TTG AGA ATC CAA GGC TCA GC-3'	5'-CTT CTC AGA CTT CCG CAG GA-3'
Collagen I	5'-CTT CAC CTA CAG CAC CCT TGT T-3'	5'-TGA CTG TCT TGC CCC AAG TTC-3'
Collagen III	5'-CAC CCT TCT TCA TCC CAC TCT T-3'	5'-TGC ATC CCA ATT CAT CTA CGT T-3'
CPT1β	5'-CCG CAG GAG GAA GGG TAG AG-3'	5'-GTC TCA TCG TCA GGG TTG TAG CT-3'
GAPDH	5'-CGG CCG CAT CTT CTT GTG-3'	5'-CAC CGA CCT TCA CCA TTT TGT-3'
GLUT4	5'-AGA GAG AGC GTC CAA TGT CCT T-3'	5'-CCG ACT CGA AGA TGC TGG TTG A-3'
IL-6	5'-TCG GAG GCT TAA TTA CAC ATG TTC-3'	5'-TGC CAT TGC ACA ACT CTT TTC T-3'
PDK4	5'-AAC CTC ACA CAA GTC AAT GGA AAA T-3'	5'-TCG ACC GTG GCC CTC AT-3'
PGC1α	5'-AAC GAT GAC CCT CCT CAC AC-3'	5'-TCT GGG GTC AGA GGA AGA GA-3'
PPARα	5'-CAA GGC CTC AGG GTA CCA CT-3'	5'-TTG CAG CTC CGA TCA CAC TT-3'
TNFα	5'-TGT CTA CTG AAC TTC GGG GTG AT-3'	5'-GGA GGC CAT TTG GGA ACT TC-3'

Table S III: Echocardiographic and physiologic parameters recorded at baseline, prior to the start of the diet.

	MALE		FEMALE		OVX	
Echocardiography, baseline	CTD (*n* =17)	HFD (*n* =17)	CTD (*n* = 16)	HFD (*n* = 18)	CTD (*n* =15)	HFD (*n* =17)
Heart rate (beats/min)	505±11.7	507±17.8	506±11.4	510±11.3	498±13	506±13.9
Anteroseptal wall thickness (mm)						
diastole	0.78±0.02	0.81±0.02	0.73±0.02	0.71±0.01	0.73±0.02	0.74±0.02
systole	1.09±0.03	1.12±0.03	1.01±0.03	0.98±0.02	1.01±0.02	1.02±0.03
Left ventricular free wall thickness (mm)						
diastole	0.68±0.01	0.70±0.01	0.57±0.01	0.61±0.01	0.60±0.01	0.60±0.01
systole	0.94±0.02	1.01±0.02	0.84±0.02	0.89±0.02	0.89±0.02	0.92±0.03
Left ventricular internal diameter (mm)						
diastole	4.38±0.08	4.43±0.06	4.02±0.05	4.03±0.06	4.03±0.06	3.98±0.04
systole	3.42±0.08	3.37±0.06	3.05±0.06	3.02±0.04	3.01±0.05	3.01±0.07
Relative wall thickness						
diastole	0.31±0.04	0.31±0.02	0.28±0.04	0.30±0.03	0.30±0.03	0.30±0.04
systole	0.55±0.08	0.60±0.06	0.56±0.09	0.59±0.08	0.59±0.08	0.62±0.14
Ejection fraction (%)	44.4±1.23	47.7±1.02	47.7±1.42	48.2±1.15	49.7±1.24	50±4.47
Fraction of shortening (%)	21.9±0.70	23.9±0.62	24.3±0.86	23.9±0.69	24.9±0.73	25.4±0.98
Cardiac Output (ml/min)	19.8±1.23	22.1±1.18	17.4±0.76	16.9±0.60	17.2±1.01	17.9±0.96
Left ventricular volume (μl)						
diastole	87.4±3.62	89.9±3.27	71.9±2.87	69.3±71.1	71.1±2.43	71.6±2.44
systole	48.8±2.71	47±2.09	36.9±1.89	35.9±1.22	35.8±1.67	35.7±1.84
E/E'	23.6±1.18	23.7±1.87	24.2±1.82	21.5±1.99	25.5±1.64	25.1±2.46
Deceleration (mm/s^2)	-29103±1859	-27190±2396	-31570±2340	-29983±1942	-30191±3286	-29582±2588
Tei index	0.49±0.03	0.49±0.04	0.52±0.04	0.5±0.04	0.54±0.047	0.51±0.04
LV mass (g)	98.37±18.47	103.9±14.26	73.3±10.38	72.7±6.15	74.9±10.4	76±9.89
Body weight (g)	28.1±2.67	29.4±1.52	21.5±1.68	22.4±1.32	22.6±2.64	23.8±2.67

Table S IV: LV hemodynamics parameters of female and male mice recorded with the PVL method after 21 wks of diet with dobutamin infusion (10 µg/kg/min).

	Male		Female		OVX	
LV Hemodynamics, 10 µg/kg/min dobutamine	CTD (*n* =8)	HFD (*n* =8)	CTD (*n* =7)	HFD (*n* =7)	CTD (*n* =8)	HFD (*n* = 9)
Heart rate (beats/min)	559±13	542±9	536±5	556±8	514±7	528±12
Volume (µl)						
End-diastole, Ved	20.6±3.85	14.9±3	9.97±1.96	13.1±1.12	10.5±2	16.5±3.11
End-systole, Ves	6.41±3.15	2.18±0.75	0.31±0.27	0.79±0.47	1.32±0.69	8±3.52
Minimum Volume, Vmin	5.34±3.26	1.8±0.94	-1.12±1.46	-2.01±2.33	-0.10±1.28	6.58±2.97
Maximal Volume, Vmax	20.8±3.86	15.85±3.25	10.24±1.94	16.97±3.26	11.03±2.01	16.37±2.72
Pressure (mmHg)						
End-diastole, Ped	4.43±0.35	4.42±0.42	4.51±0.37	3.32±0.36	4.26±0.36	4.72±0.44
End-systole, Pes	67.2±4.28	73.4±5.05	69.8±5.55	64.26±3.66	64.33±4.89	65.03±4.57
Minimum Pressure, Pmin	1.62±0.34	0.48±0.61	1.63±0.47	0.48±0.38	1.2±0.55	1.75±0.44
Maximum Pressure, Pmax	80.5±4.76	86.5±3.22	83.3±4.78	79.7±2.74	82.1±3.41	76.52±3.18
Peak rate (µL/sec)						
Filling, dV/dt max	767±90	476±46	510±31	601±88	503±66	455±58
Emptying, dV/dt min	-724±63	-540±50	-515±25	-671±64	-476±48	-458±63
Rate of pressure (mmHg/sec)						
Development, dP/dt max	9627±906	11300±273	10704±780	9619±668	10714±391	8897±913
Decline, dP/dt min	-5913±611	-6753±551	-5920±573	-5449±464	-5667±339	-5182±488
Time constant of isovolumic relaxation, Tau (msec)	8.63±1.13	8.34±1.02	9.66±1.09	9.59±0.88	8.58±1	9.42±1.19
End-diastolic pressure-volume relationship (EDPVR), 1/slope	40.07±7	60.7±17.5	68.46±17.9	65.2±12.7	52.7±14	148±43.7
End-systolic pressure-volume relationship (ESPVR), slope	9.03±3.50	6.31±0.88	15.3±4.37	16.3±3.35	12.1±3.13	10.3±2.6

8. Side-projects

I had the opportunity to work on several projects during my PhD, either projects directly linked to my main study or different. The first project in which I was involved was to understand the role of phenylephrine (PE) on autophagy and dissect the mechanism by which PE decreases the level of autophagy in neonate rat ventricular myocytes (NRVM). It was a good starting experiment for me that allowed me to learn cell culture techniques and cell experimentation in general. Soon after I made my first in vivo trial of HFD feeding in mice, this experiment helped us to determine the protocol that we will follow for the study: the type of diet, the percentage of fat, the duration, and the different tests to be performed. In parallel, I was involved in the analysis of the effects of HFD in cardiac rictor KO female mice, a study that was performed by Dr. Lifen Xu earlier. I was also implicated in the analysis of the effects of fasting-refeeding vs fasting-insulin injection on cardiac signaling. All these data are not published yet. Then I performed my first experiment where we studied the effects of HFD on cardiac function of sham- and OVX-female mice. The first results were conclusive so we decided to pursue this study involving the male, this time to describe the effect of ovarian hormones as well as gender-specific effects of HFD in mice. In parallel, I wanted to understand the mechanism by which ovarian hormones are implicated in the observations that we made in vivo. Thus, I started to study the effects of activation of estrogen signaling in NRVMs with focus on the GPER estrogen receptor, using the specific agonist G-1 and the inhibitor G-15. Unfortunately, the results were not convincing as they were not reproducible, questioning the quality of the compounds used. The timeline and priorities forced us to terminate this part of my studies. Additionally, I participated in the work for two research papers (see publications chapter).

As important continuation of the experiments described in my PhD thesis report, I evaluated the effects of ovarian hormones and gender on cardiac function in obese mice that became hypertensive after angiotensin II (Ang II) infusion. We demonstrated that 22 wks of high fat diet feeding was not sufficient to trigger a pronounced cardiac dysfunction in male, female and female lacking of estrogens. This is why we started this new project, with the aim to increase cardiac stress. Thus, we introduced the hypertension risk factor in our model, which is clinically relevant for the understanding of diabetic cardiomyopathy. Moreover, hypertension is the primary cause of diastolic dysfunction in postmenopausal women[487] and results in LV hypertrophy impairing myocardial active relaxation and the passive stiffness (compliance).[488] This study is also of interest because it evaluates gender-specificity and the role of ovarian hormones after long-term feeding and in aging mice, as the mice were followed up to 56 wks of feeding. Similar to our previous study, male, sham- and OVX-female mice were fed with fed a high fat diet (HFD, 45kJ% lard-fat) or a normal chow diet. The HFD-fed mice received Ang II during the last 4 wks of feeding via

subcutaneous infusion using mini-pumps. The mice were followed over time by blood pressure measurement, glucose tolerance tests and echocardiography. Prior to sacrifice at 56 wks, PVL analysis was performed to evaluate cardiac hemodynamics. While this study is still under analysis, our first results show that:

1. At the longer-term, the OVX female mice had a higher BW than the sham-female mice when fed with CTD, which was not the case at 22 wks of feeding. Similar to our previous study, the HFD triggered an identical body weight gain in both female groups.
2. Ang II induced the expected effects, as systolic and diastolic blood pressures as well as heart weights were increased, proving the successfulness our hypertension model. Not all animals answered in the same way to Ang II, some mice had stronger blood pressure and hypertrophy increases than others, hence the necessity to make subgroups and analyze them separately.
3. With the purpose of evaluating the glucose clearance ability of male, sham-female and OVX-female mice in response to longer-term HFD feeding and hypertension, we performed a GTT after 2 wks of Ang II infusion. In HFD-fed male mice, Ang II decreased the AUC, indicating improved glucose tolerance. Interestingly, this effect was opposite to that observed in HFD-fed sham-female mice, with higher blood glucose in sham-female than in male after 54 wks of diet and 2 wks of Ang II. Therefore, Ang II improved glucose tolerance in the male and worsened it in the female in obese mice, underlining another sexual dimorphism. The possible explanation is that Ang II increases insulin sensitivity or stimulated insulin secretion in the males and not in the females. In the OVX-female group, Ang II did not result in any changes, as for the effect of HFD, it increased glucose intolerance but this effect did not reach significance conversely to the effect observed at 22 wks of diet. This could be explained by the low number of mice analyzed so far (n=6).

The echocardiographic analysis demonstrated that:

1. After 50 wks of feeding, sham-female mice had higher ejection fractions that male mice for both diets, suggesting that their systolic function becomes better than that of the males over time. The OVX-female had similar function as the sham-female mice.
2. The relative wall thickness (RWT) during systole was also affected by aging, since the sham-female mice had a higher value than the male after CTD feeding. This suggests that females undergo more cardiac remodeling over time than males.
3. It appeared that the E/A ratio was similar between the groups at this time point, although a decrease was visible after HFD in all groups without getting significant.

After 3 wks of Ang II infusion, new effects appeared:
1. Ang II significantly increased the LV anterior and posterior wall thicknesses as well as the RWT during diastole in the OVX- but not the sham-female, suggesting that ovarian hormones may prevent Ang II-induced hypertrophy.
2. Ang II also increased LV posterior wall thickness and RWT during diastole in male. A thickening of this myocardial wall was visible in sham-female too, but to a lesser extend (not significant). If confirmed in more mice, this again suggests that ovarian hormones attenuate the cardiac hypertrophy induced by Ang II.

PVL analysis after 4 wks of Ang II infusion showed that Ang II increased the maximal and end-systole pressures developed by the heart in OVX-female mice only. This result suggests that ovarian hormones prevent the increase pressure due to Ang II and thereby play a protective role. None of the other hemodynamic parameters were affected at this stage.

Finally, we performed protein and genes expression analysis. We decided to start our analysis with the male group and our first results showed increased β-MHC protein and ANP mRNA expression as a consequence of the cardiac stress induced by Ang II. Similar to what we observed in female mice at 22 wks of diet, ANP was reduced in the HFD-fed compared to CTD-fed male mice. Therefore, male mice undergo the same cardiac ANP changes as females but simply at a later stage. Additionally, western-blotting demonstrated that Akt-pT308 was increased in the HFD group compared to the CTD. Ang II blunted this effect, since the HFD+Ang II group had similar phosphorylation levels as the CTD fed-group. Thus, Ang II impairs the HFD-induced Akt activation and thereby reduces cardioprotection.

In summary, my preliminary conclusions on our aged, HFD-fed and Ang II-treated male and female groups are as follows:
- female mice present a better systolic function than male mice at 16.5 months of age. Ang II improves glucose tolerance in HFD-fed male mice and reduces it in female mice.
- ovarian hormones prevent or attenuate Ang II-induced hypertrophy, as ovary-deficient mice presented signs of hypertrophy.
- ovarian hormones are essential to maintain normal end-systolic pressure in response to HFD, since the OVX mice presented increased LV systolic pressures.
Altogether, these results suggest that ovarian hormones exert a cardioprotective role in response to Ang II-induced hypertension and hypertrophy. The next step will be to evaluate the different mechanisms involved such as inflammation, fibrosis, autophagy, apoptosis and cardiac metabolic pathways.

9. Publications

Am J Physiol Endocrinol Metab 310: E782–E794, 2016.
First published March 15, 2016; doi:10.1152/ajpendo.00259.2015.

Neuregulin-1β promotes glucose uptake via PI3K/Akt in neonatal rat cardiomyocytes

Laura Pentassuglia, Philippe Heim, Sonia Lebboukh, Christian Morandi, Lifen Xu, and Marijke Brink
Department of Biomedicine, University of Basel and University Hospital Basel, Basel, Switzerland

Submitted 4 June 2015; accepted in final form 2 March 2016

Pentassuglia L, Heim P, Lebboukh S, Morandi C, Xu L, Brink M. Neuregulin-1β promotes glucose uptake via PI3K/Akt in neonatal rat cardiomyocytes. *Am J Physiol Endocrinol Metab* 310: E782–E794, 2016. First published March 15, 2016; doi:10.1152/ajpendo.00259.2015.—Nrg1β is critically involved in cardiac development and also maintains function of the adult heart. Studies conducted in animal models showed that it improves cardiac performance under a range of pathological conditions, which led to its introduction in clinical trials to treat heart failure. Recent work also implicated Nrg1β in the regenerative potential of neonatal and adult hearts. The molecular mechanisms whereby Nrg1β acts in cardiac cells are still poorly understood. In the present study, we analyzed the effects of Nrg1β on glucose uptake in neonatal rat ventricular myocytes and investigated to what extent mTOR/Akt signaling pathways are implicated. We show that Nrg1β enhances glucose uptake in cardiomyocytes as efficiently as IGF-I and insulin. Nrg1β causes phosphorylation of ErbB2 and ErbB4 and rapidly induces the phosphorylation of FAK (Tyr^{861}), Akt (Thr^{308} and Ser^{473}), and its effector AS160 (Thr^{642}). Knockdown of ErbB2 or ErbB4 reduces Akt phosphorylation and blocks the glucose uptake. The Akt inhibitor VIII and the PI3K inhibitors LY-294002 and Byl-719 abolish Nrg1β-induced phosphorylation and glucose uptake. Finally, specific mTORC2 inactivation after knockdown of rictor blocks the Nrg1β-induced increases in Akt-p-Ser^{473} but does not modify AS160-p-Thr^{642} or the glucose uptake responses to Nrg1β. In conclusion, our study demonstrates that Nrg1β enhances glucose uptake in cardiomyocytes via ErbB2/ErbB4 heterodimers, PI3Kα, and Akt. Furthermore, although Nrg1β activates mTORC2, the resulting Akt-Ser^{473} phosphorylation is not essential for glucose uptake induction. These new insights into pathways whereby Nrg1β regulates glucose uptake in cardiomyocytes may contribute to the understanding of its regenerative capacity and protective function in heart failure.

phosphatidylinositol 3-kinase; metabolism; tyrosine kinase; ErbB; signaling; protein synthesis

NEUREGULIN-1β (Nrg1β) and its receptors ErbB2 and ErbB4 are essential for cardiac development and also play a critical role in the healthy and diseased adult heart (45, 49, 50). Cardiomyocyte-specific ablation of ErbB2 (12, 47) or ErbB4 (21) leads to dilated cardiomyopathy with diminished contractility under basal or pressure-overload conditions. Experimental studies in which Nrg1β was administered in various rodent models of cardiac disease confirmed its beneficial action, which together with mechanistic insights obtained in cultured cardiomyocytes (17, 50, 73) led to its use in clinical trials to treat heart failure (19, 43, 58). The first two trials indeed showed a transient improvement of cardiac function (20, 30), whereas the results of several other trials, either with a recombinant human Nrg1β isoform or with the naturally occurring neuronal isoform glial growth factor 2 (GGF2), are to be expected in the near future. Recent work also implicated Nrg1β in the regenerative potential of neonatal and adult hearts (3, 25, 53). Nevertheless, the molecular mechanisms whereby Nrg1β exerts these effects in cardiac cells are still poorly understood.

Upon stimulation of cardiomyocytes by Nrg1β, the ErbB receptors act via the Src/focal adhesion kinase (FAK), the extracellular-regulated kinase (Erk)1 and 2, and the phosphatidylinositol 3-kinase (PI3K)/Akt pathways, which have been linked to distinct functions (50). Cardiac developmental and postnatal growth as well as physiological or pathological adaptations of the adult heart are regulated by the serine/threonine kinase mammalian target of rapamycin (mTOR). mTOR modulates cellular processes such as protein synthesis and energy metabolism (10, 37) and has distinct functions depending on whether it is part of mTOR complex (mTORC)1 or mTORC2. In the developing and adult heart mTORC1 activity is associated with protein synthesis and physiological hypertrophy, and mTORC2 may modulate glucose uptake, as demonstrated previously in skeletal muscle (35, 40, 57). Increased glucose uptake is critical for the survival of cardiomyocytes during the acute phase of ischemic injury, when lipid metabolism will become not only insufficient for the energy demands of the heart but will also lead to a significant increase in oxidative stress (3, 46, 72). Nrg1β is cardioprotective during ischemia (38), but its effects on glucose uptake and the involvement of mTOR have not been investigated.

In other contexts, ErbB receptor activity has been related to mTOR signaling. In breast cancer, pathological ErbB2 overexpression is associated with constitutive activation of Akt/mTOR and predicts tumor progression (52, 67, 79), and mTOR inhibitors improve the outcome of ErbB2-positive breast cancer (72). Whereas mTOR inhibition appears to be of therapeutic value in cancer, cardiomyocyte mTORC1 deficiency leads to cardiac dysfunction in mice (62, 77). The observation that recombinant human GGF2 causes phosphorylation of the mTORC1 target 70-kDa ribosomal S6 kinase (p70S6K) in cardiomyocytes (2) and that Nrg1β causes phosphorylation of Akt on the mTORC2 target site Ser^{473} (59, 76) led us to investigate whether and how mTORC1 and mTORC2 mediate one or more of the Nrg/ErbB-related cardioprotective activities.

Our study demonstrates in a model of rat neonatal cardiomyocytes that Nrg/ErbB signaling enhances glucose uptake and protein synthesis. The glucose uptake is mediated by PI3Kα/Akt/AS160. Nrg1β-induced mTORC1 activation plays a small role in the protein synthesis, whereas mTORC2 appears to not be implicated in the glucose uptake.

Address for reprint requests and other correspondence: M. Brink, Dept. of Biomedicine, Cardiobiology, Univ. of Basel and University Hospital Basel, Hebelstrasse 20, CH-4031 Basel, Switzerland (e-mail: marijke.brink@unibas.ch).

MATERIALS AND METHODS

Growth factors and inhibitors. Nrg1β was from R & D Systems, IGF-I was from Genentech, insulin, PP242, and wortmannin were from Sigma, Lapatinib and Dasatinib were from LC Laboratories, and PP2, PP3, LY-294002, Akt inhibitor VIII, U-0126, SB-203580, rapamycin, and PF573228 were from Calbiochem. Byl-719, TGX-221, Cal101, and AS605240 were kind gifts from Matthias P. Wymann, University of Basel.

Antibodies. Antibodies against mTOR-p-Ser^{2448}, mTOR-p-Ser^{2481}, mTOR, Erk1/2-p-Thr^{202}/Tyr^{204}, Akt-p-Thr^{308}, Akt-p-Ser^{473}, Akt, p70S6K1-p-Thr^{389}, p70S6K1, ULK1-p-Ser^{757}, eukaryotic initiation factor 4E-binding protein-1 (4E-BP1)-p-Ser^{65}, 4E-BP1, phosphorylated Akt substrate, AS160, and AS160-p-Thr^{642} were from Cell Signaling Technology. Antibodies against GAPDH, FAK, c-Src, ErbB2-p-Tyr^{1248}, ErbB2, and ErbB4 as well as normal goat IgG were from Santa Cruz Biotechnology. Antibodies against FAK-p-Tyr^{861} and ErbB4-p-Tyr^{1248} were from Abcam. Antibodies against FAK-p-Tyr^{397} were from BD Biosciences. Antibodies against Src-p-Tyr^{215} were from ECM Biosciences, and antibodies to ULK1 were from Sigma.

Primary neonatal cardiomyocyte isolation and transfection. Neonatal rat ventricular myocytes (NRVMs) were isolated from 1- to 2-day-old rats and transfected with nontarget ErbB2 and ErbB4 siRNA (Dharmacon) at 1 μg/3 × 10^6 cells using cardiomyocyte AMAXA nucleofactor (Lonza), as published previously (26). Two days later, the cells were treated with inhibitors and growth factors after an overnight incubation in serum-free albumin, carnitine, creatine and taurine-enriched medium (ACCT). ACCT medium consisted of 2 g/l albumin, 2 mM L-carnitine, 5 mM creatine, and 5 mM taurine (all from Sigma) in DMEM (Gibco).

Glucose uptake. NRVMs were treated with inhibitors for 30 min, followed by 30 min in the presence of growth factors and another 30 min in the presence of deoxy-D-glucose, 2-[1,2-^{3}H(N)] (Perkin-Elmer) and D-(+)-glucose (1 μCi/ml and 100 μM, respectively) in Krebs-Ringer bicarbonate buffer (115 mM NaCl, 4.7 mM KCl, 2.5 mM $CaCl_2$, 1.2 mM KH_2PO_4, 1.2 mM $MgSO_4$, 24 mM $NaHCO_3$, 10 mM HEPES, pH = 7.4, and 0.1% BSA). The glucose uptake was stopped by three washes with ice-cold PBS and lysis in NaOH. Part of the lysate was mixed with scintillation liquid, and ^{3}H was measured with a β-counter. A micro BCA protein assay (Thermo Scientific) was performed with the remaining lysate to normalize the counts/min.

Protein synthesis. To analyze the pathways by which Nrg1β stimulates protein synthesis, NRVMs were incubated for 30 min with inhibitors, as indicated in RESULTS, and then stimulated in the presence of 1 μCi/ml [^{3}H]phenylalanine (Amersham Biosciences) for 24 h. Cells were then washed with ice-cold PBS, precipitated with 10% ice-cold trichloroacetic acid for 30 min, washed with glacial EtOH 95%, dried, and lysed in NaOH for 45 min. Part of the lysate was mixed with scintillation liquid for measurement of ^{3}H with a β-counter. A DNA assay with Hoechst (Invitrogen) was performed with the remaining lysate and used to normalize the counts/min.

Protein extraction and Western blot analysis. Total protein was extracted with RIPA buffer [50 mM Tris·HCl, pH = 7.4, 150 mM NaCl, 1% Nonidet P-40, 0.25% Na deoxycholate, 0.1% SDS, 5 mM EDTA, and 0.5% phosphatase inhibitor cocktail 2 and 3 (Sigma)], and 1% protease inhibitor cocktail (Sigma) was separated by SDS-PAGE and transferred to a PVDF membrane (Amersham-GE Healthcare). After incubation with antibodies, the signal was revealed with Super-Signal West Pico Chemiluminescent Substrate (Thermo Scientific), CL-XPosure Film (Thermo Scientific), or the ChemiDoc MP System (Bio-Rad). Blots were quantified with Image Lab (Bio-Rad) and ImageJ (National Institutes of Health).

Immunoprecipitation. All procedures for immunoprecipitation were done at 4°C. Protein lysates (300 μg) were cleared with 25 μl of protein A-sepharose (Amersham-GE Healthcare) and incubated overnight with 2 μg of antibody to AS160 or normal goat IgG. A 50% slurry of protein A-sepharose (40 μl) was added for 4 h, and the beads were then washed five times with RIPA buffer and collected by centrifugation for 3 min at 3,000 rpm. The beads were resuspended in loading buffer and heated at 95°C. Supernatants were loaded on an 8% SDS-PAGE, and proteins transferred to PVDF, and phosphorylated Akt substrate and AS160 were detected as described above.

Isolation of adult mouse ventricular myocytes. Hearts were dissected from C57BL/6 mice, briefly washed in ice-cold Ca^{2+}-free perfusion buffer (135 mM NaCl, 4 mM KCl, 1 mM $MgCl_2$, 10 mM HEPES, 0.33 mM NaH_2PO_4, 10 mM glucose, 10 mM 2,3-butanedione-monoxime, and 5 mM taurine), and cannulated through the aorta for retrograde perfusion. After 5 min of acclimatization at 37°C, hearts were perfused for 7 min with digestion solution, consisting of 5,000 U collagenase (Worthington) and 5.24 U protease (Sigma) in Ca^{2+}-free perfusion buffer. The dissociated myocytes were passed through a 100-μm cell strainer and incubated with increasing concentrations of Ca^{2+} (0, 0.06, 0.24, 0.6, and 1.2 mM) that were obtained by mixing appropriate amounts of transfer *buffer A* (perfusion buffer with 5 mg/ml of BSA) with transfer *buffer B* (137 mM NaCl, 5.4 mM KCl, 0.5 mM $MgCl_2$, 10 mM HEPES, 1.2 mM $CaCl_2 \cdot H_2O$, and 5 mM glucose). Cells were seeded on laminin-coated dishes and kept in ACCT medium overnight before treatment.

Statistics. All results are expressed as means ± SE. One-way ANOVA analysis was followed by Sidak's post hoc testing using Prism 6 (GraphPad).

RESULTS

Nrg1β induces phosphorylation of the mTORC1 targets 4E-BP1, S6K, and ULK and the mTORC2 target Akt-p-Ser^{473}. First, we analyzed the temporal pattern of activation of kinases known to be part of the mTOR and Akt signaling pathways using NRVMs. Figure 1*A* shows that at 5 min, Nrg1β treatment caused phosphorylation of both ErbB2 and ErbB4 at Tyr^{1248}. At the same time, the phosphorylation of FAK and Akt was already strongly increased. The phosphorylated amounts of mTOR and the mTORC1 targets 4E-BP1, p70-S6K1, and ULK were increased later at 15 and 30 min. Lapatinib, a well known inhibitor of ErbB1 and ErbB2, blocked the phosphorylation of ErbB2 and ErbB4 as well as that of all downstream effectors (Fig. 1*A*). Moreover, a dose response experiment at 30 min confirmed specificity of the Akt response and established 10 ng/ml as optimal Nrg1β concentration for further experiments (Fig. 1*B*). Nrg1β also activated mTOR signaling in cardiomyocytes isolated from adult mouse hearts, in which increases in mTOR-pS2448 were similar to those obtained with IGF-I, and an upward bandshift was observed for 4E-BP1, indicating increased phosphorylation (Fig. 1*C*). Thus, we conclude that Nrg1β has immediate and specific stimulatory effects on mTOR-mediated signaling cascades in cardiomyocytes.

In Fig. 1*D*, the effects of Nrg1β are compared with those of IGF-I to evaluate the potency of either growth factor to activate mTOR and its effectors over a longer period of time. At 30 min, IGF-I and Nrg1β similarly increased mTOR-p-Ser^{2448}, p70-S6K1-p-Thr^{389}, Akt-p-Ser^{473}, and 4E-BP1 phosphorylation. For Nrg1β, the p70-S6K1-p-Thr^{389} and Akt-p-Ser^{473} signals decreased more rapidly than for IGF-I. Thus, at 3 h the Nrg1β-treated samples already displayed a much lesser increase compared with controls than the IGF-I-treated samples, for which the increase remained very pronounced for at least 6 h. On the other hand, the phosphorylation of 4E-BP1 persisted for up to 24 h for both growth factors. PP242, an mTOR inhibitor that blocks mTORC1 as well as mTORC2, abolished all of the Nrg1β-induced increases in phosphorylation (Fig.

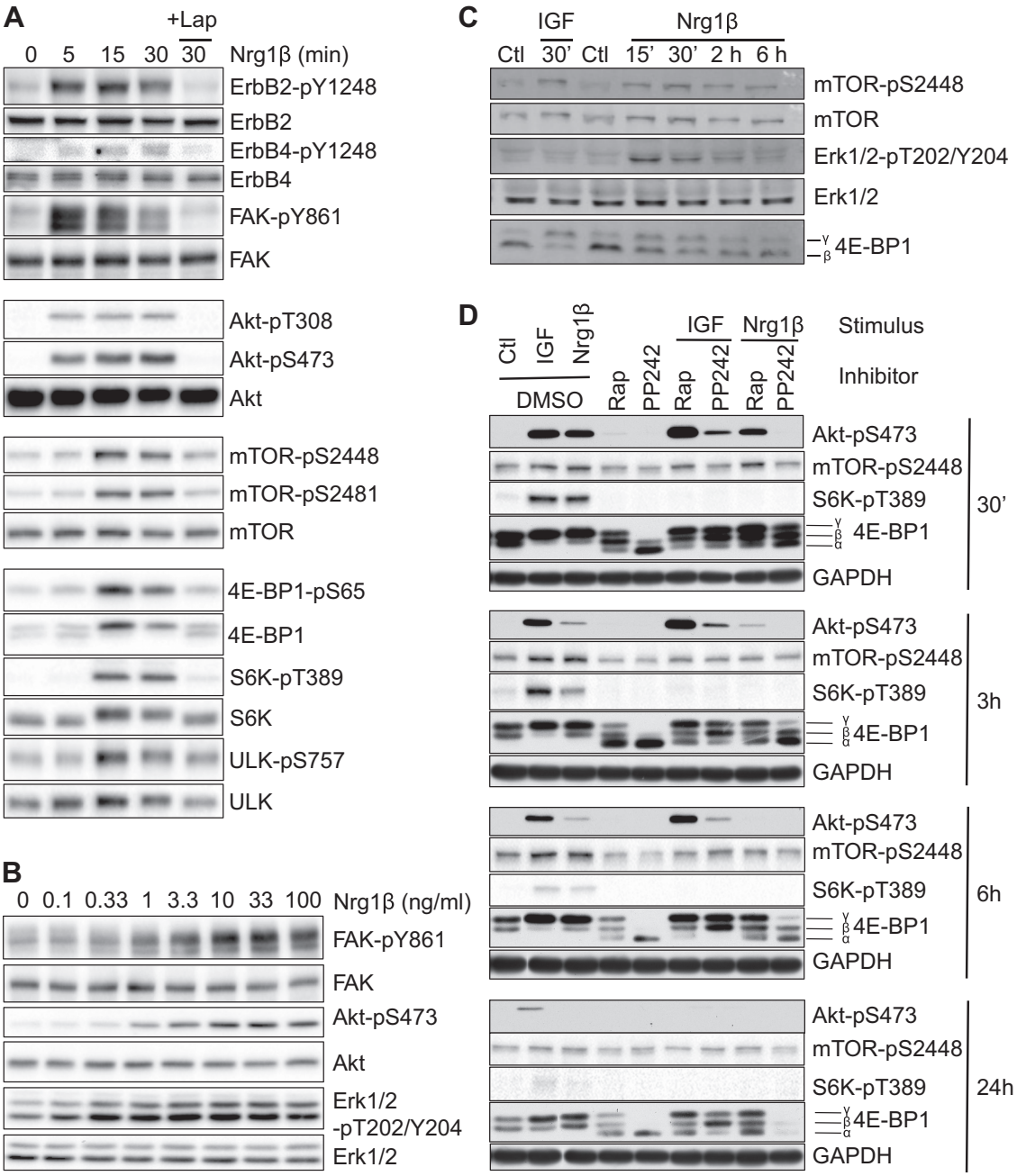

Fig. 1. Neuregulin-1β (Nrg1β) activates mammalian target of rapamycin (mTOR) complex (mTORC)1 and mTORC2 in ventricular myocytes. *A*: after overnight incubation in serum-free albumin, carnitine, creatine, and taurine-enriched medium, neonatal rat ventricular myocytes (NRVMs) were treated with Nrg1β (10 ng/ml) for 5, 15, and 30 min. Cells were pretreated with Lapatinib (Lap; 10 μM) or vehicle (DMSO) for 30 min. *B*: dose response for Nrg1β in NRVMs at 30 min. *C*: adult mouse ventricular myocytes were treated with Nrg1β (10 ng/ml) or IGF-I (20 ng/ml) and lysed for analysis by Western blotting at the time points indicated. *D*: NRVMs were treated with Nrg1β (10 ng/ml) or IGF-I (20 ng/ml) for ≤24 h in the absence or presence of rapamycin (Rap; 20 ng/ml) or PP242 (20 μM), and lysates were analyzed as in *A*. *D*: total proteins (20 μg) were analyzed by Western blotting to test for total and phosphorylated proteins as indicated. FAK, focal adhesion kinase; 4E-BP1, eukaryotic initiation factor 4E-binding protein-1; Ctl, control; S6K, p70S6K1.

1*D*). As expected, rapamycin decreased phosphorylation of p70-S6K1 and 4E-BP1 in line with its function as mTORC1 inhibitor in short-term experiments. Interestingly, rapamycin increased IGF-I-induced phosphorylation of the mTORC2 target site Ser^{473} in Akt, consistent with earlier studies (44, 68, 69, 74), whereas it did not modify the Nrg1β-induced phosphorylation of Akt at Ser^{473}. We conclude that Nrg1β/ErbB activates mTORC1-4E-BP1 in a similar manner as IGF-I, whereas it activates p70-S6K1 and mTORC2-Akt more transiently than IGF-I.

Nrg1β stimulates protein synthesis. Given the well-established function of mTORC1, we tested whether Nrg1β stimulates protein synthesis in cardiomyocytes via mTORC1. Incubation with Nrg1β for 24 h increased phenylalanine incorporation in a Lapatinib-sensitive manner (Fig. 2*A*), and rapamycin and PP242 both diminished this effect to a similar

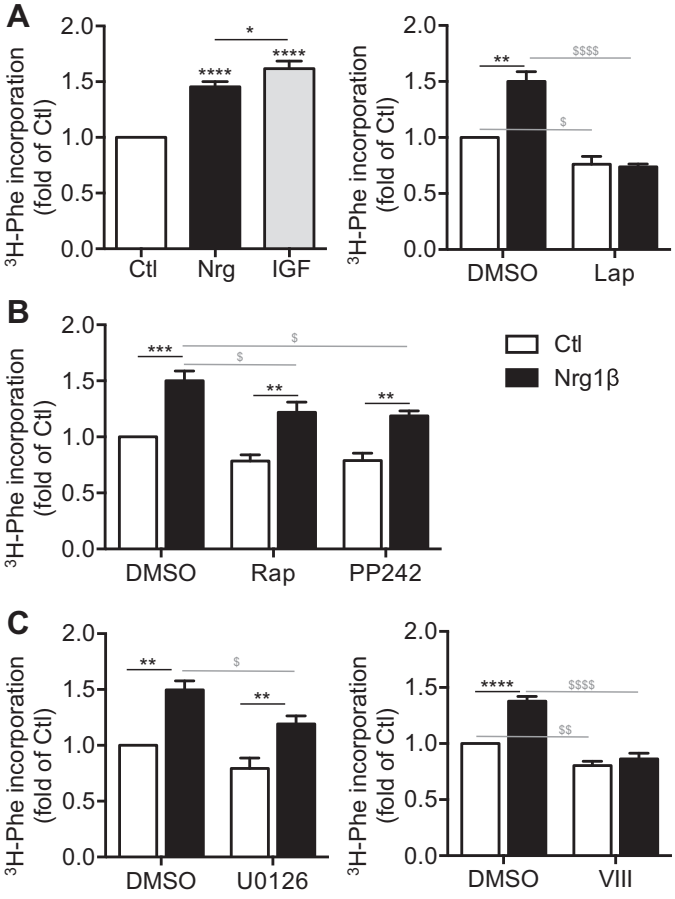

Fig. 2. Nrg1β enhances protein synthesis in part via mTORC1, Erk1/2, and Akt. After preincubation with vehicle (DMSO), Lap (10 μM), Rap (20 ng/ml), PP242 (20 μM), U-0126 (10 μM), or Akt inhibitor VIII (VIII; 20 μM) for 30 min, NRVMs were treated with Nrg1β (10 ng/ml) in the presence of [^{3}H]phenylalanine (1 μCi) for 24 h. The [^{3}H]phenylalanine incorporated into the cells was normalized for DNA content; $n = 3$. *$P < 0.05$, **$P < 0.01$, ***$P < 0.001$, and ****$P < 0.0001$, Nrg-treated vs. Ctl; \$$P < 0.05$, \$\$$P < 0.01$, and \$\$\$\$$P < 0.0001$, inhibitor- vs. corresponding DMSO-treated control.

extent (Fig. 2*B*), which suggests that mTORC1 contributes to the Nrg1β-induced protein synthesis. However, since a strong increase persisted after PP242 or Rap inhibition, mTOR-independent alternate pathways are also important in the Nrg1β-induced phenylalanine uptake. Consistent with previous studies, the Erk1/2 inhibitor U-0126 partially inhibited phenylalanine incorporation (Fig. 2*C*). Moreover, the Akt inhibitor VIII abolished the protein synthesis response, in line with the established role of Akt as upstream activator of mTORC1. We conclude that Akt and Erk1/2, as well as mTORC1 via sustained phosphorylation of 4E-BP1 (Fig. 1*D*), are implicated in the enhanced global protein synthesis after Nrg1β treatment of neonatal cardiomyocytes.

Nrg1β enhances glucose uptake. Given our observation that the effect of PP242 on protein synthesis was only modest, we next aimed at identifying other functions of mTOR in cardiomyocytes. Very little is known about the cardiac function of mTORC2, and therefore, we decided to focus on the function of the Nrg1β-induced phosphorylation of Akt at Ser^{473}, which in Fig. 1*D* was shown to be rapamycin resistant and PP242 sensitive and, therefore, most likely mTORC2 dependent. Akt is implicated in the translocation of glucose transporters to the plasma membrane and thereby contributes to insulin-induced glucose uptake after feeding (34). As mTORC2 has been reported to regulate glucose metabolism in some tissues (35, 40), we hypothesized that mTORC2-mediated phosphorylation of Akt contributes to Nrg1β-induced glucose uptake in our cardiomyocyte model. We tested this hypothesis while using IGF-I and insulin as a reference. The three stimuli induced similar increases in glucose uptake, and combinations of Nrg1β with either IGF-I or insulin did not yield any further increase (Fig. 3*A*), indicating that Nrg1β depends at least in part on the same signaling molecules as IGF-I and insulin. Lapatinib abolished the effect of Nrg1β on glucose uptake (Fig. 3*B*), implicating ErbB2 and/or ErbB4 in the response. Figure 3*C* shows that rapamycin did not have any effect at all, which excludes a role for mTORC1. On the other hand, PP242 preincubation reduced the Nrg1β-induced glucose uptake compared with that of DMSO-preincubated cells (Fig. 3*C*). In fact, PP242 reduced the Nrg1β-induced glucose uptake from 1.77- to 1.56-fold compared with the corresponding unstimulated DMSO- and PP242-preincubated controls, respectively, and therefore, the inhibition was 27% of the total increase. In additional independent experiments, PP242 reduced Nrg1β-, IGF-I-, and insulin-induced glucose uptake from 1.88-, 1.64-, and 1.90- to 1.52-, 1.56-, and 1.52-fold, respectively, vs. the corresponding unstimulated controls. This represents an inhibition of 41, 13, and 42%, respectively, for the three growth factors. Together, our data suggest that common pathways are used by the three growth factors to link receptor activation to glucose uptake and that mTORC2 may mediate part of the insulin- and Nrg1β-induced responses. Additional nonpharmacological approaches are required to prove this further (see below).

The Nrg1β-induced glucose uptake is mediated by Akt and AS160. To further characterize the PP242-sensitive signaling branch of the Nrg1β-induced glucose uptake, we assessed which kinases, in addition to those already shown in Fig. 1, were inhibited by PP242 (Fig. 4). At 30 min, Nrg1β enhanced Akt phosphorylation at Thr^{308} and Ser^{473}, although the effect was somewhat weaker than that observed for IGF-I. PP242 abolished both increases completely for Nrg1β and partially for IGF-I (Fig. 4*A*). Together with the generally accepted view that Akt-p-Ser^{473} is a direct target of mTORC2 and our finding that rapamycin does not reduce Akt-p-Ser^{473} (Fig. 1*D*), this complete inhibition by PP242 supports that mTORC2 is implicated in this Nrg1β-induced Akt phosphorylation in cardiomyocytes. In Fig. 1*A*, we showed that Nrg1β increases Akt-p-Ser^{473} already at 5 min, before mTOR phosphorylation is detectable, and therefore, we tested whether Nrg1β has a rapid, mTOR-independent phase of Akt activation. Figure 4*B* shows that PP242 inhibited the Akt-Ser^{473} phosphorylation at 5 min after Nrg1β stimulation, which indicates that mTORC2 was active and required for this early phosphorylation of Akt. Notably, Akt-p-Thr^{308} was somewhat reduced but not abolished in the PP242-pretreated cells, consistent with the notion that PDK1-mediated Akt-Thr^{308} phosphorylation is possible in the absence of mTORC2-mediated Akt-Ser^{473} phosphorylation. These reduced Akt-p-Thr^{308} amounts may explain the partially reduced glucose uptake response to Nrg1β after PP242 pretreatment. Figure 4*C* shows that the Akt inhibitor VIII abolished the Nrg1β-induced glu-

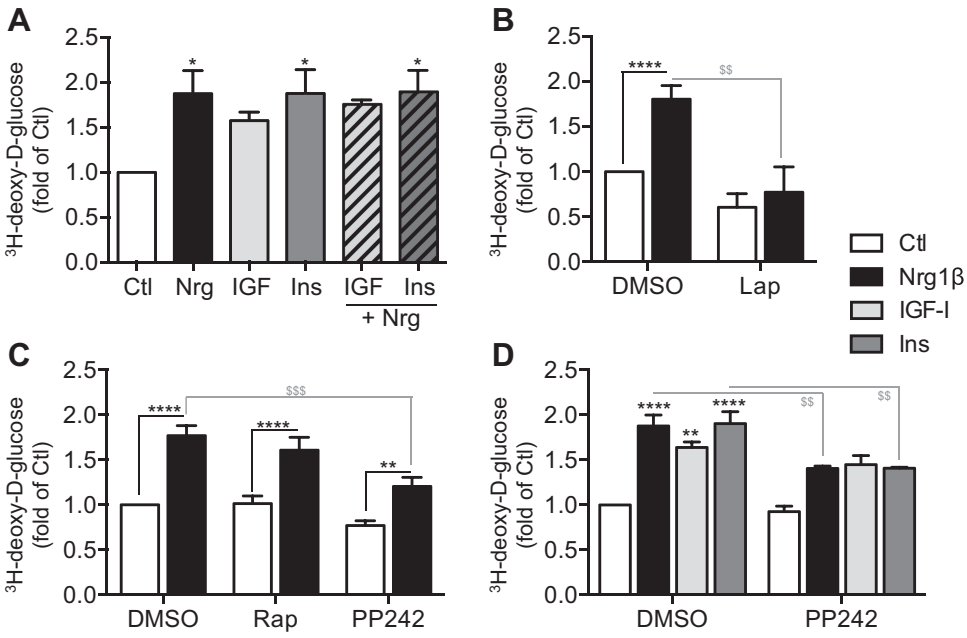

Fig. 3. Nrg1β increases glucose uptake, which is partially inhibited by PP242. *A*: NRVMs were treated for 30 min with Nrg1β (10 ng/ml), IGF-I (20 ng/ml), or insulin (Ins; 20 ng/ml) either alone or in combination as indicated. This was followed by 30 min of incubation with 1 μCi/ml [^{3}H]deoxy-D-glucose. Data were normalized for the total protein/well; $n = 3$. *B–D*: NRVMs were treated with Nrg1β (10 ng/ml) after 30 min of preincubation with vehicle (DMSO), Lap (10 μM), Rap (20 ng/ml), or PP242 (20 μM), and glucose uptake was assessed as in *A*; $n = 6$ (*B*), 7 (*C*), and 3 (*D*). $^*P < 0.05$, $^{**}P < 0.01$, and $^{****}P < 0.0001$ (vs. Ctl); \$\$\$$P < 0.001$ inhibited vs. corresponding DMSO; \$\$$P < 0.01$, inhibitor- vs. corresponding DMSO-treated control.

cose uptake, which indeed supports that Akt is a main actor in this effect.

IGF/insulin-induced Akt activation is known to cause the translocation of glucose transporters to the sarcolemma via its downstream mediator AS160 (56), but whether or not Nrg1β acts via this mechanism in cardiomyocytes is not known. Immunoprecipitation experiments demonstrated that Nrg1β raised the phosphorylation of Akt substrate AS160 in a manner similar to IGF-I (Fig. 4*D*). Moreover, an antibody to AS160-p-Thr^{642} confirmed its phosphorylation after Nrg1β stimulation (Fig. 4*E*), which is consistent with the known function of this specific phosphorylation site being indicative of enhanced glucose transporter type 4 (GLUT4) translocation to the sarcolemma. Together, these data support that Nrg1β induces glucose uptake in NRVMs via Akt and AS160 and suggest that mTORC2-mediated Akt-Ser^{473} phosphorylation may contribute to this response.

Nrg1β-induced mTORC2-mediated Akt phosphorylation at Ser^{473} is not required for the glucose uptake response. To further investigate the role of mTORC2, we knocked down its specific and essential component rictor using siRNA technologies. Figure 4*F* shows that reduced rictor protein levels were associated with lower Akt-p-Ser^{473}, confirming that mTORC2 activity was efficiently reduced. However, this was not associated with lower AS160-p-Thr^{642} (Fig. 4*F*), and consistently, glucose uptake responses to Nrg1β were not impaired (Fig. 4*G*). Together with our observations that PP242 only modestly and Akt inhibitor VIII completely inhibited the glucose uptake, these data indicate that mTORC2-mediated Akt phosphorylation is not essential for this response to Nrg1β. Thus, whereas our data demonstrate that Nrg1β activates mTORC2 and stimulates glucose uptake, the mTORC2-mediated Akt-p-Ser^{473} phosphorylation appears not to modulate this glucose uptake.

Upstream of Akt, PI3K is implicated in the Nrg1β-induced glucose uptake. We next aimed at identifying other upstream signaling molecules that mediate the Nrg1β-induced Akt activation and glucose uptake. The class 1 PI3K inhibitor LY-294002 (LY) abolished the Nrg1β-induced glucose uptake (Fig. 5*A*), whereas effects of the p38 inhibitor SB-203580 (SB) and the Erk1/2 inhibitor U-0126 did not reach significance (Fig. 5*B*). Consistently, LY blocked whereas SB only had small effects on Akt phosphorylation (Fig. 5*E*). Others have demonstrated that SB decreases glucose uptake independently of p38 MAPK inhibition (1). Therefore, PI3K is most likely the main actor upstream of Akt in the Nrg1β-induced glucose uptake. LY has been reported to also inhibit other kinases, including mTORC1, at concentrations similar to those that inhibit PI3K (13). Additional experiments with the isoform-specific PI3K inhibitor Byl-719 revealed that Nrg1β activates glucose uptake via PI3Kα (Fig. 5*C*), and this was associated with lower Akt (Thr^{308} and Ser^{473}) and Akt substrate (160 kDa) phosphorylation (Fig. 5*D*), which suggests that PI3Kα is activating both PDK1 and mTORC2. Consistently, inhibition of PI3Kβ, -δ, and -γ with TGX-221, Cal101, and AS605240, respectively, had no effect (data not shown).

Effect of Src family kinase inhibitors on the Nrg1β-induced glucose uptake. How does Nrg1β-induced ErbB2/ErbB4 phosphorylation lead to PI3K activation? Given our observation that the Nrg1β-induced Akt phosphorylation was paralleled over time by increased FAK-p-Tyr^{861} (Fig. 1*A*), we tested whether Src family kinases are implicated, because FAK is one of their direct targets (7, 61). PP2, a compound that inhibits Src family protein kinases such as c-Src, reduced the Nrg1β-induced glucose uptake (Fig. 6*A*) as well as phosphorylation of FAK at Tyr^{861} and Akt at Thr^{308} and Ser^{473} (Figs. 5*E* and 6*E*), whereas it had no effect on p70-S6K1-p-Thr^{389} (Fig. 5*E*). None of the effects was observed with PP3, a negative control for PP2. Recent studies reported that PP2 may inhibit other kinases with similar affinities and that it is less Src selective than the Src family kinase inhibitor dasatinib (Das) (4). Therefore, we also tested Das and found that it efficiently reduced FAK-p- Tyr^{861}, Akt at both tested

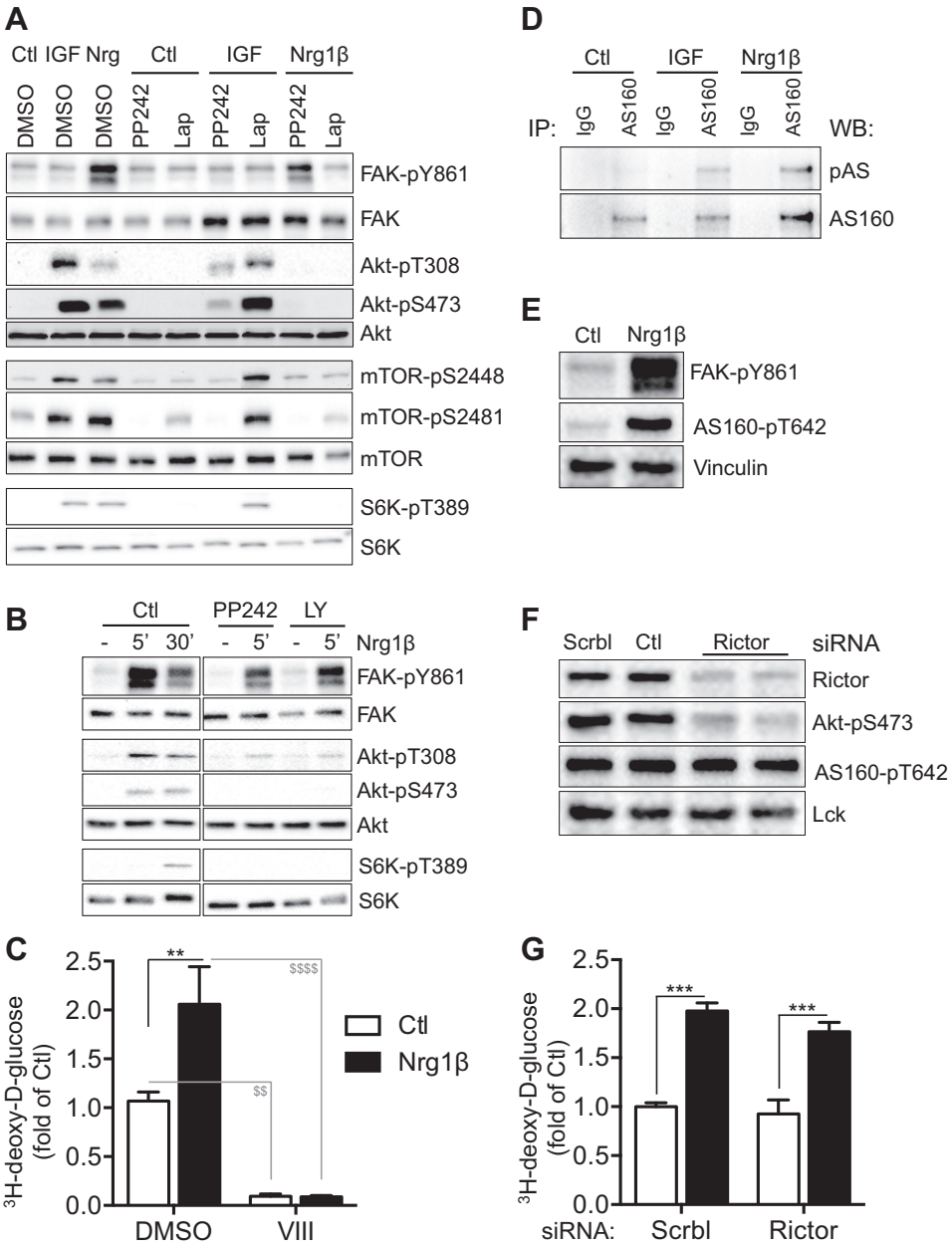

Fig. 4. The Nrg1β-induced glucose uptake is mediated by ErbB2, phosphatidylinositol 3-kinase (PI3K), and Akt. *A*: NRVMs were treated for 30 min with Nrg1β, IGF-I, or vehicle (Ctl) after 30 min of pretreatment with DMSO, PP242 (20 μM), or Lap (10 μM). Western blot (WB) analysis was performed to assess the phosphorylation status of the kinases indicated. *B*: as in *A*, LY-294002 (LY; 10 μM) was used during the preincubation, and Nrg1β treatment was done for 5 and 30 min. Images shown are cut from the same Western blot. *C*: after 30 min of pretreatment with DMSO or Akt inhibitor VIII (20 μM), NRVMs were treated for 30 min with Nrg1β or vehicle (Ctl), followed by 30 min of 1 μCi/ml [^{3}H]deoxy-D-glucose; $n = 4$. *D*: NRVMs were treated with IGF-I or Nrg1β for 30 min, and total protein extracts were immunoprecipitated (IP) for Akt substrate of 160 kDa (AS160). WBs of the precipitated proteins were analyzed with antibodies to phosphorylated Akt substrate (pAS) and AS160. *E*: after Nrg1β stimulation, total protein extracts were analyzed with a phosphospecific antibody to AS160-p-Thr^{642}. *F* and *G*: cardiomyocytes were transfected with small-interfering RNA (siRNA) to rictor immediately after their isolation using AMAXA. Stimulation with Nrg1β and protein extraction (*F*) or glucose uptake assays (*G*) followed 2 days after the transfection. $^{**}P < 0.01$ and $^{***}P < 0.001$, Nrg1β vs. Ctl; $\$\$P < 0.01$ and $\$\$\$\$P < 0.0001$, inhibitor vs. corresponding DMSO. Lck, lymphocyte-specific protein tyrosine kinase; Scrbl, scrambled.

sites (Figs. 5*E* and 6*E*), and the 160-kDa Akt substrate (not shown). A dose response experiment demonstrated that strong inhibition was obtained already at 100 ng/ml and was complete at 1 μg/ml (data not shown). Notably, Das potently reduced the Nrg1β- but not the IGF-I-induced glucose uptake (Fig. 6*B*), indicating that Das sensitivity is a unique feature of Nrg1β-induced ErbB signaling. Similarly, only Nrg1β led to increased phosphorylation of FAK at Tyr^{861} (Fig. 6*C*). In an attempt to further identify the implicated kinase, we analyzed over time the phosphorylation of Src at Tyr^{215} and Tyr^{416}, the latter site being indicative of c-Src activation. Src-p-Tyr^{215} increased at 30 min, which is much later than FAK-p- Tyr^{861}, Akt, and Akt substrate phosphorylation, excluding a role of this site in the rapid activation of Akt (Fig. 6*D*). Src-p-Tyr^{416} was already high under basal conditions and did not increase any further after Nrg1β stimulation. Das but not PP2 inhibited phosphorylation of this site (Fig. 6*E*), whereas both inhibitors negatively affected Nrg1β-induced Akt activation and glucose uptake (Fig. 6, *A* and *B*), which altogether excludes a causative role of c-Src. In conclusion, our findings indicate that one or more members of the Src kinase family (but not c-Src) are involved in the phosphorylation of FAK at Tyr^{861} and in the glucose uptake response to Nrg1β, although a causal relationship between FAK-p861 and glucose uptake and the precise mechanism involved remain to be established.

Nrg1β/ErbB-induced glucose uptake does not depend on integrin/FAK397. Src family kinases have been implicated in integrin signaling, and recent data suggest that integrin activation may promote glucose uptake (29). Ligand-induced integrin activation involves, as a first step, autophosphorylation of FAK at Tyr^{397}, which induces a conformational change and exposes a binding motif for SH2-domain-

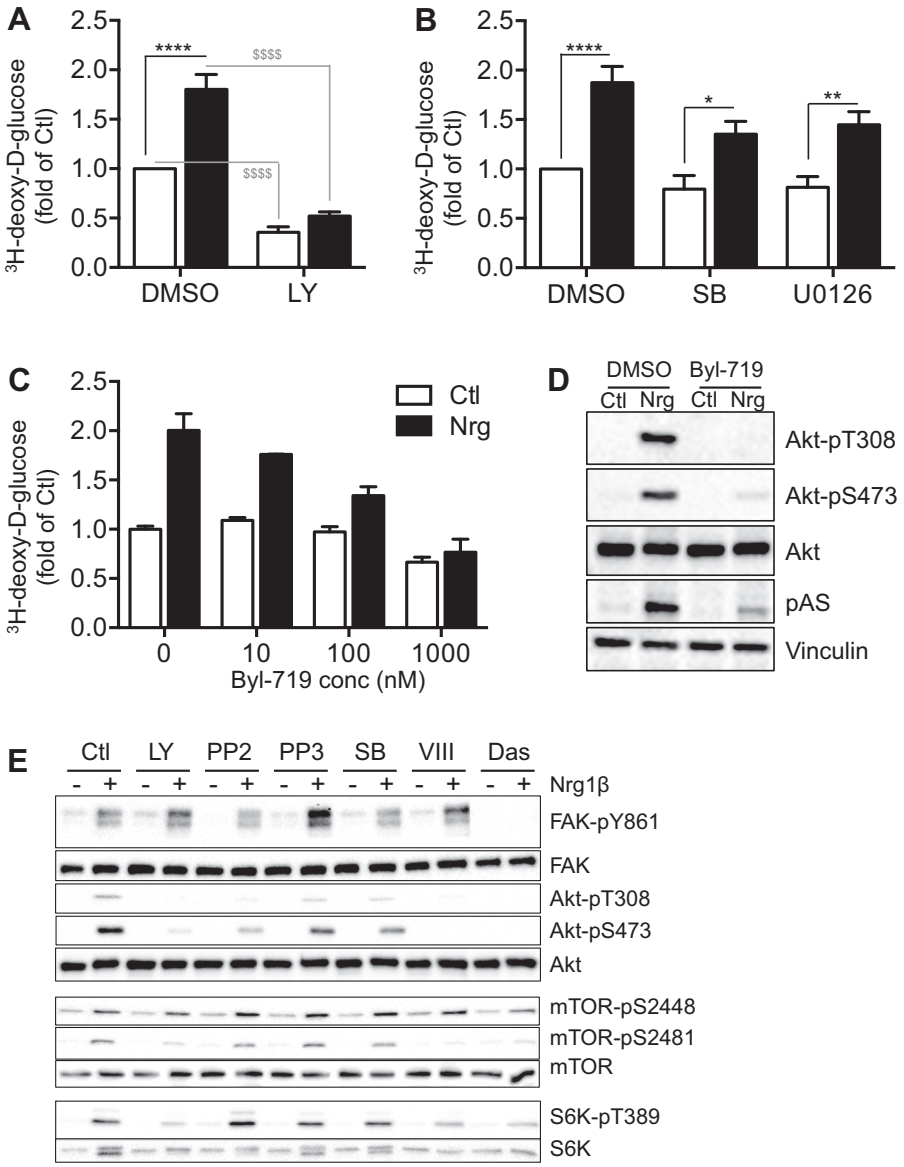

Fig. 5. Upstream of Akt, PI3Kα is implicated in the Nrg1β-induced glucose uptake. *A–D*: NRVMs were pretreated with the PI3K inhibitor LY (10 μM), the p38 inhibitor SB-203580 (SB; 10 μM), and the PI3Kα inhibitor Byl-719 (1 μM; *D*) for 30 min. NRVMs were then stimulated with vehicle (Ctl) or Nrg1β (10 ng/ml) for 30 min, and glucose uptake was assessed as in Figs. 3 and 4. *E*: inhibitors were used and cells stimulated as in *A–D* and Fig. 6. Protein extracts were analyzed by Western blotting as in Fig. 1. $*P < 0.05$, $**P < 0.01$, and $****P < 0.0001$ (vs. Ctl); $\$\$\$\$P < 0.0001$, inhibitor vs. DMSO.

containing Src-family kinases. After binding, these kinases further phosphorylate FAK at multiple sites and thereby activate it (60). To investigate whether the Nrg1β-induced glucose uptake requires signaling via integrin/FAK-p-Tyr^{397}, we used the potent FAK inhibitor PF-573228 (PF). Figure 7*A* shows that Nrg1β increased FAK-p-Tyr^{861} but did not change FAK-p-Tyr^{397} compared with untreated controls. Consistent with an earlier report (33), PF had no effect on the Nrg1β-stimulated FAK-p-Tyr^{861}, but it effectively reduced FAK-p-Tyr^{397}, Src-p-Tyr^{416}, and phosphorylation of the integrin-FAK target paxillin. Nevertheless, PF neither inhibited Nrg1β-induced mTOR and Akt signaling, as phosphorylation of mTOR and its targets Akt (Ser^{473}) and p70S6K remained high (Fig. 7*A*), nor did it affect the glucose uptake response (Fig. 7*B*), from which we conclude that these effects are integrin/FAK-p-Tyr^{397}/c-Src-independent. The data also indicate the presence of high basal integrin/FAK/Src activity in our model.

Specific downregulation of ErbB2 and ErbB4 with siRNA. Lapatinib blocked the glucose uptake and all Nrg1β-induced signaling, but as it reduced phosphorylation of both ErbB2 and ErbB4 it did not distinguish between the two receptors (Fig. 1). To define the specific role of ErbB2 and ErbB4 in the Nrg1β-induced pathways that enhance glucose uptake, we used pools of siRNA specific for ErbB2 and ErbB4. Both targeted proteins were effectively downregulated, whereas GAPDH and vinculin were not altered (Fig. 8). Knockdown of ErbB4 resulted in reduced Nrg1β-stimulated levels of FAK-p-Tyr^{861}, Akt-p-Ser^{473}, Akt-p-Thr^{308}, mTOR-p-Ser^{2448}, ULK-p-Ser^{757}, and p70-S6K1-p-Thr^{389}. ErbB2 knockdown, on the other hand, only reduced Akt-p-Ser^{473} and Akt-p-Thr^{308} (Fig. 8). Both the ErbB2 and ErbB4 siRNA knockdown abolished the Nrg1β-induced glucose uptake, showing that both ErbB2 and ErbB4 are needed for this response. The signaling data suggest that ErbB4 is implicated in the Nrg1β-induced activation of mTORC1 as well as mTORC2. ErbB2 is implicated in mTORC2 but does not seem to be required for mTORC1 activation by Nrg1β. However, as our knockdown approach was more efficient for ErbB4 than for ErbB2, coimmunoprecipitation and com-

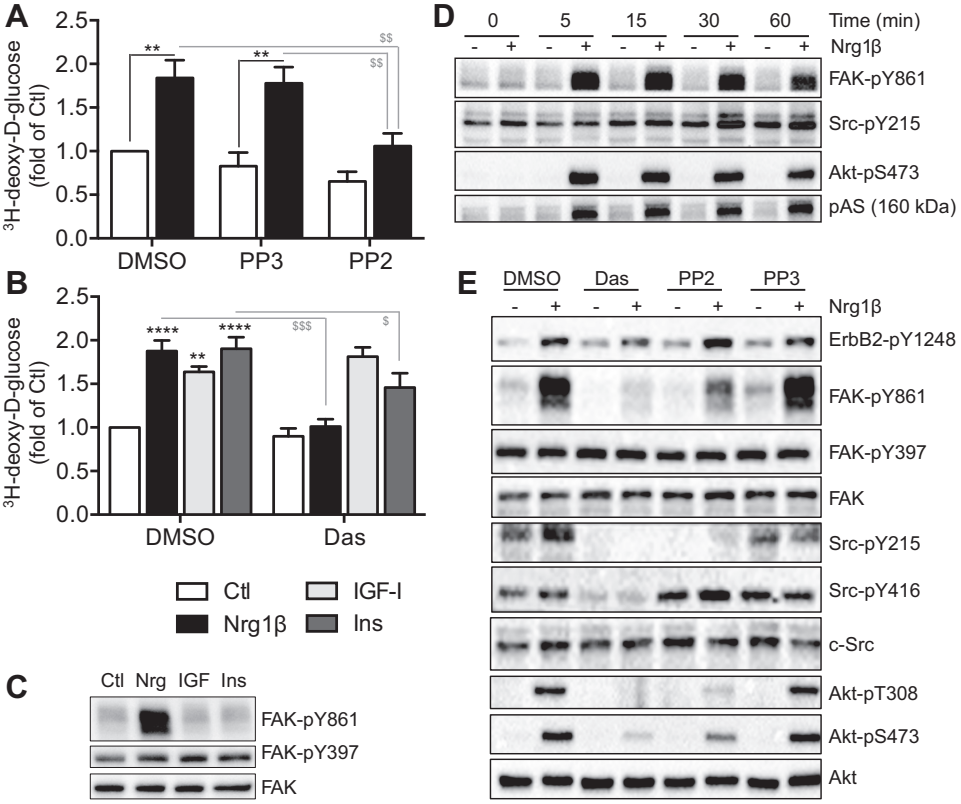

Fig. 6. Effect of Src family kinase inhibitors on Nrg1β-induced signaling and glucose uptake. *A* and *B*: NRVMs were pretreated with the inhibitor PP2 (5 μM) or dasatinib (Das; 1 μM) for 30 min. PP3 (5 μM) was used as negative control for PP2. NRVMs were then stimulated with vehicle (Ctl) or Nrg1β (10 ng/ml) or IGF-I (20 ng/ml) for 30 min, and glucose uptake was assessed as in Figs. 3–5. *C–E*: protein extracts were analyzed by Western blotting as in Fig. 1. $^{**}P < 0.01$ and $^{****}P < 0.0001$ vs. Ctl; $\$P < 0.05$, $\$\$P < 0.01$, and $\$\$\$P < 0.001$, inhibitor vs. corresponding DMSO.

plete knockout approaches are required to further investigate receptor involvement. Our data are in line with the notion that ErbB4 is the main receptor for Nrg1β, whereas ErbB2 has no extracellular binding pocket for Nrg1β but transduces specific signals when it is part of a heterodimer complex with one of the other ErbB isoforms.

DISCUSSION

Under stress conditions, cardiac microvascular endothelial cells release Nrg1β, which in a paracrine manner activates the receptor dimers ErbB2/ErbB4 and ErbB4/ErbB4, both of which are expressed in cardiomyocytes (11, 78). Upon stimulation, the ErbB receptors may act via the Erk1/2, PI3K/Akt, and Src/FAK pathways, each of which has been linked to distinct protective functions. For example, Nrg1β diminishes doxorubicin-induced sarcomere disarray in cardiomyocytes via Erk (48, 51, 59), whereas PI3K/Akt activation is responsible for the protection against basal or anthracycline-induced apoptosis (16, 22, 78) in part by reducing oxidative stress and improving mitochondrial function, calcium handling, and contractility (22, 23, 66). Independently of PI3K/Akt and Erk1/2, Nrg1β influences focal adhesion formation via Src/FAK (36).

Consistent with previous studies (2, 11, 78), we show here that Nrg1β increases global protein synthesis in neonatal cardiomyocytes. Whereas early studies implicated ErbB2 and Erk1/2 in the protein synthesis response to GGF2, here we extend the mechanistic insights by demonstrating how Nrg1β activates mTORC1 over time and by providing data that suggest its involvement in protein synthesis. However, it should be mentioned here that a large part of the Nrg1β-induced protein synthesis was not inhibitable by the mTOR inhibitor PP242, indicating pathway redundancy. Nevertheless, we show that Nrg1β increases mTOR-p-Ser^{2448} (a site that indicates mTORC1 activity) and the phosphorylated levels of two direct mTORC1 targets that regulate protein synthesis, namely p70-S6K and 4E-BP1. The Nrg1β-induced increase in 4E-BP1 phosphorylation lasted as long as that induced by IGF-I, which may explain the similar potency of the two factors to enhance protein synthesis. In contrast to IGF-I, Nrg1β only transiently affects p70-S6K phosphorylation, and rapamycin does not lead to hyperphosphorylation of Akt. These findings suggest that Nrg1β activates mTORC1 and protein synthesis without inducing the negative feedback loop that is perceived as one of the causes of insulin resistance.

Our study also demonstrates that Nrg1β increases glucose uptake. Nrg1β was reported to enhance glucose uptake in cardiomyocytes only in one earlier study, in which it was shown that the endothelium generates both Nrg1α and Nrg1β, but that only Nrg1β causes ErbB2 tyrosine phosphorylation with functional consequences such as increased glucose uptake (11). Whereas that study did not analyze the underlying pathways, our study now shows that Nrg1β increases glucose uptake via ErbB2/ErbB4 heterodimers and enhanced signaling via PI3Kα, Akt, and AS160. Given the well-established function of Akt/AS160, our data suggest that the increase in glucose uptake after Nrg1β stimulation is a consequence of GLUT4 translocation to the sarcolemma (56). Thus, whereas others have linked Akt activation by Nrg1β to pro-survival pathways (16, 22, 23, 66, 78), here we provide evidence that Nrg1β also triggers glucose uptake via this kinase.

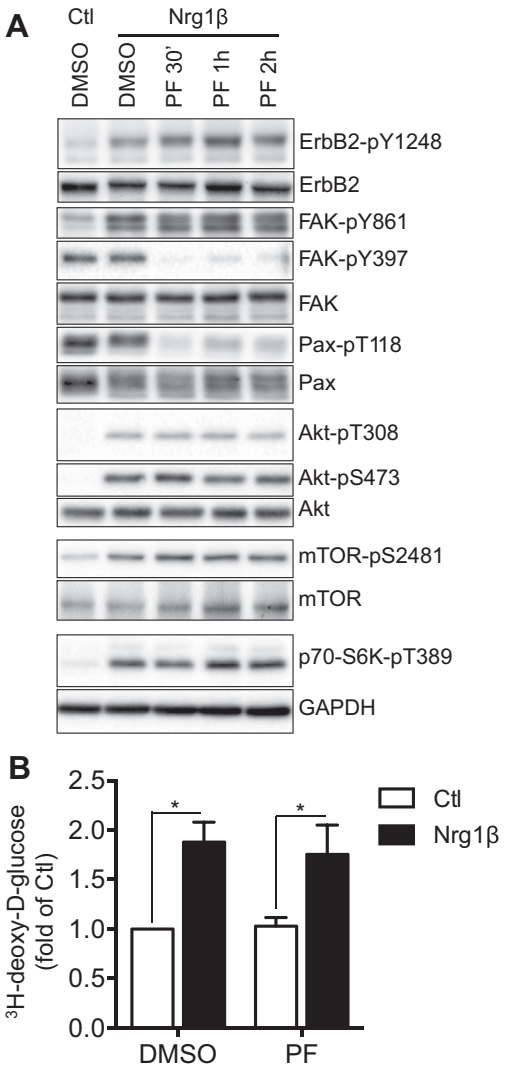

Fig. 7. FAK-p-Tyr^{397} is not implicated in the glucose uptake response to Nrg1β. *A*: NRVMs were pretreated with FAK inhibitor PF-573228 (PF; 1 μM), followed by Nrg1β treatment for 30 min. *A*: WB analysis was performed for FAK and mTOR signaling. PF preincubation was done for 30 min, 1 h, and 2 h; the DMSO control matched the 30-min time point. *B*: glucose uptake was performed as in Fig. 3 to assess the influence of integrin/FAK-p-Tyr^{397} inhibition on the Nrg1β-stimulated glucose uptake; $n = 4$. *$P < 0.05$ vs. Ctl.

This novel ErbB2/ErbB4-specific mechanism of glucose uptake may be particularly important under conditions of acute stress such as ischemic events, when the heart has to rapidly respond to maintain performance and survival of contractile cells. Whereas fatty acid and glucose oxidation are tightly regulated in the healthy heart to optimally provide it with the high amounts of energy needed for contraction, substrate use for ATP production changes under hypoxic conditions associated with, e.g., ischemia or hypertrophy. A shift from predominant fatty acid oxidation to increased carbohydrate use and glycolysis ensures continued ATP production under conditions of oxygen deficiency (31, 39). Ischemia has previously been associated with the translocation of glucose transporters to the sarcolemma (5, 46, 75). At the early stages of ischemia, the glucose allows a better adaptation and survival (5). In support of this concept, cardiac deletion of GLUT4 leads to a lower tolerance to ischemic events associated with a higher rate of ATP depletion (65). Indeed, ischemic insults acutely caused the rapid release of Nrg1β from microendothelial cells and phosphorylation of ErbB4 (15, 36), and Nrg1β ablation in endothelial cells aggravated the harmful consequences of ischemia (38), whereas intravenous injections of the EGF-like domain of Nrg1β or GGF2 improved ventricular function in rat and swine models of myocardial infarction (18, 27, 41). Our present findings suggest that an increase in glucose uptake is one of the protective mechanisms induced by Nrg1β in these conditions.

The ability of Nrg1β to stimulate glucose uptake has been reported previously for a skeletal muscle cell line (8, 64), and consistent with those in vitro studies, acute infusion of GGF2 or Nrg1β was recently shown to lower blood glucose in swine (18), rats (6), and a mouse model of type 2 diabetes (14). Whereas in L6E9 myotubes PKCζ was implicated in the glucose uptake response, here we show that in cardiomyocytes Akt activation is implicated, because Nrg1β increases AS160 phosphorylation, and the Akt inhibitor VIII abolishes this as well as the glucose uptake response. Another new finding of our study is that Nrg1β activates mTORC2 because it phosphorylated the mTORC2-specific site Ser^{473} of Akt in a PP242-sensitive manner. However, consistent with our recently published in vivo data in adult mice (63), Akt-p-Ser^{473} phosphorylation appears to not be needed for phosphorylation of substrates involved in glucose uptake. This conclusion is supported by our observation that rictor knockdown efficiently reduces Akt-p-Ser^{473} without having any effects on AS160 phosphorylation and glucose uptake. Thus, whereas a role has previously been attributed to mTORC2 in skeletal muscle (35, 40, 57), fat, and liver (24), our own data demonstrate that mTORC2 is not implicated in glucose uptake of the heart. In this setting, it should be mentioned that PI3K was recently reported to directly phosphorylate Akt at Ser^{473} and induce glucose transporter translocation (70), and thus mTORC2-dependent Ser^{473} phosphorylation of Akt appears to be dispensable in this pathway.

To the best of our knowledge, our study is the first to identify Nrg1β as an activator of PI3K/Akt-mediated glucose uptake in cardiac cells. We show unique features of this Nrg1β-induced pathway, such as its Das sensitivity, which was not observed in IGF-I-stimulated cells. Consistently, Nrg1β, but not IGF-I or insulin, induced phosphorylation of FAK at Tyr^{861}. LY did not block FAK phosphorylation, whereas Das and PP2 blocked phosphorylation of FAK and Akt as well as the glucose uptake response, suggesting that Src family kinases and FAK may be implicated either upstream of or in parallel to PI3K, consistent with previous studies in the heart (9) and noncardiac cells (42). Whether or not Src-dependent FAK-Tyr^{861} phosphorylation is implicated in transmitting the signal from ErbB to PI3K remains to be proven. Others have demonstrated that ErbB activation may also directly stimulate PI3K in cardiomyocytes (70).

Our observation that Nrg1β rapidly increases FAK-p- Tyr^{861} is consistent with a previous study on adult cardiomyocytes (36). In contrast to that study, phosphorylation of c-Src at Tyr^{416} was high in our unstimulated NRVMs, and Nrg1β did not increase this further. Das decreased c-Src-p-Tyr^{416}, suggesting that it was already active under basal conditions in our

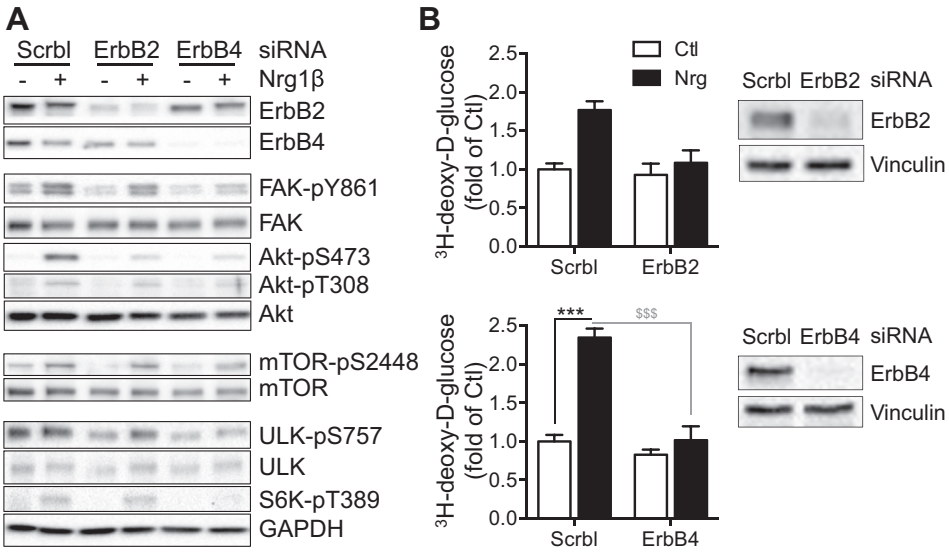

Fig. 8. The Nrg1β-stimulated glucose uptake is mediated by the ErbB2/ErbB4 heterodimer. *A*: ErbB2 and ErbB4 receptors were downregulated with pools of specific siRNAs. WB analysis was performed to assess the efficiency of the ErbB2 and ErbB4 knockdown as well as the effects on mTORC1 and mTORC2 targets. *B*: glucose uptake was measured as in Fig. 3 at 2 days after the siRNA transfection. ***$P < 0.001$, Nrg-treated vs. control; $$$$P < 0.001$, inhibitor- vs. corresponding DMSO-treated control.

model. On the other hand and consistent with Kuramochi et al. (36), Nrg1β increased the signal detected with an antibody to Src-p-Tyr^{215}. PP2 and Das, but not PP3, blocked this increase as well as the glucose uptake response. However, our observation that this phosphorylation happens later than the Akt phosphorylation excludes its role in the specific activation by ErbB2/ErbB4. We conclude that the presence of a PP2/Das-sensitive kinase, but most likely not c-Src, is important for the phosphorylation of FAK at Tyr^{861} and the glucose uptake response to Nrg1β, although the causal relationship between FAK-p-Tyr^{861} and Akt remains to be proven.

Interestingly, we found that phosphorylation of FAK at Tyr^{861} by Nrg1β does not depend on FAK phosphorylation at Tyr^{397}, a site that autophosphorylates upon integrin stimulation and leads to additional phosphorylation events after Src family kinase recruitment to SH2 domains. Our conclusion is supported by the observation that PF reduces integrin-related FAK-p-Tyr^{397} and paxillin-p-Tyr^{118} but not the Nrg1β-induced phosphorylation of FAK at Tyr^{861}. Differential inhibition by PF of these two phosphorylation events has also been reported for lung and breast cancer cells (28, 33). Thus, Nrg1β induces FAK phosphorylation independently of the classical integrin pathway.

A limitation of our own as well as other studies with different cell types and hormonal stimuli (32, 54, 71) is that pharmacological inhibition was used to implicate Src family kinases in glucose uptake responses. Since PP2 and Das, besides inhibiting multiple Src family kinases, have recently been described to have off-target effects, further studies are needed to determine which kinases inhibited by PP2 and Das are responsible for FAK-Tyr^{861} phosphorylation and the glucose uptake response to Nrg1β. It also remains possible that although the time course and PP2/Das sensitivity of FAK-Tyr^{861} phosphorylation parallels that of Akt and AS160 phosphorylation, FAK is not causally implicated in the glucose uptake. Moreover, it is also possible that ErbB directly activates PI3K (55).

Taken together, we show that Nrg1β enhances glucose uptake via ErbB2/ErbB4, PI3Kα, Akt, and AS160 (Fig. 9) and that these effects are sensitive to PP2 and Das. These novel insights provide a basis for future experimental and clinical studies in which this pathway may be exploited to increase glucose uptake, especially in states of irresponsiveness to insulin.

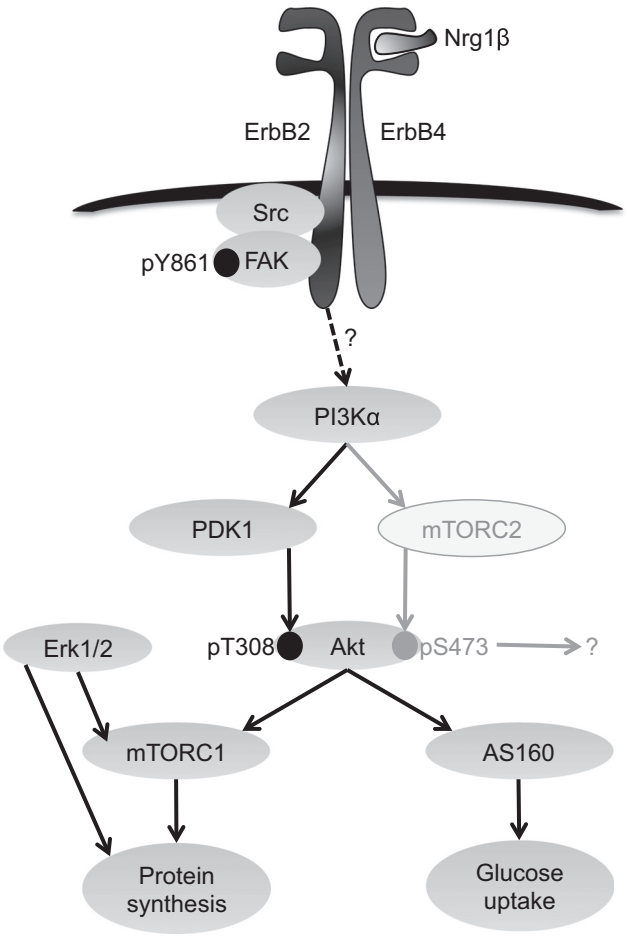

Fig. 9. Working model for the pathways that link Nrg1β to glucose uptake in cardiomyocytes.

ACKNOWLEDGMENTS

Present address of L. Pentassuglia: Acorda Therapeutics, Inc., 420 Saw Mill River Rd., Ardsley, NY 10502.

GRANTS

This work was supported by Swiss National Science Foundation Grant No. 31-135559/1, the "Stiftung für kardiovaskuläre Forschung Basel," and a career grant from the University of Basel to L. Pentassuglia.

DISCLOSURES

No conflicts of interest, financial or otherwise, are declared by the authors.

AUTHOR CONTRIBUTIONS

L.P., P.H., and M.B. conception and design of research; L.P., P.H., S.L., C.M., and L.X. performed experiments; L.P., P.H., C.M., and M.B. analyzed data; L.P., P.H., and M.B. interpreted results of experiments; L.P., P.H., and M.B. prepared figures; L.P. drafted manuscript; L.P., P.H., S.L., C.M., L.X., and M.B. edited and revised manuscript; L.P., P.H., S.L., C.M., L.X., and M.B. approved final version of manuscript.

REFERENCES

1. **Antonescu CN, Huang C, Niu W, Liu Z, Eyers PA, Heidenreich KA, Bilan PJ, Klip A.** Reduction of insulin-stimulated glucose uptake in L6 myotubes by the protein kinase inhibitor SB203580 is independent of p38MAPK activity. *Endocrinology* 146: 3773–3781, 2005.
2. **Baliga RR, Pimental DR, Zhao YY, Simmons WW, Marchionni MA, Sawyer DB, Kelly RA.** NRG-1-induced cardiomyocyte hypertrophy. Role of PI-3-kinase, $p70^{S6K}$, and MEK-MAPK-RSK. *Am J Physiol Heart Circ Physiol* 277: H2026–H2037, 1999.
3. **Bersell K, Arab S, Haring B, Kuhn B.** Neuregulin1/ErbB4 signaling induces cardiomyocyte proliferation and repair of heart injury. *Cell* 138: 257–270, 2009.
4. **Brandvold KR, Steffey ME, Fox CC, Soellner MB.** Development of a highly selective c-Src kinase inhibitor. *ACS Chem Biol* 7: 1393–1398, 2012.
5. **Broderick TL, Quinney HA, Barker CC, Lopaschuk GD.** Beneficial effect of carnitine on mechanical recovery of rat hearts reperfused after a transient period of global ischemia is accompanied by a stimulation of glucose oxidation. *Circulation* 87: 972–981, 1993.
6. **Caillaud K, Boisseau N, Ennequin G, Chavanelle V, Etienne M, Li X, Denis P, Dardevet D, Lacampagne A, Sirvent P.** Neuregulin 1 improves glucose tolerance in adult and old rats. *Diabetes Metab*. In press.
7. **Calalb MB, Zhang X, Polte TR, Hanks SK.** Focal adhesion kinase tyrosine-861 is a major site of phosphorylation by Src. *Biochem Biophys Res Commun* 228: 662–668, 1996.
8. **Canto C, Suarez E, Lizcano JM, Grino E, Shepherd PR, Fryer LG, Carling D, Bertran J, Palacin M, Zorzano A, Guma A.** Neuregulin signaling on glucose transport in muscle cells. *J Biol Chem* 279: 12260–12268, 2004.
9. **Clemente CF, Xavier-Neto J, Dalla Costa AP, Consonni SR, Antunes JE, Rocco SA, Pereira MB, Judice CC, Strauss B, Joazeiro PP, Matos-Souza JR, Franchini KG.** Focal adhesion kinase governs cardiac concentric hypertrophic growth by activating the AKT and mTOR pathways. *J Mol Cell Cardiol* 52: 493–501, 2012.
10. **Cornu M, Albert V, Hall MN.** mTOR in aging, metabolism, and cancer. *Curr Opin Genet Dev* 23: 53–62, 2013.
11. **Cote GM, Miller TA, Lebrasseur NK, Kuramochi Y, Sawyer DB.** Neuregulin-1alpha and beta isoform expression in cardiac microvascular endothelial cells and function in cardiac myocytes in vitro. *Exp Cell Res* 311: 135–146, 2005.
12. **Crone SA, Zhao YY, Fan L, Gu Y, Minamisawa S, Liu Y, Peterson KL, Chen J, Kahn R, Condorelli G, Ross J Jr, Chien KR, Lee KF.** ErbB2 is essential in the prevention of dilated cardiomyopathy. *Nat Med* 8: 459–465, 2002.
13. **Davies SP, Reddy H, Caivano M, Cohen P.** Specificity and mechanism of action of some commonly used protein kinase inhibitors. *Biochem J* 351: 95–105, 2000.
14. **Ennequin G, Boisseau N, Caillaud K, Chavanelle V, Etienne M, Li X, Sirvent P.** Neuregulin 1 Improves Glucose Tolerance in db/db Mice. *PLoS One* 10: e0130568, 2015.
15. **Fang SJ, Wu XS, Han ZH, Zhang XX, Wang CM, Li XY, Lu LQ, Zhang JL.** Neuregulin-1 preconditioning protects the heart against ischemia/reperfusion injury through a PI3K/Akt-dependent mechanism. *Chin Med J (Engl)* 123: 3597–3604, 2010.
16. **Fukazawa R, Miller TA, Kuramochi Y, Frantz S, Kim YD, Marchionni MA, Kelly RA, Sawyer DB.** Neuregulin-1 protects ventricular myocytes from anthracycline-induced apoptosis via erbB4-dependent activation of PI3-kinase/Akt. *J Mol Cell Cardiol* 35: 1473–1479, 2003.
17. **Fuller SJ, Sivarajah K, Sugden PH.** ErbB receptors, their ligands, and the consequences of their activation and inhibition in the myocardium. *J Mol Cell Cardiol* 44: 831–854, 2008.
18. **Galindo CL, Kasasbeh E, Murphy A, Ryzhov S, Lenihan S, Ahmad FA, Williams P, Nunnally A, Adcock J, Song Y, Harrell FE, Tran TL, Parry TJ, Iaci J, Ganguly A, Feoktistov I, Stephenson MK, Caggiano AO, Sawyer DB, Cleator JH.** Anti-remodeling and anti-fibrotic effects of the neuregulin-1β glial growth factor 2 in a large animal model of heart failure. *J Am Heart Assoc* 3: e000773, 2014.
19. **Galindo CL, Ryzhov S, Sawyer DB.** Neuregulin as a heart failure therapy and mediator of reverse remodeling. *Curr Heart Fail Rep* 11: 40–49, 2014.
20. **Gao R, Zhang J, Cheng L, Wu X, Dong W, Yang X, Li T, Liu X, Xu Y, Li X, Zhou M.** A Phase II, randomized, double-blind, multicenter, based on standard therapy, placebo-controlled study of the efficacy and safety of recombinant human neuregulin-1 in patients with chronic heart failure. *J Am Coll Cardiol* 55: 1907–1914, 2010.
21. **Garcia-Rivello H, Taranda J, Said M, Cabeza-Meckert P, Vila-Petroff M, Scaglione J, Ghio S, Chen J, Lai C, Laguens RP, Lloyd KC, Hertig CM.** Dilated cardiomyopathy in Erb-b4-deficient ventricular muscle. *Am J Physiol Heart Circ Physiol* 289: H1153–H1160, 2005.
22. **Gordon LI, Burke MA, Singh AT, Prachand S, Lieberman ED, Sun L, Naik TJ, Prasad SV, Ardehali H.** Blockade of the erbB2 receptor induces cardiomyocyte death through mitochondrial and reactive oxygen species-dependent pathways. *J Biol Chem* 284: 2080–2087, 2009.
23. **Grazette LP, Boecker W, Matsui T, Semigran M, Force TL, Hajjar RJ, Rosenzweig A.** Inhibition of ErbB2 causes mitochondrial dysfunction in cardiomyocytes: implications for herceptin-induced cardiomyopathy. *J Am Coll Cardiol* 44: 2231–2238, 2004.
24. **Hagiwara A, Cornu M, Cybulski N, Polak P, Betz C, Trapani F, Terracciano L, Heim MH, Ruegg MA, Hall MN.** Hepatic mTORC2 activates glycolysis and lipogenesis through Akt, glucokinase, and SREBP1c. *Cell Metab* 15: 725–738, 2012.
25. **Hao J, Galindo CL, Tran TL, Sawyer DB.** Neuregulin-1beta induces embryonic stem cell cardiomyogenesis via ErbB3/ErbB2 receptors. *Biochem J* 458: 335–341, 2014.
26. **Hauselmann SP, Rosc-Schlüter BI, Lorenz V, Plaisance I, Brink M, Pfister O, Kuster GM.** β1-Integrin is up-regulated via Rac1-dependent reactive oxygen species as part of the hypertrophic cardiomyocyte response. *Free Radic Biol Med* 51: 609–618, 2011.
27. **Hill MF, Patel AV, Murphy A, Smith HM, Galindo CL, Pentassuglia L, Peng X, Lenneman CG, Odiete O, Friedman DB, Kronenberg MW, Zheng S, Zhao Z, Song Y, Harrell FE Jr, Srinivas M, Ganguly A, Iaci J, Parry TJ, Caggiano AO, Sawyer DB.** Intravenous glial growth factor 2 (GGF2) isoform of neuregulin-1β improves left ventricular function, gene and protein expression in rats after myocardial infarction. *PLoS One* 8: e55741, 2013.
28. **Hiscox S, Barnfather P, Hayes E, Bramble P, Christensen J, Nicholson RI, Barrett-Lee P.** Inhibition of focal adhesion kinase suppresses the adverse phenotype of endocrine-resistant breast cancer cells and improves endocrine response in endocrine-sensitive cells. *Breast Cancer Res Treat* 125: 659–669, 2011.
29. **Hsieh IS, Yang RS, Fu WM.** Osteopontin upregulates the expression of glucose transporters in osteosarcoma cells. *PLoS One* 9: e109550, 2014.
30. **Jabbour A, Hayward CS, Keogh AM, Kotlyar E, McCrohon JA, England JF, Amor R, Liu X, Li XY, Zhou MD, Graham RM, Macdonald PS.** Parenteral administration of recombinant human neuregulin-1 to patients with stable chronic heart failure produces favourable acute and chronic haemodynamic responses. *Eur J Heart Fail* 13: 83–92, 2011.
31. **Jaswal JS, Keung W, Wang W, Ussher JR, Lopaschuk GD.** Targeting fatty acid and carbohydrate oxidation—a novel therapeutic intervention in the ischemic and failing heart. *Biochim Biophys Acta* 1813: 1333–1350, 2011.
32. **Kanda Y, Watanabe Y.** Thrombin-induced glucose transport via Src-p38 MAPK pathway in vascular smooth muscle cells. *Br J Pharmacol* 146: 60–67, 2005.

33. **Kline ER, Shupe J, Gilbert-Ross M, Zhou W, Marcus AI.** LKB1 represses focal adhesion kinase (FAK) signaling via a FAK-LKB1 complex to regulate FAK site maturation and directional persistence. *J Biol Chem* 288: 17663–17674, 2013.
34. **Kohn AD, Summers SA, Birnbaum MJ, Roth RA.** Expression of a constitutively active Akt Ser/Thr kinase in 3T3-L1 adipocytes stimulates glucose uptake and glucose transporter 4 translocation. *J Biol Chem* 271: 31372–31378, 1996.
35. **Kumar A, Harris TE, Keller SR, Choi KM, Magnuson MA, Lawrence JC Jr..** Muscle-specific deletion of rictor impairs insulin-stimulated glucose transport and enhances Basal glycogen synthase activity. *Mol Cell Biol* 28: 61–70, 2008.
36. **Kuramochi Y, Guo X, Sawyer DB.** Neuregulin activates erbB2-dependent src/FAK signaling and cytoskeletal remodeling in isolated adult rat cardiac myocytes. *J Mol Cell Cardiol* 41: 228–235, 2006.
37. **Laplante M, Sabatini DM.** mTOR signaling in growth control and disease. *Cell* 149: 274–293, 2012.
38. **Lemmens K, Doggen K, De Keulenaer GW.** Activation of the neuregulin/ErbB system during physiological ventricular remodeling in pregnancy. *Am J Physiol Heart Circ Physiol* 300: H931–H942, 2011.
39. **Lionetti V, Stanley WC, Recchia FA.** Modulating fatty acid oxidation in heart failure. *Cardiovasc Res* 90: 202–209, 2011.
40. **Liu H, Liu R, Xiong Y, Li X, Wang X, Ma Y, Guo H, Hao L, Yao P, Liu L, Wang D, Yang X.** Leucine facilitates the insulin-stimulated glucose uptake and insulin signaling in skeletal muscle cells: involving mTORC1 and mTORC2. *Amino Acids* 46: 1971–1979, 2014.
41. **Liu X, Gu X, Li Z, Li X, Li H, Chang J, Chen P, Jin J, Xi B, Chen D, Lai D, Graham RM, Zhou M.** Neuregulin-1/erbB-activation improves cardiac function and survival in models of ischemic, dilated, and viral cardiomyopathy. *J Am Coll Cardiol* 48: 1438–1447, 2006.
42. **Liu X, Marengere LE, Koch CA, Pawson T.** The v-Src SH3 domain binds phosphatidylinositol 3′-kinase. *Mol Cell Biol* 13: 5225–5232, 1993.
43. **Mendes-Ferreira P, De Keulenaer GW, Leite-Moreira AF, Brás-Silva C.** Therapeutic potential of neuregulin-1 in cardiovascular disease. *Drug Discov Today* 18: 836–842, 2013.
44. **Mieulet V, Lamb RF.** Tuberous sclerosis complex: linking cancer to metabolism. *Trends Mol Med* 16: 329–335, 2010.
45. **Odiete O, Hill MF, Sawyer DB.** Neuregulin in cardiovascular development and disease. *Circ Res* 111: 1376–1385, 2012.
46. **Opie LH.** Effects of regional ischemia on metabolism of glucose and fatty acids. Relative rates of aerobic and anaerobic energy production during myocardial infarction and comparison with effects of anoxia. *Circ Res* 38: I52–I74, 1976.
47. **Ozcelik C, Erdmann B, Pilz B, Wettschureck N, Britsch S, Hubner N, Chien KR, Birchmeier C, Garratt AN.** Conditional mutation of the ErbB2 (HER2) receptor in cardiomyocytes leads to dilated cardiomyopathy. *Proc Natl Acad Sci USA* 99: 8880–8885, 2002.
48. **Pentassuglia L, Graf M, Lane H, Kuramochi Y, Cote G, Timolati F, Sawyer DB, Zuppinger C, Suter TM.** Inhibition of ErbB2 by receptor tyrosine kinase inhibitors causes myofibrillar structural damage without cell death in adult rat cardiomyocytes. *Exp Cell Res* 315: 1302–1312, 2009.
49. **Pentassuglia L, Sawyer DB.** ErbB/integrin signaling interactions in regulation of myocardial cell-cell and cell-matrix interactions. *Biochim Biophys Acta* 1833: 909–916, 2013.
50. **Pentassuglia L, Sawyer DB.** The role of Neuregulin-1beta/ErbB signaling in the heart. *Exp Cell Res* 315: 627–637, 2009.
51. **Pentassuglia L, Timolati F, Seifriz F, Abudukadier K, Suter TM, Zuppinger C.** Inhibition of ErbB2/neuregulin signaling augments paclitaxel-induced cardiotoxicity in adult ventricular myocytes. *Exp Cell Res* 313: 1588–1601, 2007.
52. **Podsypanina K, Lee RT, Politis C, Hennessy I, Crane A, Puc J, Neshat M, Wang H, Yang L, Gibbons J, Frost P, Dreisbach V, Blenis J, Gaciong Z, Fisher P, Sawyers C, Hedrick-Ellenson L, Parsons R.** An inhibitor of mTOR reduces neoplasia and normalizes p70/S6 kinase activity in Pten+/− mice. *Proc Natl Acad Sci USA* 98: 10320–10325, 2001.
53. **Polizzotti BD, Ganapathy B, Walsh S, Choudhury S, Ammanamanchi N, Bennett DG, dos Remedios CG, Haubner BJ, Penninger JM, Kühn B.** Neuregulin stimulation of cardiomyocyte regeneration in mice and human myocardium reveals a therapeutic window. *Sci Transl Med* 7: 281ra45, 2015.
54. **Rosenzweig T, Aga-Mizrachi S, Bak A, Sampson SR.** Src tyrosine kinase regulates insulin-induced activation of protein kinase C (PKC) delta in skeletal muscle. *Cell Signal* 16: 1299–1308, 2004.
55. **Roskoski R Jr.** The ErbB/HER family of protein-tyrosine kinases and cancer. *Pharmacol Res* 79: 34–74, 2014.
56. **Sano H, Kane S, Sano E, Miinea CP, Asara JM, Lane WS, Garner CW, Lienhard GE.** Insulin-stimulated phosphorylation of a Rab GTPase-activating protein regulates GLUT4 translocation. *J Biol Chem* 278: 14599–14602, 2003.
57. **Sato M, Dehvari N, Oberg AI, Dallner OS, Sandström AL, Olsen JM, Csikasz RI, Summers RJ, Hutchinson DS, Bengtsson T.** Improving type 2 diabetes through a distinct adrenergic signaling pathway involving mTORC2 that mediates glucose uptake in skeletal muscle. *Diabetes* 63: 4115–4129, 2014.
58. **Sawyer DB, Caggiano A.** Neuregulin-1beta for the treatment of systolic heart failure. *J Mol Cell Cardiol* 51: 501–505, 2011.
59. **Sawyer DB, Zuppinger C, Miller TA, Eppenberger HM, Suter TM.** Modulation of anthracycline-induced myofibrillar disarray in rat ventricular myocytes by neuregulin-1beta and anti-erbB2: potential mechanism for trastuzumab-induced cardiotoxicity. *Circulation* 105: 1551–1554, 2002.
60. **Schaller MD, Hildebrand JD, Shannon JD, Fox JW, Vines RR, Parsons JT.** Autophosphorylation of the focal adhesion kinase, pp125FAK, directs SH2-dependent binding of pp60src. *Mol Cell Biol* 14: 1680–1688, 1994.
61. **Schlaepfer DD, Hunter T.** Evidence for in vivo phosphorylation of the Grb2 SH2-domain binding site on focal adhesion kinase by Src-family protein-tyrosine kinases. *Mol Cell Biol* 16: 5623–5633, 1996.
62. **Shende P, Plaisance I, Morandi C, Pellieux C, Berthonneche C, Zorzato F, Krishnan J, Lerch R, Hall MN, Ruegg MA, Pedrazzini T, Brink M.** Cardiac raptor ablation impairs adaptive hypertrophy, alters metabolic gene expression, and causes heart failure in mice. *Circulation* 123: 1073–1082, 2011.
63. **Shende P, Xu L, Morandi C, Pentassuglia L, Heim P, Lebboukh S, Berthonneche C, Pedrazzini T, Kaufmann BA, Hall MN, Ruegg MA, Brink M.** Cardiac mTOR complex 2 preserves ventricular function in pressure-overload hypertrophy. *Cardiovasc Res* 109: 103–114, 2016.
64. **Suarez E, Bach D, Cadefau J, Palacin M, Zorzano A, Guma A.** A novel role of neuregulin in skeletal muscle. Neuregulin stimulates glucose uptake, glucose transporter translocation, and transporter expression in muscle cells. *J Biol Chem* 276: 18257–18264, 2001.
65. **Tian R, Abel ED.** Responses of GLUT4-deficient hearts to ischemia underscore the importance of glycolysis. *Circulation* 103: 2961–2966, 2001.
66. **Timolati F, Ott D, Pentassuglia L, Giraud MN, Perriard JC, Suter TM, Zuppinger C.** Neuregulin-1 beta attenuates doxorubicin-induced alterations of excitation-contraction coupling and reduces oxidative stress in adult rat cardiomyocytes. *J Mol Cell Cardiol* 41: 845–854, 2006.
67. **Tomioka H, Mukohara T, Kataoka Y, Ekyalongo RC, Funakoshi Y, Imai Y, Kiyota N, Fujiwara Y, Minami H.** Inhibition of the mTOR/S6K signal is necessary to enhance fluorouracil-induced apoptosis in gastric cancer cells with HER2 amplification. *Int J Oncol* 41: 551–558, 2012.
68. **Tremblay F, Gagnon A, Veilleux A, Sorisky A, Marette A.** Activation of the mammalian target of rapamycin pathway acutely inhibits insulin signaling to Akt and glucose transport in 3T3-L1 and human adipocytes. *Endocrinology* 146: 1328–1337, 2005.
69. **Tremblay F, Marette A.** Amino acid and insulin signaling via the mTOR/p70 S6 kinase pathway. A negative feedback mechanism leading to insulin resistance in skeletal muscle cells. *J Biol Chem* 276: 38052–38060, 2001.
70. **Tsuchiya A, Kanno T, Nishizaki T.** PI3 kinase directly phosphorylates Akt1/2 at Ser473/474 in the insulin signal transduction pathway. *J Endocrinol* 220: 49–59, 2014.
71. **Valle-Casuso JC, Gonzalez-Sanchez A, Medina JM, Tabernero A.** HIF-1 and c-Src mediate increased glucose uptake induced by endothelin-1 and connexin43 in astrocytes. *PLoS One* 7: e32448, 2012.
72. **Vicier C, Dieci MV, Arnedos M, Delaloge S, Viens P, Andre F.** Clinical development of mTOR inhibitors in breast cancer. *Breast Cancer Res* 16: 203, 2014.
73. **Wadugu B, Kuhn B.** The role of neuregulin/ErbB2/ErbB4 signaling in the heart with special focus on effects on cardiomyocyte proliferation. *Am J Physiol Heart Circ Physiol* 302: H2139–H2147, 2012.
74. **Wang X, Yue P, Kim YA, Fu H, Khuri FR, Sun SY.** Enhancing mammalian target of rapamycin (mTOR)-targeted cancer therapy by

preventing mTOR/raptor inhibition-initiated, mTOR/rictor-independent Akt activation. *Cancer Res* 68: 7409–7418, 2008.

75. **Young LH, Renfu Y, Russell R, Hu X, Caplan M, Ren J, Shulman GI, Sinusas AJ.** Low-flow ischemia leads to translocation of canine heart GLUT-4 and GLUT-1 glucose transporters to the sarcolemma in vivo. *Circulation* 95: 415–422, 1997.
76. **Zagozdzon R, Bougeret C, Fu Y, Avraham HK.** Overexpression of the Csk homologous kinase facilitates phosphorylation of Akt/PKB in MCF-7 cells. *Int J Oncol* 21: 1347–1352, 2002.
77. **Zhang D, Contu R, Latronico MV, Zhang JL, Rizzi R, Catalucci D, Miyamoto S, Huang K, Ceci M, Gu Y, Dalton ND, Peterson KL, Guan KL, Brown JH, Chen J, Sonenberg N, Condorelli G.** MTORC1 regulates cardiac function and myocyte survival through 4E-BP1 inhibition in mice. *J Clin Invest* 120: 2805–2816, 2010.
78. **Zhao YY, Sawyer DR, Baliga RR, Opel DJ, Han X, Marchionni MA, Kelly RA.** Neuregulins promote survival and growth of cardiac myocytes. Persistence of ErbB2 and ErbB4 expression in neonatal and adult ventricular myocytes. *J Biol Chem* 273: 10261–10269, 1998.
79. **Zhou X, Tan M, Stone Hawthorne V, Klos KS, Lan KH, Yang Y, Yang W, Smith TL, Shi D, Yu D.** Activation of the Akt/mammalian target of rapamycin/4E-BP1 pathway by ErbB2 overexpression predicts tumor progression in breast cancers. *Clin Cancer Res* 10: 6779–6788, 2004.

Cardiovascular Research (2016) **109**, 103–114
doi:10.1093/cvr/cvv252

Cardiac mTOR complex 2 preserves ventricular function in pressure-overload hypertrophy

Pankaj Shende[1†], Lifen Xu[1†], Christian Morandi[1†], Laura Pentassuglia[1], Philippe Heim[1], Sonia Lebboukh[1], Corinne Berthonneche[2], Thierry Pedrazzini[2], Beat A. Kaufmann[1], Michael N. Hall[3], Markus A. Rüegg[3], and Marijke Brink[1]*

[1]Department of Biomedicine, University of Basel and University Hospital Basel, Hebelstrasse 20, CH-4031 Basel, Switzerland; [2]Department of Medicine and Cardiovascular Assessment Facility, University of Lausanne Medical School, Lausanne, Switzerland; and [3]Biozentrum, University of Basel, Basel, Switzerland

Received 8 January 2015; revised 16 October 2015; accepted 6 November 2015; online publish-ahead-of-print 23 November 2015

Time for primary review: 43 days

Aims Mammalian target of rapamycin (mTOR), a central regulator of growth and metabolism, has tissue-specific functions depending on whether it is part of mTOR complex 1 (mTORC1) or mTORC2. We have previously shown that mTORC1 is required for adaptive cardiac hypertrophy and maintenance of function under basal and pressure-overload conditions. In the present study, we aimed to identify functions of mTORC2 in the heart.

Methods and results Using tamoxifen-inducible cardiomyocyte-specific gene deletion, we generated mice deficient for cardiac rapamycin-insensitive companion of mTOR (rictor), an essential and specific component of mTORC2. Under basal conditions, rictor deficiency did not affect cardiac growth and function in young mice and also had no effects in adult mice. However, transverse aortic constriction caused dysfunction in the rictor-deficient hearts, whereas function was maintained in controls after 1 week of pressure overload. Adaptive increases in cardiac weight and cardiomyocyte cross-sectional area, fibrosis, and hypertrophic and metabolic gene expression were not different between the rictor-deficient and control mice. In control mice, maintained function was associated with increased protein levels of rictor, protein kinase C (PKC)βII, and PKCδ, whereas *rictor* ablation abolished these increases. *Rictor* deletion also significantly decreased PKCε at baseline and after pressure overload. Our data suggest that reduced PKCε and the inability to increase PKCβII and PKCδ abundance are, in accordance with their known function, responsible for decreased contractile performance of the rictor-deficient hearts.

Conclusion Our study demonstrates that mTORC2 is implicated in maintaining contractile function of the pressure-overloaded male mouse heart.

Keywords Heart failure • Hypertrophy • Metabolism • Signal transduction

1. Introduction

Recent studies have identified mammalian target of rapamycin (mTOR) as an important regulator of cardiac adaptations to pressure overload.[1] mTOR, an evolutionary conserved serine/threonine kinase belonging to the phosphatidylinositol 3-kinase (PI3K)-related kinase family of proteins, matches cell growth and metabolism with environmental resources and other cues.[2] Thus, it senses nutrient and energy status, growth factors, oxygen levels and stress, and adapts a range of cellular functions related to growth and metabolism correspondingly. In line with its important regulatory function, mTOR overexpression is protective in pressure-overloaded mouse hearts,[3] whereas conditional mTOR deletion causes cardiac dysfunction.[4]

mTOR has different functions depending on whether it is part of the multiprotein complex termed mTOR complex 1 (mTORC1) or mTORC2.[5,6] We recently showed that raptor (regulatory-associated protein of mTOR) is required for basal cardiac function and that adequate mTORC1 activity is even more critical in the pressure-overloaded heart. Reduced mTORC1 activity in raptor-deficient cardiomyocytes leads to heart failure and death within 2 weeks of aortic constriction.[7] While increased autophagy and apoptosis as well as changed metabolism were observed in the raptor-deficient hearts, one of the primary reasons

* Corresponding author. Tel: +41 61 265 33 61; fax: +41 61 265 23 50, E-mail: marijke.brink@unibas.ch

† The first three authors equally contributed to this work.

for the observed dysfunction is reduced protein synthesis and a lack of adaptive hypertrophy.[7]

Much less is known about mTORC2 owing to the unavailability of selective inhibitors. Early work demonstrated that by phosphorylating members of the AGC kinase family such as protein kinase C (PKC), PKB/Akt, and SGK1, mTORC2 regulates cytoskeletal actin organization, cell survival, and other processes.[8] The availability of tissue-specific knockout models for essential components of mTORC2 has recently given more insights into the *in vivo* functions of mTORC2 for some tissues. Knockout of the mTORC2 component rapamycin-insensitive companion of mTOR (rictor) in skeletal muscle showed either no phenotype[9] or impaired insulin-stimulated glucose transport and enhanced glycogen synthase activity.[10] Adipose-specific rictor-deficient mice showed increased body size, an enlarged pancreas, and hyperinsulinaemia,[10,11] whereas liver-specific rictor knockout mice revealed that mTORC2 regulates hepatic glucose and lipid metabolism.[12] mTORC2 was recently also shown to regulate size, shape, and synaptic plasticity of neurons[13,14] as well as oligodendrocyte differentiation.[15] These and other studies demonstrate that the functions of mTORC2 are diverse and specific for the tissue or cell type being analysed.

The mTORC1 inhibitor rapamycin is used as an immunosuppressant and an anticancer drug, and the interest to use it for ageing-related disease including cardiac disease is also high. Notably, rapamycin does not fully block mTORC1[16] and it was reported to activate mTORC2 and Akt, which may be anti-apoptotic.[17] On the other hand, long-term rapamycin treatment can also inhibit mTORC2.[18,19] Our present study therefore aims to uncover the cardiac function of rictor/mTORC2 using a conditional knockout approach. We report that deletion of *rictor* from cardiomyocytes inactivates mTORC2, but does not modify basal cardiac function and geometry during postnatal growth and up to an age of 54 weeks. However, rictor-deficient hearts perform less well when challenged by aortic constriction-induced pressure overload, despite the fact that their reactive hypertrophy is similar as in controls. Our data suggest that mTORC2 is implicated in the contractile response to pathological haemodynamic stress and further molecular analyses point to PKCβII and PKCδ as effectors of mTORC2 in our model.

2. Methods

2.1 Animals

Male rictor knockout and control mice on a C57BL/6 background were generated using tamoxifen-inducible Cre-recombinase under control of the cardiomyocyte-specific α-myosin heavy chain (MHC) promoter.[7] Transverse aortic constriction (TAC) and echocardiography were performed as published, using ketamine/xylazine and isoflurane, respectively.[7] Animal experiments were performed according to Guidelines for the Care and Use of Laboratory Animals and with approval of the Swiss Cantonal Authorities.

2.2 Cardiomyocyte isolation

Cardiomyocytes were isolated from control and cardiac rictor knockout (rictor-cKO) mice at 12 weeks of age as published.[20]

2.3 Protein and RNA analysis

Equal amounts of protein or RNA extracted from tissues and cultured cardiomyocytes were analysed by immunoblotting and quantitative real-time PCR as reported.[7]

2.4 Microscopic analysis

Paraffin sections of 4% paraformaldehyde-fixed tissue were processed for Picrosirius red staining to visualize fibrosis. Deoxynucleotidyl transferase dUTP nick end-labelling (TUNEL) assay was performed using an *in situ* apoptosis detection kit (Roche Diagnostics, Rotkreuz, Switzerland). Wheat germ agglutinin (WGA) staining, collagen, and caspase-3 labelling were done on cryosections fixed with 4% paraformaldehyde.[7] Cross-sectional areas were quantified by measuring at least 100 cardiomyocytes in three independent sections of 3–4 mice per group.

2.5 Statistical analysis

Data are presented as mean ± SEM. Differences in means were evaluated with two-way ANOVA (*P*-values in text), followed by Sidak's multiple comparisons tests (*P*-values in figures). For multiple measurements of the same mice, repeated-measures ANOVA was used. All statistics was performed with GraphPad Prism 6.0. *P*-values of <0.05 were considered statistically significant.

Detailed procedures, antibody sources, and buffer compositions are provided in Supplementary material online.

3. Results

3.1 Rictor deficiency does not affect cardiac weight, function, or geometry in adult mice up to 54 weeks of age or in growing young mice

To analyse the cardiac function of mTORC2, we generated cardiac-specific rictor knockout mice by crossing mice containing the floxed *rictor* gene[9,21] with mice transgenic for inducible cre-recombinase driven by the α-MHC promoter.[22] The resulting *rictor*$^{fl/fl}$ α-MHC-MerCreMer$^{Tg/0}$ mice were, at an age of 10 weeks, injected with tamoxifen to induce the deletion. These mice are hereafter referred to as rictor-cKO mice. Control mice (*rictor*$^{+/+}$ α-MHC-MerCreMer$^{Tg/0}$) underwent the same tamoxifen treatment. 18 days after the tamoxifen injections, rictor protein was lower in the rictor-cKO mice compared with the control mice in cardiac muscle, but not in skeletal muscle. Moreover, insulin-stimulated increases in Akt-pS473 were dramatically impaired while 4E-BP1 phosphorylation was not affected in the rictor-cKO hearts (*Figure 1A*). This confirms specificity of the deletion and efficient inactivation of mTORC2, because Ser473 in the hydrophobic motif (HM) of Akt is the best-established direct target of mTORC2. At this time point after induction of the deletion, no cardiac functional or geometric differences were revealed by ultrasound analysis between the control and rictor-cKO mice. To evaluate the consequences of prolonged mTORC2 inactivation under basal conditions, we performed echocardiography at 4, 6, 10, 16, and 25 weeks after tamoxifen to assess cardiac parameters at 14, 16, 20, 26, and 35 weeks of age (see Supplementary material online, *Figure S1A* and *Table S1*). At all time points, the ejection fraction (EF) and fractional shortening (FS) values of the rictor-cKO mice were similar to those of control mice. Systolic and diastolic septum and left ventricular (LV) posterior wall thickness, LV internal diameters, and LV mass-to-body weight ratios were also indistinguishable over the time period that these mice were followed. Consistently, *post-mortem* analysis at the age of 35 weeks revealed no differences in ventricular weight to tibia length ratios between the control and rictor-cKO mice. In an independent experiment with a different batch of mice, we found that even at 54 weeks of age, rictor-cKO mice were indistinguishable from control mice (*Table 1*). Notably, at both 35 and 54 weeks, rictor protein and mTORC2 activity, as assessed by the amount of Akt-pS473,

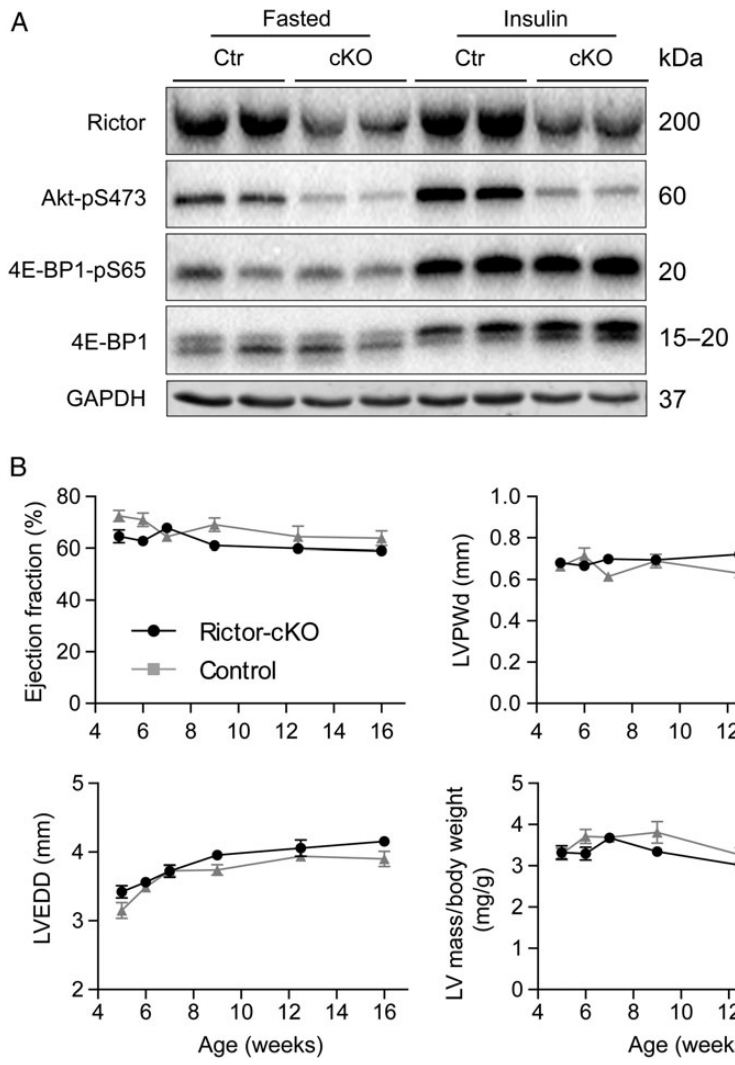

Figure 1 Baseline characterization of rictor-deficient mice at 18 days after induction of the deletion (*A*), and analysis of the consequences of rictor deficiency in young growing mice (*B*). (*A*) At 18 days after tamoxifen, overnight-fasted male mice were stimulated with vehicle ('fasted') or insulin for 2 h, sacrificed, and the left ventricle was dissected and snap-frozen for analysis by western blotting with antibodies as indicated. (*B*) Ultrasound measurements of EF, diastolic LV posterior wall thickness (LVPWd), LVEDD, and LV mass-to-body weight ratios are shown at the indicated ages. *Rictor* deletion at 10 (*A*) and 4 (*B*) weeks of age. Rictor-cKO: tamoxifen-injected α-MHC-MerCreMer/rictor$^{fl/fl}$ ($N = 9$). Controls: tamoxifen-injected α-MHC-MerCreMer/rictor$^{+/+}$ ($N = 4$). Statistical analysis: repeated-measures ANOVA.

were still significantly decreased (see Supplementary material online, *Figure S1B*).

As mTOR and Akt have been implicated in growth regulatory mechanisms, we next deleted cardiac *rictor* in growing mice at 4 weeks of age. We observed a normal increase in LV mass over time with no differences between the rictor-cKO and control mice. Cardiac growth was in proportion to whole body growth for both groups, as LV mass-to-body weight ratios were identical over time (*Figure 1B*). Moreover, EFs and all other echocardiographic parameters were normal during growth and up to an age of 16 weeks (see Supplementary material online, *Table S2*). Thus, rictor deficiency does not affect physiological cardiac growth in young mice and has no adverse effects on cardiac function in healthy adult mice kept under laboratory conditions up to 54 weeks of age, the latest time point analysed in our study.

3.2 Rictor deficiency accelerates the development of cardiac dysfunction after aortic constriction

The above data show that despite significant changes in Akt phosphorylation at Ser473, rictor-cKO mice have a virtually normal functional cardiac phenotype. We reasoned that mTORC2 may primarily function as a modulator of cardiac function during cardiac stress and therefore assessed the effect of rictor deficiency in the cardiac response to pathological pressure overload induced by TAC. Rictor-cKO and control mice were assigned randomly to sham or TAC groups for surgery at 18 or 19 days after tamoxifen. Echocardiography was performed before (see Supplementary material online, *Table S3*) and 1 week after TAC (*Figure 2A* and *Table 2*). Prior to TAC, no differences were detectable between any of the experimental groups. In the control mice, 1

Table 1 Echocardiographic parameters of control and rictor knockout mice at 54 weeks of age

	Control ($N = 6$)	Rictor-cKO ($N = 5$)
Echocardiography		
Heart rate (b.p.m.)	500 ± 28	563 ± 16
Anteroseptal wall thickness (mm)		
Diastole	0.97 ± 0.04	0.82 ± 0.07
Systole	1.36 ± 0.05	1.17 ± 0.11
LV wall thickness (mm)		
Diastole	0.75 ± 0.02	0.82 ± 0.04
Systole	1.05 ± 0.06	1.11 ± 0.07
LV internal diameter (mm)		
Diastole	4.11 ± 0.05	4.11 ± 0.2
Systole	2.88 ± 0.04	3.03 ± 0.24
Ejection fraction (%)	61.3 ± 1.4	55.9 ± 4.0
Fractional shortening (%)	32.6 ± 1.0	29.0 ± 2.7
Post-mortem analysis		
Body weight (g)	40.6 ± 1.6	39.8 ± 2.2
Ventricular weight (VW, mg)	123.2 ± 5.4	120.0 ± 5.9
VW/body weight (mg/mm)	3.05 ± 0.15	3.03 ± 0.09

Rictor deletion was induced in α-MHC-MerCreMer/rictor$^{fl/fl}$ mice at the age of 10 weeks by an intraperitoneal injection with tamoxifen for 5 consecutive days. Controls consisted of mice homozygous for the wild-type rictor gene (α-MHC-MerCreMer/rictor$^{+/+}$), injected with tamoxifen. Ultrasound analysis was performed at 44 weeks after tamoxifen. $N = 5$ for rictor-cKO and $N = 6$ for control.

week of TAC significantly increased the LV posterior and anteroseptal wall thickness while not changing the LV end-systolic and end-diastolic internal diameters. Moreover, the control mice maintained cardiac function after TAC, as their EF and FS values were similar to those measured after sham surgery. In the rictor-cKO, however, TAC significantly reduced EF and FS compared with sham-operated rictor-cKO or TAC-operated control mice. The rictor-cKO mice had higher LV end-diastolic diameters (LVEDD), an effect that was strongest at the end of systole. Moreover, although after TAC the rictor-cKO mice displayed increases in anteroseptal and LV posterior wall thickness, these increases were less pronounced than those measured in control mice. Taken together, these data indicate that the rictor-cKO mice developed signs of eccentric LV hypertrophy with a decline in cardiac function, whereas control mice were in the compensatory phase of hypertrophy after 1 week of TAC.

3.3 Rictor deficiency does not affect hypertrophy, fibrosis, or metabolic gene expression after TAC

Post-mortem analysis at 1 week after TAC revealed that the ventricular weight to tibia length ratios were not different between control and rictor-cKO mice. Thus, both groups produced similar increases in cardiac weight compared with the corresponding sham-operated groups (*Figure 2B*). In line with an unaltered hypertrophic response, atrial natriuretic peptide (ANP) and brain natriuretic peptide (BNP) were induced similarly in both groups (*Figure 2B* and *D*). TAC also increased skeletal muscle actin and decreased α-MHC mRNA levels but again, these changes happened irrespective of the absence or presence of rictor (*Figure 2C*). Notably, β-MHC mRNA transcript levels were higher in the rictor-cKO mice than in controls under sham and TAC conditions (*Figure 2C*), although the effect did not reach statistical significance at the protein level (*Figure 2D*). WGA labelling (*Figure 3A*), Picrosirius red staining (*Figure 3B*), collagen I (*Figure 3C*) and collagen III immunolabelling (not shown), as well as gene expression analysis (*Figure 3D* and see Supplementary material online, *Figure S2*) showed that cardiomyocyte cross-sectional areas, fibrosis, and metabolic gene expression were not affected by the *rictor* deletion. Thus, after 1 week of pressure overload, the altered geometry and decreased function of the rictor-deficient hearts is not associated with any differences in cardiac weight, fibrosis, or hypertrophic and metabolic gene expression compared with the control mice.

3.4 TAC increases rictor in control mice and rictor deficiency reduces protein levels of multiple PKC isoforms

Figure 4A shows that TAC caused a significant 1.65-fold increase in rictor protein in control mice, an observation that *per se* provides support for a role of rictor/mTORC2 in pressure-overload conditions. TAC also augmented rictor protein somewhat in the knockout mice ($P = 0.12$), which is explained by the fact that the gene is not excised from all cardiac cells.[22] To obtain insights into the mechanisms whereby mTORC2 supports cardiac function during pressure overload, we proceeded to analyse the phosphorylation state of several AGC kinases, direct targets of mTORC2, in cardiac protein extracts. Since rictor deficiency did not modify the hypertrophic growth response to TAC, we directed our attention to the PKC family of kinases, which have been implicated in metabolism and contractility.[23–25] One of the classical PKCs (cPKC), namely PKCα, is a well-established direct target of mTORC2,[26] and recent work shows that several other PKCs may also be regulated by mTORC2.[13] Given their known importance in cardiac disease, we set out to analyse which of the PKC isoforms were regulated in our TAC model and to what extent *rictor* deficiency modified this regulation. *Figure 4B* shows that in control mice, TAC increased total protein levels of the classical PKCβII as well as PKCδ, a novel PKC (nPKC) by 1.5- and 2.3-fold, respectively. For PKCβII, the increase was paralleled by enhanced phosphorylation of its HM residue Ser660 (*Figure 4B* and see Supplementary material online, *Figure S3A*). An antibody to Thr638/641 in PKCα/βII revealed that phosphorylation of this turn motif (TM) was also increased (*Figure 4B*). Probing with a PKCβII-specific TM site antibody confirmed that this indeed concerned phosphorylation of the PKCβII isoform and that the difference between control and rictor-cKO mice was already visible prior to surgery (see Supplementary material online, *Figure S3B*). As the above-mentioned phosphorylation sites are all typical mTORC2 targets and the increases in total and phosphorylated PKCs paralleled those observed for rictor shown in *Figure 4A*, we next assessed whether rictor/mTORC2 is required for their increased abundance under pressure-overload conditions. Indeed, the significant increases in PKCβII and PKCδ protein were absent in the rictor-cKO hearts and consistently, PKCβII-pS660 and -pT641 were lower in rictor-cKO than in control mice (*Figure 4B*).

While the rictor-cKO group had lower PKCα and -βII levels compared with the control group, the abundance of PKCδ appeared not affected by *rictor* ablation under basal (sham) conditions (*Figure 4B*). We also analysed PKCε, the other main nPKC expressed in the heart. Its protein levels were lower in the rictor-cKO than in the corresponding sham or TAC controls, and did not increase after TAC (*Figure 4B* and see Supplementary material online, *Figure S3C*).

In conclusion, our observation that TAC increases PKCβII and PKCδ along with rictor in control, but not in the rictor-cKO hearts, suggests

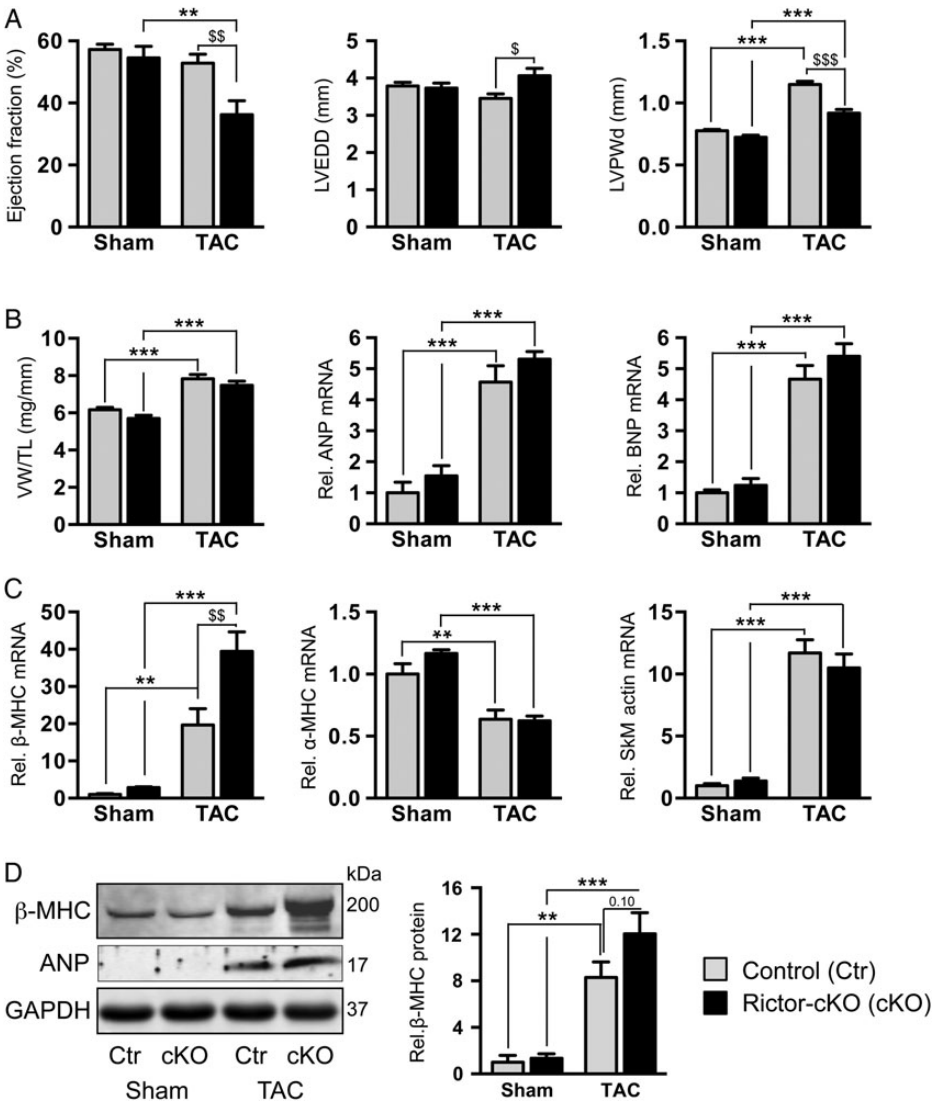

Figure 2 Rictor deficiency causes cardiac dysfunction without changing hypertrophic responses after TAC. *Rictor* deletion was induced by tamoxifen at 10 weeks of age and TAC or sham surgery performed 18–19 days later. Ultrasound was performed before (see Supplementary material online, *Table S1*) and 1 week after surgery (*A*), and the mice were sacrificed for molecular analysis immediately afterwards (*B*–*D*). (*A*) Echocardiography data of the EF, LVEDD, and diastolic LV posterior wall thickness (LVPWd). (*B*) *Post-mortem* ventricular weight to tibia length ratios (VW/TL) and quantitative RT-PCR analysis of ANP and BNP. (*C*) Quantitative RT-PCR analysis of β-MHC, α-MHC, and skeletal muscle (SkM) actin mRNA levels. (*D*) Western analysis of ANP and β-MHC proteins. Rictor-cKO are tamoxifen-injected α-MHC-MerCreMer/rictor$^{fl/fl}$ mice ($N = 5$ for sham, $N = 7$ for TAC). Controls are tamoxifen-injected α-MHC-MerCreMer/rictor$^{+/+}$ mice ($N = 6$ for sham, $N = 6$ for TAC). Two-way ANOVA *post hoc* testing: $^{**}P < 0.01$, $^{***}P < 0.001$ for TAC vs. sham; $^{\$}P < 0.05$, $^{\$\$}P < 0.01$, $^{\$\$\$}P < 0.001$ for rictor-cKO vs. control.

that the inability to increase these isozymes contributes to the reduced cardiac performance observed in our rictor-cKO mice under pressure-overload conditions. As PKCβII was already affected under basal conditions, its decrease is likely implicated directly in the development of dysfunction. Although PKCε was not increased after TAC, its strongly reduced levels in rictor-cKO hearts may have contributed to the dysfunction.

3.5 Rictor deficiency reduces Akt-pS473, Akt-pS450, as well as total Akt1 and 2 protein, while increasing Akt-pT308

Akt is the most frequently analysed target of mTORC2 and serves as an important survival kinase in the heart (for review, see Sussman *et al.*[27]).

Consistent with the baseline data obtained at 18 days after tamoxifen (*Figure 1A*) phosphorylation of Akt at its HM residue, Ser473 was also strongly reduced in the rictor-deficient hearts at 1 week after surgery, i.e. 25 days after tamoxifen, confirming that mTORC2 was to a large extent inactivated. Notably, total Akt protein was also lower in the rictor-cKO mice than in controls. Antibodies specific for total Akt1 and Akt2 protein (*Figure 4C*) revealed that both isoforms were reduced significantly. As previous studies have shown that mTORC2-mediated TM phosphorylation determines the stability and thereby abundance of Akt,[28,29] we analysed Akt-pS450. *Figure 4C* shows that phosphorylation of this site was indeed strongly diminished in the rictor-cKO hearts. Notably, Akt phosphorylation at Thr308, thought to be key for Akt activity,[30] was not reduced despite a clear lack of phosphorylation at

Table 2 Physiological and echocardiographic parameters of control and rictor knockout mice at 1 week after sham or TAC surgery

	Control		Rictor-cKO	
	Sham ($N = 7$)	TAC ($N = 6$)	Sham ($N = 5$)	TAC ($N = 7$)
Echocardiography				
Heart rate (b.p.m.)	539 ± 25	495 ± 14	473 ± 16	514 ± 13
Anteroseptal wall thickness (mm)				
Diastole	0.77 ± 0.01	1.04 ± 0.02***	0.73 ± 0.02	0.89 ± 0.03***,$$$
Systole	1.03 ± 0.02	1.39 ± 0.03***	0.97 ± 0.04	1.12 ± 0.04*,$$$
LV posterior wall thickness (mm)				
Diastole	0.78 ± 0.01	1.15 ± 0.03***	0.72 ± 0.02	0.92 ± 0.03***,$$$
Systole	1.03 ± 0.02	1.36 ± 0.03***	0.97 ± 0.04	1.07 ± 0.05*,$$$
LV internal diameter (mm)				
Diastole	3.79 ± 0.10	3.46 ± 0.13	3.73 ± 0.13	4.06 ± 0.20$
Systole	2.67 ± 0.10	2.55 ± 0.16	2.70 ± 0.18	3.38 ± 0.26$$
Ejection fraction (%)	57.2 ± 1.7	52.8 ± 3.2	54.6 ± 3.7	36.2 ± 4.5**,$$
Fractional shortening (%)	29.6 ± 1.1	26.6 ± 2.0	27.9 ± 2.4	17.3 ± 2.3**,$$
Post-mortem analysis				
Body weight (g)	29.0 ± 0.4	26.6 ± 1.1**	26.9 ± 0.8	27.1 ± 0.7
Ventricular weight (VW, mg)	112.4 ± 2.0	143.7 ± 4.2***	103.9 ± 3.1	135.9 ± 4.1***
VW/tibial length (mg/mm)	6.17 ± 0.13	7.84 ± 0.24***	5.69 ± 0.18	7.49 ± 0.22***

*$P < 0.05$, **$P < 0.01$, ***$P < 0.001$: TAC- vs. corresponding sham-operated group.
$$P < 0.05$, $$$P < 0.01$, $$$$P < 0.001$: knockout vs. corresponding control group.

Ser473 and Ser450. Consistent with earlier studies,[4,31] Akt-pT308 appeared even somewhat higher in the rictor-cKO than in control mice ($P = 0.035$ in two-way ANOVA), although upstream of Akt-pT308 no compensatory change in phosphoinositide-dependent kinase 1 (PDK1) phosphorylation was observed (see Supplementary material online, *Figure S4A*). In sham-operated mice, this went along with slightly enhanced phosphorylation of the Akt targets GSK3β and TSC2 (see Supplementary material online, *Figure S4A*). In an independent cohort of mice sacrificed at 18 days after tamoxifen in the fasted or insulin-stimulated state, rictor deficiency did not change phosphorylation of the Akt targets AS160 and FoxO1/3a (see Supplementary material online, *Figure S4B*). Our results are consistent with the view that Akt phosphorylation by mTORC2 is not required for its Thr308 phosphorylation by PDK1[32] and with what has been described for liver,[12] skeletal muscle,[9] Purkinje cells,[13] and other studies in which it was reported that Akt is still activated to a significant extent in mTORC2-deficient cells. Our findings show that also in the heart, the loss of mTORC2-mediated Akt phosphorylation does not reduce Akt activity towards several of its substrates.

3.6 Analysis of apoptosis in rictor-deficient hearts and adult cardiomyocyte cultures

Akt is known to propagate the effects of PI3K within the nucleus via FoxOs and thereby may regulate apoptosis.[33,34] Some studies support that mTORC2 is needed specifically for the function of Akt to phosphorylate FoxO, but not for other functions of Akt.[35] A recent study shows in cultured cardiomyocytes and ischaemic hearts that mTORC2 inactivation by Torin or shRNA enhances, whereas mTORC2 activation via PRAS40 decreases oxidative stress-induced apoptosis, and suggests that this happens via Akt-pS473 and FoxO.[36] We therefore tested whether mTORC2 deficiency increased apoptosis in our model by analysing cleaved caspase-3 and performing TUNEL assays. After TAC, the rictor-cKO mice ($N = 6$) had 2.2-fold more cleaved caspase-3-positive cells than the control mice ($N = 5$) and consistently, they also contained more TUNEL-positive cells (*Figure 5A* and *B*). However, only very few apoptotic cells were detectable and these were all part of the non-cardiomyocyte compartment of the heart as identified by double labelling with antibodies to myomesin. Our finding that cardiomyocyte apoptosis was not detectable in sections of the whole heart was in apparent contrast with previous work,[36] and we therefore went on to analyse apoptosis by western blotting after isolation of cardiomyocytes from the adult control and rictor-cKO hearts. *Figure 5C* shows that rictor was below detection levels in this cardiomyocyte fraction of the heart, which confirms efficiency and cardiomyocyte specificity of the deletion. Cleaved caspase-3 was higher in rictor-depleted cardiomyocytes immediately (0 h) or 24 h after their isolation. These data show that mTORC2 prevents apoptosis in adult cardiomyocytes, at least during the isolation procedure of these cells, which is very likely associated with hypoxic and/or other stress. Nevertheless, our observation that overall cardiac weight, fibrosis, and cardiomyocyte cross-sectional areas were not changed by the deletion together with the fact that we did not detect any apoptotic cardiomyocytes in the *in situ* heart indicates that apoptosis is not a primary reason for the dysfunction measured in rictor-deficient pressure-overloaded hearts. This conclusion is further supported by our observation that phosphorylated FoxO1/3 was not altered by the *rictor* deletion (see Supplementary material online, *Figure S4B*) and consistently, multiple FoxO target genes (ERRα, MCD1, and CPT1b) were indistinguishable between control and rictor-cKO hearts (data not shown).

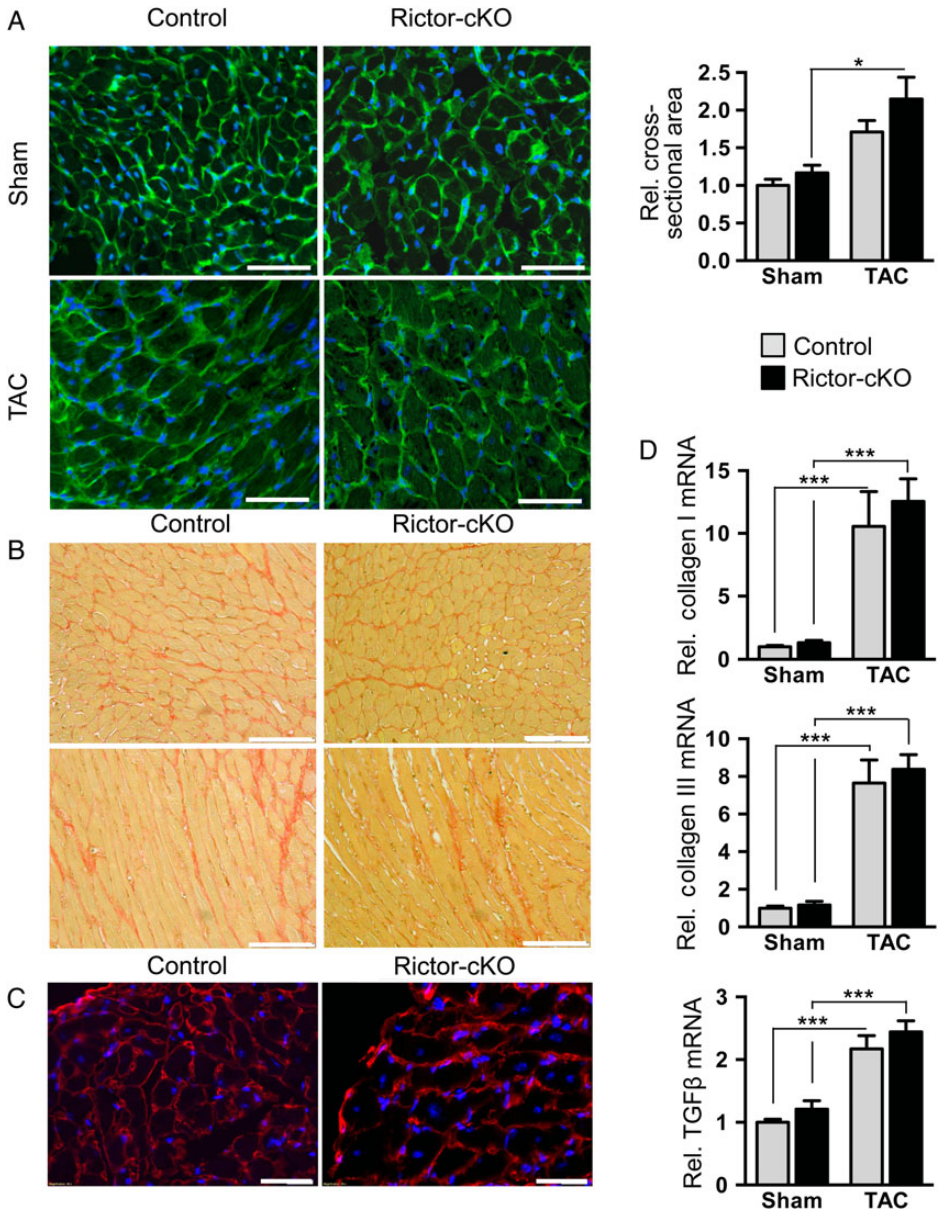

Figure 3 Rictor deficiency does not change cardiomyocyte cross-sectional areas or fibrosis after aortic constriction. Cardiac tissue of mice of *Figure 2* was either frozen in OCT (*A* and *C*) or fixed in paraformaldehyde, followed by dehydration and embedding in paraffin (*B*), or snap-frozen in liquid nitrogen for isolation of RNA and quantitative RT-PCR analysis (*D*). (*A*) WGA staining (left) and quantitative analysis of the cardiomyocyte cross-sectional area (right). (*B*) Picrosirius red staining for analysis of fibrosis. (*C*) Immunolabelling with an antibody to collagen I followed by a rhodamine-labelled secondary antibody. (*B* and *C*) TAC-operated mice. (*D*) Quantitative RT-PCR of collagen I and III and transforming growth factor (TGF)β to evaluate fibrosis ($N = 5–6$ mice per group). Two-way ANOVA *post hoc* testing: $^{*}P < 0.05$; $^{***}P < 0.001$ for TAC vs. the corresponding sham control. The scale bars represent 100 μm.

3.7 Rictor deficiency blunts signalling via PRAS40, mTORC1, and rpS6

Next to the Akt targets GSK3β, TSC2, and AS160 described under Section 3.5, reduced Akt levels in rictor-deficient hearts could, via PRAS40 and TSC, diminish mTORC1 activity. Since changed signalling via mTORC1 may, at least in part, explain the functional phenotype of the rictor-cKO mice, we tested whether mTORC2 inactivation modified signalling via mTORC1. Whereas *Figure 6A* shows that phosphorylation of the mTORC1 targets 4E-BP1 and UNC-51-like kinase 1 (ULK1) were not affected by *rictor* ablation, *Figure 6B* shows a trend towards lower S6-pS240/244 in rictor-deficient hearts ($P = 0.068$ in two-way ANOVA), suggesting reduced signalling via mTORC1/p70-S6K1. Consistently, mTOR phosphorylation at Ser2448, a target of p70-S6K1 indicative of mTORC1 activation, was decreased after *rictor* deletion ($P = 0.006$ in two-way ANOVA, *Figure 6B*). Furthermore, PRAS40, a target of Akt and component and negative regulator of mTORC1, was less phosphorylated in the rictor-cKO mice ($P = 0.011$ in two-way ANOVA, *Figure 6B*). Our findings suggest that mTORC2 may, possibly via Akt and

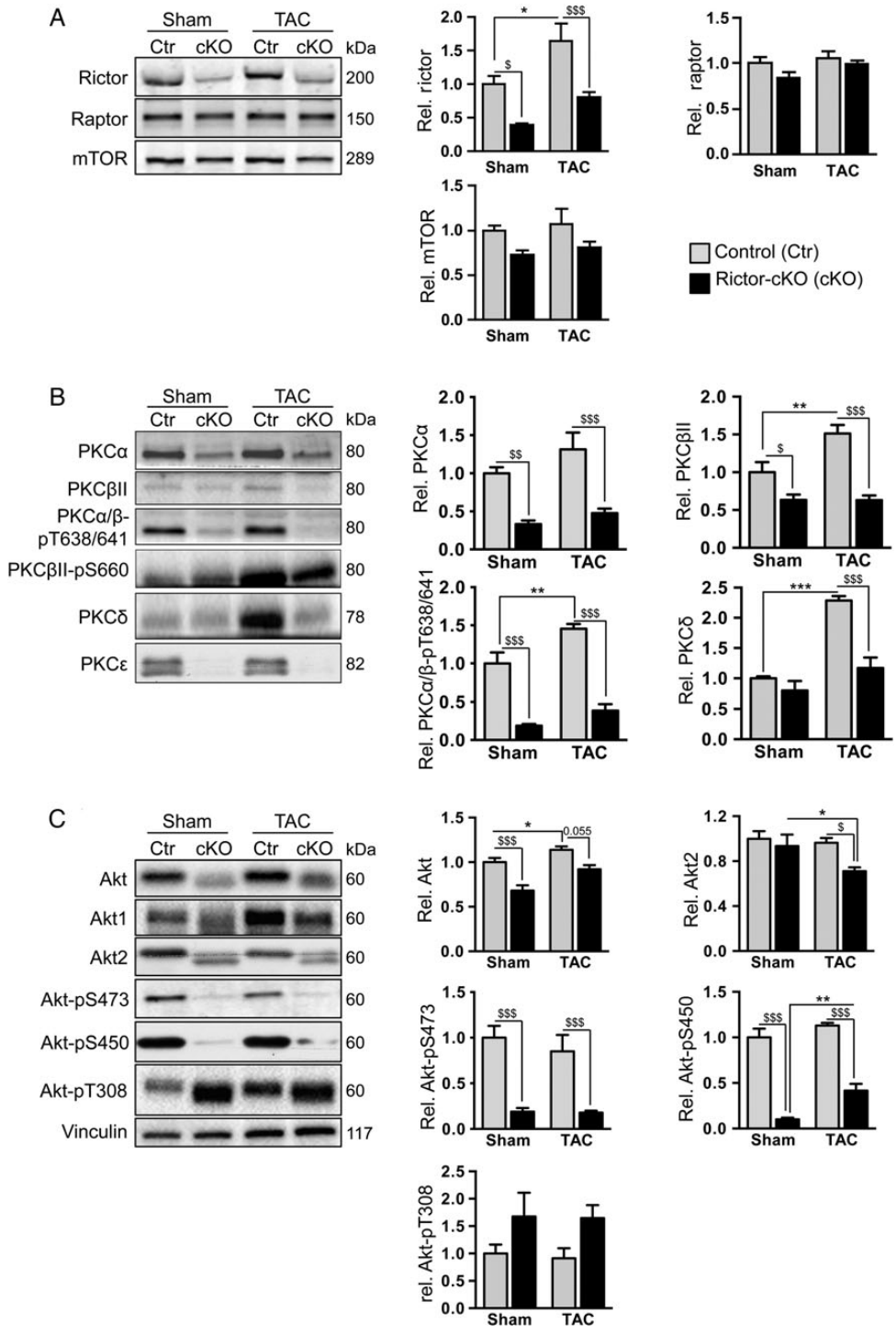

Figure 4 Effects of TAC and *rictor* ablation on AGC signalling at 1 week after surgery. Examples of western blots incubated with the antibodies as indicated (left). Quantification after normalization to the corresponding loading controls (right). The normalized data are expressed relative to the sham-operated controls. Control and rictor-cKO mice as in *Figure 2*. $N = 5–7$ per group. Two-way ANOVA *post hoc* testing: $^{*}P < 0.05$, $^{**}P < 0.01$, $^{***}P < 0.001$ for TAC vs. sham; $^{\$}P < 0.05$, $^{\$\$}P < 0.01$, $^{\$\$\$}P < 0.001$ for rictor-cKO vs. control.

PRAS40, regulate mTORC1-mediated p70-S6K1 and rpS6 phosphorylation. We also analysed AMPKα, as it is known to independently repress mTORC1 signalling through specific phosphorylation sites on mTOR, raptor, and TSC2 (reviewed in Shimobayashi and Hall[37]). AMPKα phosphorylation was increased in the rictor-deficient hearts ($P = 0.012$ in two-way ANOVA). Thus, AMPK may have blocked mTORC1 activity towards p70-S6K1 in parallel to PRAS40. Notably, the observed increase in AMPKα phosphorylation is indicative of increased AMP/ATP ratios, suggesting that energy availability is decreased in the rictor-cKO hearts. Indicative of metabolic stress is also the observed induction of β-MHC gene expression in the rictor-deficient mice (*Figure 2*).

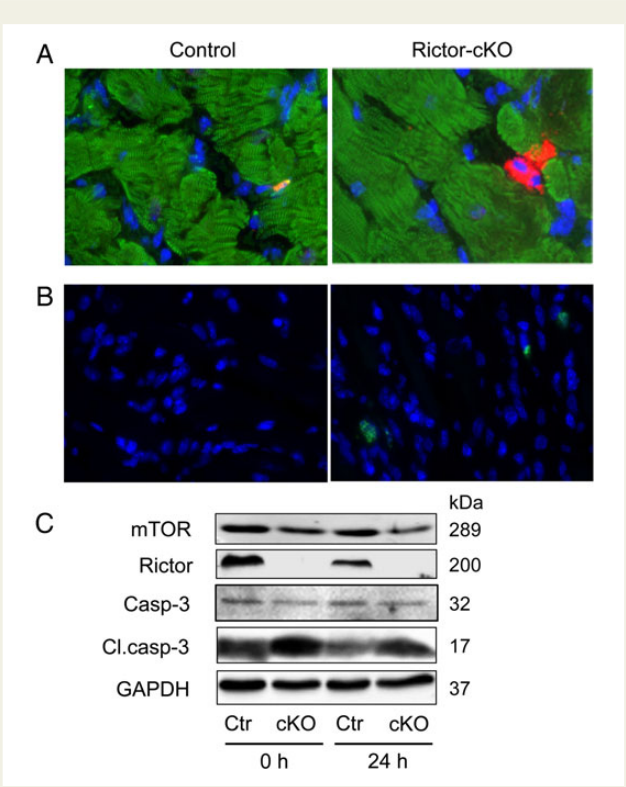

Figure 5 mTORC2 inactivation increases apoptosis in non-myocyte cells of the heart. Cardiac tissue of the mice of *Figure 2* was frozen in OCT (*A*) or fixed in paraformaldehyde, followed by dehydration and embedding in paraffin (*B*). (*A*) Immunostaining with an antibody against cleaved caspase-3 fragment followed by an Alexa555-labeled secondary antibody. Double labelling of the same section with an antibody to myomesin followed by an Alexa488-labelled antibody was performed to identify cardiomyocytes. (*B*) TUNEL assay was performed on paraffin sections. (*A* and *B*) Nuclei were stained with DAPI. For *C*, primary cardiomyocyte cultures were prepared from adult control and rictor cardiac knockout (cKO) mice and proteins extracted immediately (0 h) or 1 day after the isolation (24 h). Caspase-3 was analysed by western blotting.

4. Discussion

4.1 Rictor/mTORC2 is implicated in the response to pressure overload

The main objective of the present study was to elucidate the function of mTORC2 in the heart. Our experiments demonstrate that haemodynamic stress causes cardiac dysfunction in mice deficient for rictor, an essential component of mTORC2, whereas control mice with normal mTORC2 activity display maintained function. Cardiac mTORC2 inactivation does not cause any obvious basal phenotype during postnatal growth or adulthood up to 54 weeks of age. Interestingly, TAC increased overall ventricular weight in the rictor-cKO mice as much as in the control mice, but increases in LV wall thickness were less pronounced and associated with increased LV internal diameters, reminiscent of eccentric hypertrophy. Rictor deficiency did not affect any of the TAC-induced hypertrophic markers ANP, BNP, smooth muscle actin, and skeletal muscle actin, nor did it modify metabolic gene expression or fibrosis. Taken together, our results indicate that mTORC2 is important for contractile performance in acute pressure-overload conditions, without affecting reactive hypertrophic responses.

4.2 Rictor/mTORC2 is required for increased PKCβII and PKCδ protein levels during pressure overload

The role of mTORC2 during haemodynamic stress is further supported by our observation that rictor protein levels increase concomitant with maintained function in pressure-overloaded control hearts. This increase is paralleled by enhanced phosphorylation of PKCα and PKCβII. Because mTORC2 has been implicated in the phosphorylation of multiple PKC family members,[13,26,28,38,39] our results suggest that cardiac mTORC2 participates in the response to haemodynamic stress via these effectors. The reduced phosphorylated levels of these PKCs after cardiac *rictor* ablation consolidate this view.

Total protein levels of PKCβII, PKCδ, and, albeit to a lesser extent, PKCα ($P = 0.16$) are also higher after TAC in control hearts, but not in rictor-deficient hearts. Consistent with earlier work in murine embryonic fibroblasts, where evidence was provided that co-translational TM site phosphorylation by mTORC2 regulates stability and thereby the abundance of PKCα,[27,39] we here show that enhanced TM phosphorylation of PKCα and PKCβII after TAC is associated with their increased abundance, whereas decreased phosphorylation of the same sites after *rictor* deletion is associated with their reduced abundance. Notably, the decrease in phosphorylated PKC was stronger than that in total PKC, indicating that the remaining protein was less phosphorylated. Similarly, the strongly reduced Akt and PKCε abundance in our rictor-deficient hearts is very likely related to reduced mTORC2 phosphorylation, in line with previous mechanistic studies.[13,28] On the other hand, mTORC2 did not appear to regulate PKCδ in MEFs[28,39] or neurons,[13] and earlier work demonstrated TM autophosphorylation of PKCδ.[40,41] Our data therefore suggest that PKCδ stability may be regulated in a cell type-specific manner. It remains to be proven whether the decrease in PKCδ is explained by a direct mTORC2-mediated mechanism because unlike Akt and other PKCs that we measured, PKCδ appeared not reduced under basal conditions. We therefore cannot exclude the possibility that decreased PKCδ abundance after TAC is secondary to, for example, the observed cardiac or metabolic stress. Speaking against this is that cardiac stress has previously been associated with increased rather than decreased PKCδ. Alternatively, mTORC2-mediated PKCε reductions could be responsible for the lowered PKCδ, as published previously,[42] because PKCε is an established direct mTORC2 target.[26,28,39]

4.3 Functional consequences of reduced PKCβII and PKCδ after TAC

Phosphorylation of the three conserved serine/threonine residues on cPKCs and nPKCs takes place shortly after synthesis and is needed for their intracellular distribution, stability, and catalytic activity.[43,44] These phosphorylation events cause a stable but still 'closed' inactive enzyme conformation and prepare them for subsequent activation by lipid second messengers, such as diacylglycerol (DAG) and Ca^{2+}. In pressure-overload models, stimulation of angiotensin AT_1 and α_1-adrenergic receptors will, via Gq and DAG, stimulate the PKCs. Increased PKC expression and activity was previously thought to cause the pathological hypertrophy together with ERK1/2 and p38 stress-activated kinases. However, consistent with our observation that decreased levels of two cPKCs were not associated with any

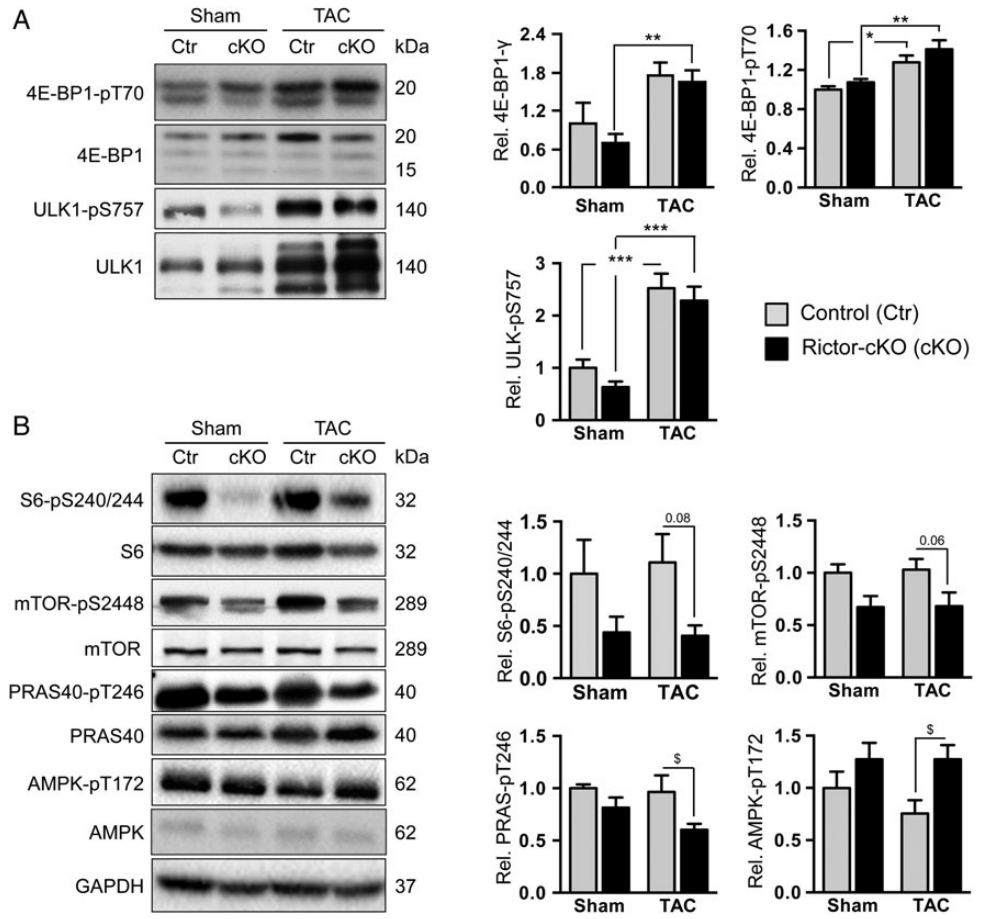

Figure 6 Effect of *rictor* deletion on mTORC1, PRAS40, and AMPK. Examples of western blots incubated with antibodies as indicated (left). Quantification after normalization to the corresponding loading controls (right). The normalized data are expressed relative to the sham-operated controls. Control and rictor-cKO mice as in *Figures 2* and *4*. $N = 5–7$ per group. Two-way ANOVA *post hoc* testing: $^{*}P < 0.05$, $^{**}P < 0.01$, $^{***}P < 0.001$ for TAC vs. sham; $^{\$}P < 0.05$ for rictor-cKO vs. control.

effects on the hypertrophic response, genetic ablation of the cPKC family members does not prevent cardiac hypertrophy.[45] Instead, the cPKCs are today thought to be involved in the regulation of cardiac contractility.[23] Studies with PKC knockout mice have demonstrated that the β and γ isoforms are, in contrast to PKCα, positively affecting contractility. Thus, PKCβ/γ null mice show more severe failure, whereas PKCα null mice are less susceptible to heart failure following long-term pressure-overload or myocardial infarction injury.[45] Based on these studies, we think that our phenotype is related to the inability of the rictor-deficient hearts to increase PKCβII and perhaps also PKCγ, which we did not test in the heart but was strongly decreased after *rictor* ablation in neuronal tissue.[13]

Regarding the nPKCs, a study published during the revision of our manuscript demonstrated that PKCδ and PKCε depress reactive hypertrophy, but that it required deletion of both genes to reveal this function, because redundancy masked the effect after ablation of the individual genes. The lack of a phenotype under basal conditions in our study with both nPKCs being strongly decreased after *rictor* ablation is consistent with that study, in which combined embryonic ablation of PKCδ and PKCε showed no phenotype under basal conditions.[35] The lack of a significant effect on pressure-overload hypertrophy in the rictor-deficient mice may be due to residual PKCδ and PKCε protein, inherent to the inducible MerCreMer model that we used.

Besides contractile deficiency, the decreased cardiac performance may be related to the energy resources available for contraction, as mTORC2 has been implicated in the regulation of metabolism in various tissues.[37,46] In support of this idea, AMPK phosphorylation levels were increased in the rictor-cKO hearts indicative of a reduced ATP availability. Moreover, β-MHC expression was induced, which, as this isoform generates force in an energetically more economic manner than the α-isoform, may represent a compensatory energy-preserving effort after *rictor* ablation. Akt2 regulates Glut4 translocation to the sarcolemma, a process that is enhanced during the cardiac pressure-overload response to ensure that energy supplies match the increased work. However, although Akt2 abundance was strongly reduced in the rictor-cKO hearts, the phosphorylation of its downstream mediator AS160 was not affected (see Supplementary material online, *Figure S4B*). Finally, the lack of a robust PKCδ increase after TAC, possibly secondary to decreased PKCε,[42] may explain metabolic insufficiency after *rictor* ablation, because it has been shown previously that hearts lacking PKCδ lose their capacity to adapt metabolically.[47,48] In conclusion, our data suggest that the lacking increases in PKCβII and

PKCδ contributed to the dysfunction observed after pressure overload for the rictor-deficient hearts.

4.4 Reduced phosphorylation of Akt at Ser473 and Ser450 after *rictor* ablation does not reduce Akt substrate phosphorylation

Next to the above-discussed PKCs, the protein abundance of the best-established mTORC2 target Akt was reduced in the rictor-cKO mice and this applies to Akt1 as well as Akt2. Because Akt was not increased in our TAC model, its reduced expression is most likely not a primary cause of the dysfunction measured in the rictor-cKO mice. The lack of a functional or morphological phenotype under physiological conditions in growing and adult mice suggests that the residual protein amounts were sufficient for normal cardiac function or that a high level of redundancy in cardiac signalling exists and alternate pathways compensate for the deletion. The latter possibility is supported by the fact that phosphorylation of Akt at Thr308 was not impaired and that the Akt targets GSK3β, TSC, and AS160 mirrored the Akt-pT308 levels, indicating normal Akt activity under basal conditions. These results imply that the mTORC2-mediated Akt phosphorylation is not essential for basal cardiac function. Consistently, cardiac deletion of mTOR[4] caused a basal phenotype that was very similar to that of mice in which raptor was lacking,[7] which indicates that mTOR acts predominantly as part of mTORC1. Similar observations were noted for other organs, including skeletal muscle,[9,10] kidney,[49] or adipose tissue[11] in all of which rictor deficiency does not cause any strong baseline phenotype. Along similar lines, mTORC2-mediated HM site phosphorylation appears not essential for the growth regulatory activity of Akt at physiological levels of insulin stimulation.[50] The latter study suggests that only the maximal levels of Akt activity are limited in the absence of HM phosphorylation, for example, when insulin stimulation is increased.[50] In analogy, our data obtained with the TAC model suggest that in the heart, the mTORC2-mediated phosphorylation becomes functionally important when mTORC2 targets are significantly activated, which we demonstrated for PKCβII and PKCδ, but not for Akt. It is of note that our study was performed with male mice. Given the known effect of female hormones on Akt signalling, it remains to be demonstrated whether mTORC2 deficiency impacts one or more targets of Akt in the female heart.

4.5 mTORC2 inactivation does not modify physiological or pathological cardiac growth

Our previous work shows that mTORC1 is essential for the cardiac adaptation to pressure overload with protein synthesis inherent to cardiomyocyte hypertrophy being one of the prior mechanisms implicated.[7] Upstream of mTORC1 and downstream of mTORC2 Akt can activate protein translation via TSC1/TSC2 and Rheb. Akt regulates normal postnatal cardiac growth,[51] it may get activated by pressure overload,[52] and transgenic overexpression of active Akt1 induces cardiac hypertrophy.[53,54] Whether or not mTORC2, via Akt or other pathways, contributes to cardiac growth responses was unclear at the onset of our study. As *rictor* deletion neither affected cardiac weight and cardiomyocyte cross-sectional areas after TAC, nor changed physiological postnatal cardiac growth, we conclude that mTORC2 is not required for cardiac protein synthesis. This is further supported by our observation that 4E-BP1, main mediator of protein synthesis downstream of mTORC1, was increased after TAC in the rictor-cKO as much as in control mice. Moreover, Akt-pT308 was increased along with enhanced phosphorylation of targets involved in growth responses, such as TSC2 and GSK3β. In contrast, *rictor* ablation decreased S6K1 phosphorylation. While this effect may be secondary to decreased PKC activity,[41,41,55,56] it had no consequences for cardiac weight or cardiomyocyte cross-sectional area in our model, consistent with earlier work.[57] Thus, the heart behaves like several other organs from which *rictor* has been removed without affecting an increase in organ weight, including skeletal muscle,[9,10] adipose tissue,[11] and kidney.[49] We conclude that increased global protein synthesis intrinsic to physiological growth or pathological cardiac hypertrophy does not depend on mTORC2.

Taken together, our study points to a beneficial function of mTORC2 in the heart during haemodynamic stress. We identified several kinases that were reduced in rictor-deficient hearts. As cardiac dysfunction occurred only after haemodynamic stress, we conclude that the kinases that were increased concomitant to rictor in control but not in rictor-cKO hearts, namely PKCβII and -δ, are implicated in the beneficial effects of mTORC2. As several compounds inhibiting both mTOR complexes are in clinical trials for the treatment of cancer, special attention should be paid in these studies to patients with concurrent cardiovascular diseases such as hypertension or valve disease. On the other hand, our insights into cardiac mTORC2 signalling may also open new avenues for the treatment of cardiac disease.

Supplementary material

Supplementary material is available at *Cardiovascular Research* online.

Conflict of interest: none declared.

Funding

This work was supported by the Swiss National Science Foundation (grant no. 31-135559/1), the 'Stiftung für Kardiovaskuläre Forschung Basel', and the 'Novartis Foundation for Medical-Biological Research'.

References

1. Sciarretta S, Volpe M, Sadoshima J. Mammalian target of rapamycin signaling in cardiac physiology and disease. *Circ Res* 2014;**114**:549–564.
2. Dibble CC, Manning BD. Signal integration by mTORC1 coordinates nutrient input with biosynthetic output. *Nat Cell Biol* 2013;**15**:555–564.
3. Song X, Kusakari Y, Xiao CY, Kinsella SD, Rosenberg MA, Scherrer-Crosbie M, Hara K, Rosenzweig A, Matsui T. mTOR attenuates the inflammatory response in cardiomyocytes and prevents cardiac dysfunction in pathological hypertrophy. *Am J Physiol Cell Physiol* 2010;**299**:C1256–C1266.
4. Zhang D, Contu R, Latronico MV, Zhang JL, Rizzi R, Catalucci D, Miyamoto S, Huang K, Ceci M, Gu Y, Dalton ND, Peterson KL, Guan KL, Brown JH, Chen J, Sonenberg N, Condorelli G. MTORC1 regulates cardiac function and myocyte survival through 4E-BP1 inhibition in mice. *J Clin Invest* 2010;**120**:2805–2816.
5. Wullschleger S, Loewith R, Hall MN. TOR signaling in growth and metabolism. *Cell* 2006;**124**:471–484.
6. Laplante M, Sabatini DM. mTOR signaling in growth control and disease. *Cell* 2012;**149**:274–293.
7. Shende P, Plaisance I, Morandi C, Pellieux C, Berthonneche C, Zorzato F, Krishnan J, Lerch R, Hall MN, Ruegg MA, Pedrazzini T, Brink M. Cardiac raptor ablation impairs adaptive hypertrophy, alters metabolic gene expression, and causes heart failure in mice. *Circulation* 2011;**123**:1073–1082.
8. Oh WJ, Jacinto E. mTOR complex 2 signaling and functions. *Cell Cycle* 2011;**10**:2305–2316.
9. Bentzinger CF, Romanino K, Cloetta D, Lin S, Mascarenhas JB, Oliveri F, Xia J, Casanova E, Costa CF, Brink M, Zorzato F, Hall MN, Ruegg MA. Skeletal muscle-specific ablation of raptor, but not of rictor, causes metabolic changes and results in muscle dystrophy. *Cell Metab* 2008;**8**:411–424.
10. Kumar A, Harris TE, Keller SR, Choi KM, Magnuson MA, Lawrence JC Jr. Muscle-specific deletion of rictor impairs insulin-stimulated glucose transport and enhances basal glycogen synthase activity. *Mol Cell Biol* 2008;**28**:61–70.
11. Cybulski N, Polak P, Auwerx J, Ruegg MA, Hall MN. mTOR complex 2 in adipose tissue negatively controls whole-body growth. *Proc Natl Acad Sci USA* 2009;**106**:9902–9907.

12. Hagiwara A, Cornu M, Cybulski N, Polak P, Betz C, Trapani F, Terracciano L, Heim MH, Ruegg MA, Hall MN. Hepatic mTORC2 activates glycolysis and lipogenesis through Akt, glucokinase, and SREBP1c. *Cell Metab* 2012;**15**:725–738.
13. Thomanetz V, Angliker N, Cloetta D, Lustenberger RM, Schweighauser M, Oliveri F, Suzuki N, Ruegg MA. Ablation of the mTORC2 component rictor in brain or Purkinje cells affects size and neuron morphology. *J Cell Biol* 2013;**201**:293–308.
14. Huang W, Zhu PJ, Zhang S, Zhou H, Stoica L, Galiano M, Krnjevic K, Roman G, Costa-Mattioli M. mTORC2 controls actin polymerization required for consolidation of long-term memory. *Nat Neurosci* 2013;**16**:441–448.
15. Bercury KK, Dai J, Sachs HH, Ahrendsen JT, Wood TL, Macklin WB. Conditional ablation of raptor or rictor has differential impact on oligodendrocyte differentiation and CNS myelination. *J Neurosci* 2014;**34**:4466–4480.
16. Choo AY, Yoon SO, Kim SG, Roux PP, Blenis J. Rapamycin differentially inhibits S6Ks and 4E-BP1 to mediate cell-type-specific repression of mRNA translation. *Proc Natl Acad Sci USA* 2008;**105**:17414–17419.
17. Wang X, Yue P, Kim YA, Fu H, Khuri FR, Sun SY. Enhancing mammalian target of rapamycin (mTOR)-targeted cancer therapy by preventing mTOR/raptor inhibition-initiated, mTOR/rictor-independent Akt activation. *Cancer Res* 2008;**68**: 7409–7418.
18. Sarbassov DD, Ali SM, Sengupta S, Sheen JH, Hsu PP, Bagley AF, Markhard AL, Sabatini DM. Prolonged rapamycin treatment inhibits mTORC2 assembly and Akt/PKB. *Mol Cell* 2006;**22**:159–168.
19. Lamming DW, Ye L, Katajisto P, Goncalves MD, Saitoh M, Stevens DM, Davis JG, Salmon AB, Richardson A, Ahima RS, Guertin DA, Sabatini DM, Baur JA. Rapamycin-induced insulin resistance is mediated by mTORC2 loss and uncoupled from longevity. *Science* 2012;**335**:1638–1643.
20. Nagata K, Liao R, Eberli FR, Satoh N, Chevalier B, Apstein CS, Suter TM. Early changes in excitation-contraction coupling: transition from compensated hypertrophy to failure in Dahl salt-sensitive rat myocytes. *Cardiovasc Res* 1998;**37**:467–477.
21. Polak P, Cybulski N, Feige JN, Auwerx J, Ruegg MA, Hall MN. Adipose-specific knockout of raptor results in lean mice with enhanced mitochondrial respiration. *Cell Metab* 2008;**8**:399–410.
22. Sohal DS, Nghiem M, Crackower MA, Witt SA, Kimball TR, Tymitz KM, Penninger JM, Molkentin JD. Temporally regulated and tissue-specific gene manipulations in the adult and embryonic heart using a tamoxifen-inducible Cre protein. *Circ Res* 2001;**89**:20–25.
23. Liu Q, Molkentin JD. Protein kinase C alpha as a heart failure therapeutic target. *J Mol Cell Cardiol* 2011;**51**:474–478.
24. Palaniyandi SS, Sun L, Ferreira JC, Mochly-Rosen D. Protein kinase C in heart failure: a therapeutic target? *Cardiovasc Res* 2009;**82**:229–239.
25. Duquesnes N, Lezoualc'h F, Crozatier B. PKC-delta and PKC-epsilon: foes of the same family or strangers? *J Mol Cell Cardiol* 2011;**51**:665–673.
26. Guertin DA, Stevens DM, Thoreen CC, Burds AA, Kalaany NY, Moffat J, Brown M, Fitzgerald KJ, Sabatini DM. Ablation in mice of the mTORC components raptor, rictor, or mLST8 reveals that mTORC2 is required for signaling to Akt-FOXO and PKCalpha, but not S6K1. *Dev Cell* 2006;**11**:859–871.
27. Sussman MA, Volkers M, Fischer K, Bailey B, Cottage CT, Din S, Gude N, Avitabile D, Alvarez R, Sundararaman B, Quijada P, Mason M, Konstandin MH, Malhowski A, Cheng Z, Khan M, McGregor M. Myocardial AKT: the omnipresent nexus. *Physiol Rev* 2011;**91**:1023–1070.
28. Ikenoue T, Inoki K, Yang Q, Zhou X, Guan KL. Essential function of TORC2 in PKC and Akt turn motif phosphorylation, maturation and signalling. *EMBO J* 2008;**27**: 1919–1931.
29. Oh WJ, Wu CC, Kim SJ, Facchinetti V, Julien LA, Finlan M, Roux PP, Su B, Jacinto E. mTORC2 can associate with ribosomes to promote cotranslational phosphorylation and stability of nascent Akt polypeptide. *EMBO J* 2010;**29**:3939–3951.
30. Alessi DR, James SR, Downes CP, Holmes AB, Gaffney PR, Reese CB, Cohen P. Characterization of a 3-phosphoinositide-dependent protein kinase which phosphorylates and activates protein kinase B alpha. *Curr Biol* 1997;**7**:261–269.
31. Zhu Y, Soto J, Anderson B, Riehle C, Zhang YC, Wende AR, Jones D, McClain DA, Abel ED. Regulation of fatty acid metabolism by mTOR in adult murine hearts occurs independently of changes in PGC-1alpha. *Am J Physiol Heart Circ Physiol* 2013;**305**: H41–H51.
32. Garcia-Martinez JM, Alessi DR. mTOR complex 2 (mTORC2) controls hydrophobic motif phosphorylation and activation of serum- and glucocorticoid-induced protein kinase 1 (SGK1). *Biochem J* 2008;**416**:375–385.
33. Brunet A, Park J, Tran H, Hu LS, Hemmings BA, Greenberg ME. Protein kinase SGK mediates survival signals by phosphorylating the forkhead transcription factor FKHRL1 (FOXO3a). *Mol Cell Biol* 2001;**21**:952–965.
34. Aoyama T, Matsui T, Novikov M, Park J, Hemmings B, Rosenzweig A. Serum and glucocorticoid-responsive kinase-1 regulates cardiomyocyte survival and hypertrophic response. *Circulation* 2005;**111**:1652–1659.
35. Song M, Matkovich SJ, Zhang Y, Hammer DJ, Dorn GW II. Combined cardiomyocyte PKCdelta and PKCepsilon gene deletion uncovers their central role in restraining developmental and reactive heart growth. *Sci Signal* 2015;**8**:ra39.
36. Volkers M, Konstandin MH, Doroudgar S, Toko H, Quijada P, Din S, Joyo A, Ornelas L, Samse K, Thuerauf DJ, Gude N, Glembotski CC, Sussman MA. Mechanistic target of rapamycin complex 2 protects the heart from ischemic damage. *Circulation* 2013;**128**: 2132–2144.
37. Shimobayashi M, Hall MN. Making new contacts: the mTOR network in metabolism and signalling crosstalk. *Nat Rev Mol Cell Biol* 2014;**15**:155–162.
38. Sarbassov DD, Ali SM, Kim DH, Guertin DA, Latek RR, Erdjument-Bromage H, Tempst P, Sabatini DM. Rictor, a novel binding partner of mTOR, defines a rapamycin-insensitive and raptor-independent pathway that regulates the cytoskeleton. *Curr Biol* 2004;**14**:1296–1302.
39. Facchinetti V, Ouyang W, Wei H, Soto N, Lazorchak A, Gould C, Lowry C, Newton AC, Mao Y, Miao RQ, Sessa WC, Qin J, Zhang P, Su B, Jacinto E. The mammalian target of rapamycin complex 2 controls folding and stability of Akt and protein kinase C. *EMBO J* 2008;**27**:1932–1943.
40. Li W, Zhang J, Bottaro DP, Pierce JH. Identification of serine 643 of protein kinase C-delta as an important autophosphorylation site for its enzymatic activity. *J Biol Chem* 1997;**272**:24550–24555.
41. Parekh D, Ziegler W, Yonezawa K, Hara K, Parker PJ. Mammalian TOR controls one of two kinase pathways acting upon nPKCdelta and nPKCepsilon. *J Biol Chem* 1999;**274**: 34758–34764.
42. Basu A, Sridharan S, Persaud S. Regulation of protein kinase C delta downregulation by protein kinase C epsilon and mammalian target of rapamycin complex 2. *Cell Signal* 2009;**21**:1680–1685.
43. Gallegos LL, Newton AC. Spatiotemporal dynamics of lipid signaling: protein kinase C as a paradigm. *IUBMB Life* 2008;**60**:782–789.
44. Freeley M, Kelleher D, Long A. Regulation of protein kinase C function by phosphorylation on conserved and non-conserved sites. *Cell Signal* 2011;**23**: 753–762.
45. Liu Q, Chen X, Macdonnell SM, Kranias EG, Lorenz JN, Leitges M, Houser SR, Molkentin JD. Protein kinase C{alpha}, but not PKC{beta} or PKC{gamma}, regulates contractility and heart failure susceptibility: implications for ruboxistaurin as a novel therapeutic approach. *Circ Res* 2009;**105**:194–200.
46. Cornu M, Albert V, Hall MN. mTOR in aging, metabolism, and cancer. *Curr Opin Genet Dev* 2013;**23**:53–62.
47. Mayr M, Chung YL, Mayr U, McGregor E, Troy H, Baier G, Leitges M, Dunn MJ, Griffiths JR, Xu Q. Loss of PKC-delta alters cardiac metabolism. *Am J Physiol Heart Circ Physiol* 2004;**287**:H937–H945.
48. Mayr M, Metzler B, Chung YL, McGregor E, Mayr U, Troy H, Hu Y, Leitges M, Pachinger O, Griffiths JR, Dunn MJ, Xu Q. Ischemic preconditioning exaggerates cardiac damage in PKC-delta null mice. *Am J Physiol Heart Circ Physiol* 2004;**287**: H946–H956.
49. Godel M, Hartleben B, Herbach N, Liu S, Zschiedrich S, Lu S, Debreczeni-Mor A, Lindenmeyer MT, Rastaldi MP, Hartleben G, Wiech T, Fornoni A, Nelson RG, Kretzler M, Wanke R, Pavenstadt H, Kerjaschki D, Cohen CD, Hall MN, Ruegg MA, Inoki K, Walz G, Huber TB. Role of mTOR in podocyte function and diabetic nephropathy in humans and mice. *J Clin Invest* 2011;**121**:2197–2209.
50. Hietakangas V, Cohen SM. Re-evaluating AKT regulation: role of TOR complex 2 in tissue growth. *Genes Dev* 2007;**21**:632–637.
51. Shiojima I, Yefremashvili M, Luo Z, Kureishi Y, Takahashi A, Tao J, Rosenzweig A, Kahn CR, Abel ED, Walsh K. Akt signaling mediates postnatal heart growth in response to insulin and nutritional status. *J Biol Chem* 2002;**277**:37670–37677.
52. Naga Prasad SV, Esposito G, Mao L, Koch WJ, Rockman HA. Gbetagamma-dependent phosphoinositide 3-kinase activation in hearts with in vivo pressure overload hypertrophy. *J Biol Chem* 2000;**275**:4693–4698.
53. Shioi T, McMullen JR, Kang PM, Douglas PS, Obata T, Franke TF, Cantley LC, Izumo S. Akt/protein kinase B promotes organ growth in transgenic mice. *Mol Cell Biol* 2002;**22**: 2799–2809.
54. Condorelli G, Drusco A, Stassi G, Bellacosa A, Roncarati R, Iaccarino G, Russo MA, Gu Y, Dalton N, Chung C, Latronico MV, Napoli C, Sadoshima J, Croce CM, Ross J Jr. Akt induces enhanced myocardial contractility and cell size in vivo in transgenic mice. *Proc Natl Acad Sci USA* 2002;**99**:12333–12338.
55. Moschella PC, Rao VU, McDermott PJ, Kuppuswamy D. Regulation of mTOR and S6K1 activation by the nPKC isoforms, PKCepsilon and PKCdelta, in adult cardiac muscle cells. *J Mol Cell Cardiol* 2007;**43**:754–766.
56. Wang L, Rolfe M, Proud CG. Ca(2+)-independent protein kinase C activity is required for alpha1-adrenergic-receptor-mediated regulation of ribosomal protein S6 kinases in adult cardiomyocytes. *Biochem J* 2003;**373**:603–611.
57. McMullen JR, Shioi T, Zhang L, Tarnavski O, Sherwood MC, Dorfman AL, Longnus S, Pende M, Martin KA, Blenis J, Thomas G, Izumo S. Deletion of ribosomal S6 kinases does not attenuate pathological, physiological, or insulin-like growth factor 1 receptor-phosphoinositide 3-kinase-induced cardiac hypertrophy. *Mol Cell Biol* 2004;**24**: 6231–6240.

Acknowledgments

I would like to first acknowledge Prof. Dr. Marijke Brink for giving me the opportunity to do one the greatest achievements of my personal and professional live. I would like to thank her for her guidance, support, and understanding. It was a great challenging experience that enforces me in my will of continuing research.

I would like to thank my Ph.D. committee members: Prof. Dr. Markus A. Rüegg and Prof. Dr. Thierry Pedrazzini, for their supervision and the time and efforts spent in the accompaniment of my project.

I want to give a special thanks to Lifen for the precious help that she gave me all along my study. Her broad knowledge, her technical and surgical skills were essential for the successful conduction of my projects. Thank you Lifen for your scientific support, presence and friendship. We spent great time with the mice and also without!

I also want to thank the other members of the laboratory, Christian who gave me a great technical support whenever I had questions; and Philippe who was always present for science and fun, I will take my revenge in table tennis…one day! It is of course, without forgetting Laura from whom I learned molecular analysis technique, she is a good teacher. I am also grateful to have met Fabienne, we had enjoyable discussions! Finally I thank Stéphanie for being a such supportive friend and also an excellent scientific collaborator, thank you for everything!

My final thanks is going to Dr. Mohamed Chami and his team from the C-CINA, Biocenter of Basel. They made a great job in the analysis of cardiac autophagy by TEM in our animal study.